The Detection of Potato Cyst Nematode (PCN) Infestation Using Remotely Sensed Imagery

Thesis

UNRESTRICTED

The Detection of Potato Cyst Nematode (PCN) Infestation Using Remotely Sensed Imagery

William Loveland Heath BSc (Hons)

A thesis submitted in partial fulfilment of the requirements of the Open University for the degree of Doctor of Philosophy

October 2003

Harper Adams University College, Newport, Shropshire in collaboration with Rothamsted Research

Submission date: 24 October 2003
Award date: 19 July 2004

ProQuest LLC.
789 East Eisenhower Parkway
P.O. Box 1346
Ann Arbor, MI 48106 – 1346

Declaration

No part of this work has been submitted for the award of a qualification at this or any other institution. All published work has been fully referenced.

Signed

William L. Heath

Abstract

The Detection of Potato Cyst Nematode (PCN) Infestation Using Remotely Sensed Imagery.

Potato cyst nematodes (PCN) *Globodera pallida* Stone *and G. rostochiensis* (Wollenweber) are economically-important pests which cause significant losses to potato production world-wide. Population control is a major objective of a sustainable management strategy as nematodes are persistent and reproductive rates can be high. Current methods of determining PCN population densities are both expensive and time consuming: an advance on current sampling methods would facilitate the application of precision farming methods to PCN management.

The potential for using light reflected from the potato canopy as an assay to detect PCN infestation is investigated. Spectral reflectance was measured from the canopy of commercial potato crops, individual plants and single leaves with a field spectrometer, airborne remote sensing and from SPOT and Ikonos satellite images. Comparisons between the reflectance from healthy and infected plants revealed a significant reduction in green (*c.* 550nm) reflectance from infested plants, and this was consistent across seasons, cultivars and imaging methods. The strongest results were seen early in the crop cycle, although full canopy development is desirable in airborne and satellite image analysis.

Yield-limiting pathogens are frequently reported as increasing visible reflectance by reducing chlorophyll concentration in the leaves of afflicted plants. The spectral response to PCN infestation is distinct from that from common plant stress factors and a PCN-specific detector system is proposed.

A viable commercial PCN assay would need to be timely, reliable and cost-effective. Whilst aircraft and satellite platforms offer the rapid acquisition of data from large areas, these imaging methods are heavily dependent on weather conditions. Results from data collected using a hand-held chlorophyll meter in this investigation indicate that a closed, or semi-closed imaging system (enclosing or covering the plant canopy) would be suited to the detection of PCN under field conditions and less susceptible to inclement weather.

Acknowledgements

William Heath was in receipt of a Research Studentship funded by Harper Adams University College through the Sustainable Arable LINK programme 112, Integrated Management Strategies for Potato Cyst Nematodes.

Field spectrometers and associated equipment have been made available to this project by the Natural Environment Research Council (NERC) Equipment Pool for Field Spectroscopy (EPFS).

Airborne spectral data were collected for this investigation by the NERC Airborne Remote Sensing Facility (ARSF), Didcot, Oxfordshire, UK. in 2001 and 2002.

Thanks are expressed to:

Dr Edward Milton and Karen Anderson from NERC EPFS for training and advice on the use of field spectrometers. Karen is remembered for her 'can-do' attitude to arranging loans of EPFS equipment.

Fabrizio Tadina and the crew of the NERC Airborne Remote Sensing Facility (ARSF) for their (successful) efforts to obtain airborne spectral data despite extended periods of unfavourable weather.

Dr Helen Ougham and Prof. Sid Thomas of the Institute for Grassland Research (IGER), Aberystwyth for the use of their camera and filter equipment.

Dr Andrew Wilson from the Centre for Ecology and Hydrology (CEH) for his patience and advice on the processing of airborne remote sensing data.

Dr Simon Edwards and Katya Pirgozliev from Harper Adams University College for instruction, support and assistance with laboratory procedures for the polymerase chain reaction (PCR) species determination of PCN.

Dr Stephen Minnis, Dr Simon Woods and Dr Ivan Grove from Harper Adams University College for instruction and advice on laboratory techniques for working with cyst nematodes.

Victoria Talbot from Harper Adams University College for assistance and instruction in the laboratory determination of soil nutrient concentration levels.

Charles Murray and the staff of the Crop and Environment Research Centre at Harper Adams for assistance and support with field and glasshouse experiments.

My Director of Studies, Dr P.P.J. Haydock and Supervisors, Dr A. Wilcox and Dr Ken Evans for their unstinting support and guidance throughout this project.

Mr R Belcher, Mr A. Craddock and Mr M. Bubb for the use of their fields in airborne and satellite remote sensing experiments.

Mathew Back and Jacqueline Pratt for assistance with field trials, good humour and good company whilst sharing an office with me for four years.

With special thanks to my wife Sara for her support and encouragement over many years, and her patience and tolerance when writing this thesis took priority over family life.

Statement of advanced studies

During the tenure of this project, in addition to conducting and reporting the experiments in this manuscript, the author has:

- Completed an M.Sc. unit in statistical procedures;
- completed a course in technical writing skills;
- received training in laboratory procedures for the extraction and quantification of cyst nematodes from plant and soil samples;
- received training in PCN species determination by the polymerase chain reaction (PCR) method;
- attended weekly research seminars at Harper Adams University College and given a presentation;
- given a presentation at the Harper Adams Postgraduate Colloquium. December 1999;
- presented a poster at the Association of Applied Biologists 'Offered Papers in Nematology' meeting, Linnean Society, London. December 14th, 1999;
- presented a poster at the Association of Applied Biologists conference 'Potato Cyst Nematode Management'. Harper-Adams University College, Shropshire. June 6th, 2000;
- presented a poster at the Association of Applied Biologists conference 'Remote Sensing in Agriculture'. Cirencester. June 26th-28th, 2000;
- presented a poster at the Harper-Adams University College Open Day. July 13th, 2000;
- attended a training course in the use of Sokkia DGPS equipment and Sokkia Midas GIS software, Steanne Solutions, Manchester. July 20th-21st, 2000;
- delivered the Institute of Electrical Engineers Retired Engineers Lecture. 'Electronics in Agriculture'. Stone, Staffordshire. October 24th, 2000;
- attended the Annual Conference of the NERC Airborne Remote Sensing Facility. BGS Keyworth. Nottingham. December 12th-13th, 2000;
- attended a statistics workshop 'Logistic Regression' by Eleanor Allen of the University of Reading, Harper Adams University College. January 17th, 2001;
- attended the Society of Chemical Industry conference 'In-Field Monitoring of Soil and Crop Factors'. Belgrave Square, London. January 23rd, 2001;

- attended the Association of Applied Biologists 'Offered Papers in Nematology' meeting, Linnean Society. London. December 11th, 2001;

- attended the NERC Equipment Pool for Field Spectroscopy 'Field Spectral Measurements in Remote Sensing' meeting. University of Southampton. April 15th-16th, 2002;

- attended the Society of Chemical Industry conference 'Application of Remote Sensing in Agriculture'. Belgrave Square, London. January 15th, 2002;

- presented a paper at the NERC Airborne Remote Sensing Facility Workshop, Rutherford Appleton Laboratory. December 16th-17th, 2002.

Table of contents page

List of figures

List of tables

page

List of plates

page

1. Introduction

1.1. Potato cyst nematodes (PCN).

Potato cyst nematodes (PCN) *Globodera pallida* (Wollenweber) *and G. rostochiensis* Stone are microscopic (< 1mm) invertebrates that can survive in the soil for many years within a protective cyst (Evans & Stone, 1977). The potato *Solanum tuberosum* is one of the world's most important crops, ranking 4th behind wheat, rice and corn as a food source (Ulrich, 1993; Brodie, 1998). Potato cyst nematodes inflict significant loss on potato crops, with yield losses estimated at 9% of the UK harvest (Evans & Stone, 1977), and are economically important pests in temperate regions of the world (Brodie *et al.*, 1993; Evans, 1993). Potato cyst nematodes have been classified as A2 quarantine pests by the European Union, which prohibits seed-tuber production on infested land (Cotten, 1991; Ward & Hockland, 1996).

1.1.1. Background and history.

Potato cyst nematodes are highly specialised and successful parasites of agricultural crops (Turner & Evans, 1998). Six species of the genus *Globodera* are known to be parasites of the Solanaceae, although only *G. rostochiensis* and *G. pallida* are serious pests of potato crops worldwide (Evans & Stone, 1977).

Solanum species, from which the domesticated potato *S. tuberosum* ssp. tuberosum derives, are native to the mountainous western region of South America, extending into southern areas of North America. Two regions are notable for the diversity of wild *Solanum* plants: Central Mexico and the Andean region between Peru and Argentina, leading to speculation that the *Solanaceae* plant genus originated from those areas (Evans *et al.*, 1975a; Franco *et al.*, 1998). The authors also suggest that the distribution and

speciation of PCN in this region represents a strong indicator for the co-evolution of these obligate parasites with their *Solanaceae* hosts on the Andean plateau.

Although extensively cultivated by Andean Indians prior to the arrival of Spanish explorers in 1531 (Turner & Evans, 1998) the potato was unknown outside of South America before the sixteenth century (Franco *et al.*, 1998). Poorly suited to the long summer days of northern latitudes, early introductions were probably exotic morsels for a wealthy few. Although the potato eventually became widely cultivated, European potato crops of the eighteenth and early nineteenth centuries were largely descended from two introductions of *S. tuberosum* ssp. *andigena* to Spain and England some three hundred years earlier (Turner & Evans, 1998). The resulting narrow genetic base rendered the potato crop vulnerable to a single pathogen and a severe outbreak of potato blight (*Phytophthora infestans*) in 1845 caused widespread loss in the European potato crop and a catastrophic famine in Ireland. These events prompted a renewed interest in the diversity of native South American potatoes.

1.1.2. Distribution and spread.

Turner & Evans (1998) suggest that PCN were introduced to Europe with the many *Solanum* spp. lines imported for the development of blight resistance in the 1850's, citing the chronology of PCN discovery (some 30 years later) as a major indicator for this theory. Franco *et al.* (1998) support the post-potato famine conclusions of Turner & Evans and add that further introduction occurred in the first quarter of the twentieth century as interest in potato varieties grew, although no evidence or further details are supplied in support of this statement. Some transfer of PCN to Europe may also have taken place due to the re-use of potato sacks for the import of guano (Evans *et al.*, 1975a). Brodie & Mai (1989) suggest that a localised outbreak of *G. rostochiensis* was introduced to New York State, USA, in soil adhering to military equipment returning from Europe after the First World War.

While these theories are entirely plausible, evidence on the manner of PCN dissemination remains largely circumstantial.

Regardless of the method of their dissemination however, PCN are indisputably present in most temperate regions where potatoes are grown and constitute a major limiting factor to crop yield and sustainable production in the UK (Evans & Stone, 1977; Evans & Haydock, 2000). Once introduced to a region, PCN can be spread by tillage, harvesting or wind. Soil adhering to farm machinery or seed tubers is a primary method by which PCN are introduced to uninfested areas (Boag, 1985; Haydock & Evans, 1998b).

1.1.3. Pathogenicity.

Potato cyst nematodes are reported by Evans & Haydock (2000) to be the single most important factor limiting potato production in the UK. United Kingdom potato growers incur direct costs of *c.* £8M on nematicides in addition to a loss of revenue from reduced yield. The time and labour required to apply these chemicals and the opportunity cost of dedicated potato machinery left idle during extended rotations must be taken into consideration when the economic impact of PCN is assessed (Haydock & Evans, 1998b).

Potato cyst nematodes invade the roots of developing potato plants, damaging the root structure and reducing the nutrient uptake of the plant (Evans & Stone, 1977). In contrast to root-knot nematodes (*Meloidogyne* spp.) which migrate intracellularly, PCN cut through root cells, causing extensive damage, often destroying cells in their path (Evans & Stone, 1977; Von Mende *et al.*, 1998). Once established, PCN induce the formation of extensive feeding sites from the fusion of many cells (Viglierchio, 1991). The juvenile nematodes remain static and progress through a series of moults, withdrawing nutrients from the plant (Evans & Stone, 1977).

Several theories have been advanced to describe the ways in which PCN reduce growth and yield of potato crops. Invasion of roots by PCN, and subsequent feeding on plant metabolites was suggested by Schans (1991) as a primary cause of reduced growth, while Evans *et al.* (1977) investigated the volume of soil exploited by the roots of infested plants. Whilst concluding that stunted root development can lead to a deficiency in uptake of the nutrient most limiting to growth, they cite another factor, possibly a nematode secretion, as reducing growth in young plants which draw on nutrient reserves from the seed tuber.

In addition to direct pathogenesis, invasion by PCN is implicated in the occurrence and severity of fungal infection in potato crops (Evans, 1987; Back *et al.*, 2002). Endo (1975) lists several instances of fungal and viral transmission by cyst and root-knot nematodes.

1.1.4. Life history.

Potato cyst nematodes remain dormant in the soil for many years (Turner, 1996). Extensive hatching (*c.* 60-80%) occurs only in response to stimulation from root exudates secreted by a host plant (Rawsthorne & Brodie, 1986). Infective juveniles invade the root of a host plant, using repeated thrusts from their sharp stylet to puncture the root cortex. The stylet is similarly used to penetrate cell walls as the nematode migrates intercellularly towards a static feeding site (Evans & Stone, 1977).

Second stage juveniles are vermiform and pass through a series of moults, differentiating into male and female at juvenile stage three (Fig. 1.1.). Multiplication is dependent on the initial population density, as not all juveniles find a vacant root space and more are diverted to smaller, less suitable lateral roots. Here, a greater proportion become male due to limited resources (Evans & Stone, 1977; Phillips & Trudgill, 1998). Females become saccate and expand to protrude through the root cortex.

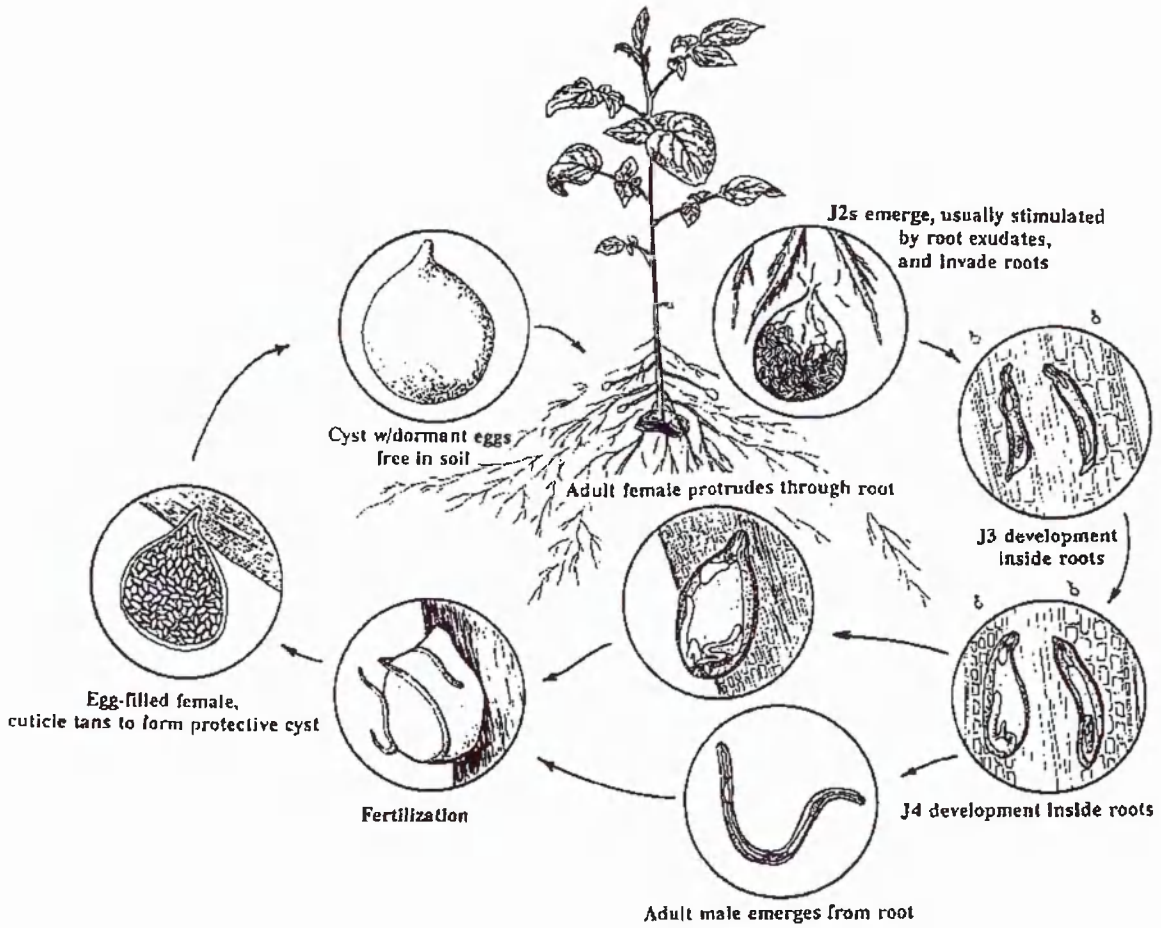

Figure 1.1. Potato cyst nematode lifecycle (source Brodie *et al.*, 1993).

The swollen females are fertilised by vermiform adult males before expiring and discharging into the soil as cysts (Evans & Stone, 1977). These can contain up to 400 eggs (Brodie *et al.*, 1993) and may remain viable for up to fifteen years in soil (Whitehead, 1986).

A proportion of the embryonated juveniles will die or hatch spontaneously in the absence of a host crop, leading to a natural decline of *c.* 20-30% per annum (Jones, 1970). This figure can vary and Turner (1996) has reported an annual decline of less than ten percent.

1.1.5. Management.

Phytosanitary measures to prevent cysts spreading to uninfested areas are an obvious first step in PCN management strategy. Low initial populations of PCN can multiply by up to seventy-fold in one season (Evans & Trudgill, 1992) and population decline alone is seldom sufficient to keep populations in check. Effective measures to control PCN infestation are essential where an infestation is already present, and may be necessary to restrict population growth and maintain the long-term viability of production land. However, measures such as the application of granular nematicides at low initial population densities may not result in an economic return for the current crop (Haydock & Evans, 1998a; Evans & Haydock, 2000).

Extended rotations, incorporation of chemical nematostats and the planting of resistant cultivars are accepted methods of PCN control (Whitehead, 1986; Evans & Haydock, 2000), although they are seldom sufficient if used in isolation. Integrated management strategies combine these methods according to the infestation levels and species present (Fleming *et al.*, 1998). Granular nematostats are more effective at protecting the crop from root damage than at reducing population levels and decline rates during extended rotations are variable (Evans & Haydock, 2000). The repeated use of partially-resistant cultivars can select for virulence (Turner, 1990) and problem fields (high populations, slow decline) may require the application of fumigant biocides before the land can be profitably returned to potato production.

The repeated application of granular nematicides can result in substantially reduced persistence of the active compounds (Smelt *et al.*, 1987), as might elevated soil temperature, moisture and pH (Ambrose *et al.*, 2000). Although the high cost of fumigant biocides presents a substantial disincentive to their repeated application, there is some

indication that this 'method of last resort' is likely to suffer reduced efficacy when used repeatedly (Ou *et al.*, 1995).

As an introduced organism, PCN have few natural predators in potato growing regions outside of South America (Phillips & Trudgill, 1998). Some predation by birds is possible; Franco *et al.* (1998) mention the limited survival of cysts ingested by birds. Several fungal organisms are known to be parasites of PCN cysts. Attempts to culture fungi as biological control agents, however, have shown limited success (Brodie *et al.*, 1993; Crump, 1998; Davies, 1998).

1.1.6. The *G. pallida* problem.

Globodera pallida and *G. rostochiensis* are similar in both appearance and physiology and were first distinguished by Stone (1972). The former presents a considerably greater challenge to agronomists, researchers and growers. *Globodera pallida* is replacing *G. rostochiensis* in many fields, is less susceptible to control measures, and remains viable for longer than *G. rostochiensis* (Evans, 1993; Whitehead & Turner, 1998). With no available potato cultivar having full resistance to *G. pallida,* (Evans, 1993; Phillips & Trudgill, 1998) repeated use of partially resistant cultivars will promote the selection of increasingly virulent populations (Whitehead, 1986; Turner, 1990).

Globodera pallida quickly replaces *G. rostochiensis* when cultivars with full resistance to *G. rostochiensis* are grown (Evans & Stone, 1977) and preferential selection of *G. pallida* continues to compound an already serious problem. Despite the adoption of integrated control management, including an annual expenditure on nematicides of *c.* £8 million, *G. pallida* populations have increased in number and severity over the last 25 years (Evans & Haydock, 2000; Minnis *et al.,* 2002). The widespread adoption of cultivars resistant to *G.*

rostochiensis has led to the predominance of *G. pallida,* which is now present in 92% of infested sites (Minnis *et al.*, 2002).

The two most widely-used methods for controlling PCN populations, granular nematicides and extended rotations, are less effective against *G. pallida.* An extended hatching period adds to the difficulty of controlling *G. pallida* with granular nematicides, which frequently degrade below an effective concentration before the peak of *G. pallida* hatching takes place (Evans, 1993; Ambrose *et al.*, 2000). Longer rotations are required as *G. pallida* decline at a slower rate. In the absence of a host crop, *G. pallida* can persist at yield-reducing levels for up to eight years longer than *G. rostochiensis* (Evans, 1993).

1.1.7. Within-field distribution.

Cyst nematodes are virtually immobile (Been & Schomaker, 1995), with only hatched juveniles having a motile range of *c.* one metre, and remain close to their point of gestation unless transported by external forces. Introduced cysts multiply on subsequent host crop rotations and develop into discrete foci (Southey, 1974; Boag *et al.*, 2000), leading to an aggregated distribution within the cultivated area (Southey, 1974). Particular care is therefore required to detect a recent and localised infestation.

Nematode density within developing foci has been described as resembling a negative binomial distribution (Seinhorst, 1982; Schomaker & Been, 1992), while Boag & Topham (1984) applied Taylor's Power Law to species-specific (non cyst) nematode population aggregation. Been & Schomaker (1995), however, pointedly note that the similarity of a distribution function with empirical results is insufficient reason to accept it as a general model.

1.1.8. Population density estimation.

Both small and persistent, PCN cysts form a tiny fraction of the soil mass that they inhabit and detecting, quantifying and identifying populations is laborious (Boag & Neilson, 1994). The practical detection threshold (for statutory sampling) of one cyst per 500g soil sample represents a probable field population of two million cysts per hectare (Trudgill *et al.*, 1987). Advisory samples collected from production land generally use a 200g sub-sample, inevitably leading to a further increase in the detection threshold.

There are two methods of sampling for PCN which have been recognised by the European and Mediterranean Plant Protection Organisation (EPPO): collecting samples of soil for the extraction of cysts, or by lifting plants and examining their roots for juveniles or cysts (Haydock & Perry, 1998). The former method is most commonly adopted (Southey, 1974).

1.1.8.1. Sampling strategies.

The spatial heterogeneity and aggregated distribution of cyst nematode populations require that sampling, whether from soil or roots, must be carried out in a systematic and thorough manner. It is self-evident that any sampling scheme which ignores large areas of the field will be less reliable at detecting PCN than a more comprehensive method. The collection and processing of multiple soil samples, however, is labour-intensive and expensive and some attempts have been made to automate the collection of soil samples.

One device used suction to collect cysts (Anon. 1972). Wire combs disturbed the soil surface as a low-suction vacuum device drew cysts and other light material into a collection bag. This approach has the advantage of covering a large area of the field quickly, and with little effort. The resulting sample was said to be concentrated with heavier soil particles left behind. However, the force required to lift cysts from the

surrounding soil matrix will depend heavily on the soil type and moisture content - compare the binding nature of a wet, clay soil to that of a dry, sandy loam. It would appear unlikely, therefore, that this method can produce comparable results across a range of soil types and moisture levels.

Cooke *et al.* (1979) describe an automatic soil sample collector mounted on a lightweight all-terrain vehicle. This device was able to collect samples rapidly across a wide area, although only on cultivated soil. Samples appear to have been collected from close to the surface, where heat from the Californian sun might reduce the viability of cyst nematodes and, although Boag & Neilson (1994) consider cyst nematodes to be randomly distributed throughout the plough layer (*c.* 20cm), a shallow sampling method might need to allow for mechanical damage, the harsher environment and possible bird predation of cysts close to the soil surface.

The United States Department of Agriculture developed a wheel sampler, described by Brodie *et al.* (1993). This consisted of one or more wheels, fitted with hollow probes and mounted behind a tractor. Sampling intensity could be varied with the number and spacing of the wheels. Although not specified, the sampling depth is unlikely to have been greater than 2-3cm and might be expected to vary with soil conditions.

All such devices collect bulk samples which cannot convey information on nematode distribution within the area sampled, and care must be taken to ensure that the machinery is cleared of all soil before sampling subsequent sub-field survey blocks.

1.1.8.2. Current detection methods.

Soil samples (in Europe) are collected with a hollow probe, or auger (Southey, 1974). Turner (1993) evaluated the performance of three types of auger, rejecting a fourth as

unsuitable for local conditions. Her results show that 120 samples collected with a small (3ml) auger detected PCN in 68% of the 87 fields sampled while 30-36 cores from augers of 10-12ml capacity detected PCN in 64%, showing little advantage from the more labour-intensive method.

1.1.8.3. Sampling patterns.

Several studies have compared the detection efficiency of spatial patterns and sample intensity for the detection and quantification of cyst nematodes. The metric of efficiency being generally taken as a percentage of the mean of all methods. Church *et al.* (1959) suggested that sample cores should be taken from 50 points from a field of up to 4 ha, collecting a bulk sample of at least 1kg, but preferably 2.5 kg. Two hundred grams of soil is then taken from each bulk sample for analysis. Accuracy improved with the number of sample points, as did the time and effort required. Turner (1993) also identified a positive relationship between core numbers and detection efficiency, but found no significant advantage in taking more than 36 cores per two hectare sample area. As mentioned previously, the heterogeneity of infestation is critical to the success or failure of a sampling regime and Turner's results may not be transferable to other infestation conditions. Turner also compared the percentage of cysts detected when using different sampling patterns. Her conclusion that the patterns tested are equally capable of detecting PCN is difficult to reconcile with her reported results where, at low PCN levels, a perimeter pattern detected only three-quarters of the cysts found when using a zig-zag design. Evans *et al.* (2000) report that a perimeter design performed poorly and was less consistent that the other methods tested. A perimeter sampling pattern may have some validity for the detection of recently-introduced infestations carried on farm machinery and therefore likely to be located close to field access points (Boag & Neilson, 1994). However, perimeter sampling covers only a small proportion of the field area and infestations introduced by other means, e.g. contaminated seed or cysts carried in slurry, may escape detection.

The sampling methods investigated by Turner (1993) did not include a regular, grid-based sample design and Church *et al.* (1959) found sampling at points on a regular grid to significantly reduce sampling errors. Schomaker & Been (1992) also recommend the use of a grid-based sampling strategy. When simulating various sampling patterns and orientations from a large number of existing 200g point samples, Evans *et al.* (2000) found a regular grid-based sampling scheme to be the most consistent method. They were, however, able to report higher detection from both 'X' and 'W' path sampling strategies than from their grid-based simulation.

When compared to a regular grid pattern, both 'X' and 'W' sampling patterns will concentrate sampling points near to the intersection of the sampling lines whilst ignoring large areas of the field where the lines diverge. A logical explanation for the superiority of these sampling patterns is therefore difficult to envisage, particularly as the reported variation with pattern orientation points to an element of chance inherent in irregular sampling patterns. The sampling patterns investigated by Evans *et al.* (2000) were tested on a single field, which was also sampled as halves and quarters. The relatively high and even infestation of the quarter-field areas (50-83 eggs g^{-1}) indicate that this was an established population which had been distributed throughout the field over a number of years. The relative merit of each sample pattern tested might well be very different when assessing a field with recent and localised infestation foci.

Of seven examples from international statutory sampling practice quoted by Haydock & Perry (1998), five countries used a grid pattern, one used either grid or 'W' patterns and the seventh used a 'W' design. The bulk of advisory practice was listed as using the 'W' approach, which offers a shorter path than grid schemes for the same number of sample points. An important consideration when comparing sampling patterns is the maturity of

the PCN infestation: recently introduced populations exhibiting greater heterogeneity than those which have spread through cultivation over a number of rotations (Evans *et al.*, 1998; Riding *et al.*, 2000). An element of chance is inherent in any sub-sampling strategy and this is amplified by low or patchy infestation, with all methods approaching a common mean as PCN distribution spreads across the field. All but the most homogeneous fields would require multiple replication before an accurate comparison between sampling strategies can be made.

Wood *et al.* (1983) compared the New Zealand practice of inspecting plant roots for visible cysts with UK and Dutch soil-sampling methods for the detection of low levels of PCN infestation. Although the authors concluded that inspecting live roots in the field was 80-120 times more likely to detect foci than soil sampling, their method has limited application to advisory PCN survey. Field inspection of roots from the growing crop must be carefully timed to allow the cysts to emerge from the root and before they detach into the soil. The timing of hatch, motility and invasion by PCN is influenced by the species present (Robinson *et al.*, 1987a; Webley & Jones, 1981), accumulated temperature (Magnusson, 1986) and soil moisture and soil type (Robinson *et al.*, 1987b). A history of early cropping can also select for a faster-hatching population (Hominick, 1982), making accurate timing of root inspection subject to considerable uncertainty.

The visual inspection of the roots from 150-170 plants per hectare may be practicable (if time-consuming) in dry, sandy soil, but would present a daunting prospect in a field of wet clay, where the roots must be cleaned sufficiently to enable cysts to be seen (Cotten, 1991). The number of plants that can be sampled from a field crop will be subject to constraints of time and expense, and the problem of aggregation when selecting a very small proportion of the crop for analysis must surely outweigh any additional accuracy that the method has to offer.

1.1.8.4. Laboratory processing.

1.1.8.4.1. Soil samples.

Bulk soil samples from the field are dried, crushed and passed through a sieve of 4mm to remove stones (Shepherd, 1986). Samples are then thoroughly mixed before removing a sub-sample for analysis. Church *et al.*(1959) recommend that a minimum of 200g dry soil be examined.

A variety of methods are employed to extract cysts from the dried soil sample, with the most common being flotation in a Fenwick can. The Fenwick can is a tapering container, filled with water, and having a sloping collar attached to the neck. Soil samples are washed into the Fenwick can by a constant flow of water whereupon cysts and other buoyant material are carried over the collar and into collecting sieves (Shepherd, 1986). The 'float' is collected in a wrap of fine-meshed material and dried, before being loaded onto an examination plate where the cysts are counted and a subset selected as representative of the remaining cysts (Turner, 1998). The sub-sample of cysts (usually 50) are soaked in water for 24 hours before being crushed between an aluminium slide with a 0.5mm depression and a glass cover. The eggs released by crushing are washed into a 50ml solution and, after thorough mixing, one ml is removed and placed in a counting slide under a microscope. The final count is expressed as eggs per gram of (dry) soil. No account is taken of variation in soil density, and some interpretation is required to assess the number of juveniles present within migratory range of the root mass.

1.1.8.4.2. Root invasion.

While Wood *et al.* (1983) describe the New Zealand method of inspecting roots from plants in the field, UK practice is to harvest the entire plant, wash and separate the roots, then select a two gram sub-sample from the total root mass for laboratory analysis (Hooper, 1986). The root sub-sample is stained and macerated to release the nematodes and form a 200ml solution. One percent of the macerated root solution is withdrawn for counting under a microscope and errors are kept to a minimum by thorough mixing of both the root sample and the macerated suspension.

A simple count of the total number of juveniles per unit of root fails to take into account the amount of nutrition that the nematode has withdrawn from the plant. The method also lacks a factor to account for the amount of physical disruption to the root structure and metabolic pathways caused by differences due to the various juvenile stages or gender. Males do not feed after juvenile stage three and are thought to require less than one hundredth of the amount of food needed by a female (Evans & Stone, 1977). A recently-invading juvenile will have developed a limited syncytium and mechanical damage to the root will be confined to the entry location and migration pathway. Under current procedures, however, this juvenile will be accorded equal significance to a mature (juvenile stage 5) female which will have developed a much larger syncytium, potentially blocking multiple segments of the root (Jones, 1970) and have expanded to burst through the outer cortex of the root (Endo, 1987).

1.2. Effects of PCN on plant and canopy.

Inspecting the growing crop for signs of poor growth ('field walking') is a long-established and traditional procedure for the detection of disease or pathogens, and may give an indication of nematode infestation once populations have reached yield-reducing levels. An example of a less subjective approach is that of Evans (1987) who studied foliage

symptoms of potato plants infected with PCN and the fungal pathogen *Veticillium dahliae.* His 'early dying' scores may, however, relate more to the fungal disease than to the population density of PCN, although considerable interaction is evident in his results from *c.* eight weeks after planting. However, Southey (1974) concluded that the inspection of the potato canopy was unsuitable for the detection of PCN as symptoms of infestation varied between soil types and with environmental factors. Brown (1969) noted that substantial yield-loss could occur before symptoms of PCN infestation became apparent in the haulm. Dale & Brown (1989), however, were able to assess nematode damage of potato by inspection of the foliage and reported significant correlation between foliage scores and yield loss due to PCN. Sabins (1996) notes that symptoms of plant stress can be recorded by light-sensitive instruments (i.e. a spectrometer) before they become visible to the human eye, and the analysis of light reflected from the crop canopy has been used in many crop-monitoring experiments (e.g. Al-Abbas *et al.*, 1974; Bacci *et al.*, 1991; Bauer, 1986; Blazquez & Edwards, 1986).

The canopy of a potato crop represents the only significant plant element available to a remote sensing spectrometer and the delelopment of a spectral assay to detect PCN is predicated on the hypothesis that nematode infestation produces a measurable change in leaf reflectance. Some consideration is warranted, therefore, to the possible mechanisms by which PCN infestation might induce measurable change in the potato crop canopy and the light reflected from it.

1.2.1. Canopy geometry and development.

Haverkort & Trudgill (1995) suggest that PCN cause morphological changes which inhibit leaf expansion and that plant resources are directed away from canopy development. They reported that potato plants infested with PCN had fewer and shorter stems with smaller and thicker leaves. Infestation by PCN caused the percentage of haulm dry matter to increase,

leading Fatemy & Evans (1986) to postulate that infested plants have smaller cells and a greater ratio of cell-wall material to cell content than uninfested plants. Gausman *et al.* (1975) also reported that the leaves of cotton (*Gossypium hirsutum*) infested by the nematode *Rotylenchulus reniformis* were smaller, darker and had a more compact mesophyll than uninfested plants. They, unlike Fatemy & Evans (1986), did not observe a significant change in leaf thickness from infested plants.

Lauer *et al.* (1989) found the leaves of soybean (*Glycine max*) to be diaheliotropic – orientating their adaxial surface toward the sun and tracking the solar position throughout the day. Conversely, leaves of plants deficient in inorganic phosphate turned away from the sun at times of peak solar radiation, placing the leaf parallel to the sun's rays. The authors suggest that P-deficient plants are unable to process all of the intercepted energy and so avoid direct sunlight. This would indicate that plants are not able to regulate the absorption of light internally, and that absorption of incident light is undiminished by P-deficiency. No reports linking this phenomenon to the potato were found in the literature.

1.2.2. Leaf composition of infested plants.

Fatemy *et al.* (1985) measured elevated levels of abscisic acid (ABA) in the leaves of Pentland Dell (+28%) and Cara (+14%) plants infested with 250 eggs g^{-1} of *G. rostochiensis.* Cara is both resistant and tolerant to *G. rostochiensis,* whereas Pentland Dell is neither. This was, however, a pot experiment and the Cara plants, with their extensive rooting habit (Evans & Haydock, 1990), may have become root-bound in the 1000g soil of the containers. Exogenously applied ABA reduced the growth and water consumption of both cultivars. Stomatal resistance was increased, causing a reduction in transpiration, although this effect lasted only two and six days from the time of application.

Van Staden & Dimalla (1977) found that infestation by *Meloidogyne incognita* (root-knot nematode) increased the level of cytokinin in the roots of tomato plants (*Lycopersicon esculentum*). Tomato plants susceptible to *M. incognita* had higher levels of cytokinins in their roots when compared with a resistant variety. Plants with elevated cytokinin levels were invaded by a greater number of nematodes.

Cytokinins are plentiful in young leaves and enhance cell division and expansion, leading to the development of larger cells (Salisbury & Ross, 1992). The ratio of cytokinin to auxin also regulates the production of roots and shoots (Raven *et al.*, 1998). Changes in the translocation or abundance of cytokinins may provide a potential link between nematode damage and the reduction in the shoot-root ratio of PCN-infested plants reported by Haverkort & Trudgill (1995) and a substantial decrease in the ratio of lateral to main roots found by Evans *et al.* (1977).

1.2.3. Nutrient uptake and mineral balance.

Potato cyst nematodes exert a clear influence on the nutrient uptake of potato plants (Evans & Haydock, 1990) and both potassium and phosphorus concentration is reduced in the haulm of potato plants infested by PCN. Significant changes in the chemical composition of a potato canopy were related to PCN infestation by Trudgill *et al.* (1975b). Their findings indicated that infestation decreased the concentration of phosphorus (P) and potassium (K) in the leaves while, at the same time, increasing plant calcium and sodium uptake. Nitrogen (N) concentration of haulm dry matter was not affected. Evans *et al.* (1977) found the uptake of inorganic nutrients was inhibited by PCN infestation and concluded that growth and yield of infested plants is restrained by whichever nutrient is limiting at the time.

Trudgill (1980) investigated the effects of infestation by *G. rostochiensis* on the haulm nutrient content of potato cv. Pentland Crown. Concentrations of N, P and K were reduced in haulm dry matter. Nitrogen and phosphorus were thought more likely to be limiting than potassium, which did not fall to a level of deficiency. Experiments with an enhanced supply of each nutrient indicated that PCN reduced the ability of potato plants to take up additional potassium from the soil.

Grove *et al.* (1999) observed that the leaves of PCN-infested plants were darker in colour, and suggested that this might be due to a deficiency in phosphorus. They noted that high soil pH reduced P availability and associated reduced yield with lower P uptake by infested plants. Ulrich (1993) states that potato plants deficient in P are stunted and of darker green colour than non-deficient plants.

De Ruijter & Haverkort (1999) suggest that P deficiency due to PCN infestation appears to have been limiting to plant development. This reduction was exacerbated by a lower P availability at pH 6.1 (vs. pH 4.8) which agrees with Grove *et al.* (1999). Foliar N, P and K concentrations were reduced by nematodes at 61 DAP, although only P concentration was correlated with reduced biomass. The authors dismiss a possible effect from fumigation and irradiation of the soil from control replicates, despite noting that these treatments may have killed other soil organisms which interact with the plants. Whitehead *et al.* (1994) report that application of the fumigant biocide Telone™ increased yield by a greater margin than might have been expected from a reduction in the PCN population. Nitrogen availability may be responsible for the unexpected increase in biomass as Minnis (2000) concluded that soil fumigation can result in elevated levels of nitrogen becoming available to subsequent crops.

Been & Schomaker (1986) found that concentrations of N, P and K in the haulm of potato cv. Irene were reduced by increasing infestation by *G. pallida*. This reduction only became apparent, however, when comparing plants with a similar total haulm weight, which may have been due to differences in plant age if the growth of infested plants was retarded.

Viglierchio (1987) found reduced levels of P and K in leaves of tomato plants (*Lycopersicon esculentum*) heavily infected with *Meloidogyne hapla, M. incognita* and *M. javanica*. Potassium concentration in leaves of sugar beet (*Beta vulgaris*) were greatly reduced by *M. hapla, M. incognita* and *M. javanica* and halved by infestation with the beet-cyst nematode *Heterodera schachtii*. These results were, however, presented as relative to leaf calcium (Ca) content and due to the marked rise in Ca linked to nematode infestation (Trudgill *et al.* 1975b; Evans, 1982; Fatemy & Evans, 1986) it is not clear whether calcium content increased or P and K reduced in response to nematode infestation.

Grove *et al.* (1999) reported that N, P and K concentrations were reduced at 58 DAP in potato cv. Santé infested with a mixed population of *G. rostochiensis* and *G. pallida*. Their measurements were, however, taken from whole plant dry matter and a reduction in the haulm content may be partially offset by the accumulation of N, P and K in roots as reported by Trudgill *et al.* (1975a).

The comparison of studies on different nematode species must be approached with caution as invasion, migration and feeding methods vary widely (Endo, 1975; Jones, 1981). Trudgill *et al.* (1975a) reviewed previous papers on the translocation of nutrients and minerals to and from the canopy. Studies on *Meloidogyne incognita* and *Pratylenchus penetrans* showed little or no change in leaf concentrations of K, Na, P and N. *Meloidogyne javanica* and *P. vulnus* (walnut, roses) reduced K transport to the haulm.

Jenkins & Malek (1966) found considerable differences in the amount of nutrients in roots and haulm of vetch from infestation by one endoparasitic species (*M. hapla*) and three ectoparasitic nematodes while Hunter (1958) found no difference in the concentration of P, N, Ca and Mg in the leaves of tomato plants infected with *M. incognita.*

Grove *et al.* (1999) were unable to determine which nutrient or nutrients were limiting to PCN-infested potato plants from a review of the literature, whilst Been and Schomaker (1986) noted that previous studies on the influence of nematodes on mineral transport to the top of plants were not directly comparable. Different methods had been used to determine nematode densities, and metrics were sometimes vague, e.g. 'high' or 'low' populations. Sampling had not been sufficiently frequent to describe the considerable change in mineral content during the growing period. Perhaps the most significant implication of this paper is that, quite possibly, many of the changes in mineral concentration found by earlier studies are the result of nematode-induced delayed maturity of the plant and therefore have a once-removed correlation with PCN infestation.

Nutrients and minerals are present in the haulm at very low concentrations, usually less than one percent of dry matter (Ulrich, 1993) and it appears unlikely that changes in the concentrations of these elements can be detected directly. The investigation must, therefore, concentrate on the symptoms of mineral and nutrient deficiency (or excess) as they affect the structure, colour and geometry of the plant canopy.

1.2.4. Turgor.

Plant-parasitic nematodes are known to alter stomatal conductance, transpiration and leaf water potential in infested plants (Fatemy & Evans, 1986; Schans, 1991; Verma *et al.*, 1993). Water affects every aspect of plant development and vigour and forms *c.* 50% by volume of cell-wall material and *c.* 95% of the protoplasm (Slatyer, 1967). The balance

between water uptake and transpiration to the atmosphere will determine the amount of water contained in the leaf. Turgor affects cell expansion, and desiccation is known to increase near-infrared reflectance from the leaf as cells shrink away from each other (Wooley, 1971).

1.2.5. Water uptake.

Much has been written about PCN-induced water stress. The potato is a comparatively shallow-rooted (*c.* 40-50cm) plant (Brodie *et al.*, 1993) and the greater rooting habit of some cultivars has been cited as a possible tolerance mechanism to PCN damage (Evans & Haydock, 1990). Evans *et al.* (1977) report that infested plants had reduced root formation, with lateral root development most affected. The roots of infested plants exploited a smaller volume of soil and did not penetrate as deeply as roots from uninfested controls, which were able to access water reserves from lower soil levels in a dry period.

Fatemy & Evans (1986) report that water uptake per g (fresh root) declined markedly (from 6.1g to 1.7g /day) in Arran Banner infested with *G. pallida* at 0, 10, 50 and 250 eggs g^{-1} soil, possibly because multiple PCN invasion can block all segments of a root, substantially impeding longitudinal water movement (Jones, 1981). A reduction in the shoot-to-root ratio of PCN-infested plants (Haverkort & Trudgill, 1995) would, however, indicate that the plant canopy is affected to a greater degree than the roots, resulting in a reduction in plant water requirements per gram of root.

1.2.6. Water use efficiency.

Fatemy & Evans (1986) found an increase in water use efficiency (WUE), reported as transpiration ratio (= water used per unit dry matter produced) to be confined to a period similar to that of nematode invasion and development (*c.* 45 days) for a late-maturing cultivar (Arran Banner). They suggest that cultivars with later maturity may be able to maintain growth beyond the stage of peak nematode-induced damage. Schans (1991) also

reported increased WUE, although this was contradicted by Schans & Arntzen (1991) who found WUE of four cultivars to be reduced at 30 and 49 DAP, although not at 60 DAP.

1.2.7. Stomatal regulation and cation-ion balance.

Leaves of plants infested with nematodes release less water to the atmosphere due to closure of their stomata (Schans & Arntzen, 1991). Evans *et al.* (1975b) considered that PCN-induced stomatal closure might be a drought response due to lower leaf water potential, although Schans (1991) found no reduction in leaf water content of infested potato plants. Epstein & Grant (1973) recorded a poor correlation between relative water content of leaves (RWC) and leaf diffusive resistance of potato cultivars Katahdin and Russet Burbank, and were unable to relate stomatal opening to RWC. Evans *et al.* (1975b) found stomatal resistance to be greater in the leaves of Pentland Dell plants heavily infested with PCN, while lightly infested plants maintained a low stomatal resistance, including the duration of a dry period.

Wilcox-Lee & Loria (1987) reviewed studies of nematode effects on transpiration and stomatal conductance, including several papers on PCN. Transpiration was generally reduced as was the transpiration ratio (section 1.2.6). However, the authors note that the transpiration ratio increased with time and that the experiments were conducted for differing durations, and with variable PCN population densities.

Potassium is known to directly regulate stomatal opening by the translocation of K+ ions into and out of guard cells (Fisher, 1968; Salisbury & Ross, 1992). Although young potato plants can obtain sufficient potassium from the seed tuber, older plants which draw potassium from the soil become deficient when infested with cyst nematodes (Trudgill *et al.*, 1975a). Evans *et al.* (1977) noted a reduced uptake of inorganic nutrients by infested plants. This was particularly the case for potassium: the K concentration was more than

halved at eleven weeks from planting (cv. Pentland Dell, Pi 142 eggs g^{-1} soil of *G. rostochiensis*). In addition to functioning as a stomatal regulator, potassium activates enzymes required for photosynthesis and transpiration (Salisbury & Ross, 1992).

Increased calcium (Ca) uptake by infested plants, as reported by Trudgill *et al.* (1975b), is a further potential link mechanism between nematode infestation and reduced transpiration. Fisher (1968) reported that the replacement of potassium with calcium completely inhibited stomatal opening and Willmer & Mansfield (1969) note that an addition of $CaCl_2$ negated stomatal opening induced by KCl. Trudgill *et al.* (1975b) report a near-doubling of sodium (Na) content from the haulm of heavily-infested Pentland Dell potato plants when compared with plants having the lowest infestation. Willmer & Mansfield (1969) found that the addition of Na stimulated stomatal opening more than KCl, although whether this effect was also negated by calcium is not stated. The accumulation of abscisic acid in the leaves of infested potato plants noted by Fatemy *et al.* (1985) also induces plants to close their stomata and therefore transpire less water into the atmosphere.

1.2.8. Photosynthesis.

A consequence of nematode-induced stomatal closure is reduced photosynthetic activity. Plants must open their stomata to perform photosynthesis (Blankenship, 2002) and disruption of stomatal regulation will have a negative effect on plant growth in addition to any direct pathogenesis of mechanical damage or nutrient withdrawal by PCN in the roots.

That *G. pallida* directly inhibits stomatal opening was confirmed by Schans (1991), who compared the stomatal conductance of infested and uninfested plants at increased CO_2 levels and in darkness. Transpiration in darkness of cv. Darwina was reduced at three days after inoculation with hatched second-stage juveniles (J2's). Schans & Arntzen (1991)

report that *G. pallida* inhibited photosynthesis to a greater extent than could be explained by the reduction of transpiration, and suggest that a second, possibly biochemical, factor was responsible for the disparity. Franco (1980) noted that total photosynthesis was reduced in three potato cultivars inoculated with *G. rostochiensis* at 0, 160 and 800 eggs g^{-1} soil. The photosynthetic rate per unit area of leaf varied, however, with susceptible cultivars (Maris Peer and Pentland Dell) exhibiting an initial increase in response to 'moderate' infestation (160 eggs g^{-1} soil), whilst the resistant (to *Globodera rostochiensis*), variety Maris Piper had a reduced photosynthetic rate at moderate and high infestation levels.

1.2.9. Leaf colour.

Photosynthetic pigments absorb up to 85% of visible light incident upon a leaf (Carter, 1993) and a reduction in photosynthetic activity would seem to imply that reflectance of visible light must increase as absorption by photosynthetic molecules is reduced. The opposite effect of nematode infestation on leaf reflectance was reported by Gausman *et al.* (1978) and Grove *et al.* (1999). Gausman *et al.* describe an increased chlorophyll concentration per unit leaf area for infected plants. Grove *et al.* noted that leaves of infested plants appeared darker than the leaves of uninfested plants.

Leaves appear darker because they are absorbing more of the incident light and, under constant irradiance, more energy is being intercepted by the photosynthetic molecules. Photosynthetic activity is reduced however; Wallace (1987) surmises that nematode infestation inhibits the calvin cycle whereby energy from light is transformed into chemical forms. Surplus energy must be dissipated quickly to avoid damaging photo-oxidation of the chlorophylls (Gates *et al.*, 1965) and energy is lost mostly by heat and some fluorescence (Hodáňová, 1985). Lili *et al.* (1991) show photographic (infrared) evidence of elevated canopy temperature for winter wheat (cv. Arminda) infested with *Heterodera*

avenae. The mean temperature difference between lightly and heavily infested plots was *c.* 2° C.

The inference gained from these findings is that the leaves of nematode-infested plants continue to absorb visible light, and may increase the percentage of incident radiation intercepted. Surplus energy is then dissipated as heat or fluorescence, while the suspension of diaheliotropic movement by soybean leaves (section 1.2.1) noted by Lauer *et al.* (1989) may form another, more sophisticated response to excess energy. A general orientation of leaves away from the solar position would reduce the amount of light incident upon the leaf and, therefore, the amount of light reflected: the leaf then appears darker to a human eye or a spectrometer.

1.3. Light.

Passive remote sensing measures the amount and distribution of energy derived from an external source. Solar radiation is by far the greatest source of energy to the earth and its atmosphere (O'Hare & Sweeney, 1986).

Light becomes visible directly from the source (sun, light bulb) and/or when reflected from surrounding objects. This 'visible' light is just one manifestation of a pervasive energy form called electromagnetic radiation (EMR). All objects at a temperature above 0° Kelvin (-273°C) emit EMR, a sinusoidal waveform of alternating electrical and magnetic polarity (Fig. 1.3.1.) which can be detected by its interaction with matter (Sabins, 1996). Although an electromagnetic waveform, the interaction of EMR with matter is more consistent with particle theory (Curran, 1985) and EMR is often considered as a stream of particles called photons (Lillesand & Kiefer, 1993; Sabins, 1996; Mather, 1999).

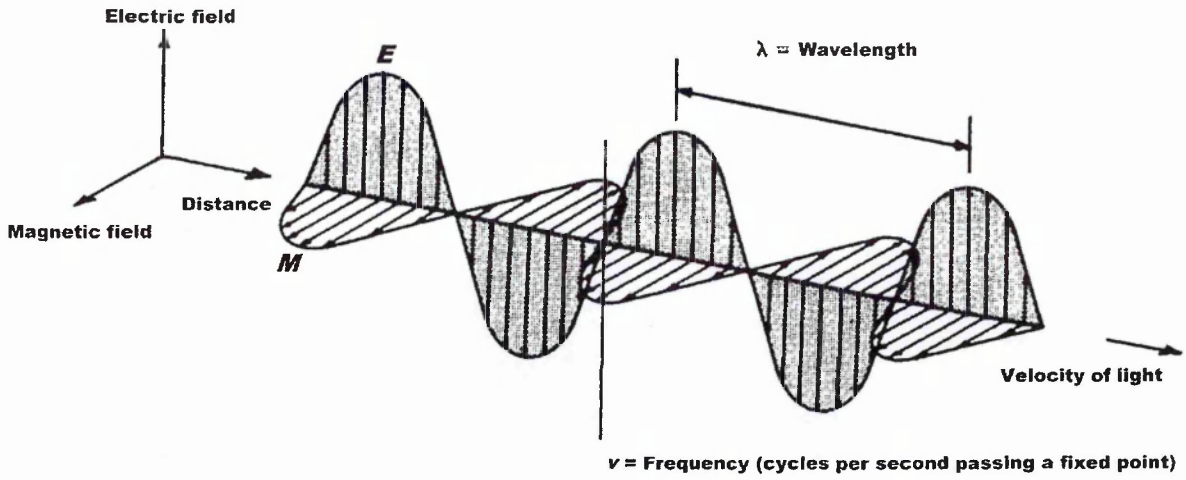

Figure 1.3.1. Electromagnetic waveform (after Lillesand & Kiefer, 1993).

Frequency (*hertz*, the number of electrical and magnetic charge reversals sec^{-1}) of EMR increases with the temperature of the emitting object (Lo, 1985; Lillesand & Kiefer, 1993). The wavelength of EMR is calculated as the distance between two identical positions (e.g. peaks) on subsequent waveforms and is a function of both speed and frequency. Electromagnetic radiation travels at the speed of light (*c.* $3 \times 10^8 m\ sec^{-1}$) and wavelength is inversely related to frequency. The unit of wavelength measurement is the metre although the nanometer (nm, 1×10^{-9} m) is frequently used due to the extremely short wavelengths in some regions of the solar spectrum (Sabins, 1996). Some publications use the micron (μm, 1×10^{-6}m), particularly when discussing longer waveband regions (e.g. thermal or radar EMR). Solar radiation, with a peak intensity (dominant wavelength) at *c.* 470nm (prior to atmospheric attenuation) equates to the energy emitted from an object at *c.* 5,900°K (Mather, 1999), and covers a wide range of frequencies and wavebands. Diagrammatic representation of the solar spectrum (Fig. 1.3.2.) is often presented in logarithmic form due to the several orders of magnitude covered by solar radiation (Lillesand & Kiefer, 1993).

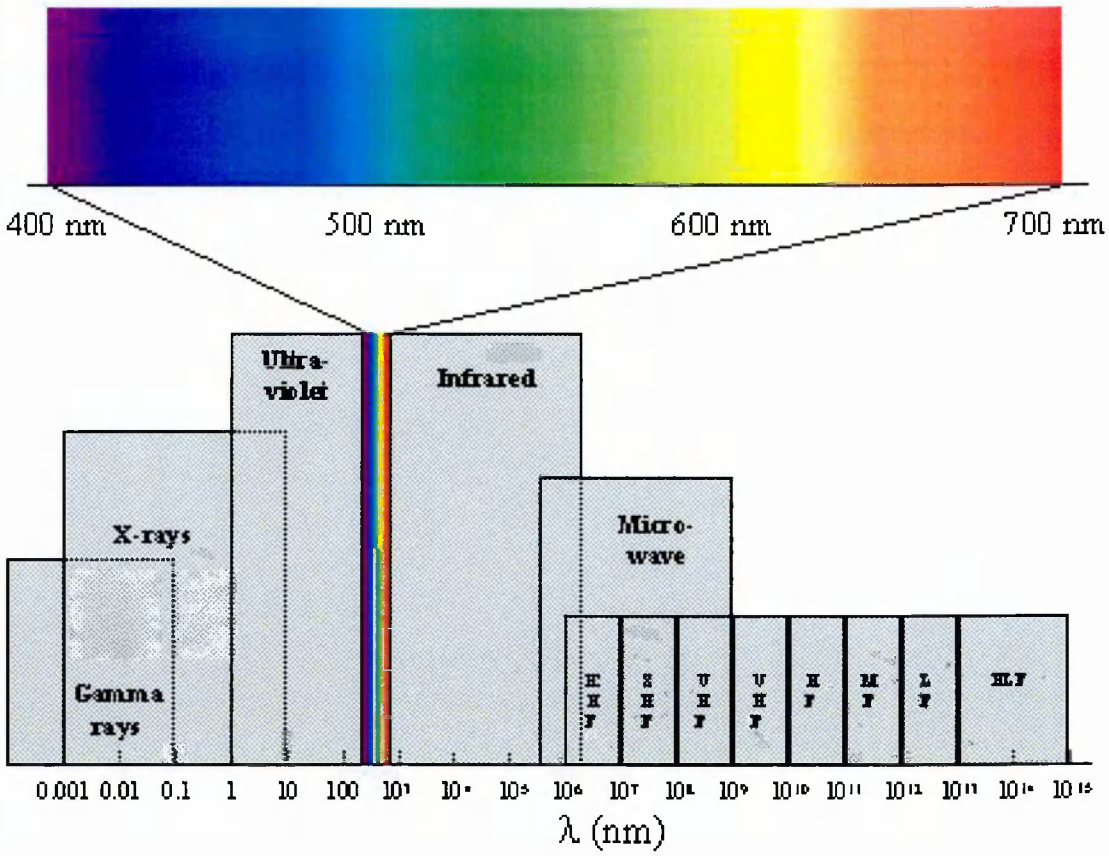

Figure 1.3.2. Solar spectrum on a logarithmic scale (source http://www-class.unl.edu/phys151/041598.html).

Solar radiation is at its most intense in the visible region which accounts for almost half of all solar energy (Mather, 1999). The human eye is sensitive to EMR over this small fraction of the solar spectrum (*c.* 400-700nm) although photosensitive instruments and some animals can detect EMR beyond these boundaries. The waveband region used for remote sensing generally ranges from 450nm to 2500nm (Jackson, 1986). Electromagnetic radiation beyond *c.* 3000nm is mainly heat re-radiated from the Earth's surface (Lillesand & Kiefer,1993).

1.3.1. Light as energy.

Given a constant angle of illumination, three factors combine to determine the amount of energy incident upon an object:

- The temperature (and size) of the source;

- the frequency of EMR;
- attenuation by intervening matter (e.g. atmospheric particles).

Higher temperature leads to more intense radiation, according to the Stefan-Bolzmann law $M= \sigma T^4$ where M is the total energy radiated, T is the absolute temperature in degrees Kelvin of the emitting object and σ is the Stefan-Bolzmann constant ($5.6697 \times 10^{-8} W\ m^{-2}\ K^{-4}$) (Lillesand & Kiefer, 1993). The energy transferred by EMR rises with frequency according to Planck's law $E= hf$, where E is energy, h is Planck's constant (6.625×10^{-34} Joules sec^{-1}) and f denotes frequency (Mather, 1999).

1.3.2. Attenuation by the Earth's atmosphere.

The Earth's atmosphere both absorbs some solar energy and reflects some back into space (O'Hare & Sweeney, 1986). Attenuation by the Earth's atmosphere modifies the distribution of incoming energy by selectively absorbing or scattering certain wavelengths. Atmospheric scattering is caused by the absorption of radiation by atoms or molecules. These then re-radiate the photons in all directions (Jensen, 2000).

Two atmospheric processes affect the visible spectrum in particular. Rayleigh scattering occurs when particles or aerosols with a diameter smaller than the wavelength intercept photons (Mather, 1999). Rayleigh scattering by the atmosphere is most pronounced at shorter wavelengths, being inversely proportional to the fourth power of wavelength (Lillesand & Kiefer, 1993), biasing the spectral distribution towards longer wavelengths. Rayleigh scattering of short wavelengths is responsible for the blue appearance of the sky and, due to a longer path and greater attenuation at low sun azimuth, the red glow of the setting sun (Lillesand & Kiefer, 1993; Mather, 1999).

Mie scattering is caused by particles having radii close to the wavelength of EMR, e.g. smoke, dust or salt aerosols. Mie scattering also biases the distribution of incident light

towards longer wavelengths, although to a far lesser degree than Rayleigh scattering. Larger elements, e.g. water droplets and ice particles in clouds, have radii greater than 10μm and do not affect the distribution of visible light (Mather, 1999; Jensen, 2000).

1.3.3. Scattering of light.

Rayleigh scattering is dominant under clear skies, with Mie scattering gaining in significance under conditions of haze (Lillesand & Kiefer, 1993). Diffuse (scattered) light is omnipresent: without diffuse light it would not be possible to see objects in shadow. Atmospheric scattering of blue light is more than twice that of red light (Sabins, 1996). A logical conclusion from this would be that shadows and shaded surfaces contain a disproportionate amount of blue light and this disparity can be expected to increase under clear skies when Rayleigh scattering becomes the dominant cause of diffuse light. Diffuse light also reaches the human eye (or remote sensing optic) and forms a background 'haze' which reduces the contrast of light reflected from the object in view. The strong element of selective scattering at blue wavelengths both reduces the amount of energy available to the sensor and obscures variability of blue reflectance by objects. Ratio analysis between blue and other wavelengths will also be confounded by selective scattering and blue wavebands are rarely used in remote sensing (Mather, 1999).

Many gasses and particles absorb solar energy at distinct wavelengths and water vapour affects several regions in the near and mid-infrared. Oxygen is responsible for a narrow and pronounced absorption feature at 760nm and atmospheric water absorbs at 940nm and 1,100nm (Milton *et al.*, 1995). Major water absorption bands at *c.* 1450nm and 1950nm reduce the amount of incident energy to levels which are insufficient to obtain reliable signals, thus precluding the use of these wavelengths for spectral analysis. Regions of the spectrum where sufficient energy reaches the ground to enable reliable detection and

measurement are used for remote sensing and referred to as 'atmospheric windows' (Lillesand & Kiefer, 1993; Jensen, 2000).

1.3.4. Physical basis of spectral properties.

Whilst instruments can quantify the amount and distribution of light incident upon an object, such measurement conveys no information about the object itself. Photons of EMR interact with a surface at a molecular scale and are selectively absorbed, transmitted or reflected (Wooley, 1971). It is these interactions which modify the amount and distribution of radiant light and are governed by the composition of the object. Transmitted light passes through the object and the exit flux can be measured on the far side. Measurement of transmission is seldom convenient for remote sensing of larger areas, or where access to the target is limited. Light which is not transmitted or absorbed will be reflected, and it is this reflectance which may be related to the structure and composition of the leaf.

Molecules possess discrete energy levels and can absorb energy (photons) only at specific wavelengths. Absorption of light at wavelengths shorter than *c.* 800nm is achieved by the electronic transition of atoms to a higher energy level, whilst absorption above *c.* 800nm causes a rotation and stretching of the chemical bonds between atoms (Baret, 1995). Goetz (1992) presents a description of the complex interaction with molecular structures and the way in which photon energy is transferred to the orbit of atoms within the molecule. One striking example which is pertinent to this investigation is the sensitivity of this process shown by the different absorption maxima of chlorophyll *a* (428nm and 660nm) and chlorophyll *b* (452.2nm and 641.8nm) in dried diethyl ether (Lichtenthaler, 1987). Both pigments have an essentially identical molecular structure of 120+ atoms with only one CH_3 side-group of chlorophyll *a* changed to CHO in chlorophyll *b* (Volk, 1998), yet these two pigments have significantly different absorption characteristics.

1.4. Interaction of light with the plant canopy.

Leaves are almost entirely transparent to all light in the first instance. The cuticle and cuticular waxes reflect only a small proportion of incident light, except at very high angles of incidence (Gates *et al*, 1965; Knibling, 1970). Photons are able to pass through the various elements of the leaf structure and would pass directly through the leaf but for scattering by structural elements of the leaf mesophyll. Scattering occurs as a result of refraction, primarily at the junction of hydrated cell walls and the inter-cellular air spaces (Gausman, 1974; Vogelmann, 1989). Refractive scattering of visible light is seen as a mechanism to increase the path-length of a photon within the leaf and thus the probability of interception by a photosynthetic pigment (Buschmann & Nagel, 1993). The number of air space-cell wall interfaces encountered, rather than the size of the spaces determines the extent of scattering (Walter-Shea & Norman, 1991). Sinclair *et al.* (1973) concluded that the microfibril structure of cell walls also contributes to internal scattering.

1.4.1. Visible wavelengths and photosynthetic pigments.

The visible region (400 to 700nm) (Fig. 1.4.1.) is relatively free of absorption by water in leaf tissues (Hodáňová, 1985) and is widely used for remote sensing of vegetation.

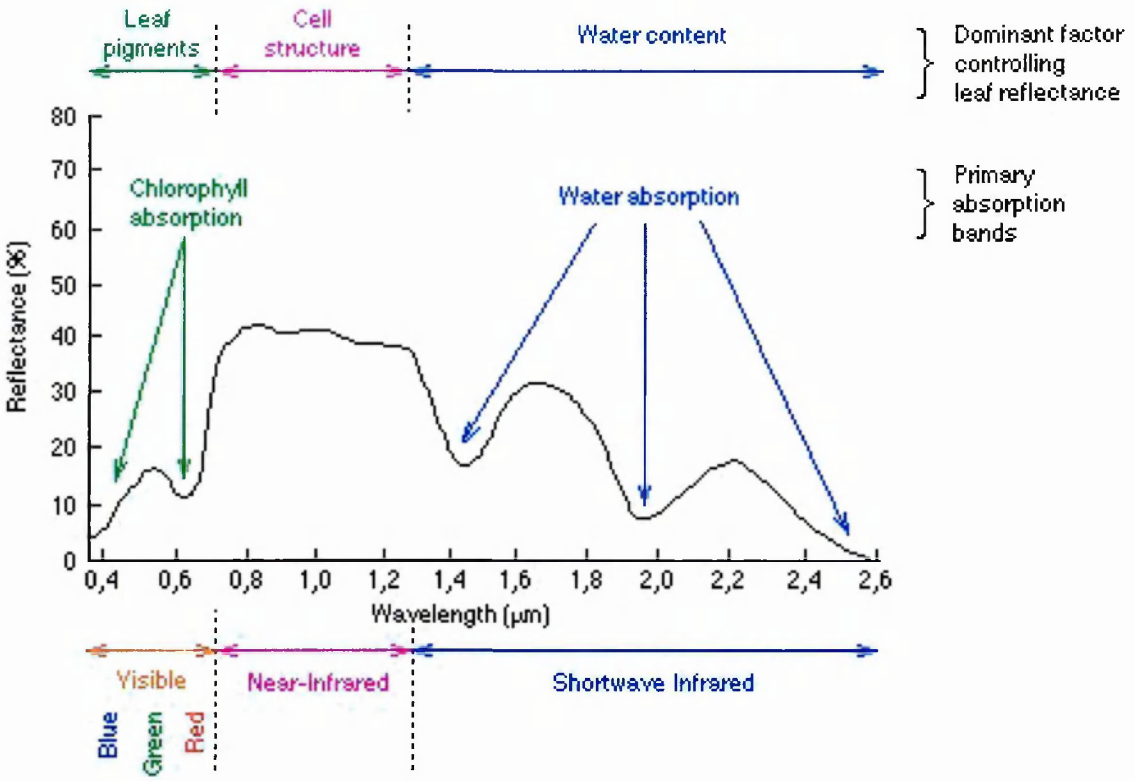

Figure 1.4.1. Leaf absorption regions
(source: http://www.tbrs.arizona.edu/education/553-2002/Ch5_Veg-slides.pdf).

Chlorophylls *a* and *b* dominate the spectral response of plants at visible wavelengths (Hoffer & Johannsen, 1969; Guyot, 1990) and form *c.* 65% of leaf photosynthetic pigments, with xanthophylls contributing *c.* 29% and carotenes *c.* 6% (Gates *et al.*, 1965). Chlorophyll *a* is approximately three times as abundant as chlorophyll *b* (Lichtenhaler, 1987). These ratios are variable and are indicative of plant physiology (Peñuelas *et al.*, 1995).

All of the predominant photosynthetic pigments absorb blue light, but only chlorophyll absorbs at red wavelengths (Gates *et al.*, 1965; Knibling, 1970). Gates *et al.* (1965) measured the spectral reflectance of green and albino leaves from the same variegated geranium (*Hedera helix*) plant and showed reflectance of visible light from the albino leaf to be *c.* four times that of the green leaf. Knibling (1970) also measured a large increase in the reflectance of visible light from white leaves of a variegated geranium when compared

with green leaves. He concluded from this that chlorophyll, absent in the white leaves, was responsible for the strong absorption of visible light.

Lichtenhaler (1987) examined the absorption spectra of chlorophyll *a*, chlorophyll *b* and carotenoids in pure diethyl ether. Carotenoid absorption was strongly centred around 450nm (blue) and insignificant at 550nm (green). Chlorophyll *a* and *b* absorbed at two strong and sharply defined peaks in the red and blue sections of the visible region (section 1.3.4). Neither chlorophyll displayed significant absorption between the red and blue peaks, although a localised increase is visible at around 600nm (orange). The absorption spectrum of chlorophyll *b* extends further into the blue-violet region than that of chlorophyll *a*. Photosynthetic pigments accumulate in the leaf during maturation, resulting in a decrease in visible reflectance (Walter-Shea & Norman, 1991). As the leaf matures and chlorophyll concentration increases, red and blue chlorophyll absorption extends further into both flanks of the green peak, and the leaf appears darker (Gates *et al*, 1965).

1.4.2. Near-infrared wavelengths and leaf structure.

Infra-red light occurs in that region of the spectrum beyond the red end of the human visible range, 750nm to 2500nm (Fig. 1.4.1). In contrast to their minimal reflection at visible wavelengths, plants are strong reflectors of infra-red light and appear as bright objects on infra-red images (Sabins, 1996). Only 5-8% of near-infrared energy fails to emerge from the leaf (Knibling, 1970). The combined reflectance and transmittance spectra (1 – absorption) of a multi-layered plant canopy shows that *c.* 85-90% of incident light is absorbed at visible wavelengths and only *c.* 5-10% beyond 750 nm (Walter-Shea & Norman, 1991; Guyot, 1990). This sharp contrast in absorption is characteristic of photosynthesising vegetation and provides the basis of most widely-used vegetation indices. Reflectance at near-infrared wavelengths is driven by multiple internal scattering by leaf structural elements (section 1.4) and photons are scattered from the leaf in all

directions (Gausman, 1974). In contrast to the visible region, near-infrared light is not absorbed by photosynthetic pigments. Gates *et al.* (1965) found identical NIR reflectance from green and white geranium leaves, despite very large differences in visible reflectance mentioned earlier. Absorption spectra of isolated chloroplasts indicated that photosynthetic pigments were completely transparent to infrared radiation. Near-infrared reflectance was found to be similar for both the green and white (no chlorophyll) parts of variegated geranium leaves by Knibling (1970) who noted that near-infrared reflectance was independent of the presence or absence of chlorophyll.

Earlier studies have demonstrated that near-infrared reflectance is reduced when refractive junctions within the leaf are displaced. Knibling (1970) infiltrated leaves of bean plants (*Phaseolis vulgaris*) with water and reflectance from the leaf was reduced at all wavebands between 400nm and 1200nm. A similar experiment was conducted by Gausman *et al.* (1974) who infiltrated leaves of four plant genera, including tomato (*Lycopersicon esculentum*). This action replaced the air in intercellular spaces of the leaf with liquids (water, cottonseed oil, hexane) of varying indices of refraction. As expected, reflectance at near-infrared wavelengths was strongly reduced and Gausman *et al.* concluded that refraction between the moist cell walls and air in leaf cavities was responsible for the strong scattering of infrared light. Reflectance in the visible region was also reduced, although an impairment of the scattering process can be expected to detract from the absorption of visible light and result in an increase of visible reflectance. Gausmann *et al.* do not mention transmittance. Scattering by leaf elements is largely independent of wavelength (Gates *et al.*, 1965) and a later paper by Buschmann & Nagel (1993) provides a clue to the mechanism of reduced visible reflectance: photons were passing through the leaf with minimal scattering or absorption. The authors cite increased transmittance at 800nm (near-infrared) of infiltrated leaves and, although not mentioned in their paper, a similar process can be expected to occur at visible wavelengths.

1.4.3. Canopy geometry.

Reflectance from the canopy of a growing crop is more complex than a sum of reflectance from individual leaves. Visible reflectance is reduced and near-infrared reflectance enhanced with increasing biomass concentration (Hatfield & Pinter, 1993). The three-dimensional canopy structure can have a marked effect on reflectance and control e.g. the contribution of background material or shadow to the canopy spectrum. This influence is not specific to particular canopy variables and different canopies may have very similar reflectance spectra (Baret, 1995). Several aspects of canopy geometry affect spectral reflectance, including the compound leaf area and the angle at which leaves are oriented with respect to the solar position and the recording instrument. Leaf area index (LAI) is the single side area of leaves, divided by the total area and can attain values at several times unity as the canopy expands and multiple leaf-layers develop. Leaf area index has a significant impact on the amount and distribution of light reflected from the canopy and the ratio between red and near-infrared is sensitive to the combined effects of LAI and leaf angle (Verhoef & Bunnik, 1981; Guyot, 1990).

Asner (1998) measured the effects of leaf angle distribution (LAD) on canopy reflectance and found that reducing LAD from 80° to 0° increased reflectance, and that this was a non-linear response. Stress causes the geometry of a plant to change (e.g. leaf droop and curl) (Jackson, 1986) and leaf angle distribution may change throughout the day (Jensen, 2000). Verhoef & Bunnik (1981) indicated that while reflectance from errectophile (near vertical) leaves is variable at different view angles, reflectance from a canopy having planophile leaves (*c.* 11° average inclination, similar to a potato canopy) was almost invariant at +-30° view angle (E-W) with the sun at 30° before local noon. This study used data from a reflectance model and not empirical measurements. These results are unlikely to hold for N-S angles however, where the solar elevation at higher latitudes does not approach 90

degrees. This factor is relevant to the flight direction and sensor angle range of airborne data and may affect the repeatability of satellite data recorded from off-nadir elevations.

Wind movement can modify the canopy geometry and leaf surface differences will influence the spectral signature if wind moves the canopy to such an extent that abaxial surfaces are presented to the sensor. The mesophyll of dicotyledon plants, e.g. *solanum* spp. is differentiated. A layer of tightly-packed palisade mesophyll cells is situated under the adaxial epidermis, while the abaxial spongy mesophyll consists of loosely-arranged cells with larger air-spaces between them (Wooley, 1971). Reflectance from the abaxial surface is higher at visible wavelengths, but lower than from the adaxial surface in the near-infrared region. The inversion by wind of elements of a broad-leaved canopy is to be expected in gusty conditions and wind effects are likely to be localised and variable. Spectral reflectance data obtained under conditions of significant wind strength may therefore contain errors that cannot be verified or eliminated during subsequent analysis.

1.5. Remote sensing.

Sir Isaac Newton found that visible light would divide into a spectrum of colours (wavebands) when refracted through a glass prism. Joseph Fraunhofer discovered narrow absorption bands in solar radiation and Neils Bohr linked these to absorption to the atomic structure of intervening gasses (Campbell, 1996).

In very basic terms, a spectrometer admits EMR through an opening or lens. This energy is then refracted through a prism and a single detector moved through an arc corresponding to the spread of refracted energy (Milton, 1987). Later instruments use a static array of detectors. The instrument converts each division of EMR into an electronic signal and records this as the digital number (DN) for that waveband. Comparison of the DNs for

each waveband can signal the wavelength and magnitude of absorption features and these are then related back to the composition of the target object.

The earliest spectroscopic devices were used to study human vision around 1915 (Ives, 1915). Later developments were concerned with the study of paint pigments and sources of light (Hunter, 1942; Hammond *et al.*, 1960). Instruments to investigate the photosensitivity of plants began to be developed in the 1960's. The first Landsat satellite was launched in 1972 and a field radiometer, the Exotech-100, was designed to record at similar wavebands to those of the satellite instrument (Milton, 1987).

The nomenclature of remote sensing can be confusing. Wavelength (described in section 1.2.1) is the distance between two identical points on successive waveforms of EMR while the term *waveband* refers to the range of wavelengths (e.g 450nm-460nm) recorded as a single value by the sensing instrument. Spectral resolution is a measure of the narrowest spectral feature that can be resolved by a spectrometer, usually represented as the full-width at half-maximum (FWHM) of the instrument's response to a monochromatic signal (Analytical Spectral Devices Inc; www.asdi.com). Spectral sampling interval is the distance in wavelength units (e.g. nm) between data points in the measured spectrum.

The terms radiometry, spectrometry and spectroscopy often appear in the literature devoid of any definition. Milton (1987) defines a radiometer (and thus radiometry) as recording electromagnetic radiation (EMR) in a limited number of discrete bands. Milton further defines a spectrometer (or spectroradiometer) as recording a continuous spread of wavebands. Campbell (1996) suggests that the collection of spectral data in a limited number of wavebands is properly described as spectrometry, whilst spectroscopy refers to the collection of hyperspectral data (a large number of narrow wavebands).

1.5.1. Field spectroscopy.

Modern field spectrometers are capable of high spectral resolution (~1-2nm). Ideally mounted on a tripod stand, they are static and can integrate a reflectance signal for an extended period, usually 1-2 seconds. The reflectance (or radiance) spectrum is measured as a large number of narrow and often contiguous wavebands. Figure 1.5.1. shows reflectance recorded from a typical potato canopy at 512 discrete wavebands of 1.5nm width using a GER 1500 spectrometer (Geophysical and Environmental Research Corp., New York). There is little attenuating atmosphere between the target and sensor and comparative spectra recorded from a reference panel are used to compensate for changes in incident radiation. A field spectrometer records a single spectrum from a limited field of view, typically 4-10cm diameter.

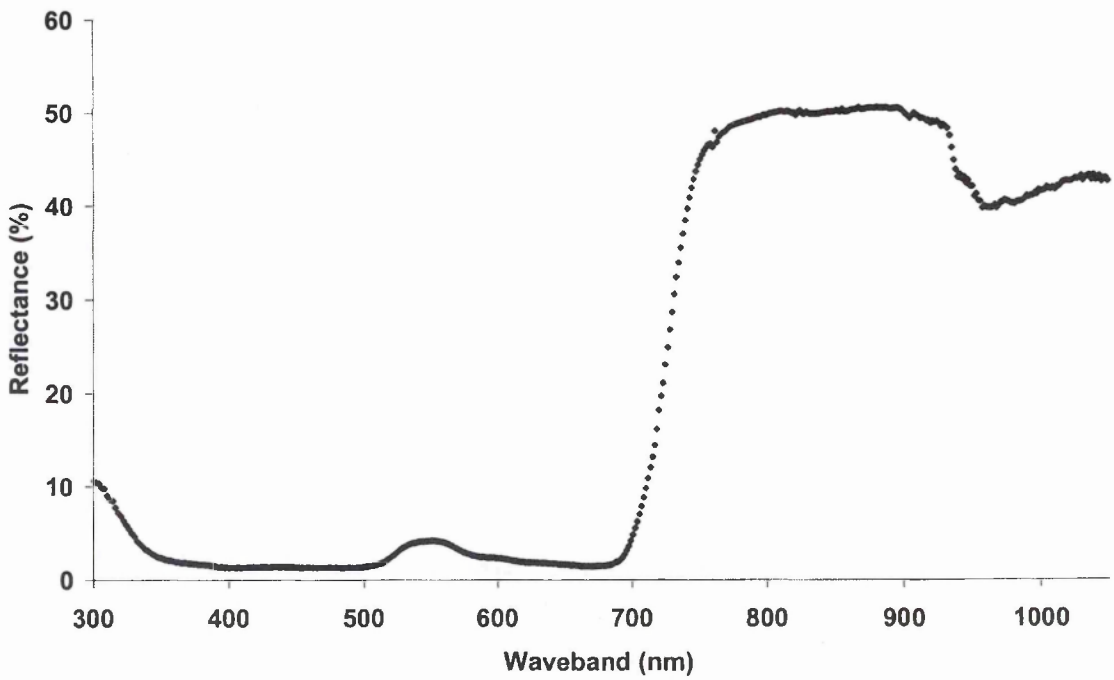

Figure 1.5.1. Spectral reflectance from a potato plant canopy at 512 wavebands. Recorded during the 2000 field experiment using a GER 1500 spectrometer.

Reflectance values measured in field spectroscopy are the percentage of incident radiation that is re-radiated from the target. Solar radiation fluctuates substantially under conditions of cloud, and imperceptibly (although not to the instrument) over short timescales under clear skies (Milton & Goetz, 1997) and incident radiation is assessed by measuring the

reflectance from a calibration panel having near-100% reflectance. The ratio between target and panel reflectance will be affected by changes in incident radiation between the two measurements and these should be made as closely as possible.

Some spectrometers e.g. the GER 1500 can be used in tandem to record the panel and target in a near-simultaneous timeframe. Reflectance from the panel is much higher than from vegetation and the instrument records the panel reflectance over a shorter integration period so the measurements are not wholly synchronous. The Cropscan instrument (Cropscan Inc., Rochester, MN, USA) employs an upward-facing sensor to measure solar irradiance concurrently with the target measurement.

Reflectance from natural surfaces, including the canopy of field crops, is not truly Lambertian (diffuse) and field spectrometer measurements should be taken from a consistent direction relative to the solar position. Variability in reflectance occurs along the principle solar plane (the solar azimuth and reciprocal) and is least in the orthogonal plane. Milton *et al.* (1995) note that most field reflectance data had been collected from the nadir position. View angle, the direction from which a sensor is aimed at the target, is a contributing factor in the reflectance values measured.

Milton (1987) suggested that field spectrometers should be mounted on a mast or tripod to ensure a consistent view angle to the target and reference panel. The instrument should be at least one metre above the target and the operator should wear dark clothing and remain in the shaded direction from the instrument. Kollenkark *et al.* (1982) measured the effects of crop row direction and sensor altitude on reflectance measurements of soybean (*Glycine max*) and Daughtry *et al.* (1982) conducted a similar investigation on row-width and sensor altitude. These studies have shown that care must be taken to ensure that the sensor does not record a variable amount of soil or shadow from partial canopy cover. Careful

alignment of the spectrometer will avoid soil and shadow effects where the sensor field-of view is completely filled by the target, as would be the case with most ground-based reflectance measurements of mature vegetation canopies.

Field spectrometers are useful for investigating the reflectance patterns of healthy and infected plants. However, a large number of recordings are necessary in order to obtain a representative sample from a heterogeneous target (Milton *et al.*, 1995) and data collection is usually limited to within two hours of solar noon to minimise diurnal changes due to e.g. leaf droop or solar elevation and azimuth factors. Movement through a dense, mature crop is often difficult and intensive monitoring of large areas may not always be practicable within this time limit.

1.5.2. Airborne remote sensing.

The mounting of a spectrometer on an aircraft can facilitate the collection of spectral measurements over a wide area and in a short period of time. The collection of a sequence of single spectra would not fully exploit the capabilities of the aircraft platform and airborne sensors are designed to collect a large number of spectra simultaneously. Each spectrum can then be used to form a point in a grid of data values; the 'pixels' of an image covering an area of the target surface.

The airborne instrument described here is the CASI-2 instrument (Itres Research, Calgary, Alberta, Canada). The CASI-2 uses a two-dimensional detector array of 512 elements across the direction of travel and 288 elements, each recording a discrete waveband, along the direction of travel (Jensen, 2000). The entire swath width is imaged simultaneously by 512 detector elements (Fig. 1.5.2.).

The CASI-2 cannot record 512 pixels width in all 288 wavebands at aircraft speeds and some compromises are required. Operated in spatial mode, the CASI-2 will record a swath 512 pixels wide in nineteen spectral bands (several waveband sensors in each group). Enhanced spectral mode can record all 288 wavebands at a width of 101 pixels. There are other, similarly restricted, permutations of width and waveband settings. Spatial resolution (pixel size) is dependent upon the height of the aircraft above the target while aircraft speed, illumination and waveband settings determine the pixel length (Jensen, 2000). Aircraft (and satellite) sensors measure radiance without correction for changes in solar irradiance. The CASI-2 does include an upward-viewing incident light sensor (ILS), although this is affected by changes in aircraft attitude (due to turbulence) and is not currently used to correct for irradiance (Milton *et al.*, 2000; A.K. Wilson, personal communication, December 2002).

One inevitable consequence of imaging a swath of pixels is that the sensor view angles vary across the aircraft track (Fig. 1.5.2.). The CASI-2 instrument operated by the Natural Environment Research Council Airborne Remote Sensing Facility (NERC ARSF, Kidlington, Oxford, UK) has a custom lens which spans 54.4° and airborne data from instruments of this design should be collected when flying along the principal solar plane to reduce directional reflectance effects.

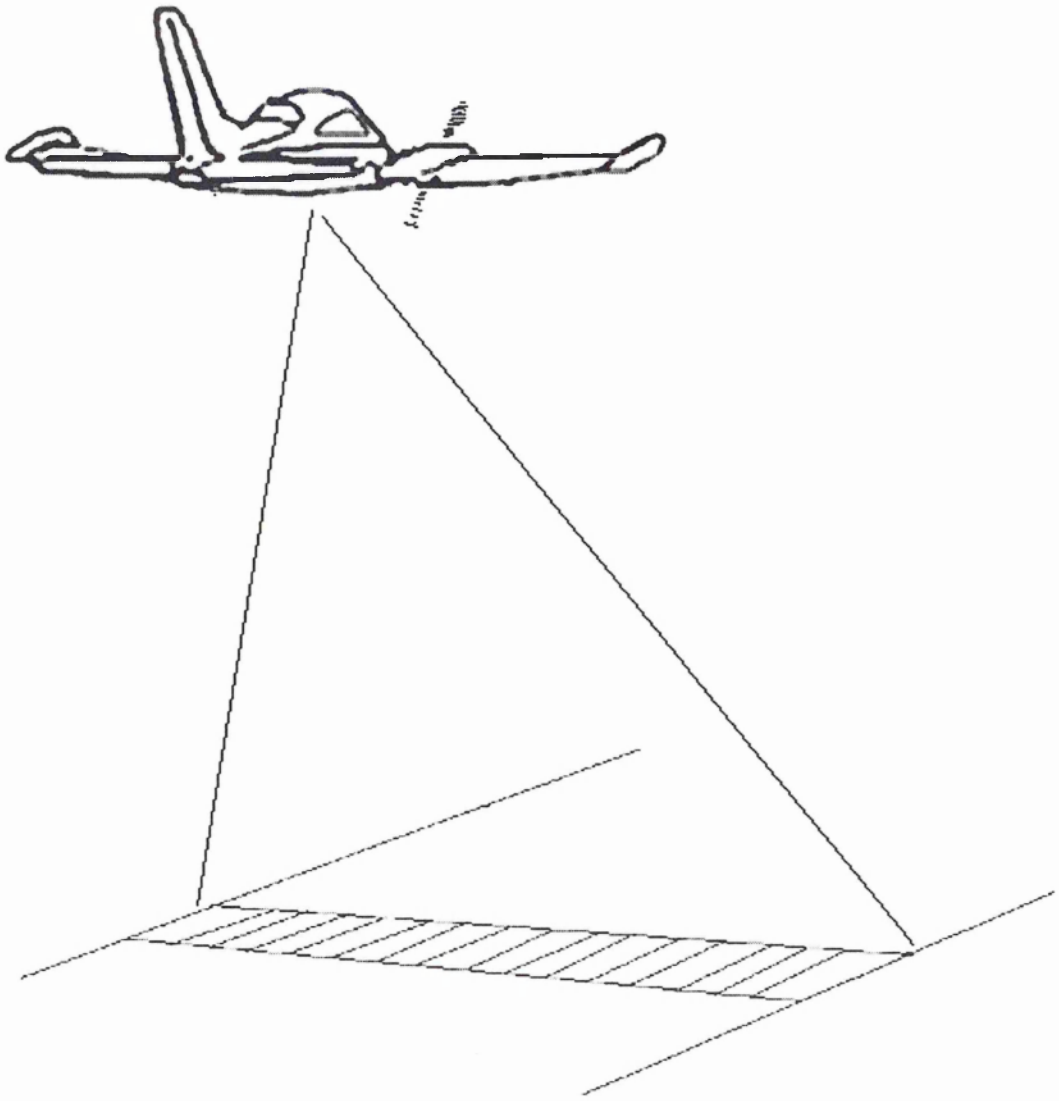

Figure 1.5.2. Schematic of airborne imaging geometry showing across-track pixels and variable sensor-view angle.

The collection of 'ground-truth' data using field spectrometers is required where an airborne or satellite remote sensing experiment is likely to be repeated under different atmospheric conditions. A series of light and dark calibration targets are recorded with field equipment and the results compared with aircraft data. This enables future users of the data to quantify the influence of the atmosphere at the time of collection.

1.5.3. Satellite remote sensing.

A large number of satellite instruments are orbiting the earth. Many record at resolutions which would not permit the identification of individual fields on the European scale, and this discussion will be restricted to the satellites used in this study, plus a brief history of

the first remote-sensing satellites, the ERTS/Landsat Program. Sensor details for the SPOT satellites are listed in Appendix A and for the Ikonos satellite in Appendix B.

1.5.3.1. ERTS (Landsat).

The United States Department of Interior initiated the Earth Resources Technology Satellites (ERTS) program in 1967. ERTS-1 was launched in 1972 and was the first unmanned satellite designed to acquire multispectral data from terrestrial surfaces (Lillesand & Kiefer, 1993). The waveband configuration of this satellite is strongly suggestive of vegetation monitoring. ERTS-1 was subsequently renamed Landsat-1

Landsats 1-5 carried a Multispectral Scanner (MSS) instrument. The Landsat MSS had four wavebands of a nominal 80m resolution. Landsats 4 and 5 carried the Themic Mapper (TM) instrument in addition to the MSS. The Landsat TM has seven wavebands, three visible and three NIR/MIR wavebands at 30m resolution, plus a thermal band of 120m resolution. Landsat 6 was to have carried the Enhanced Themic Mapper (ETM), but failed at launch (Lillesand & Kiefer, 1993). Landsat 7 was successfully launched in 1999 and carries the ETM+ instrument, which has a thermal band upgraded to 60m resolution and improved calibration facilities (Jensen, 2000).

1.5.3.2. Scanning method.

Landsat TM and ETM+ scan a scene by moving a mirror to the left and right, 'sweeping' the image swath. Landsat images were passed over in favour of data from the SPOT satellite which records the full swath width simultaneously. Fixed-view sensors have a longer dwell-time and this should improve their accuracy (Jensen, 2000). This advantage would be negated if individual elements of a fixed-sensor array were less sensitive than a single sensor behind a moving mirror. The latest generation of high spatial resolution satellites employ fixed sensor arrays, indicating that limitations of sensor size and sensitivity have been overcome.

1.5.3.3. SPOT (Satellite Pour l'Observation de la Terre).

SPOT-1, the first SPOT satellite, was launched in 1986 and followed by SPOT-2 in 1990, SPOT-3 in 1993 and SPOT-4 in 1998. SPOT-3 failed in orbit and SPOT-2 has been reactivated. Images from SPOT-2 and SPOT-4 have been tasked for this investigation. SPOT satellites carry two HRV (High Resolution Visible) sensors which have a nominal 20m resolution red, green and NIR channels, plus a Mid-IR band on SPOT-4 (Mather, 1999).

1.5.3.4. Ikonos: Space Imaging Inc.

The first Ikonos satellite was lost eight minutes after being launched in April 1999. A second satellite was successfully launched in September 1999 (Jensen, 2000) and a four-meter resolution multispectral image from this satellite was used in this investigation. The Ikonos instrument records blue, green, red and NIR wavebands and, like the SPOT HRV, the whole swath is recorded simultaneously. Both SPOT and Ikonos are able to image areas to the side of their orbit track. This greatly increases the chance of obtaining a cloud-free image, but has implications for off-nadir view angles which must be carefully considered when comparing images. SPOT would, without the ability to scan sideways, only be able to image a specific area every twenty-six days (Jensen, 2000). One cloud on one day over the target would prevent an image being obtained, and this could not be considered a practicable timescale for vegetation studies.

1.5.4. Limitations (of all platforms).

The total amount of light reflected from the surface is a function of pixel area and reduces dramatically as pixel size is reduced. The actual field of view (FOV) of the sensor may be round, although this is transformed to square pixels for image display. The area of a round pixel is Πr^2. Π is a constant and reducing the radius decreases the pixel area in the ratio of $(r_1 - r_2)^2$.

From this diminishing surface signal, we now wish to divide up the reflected radiation into ever finer wavebands to achieve higher spectral resolution. Hyperspectral instruments typically divide the incoming energy between several hundred discrete sensors (GER 1500= 512; CASI-2= 288). The assumption is of a linear relationship here, N wavebands each contain 1/N of the total signal. That in itself would be limiting, however, the amount of energy reaching the sensor reduces at shorter wavelengths and the amount of energy penetrating the atmosphere is also greatly reduced. Current sensors are operating at the limits of technology, and noise (stray photons or electrons) becomes the limiting factor. Noise can be reduced by increasing the integration time (averaging over many readings) when static instruments are used, although this can cause problems with fluctuation of lighting conditions. For moving sensor platforms (aircraft, satellite), extending the integration period enlarges the pixel size and reduces spatial resolution.

1.6. Vegetation indices.

Vegetation indices are algebraic formulae which contrast two or more measured parameters, e.g. reflectance at specific wavebands. They are designed to enhance the information conveyed by their constituent parameters, either by reducing the effects of external factors (e.g. fluctuation in solar irradiance) which operate on the numerator and denominator simultaneously, or because two (or more) factors respond to vegetation status in opposing directions. A wide variety of indices have been developed to estimate the quantity and status of photosynthetically active vegetation. Many of these indices attempt to reduce the contribution from abiotic factors such as soil colour and atmospheric attenuation.

1.6.1. Basic principles.

Many vegetation indices are predicated on the contrast between high absorpance of visible light by chloroplasts and widespread scattering of light (section 1.4) at near-infrared (NIR) wavelengths by leaf structural elements (Campbell, 1996). Plotted as magnitude of reflectance versus wavelength, a sharp rise in reflectance can be observed between the red and NIR regions. This feature is a characteristic of photosynthesising vegetation and has become known as the 'red edge' (Steven *et al.*, 1990; Lillesand & Kiefer, 1993). The majority of multispectral vegetation indices fall into two broad groups; ratio indices and perpendicular indices (Danson *et al.*, 1995).

1.6.1.1. Ratio indices.

Conventional ratio indices measure the slope in red-NIR space resulting from high chlorophyll absorption (low reflectance) at red wavelengths and the much higher level of radiation reflected by plants in the NIR region (Steven & Jaggard, 1995). Ratio indices have the advantage that changes in incident light affect both numerator and denominator in approximately equal measure and Lillesand & Kiefer (1993) note that ratio indices are almost impervious to changes in aspect and the strength of illumination. Ratio indices are, however, sensitive to changes in background reflectance, such as the colour and brightness of soil (Huete, 1988).

The ratio between red and NIR reflectance as an indicator of plant health has been used for many years. Jordan (1969) described the ratio vegetation index (RVI), calculated as NIR / Red. A development of RVI, the normalised difference vegetation index (NDVI), was suggested by Rouse *et al.* (1973) and has been the most widely used index for many years (Sabins, 1996). NDVI restricts the range of output values to between –1 and one and is calculated as $\frac{NIR - Red}{NIR + Red}$. The behaviour of NDVI at high LAI is of particular importance

for the study of crop canopies having a high percentage of ground cover. NDVI is highly sensitive to the amount of green vegetation in the sensor view, and 'saturates' at *c.* 80% ground cover (Qi *et al.*, 1994).

1.6.1.2. Soil background effect on multispectral vegetation indices.

The reflectance curve of bare soil rises from low values (≤10%) at short wavelengths, forming a near-linear (slightly convex) curve into the near infrared spectral region. The magnitude and slope of the soil reflectance signal is influenced by soil type, roughness and soil moisture (Myers & Allen, 1968; Rondeaux *et al.*, 1996). Organic soils have a steeper slope line than mineral soils and dry soil is more reflective than wet soil. Incomplete ground cover exposes soil background to the sensor, incorporating the spectral characteristics of soil in the recorded reflectance spectrum. Soil can also reflect NIR radiation penetrating a plant canopy while red light (largely absorbed by photosynthetic pigments) does not penetrate the canopy to the same extent (Heute, 1988).

The disparity between soil and vegetation spectra can make interpretation of ratio indices problematical unless the amount and brightness of the background is known and a correction factor applied. Red : NIR ratio indices are comparing two regions where the contribution from soil, the main background feature, exhibits substantial and opposing differences to the plant canopy reflectance. Reflectance from soil is generally higher at red wavelengths and lower in the NIR region than reflectance from vegetation and this makes ratio indices sensitive to both soil brightness and the percentage of canopy cover in the sensor field of view. Qi *et al.* (1994) demonstrated how the transition from dry to wet soil resulted in a large change in NDVI measurements, which were depressed by bright, sandy soil and elevated by almost fifty percent by a wet clay background. This result was, however, obtained from aircraft data over a cotton (*Gossypium hirsutum*) crop of only 5-

10% ground cover and a large fraction of the measured radiation will have emanated from the soil.

Much effort has been expended in countering the problem of soil-induced variability, leading to the development of several vegetation indices which are claimed to be less sensitive to background reflectance. Huete (1988) developed the soil-adjusted vegetation index (SAVI) by adding a constant to the NDVI calculation. SAVI is thus calculated as $\frac{NIR - Red}{NIR + Red + L} * (1 + L)$. The constant factor 'L' was set at a value of 0.5 for intermediate vegetation cover. The SAVI is a ratio index in which vegetation isolines (lines drawn through pixels representing identical vegetation fractions at different brightness) converge at a point of negative X and Y values. This displacement appears to partially compensate for a non-linear response of ratio indices to increasing biomass.

The optimised soil adjusted vegetation index (OSAVI) was described by Rondeaux *et al.* (1996) as $\frac{NIR - Red}{NIR + Red + 0.16}$. This index is similar to SAVI, although an 'L' value of 0.16 was found to give the least variation with soil brightness across a range of canopy densities (De Koeijer *et al.*, 2000). The low 'L' factor also avoided the requirement to multiply the whole by 1+L to maintain the dynamic range of the index.

Qi *et al.* (1994) developed a modified soil adjusted vegetation index (MSAVI), using the diverging soil-brightness effect on ratio and perpendicular indices to pre-calculate the L factor of SAVI. The authors then developed a recursive version, MSAVI-2, which removed the necessity of pre-calculating the ratio and perpendicular soil factors.

1.6.1.3. Perpendicular indices.

Perpendicular vegetation indices take as their reference a soil line in red-NIR space which represents reflectance from bare soil at varying degrees of brightness (i.e. wetness). The soil line gradient can vary with soil type and surface texture and is not constant between different study areas. Perpendicular indices take the orthogonal distance of a pixel from the soil line as indicative of vegetation density and status.

The perpendicular vegetation index (PVI) (Richardson & Wiegand, 1977) accommodates soil lines of differing slopes, although these must either be estimated or deduced from the data for each site. PVI is calculated as $\sqrt{(\mathrm{Red}_s - \mathrm{Red}_v)^2 + (\mathrm{NIR}_s - \mathrm{NIR}_v)^2}$ and this assumes that vegetation isolines are parallel to the soil line. A weakness of this approach is that the response to increasing vegetation cover is not linear. Red reflectance begins to saturate at *c.* LAI = 3, whilst NIR reflectance from a planophile canopy continues to increase to *c.* LAI = 5 (Guyot, 1990).

Heute (1988) found that vegetation isolines became steeper with increasing vegetation density. Orthogonal indices are therefore less suited to dense vegetation cover as the disparity between the steepening vegetation isolines and the assumed parallel isolines becomes significant. Baret *et al.* (1989) developed the transformed soil adjusted vegetation index (TSAVI), which does allow for steepening vegetation isolines, although TSAVI is actually a ratio index which includes an empirical (or estimated) soil-line slope and intercept in the equation. The weighted difference vegetation index (WDVI) (Clevers, 1989) is a difference-perpendicular hybrid index, being calculated as NIR - (*s**Red) where *s* is the slope of the soil line. The ratio of NIR : Red reflectance is assumed to be similar for wet and dry soil and therefore the factor *s**Red is derived by subtracting soil NIR reflectance from the crop NIR measurement. The soil line slope of mineral soils was found

to be close to unity by Rondeaux *et al.* (1996) and Clevers reported a similar value from his own experimental area. The WDVI index reduces to NIR-Red under these circumstances and difference indices would appear to be sensitive to fluctuation of incident radiation. The value of NIR-Red does not remain constant at increased overall reflectance levels as would NIR/Red.

The accuracy of perpendicular indices may be compromised by a difficulty in determining an accurate soil line. Some scatter among the pixels forming the soil line is inevitable, and it is from a line drawn through this scatter that the perpendicular offset is calculated. Bare soil in an agricultural setting is likely to be compacted (e.g. farm tracks) or spoil areas and might exhibit different spectral reflectance characteristics than tilled soil beneath a crop canopy.

1.6.2. Pigment ratios.

Peñuelas *et al.* (1995) investigated the ratio of wavebands associated with the major absorption features of photosynthetic pigments. The basis of this method is that, while all photosynthetic pigments absorb at blue wavelengths, chlorophyll alone is responsible for the major absorption feature at *c.* 675nm (Gates *et al.*, 1965). Peñuelas *et al.* describe a Normalised Pigment Difference Index (NDPI) to assess pigment ratio as a proxy for plant health status. Calculating NDPI as $(R^{680}-R^{430}) / (R^{680}+R^{430})$, and quoting Peñuelas *et al.* (1993) and Peñuelas *et al.* (1994), they report this ratio to be highly correlated with the ratio of caroteniods and chlorophyll *a*. Developing this line of enquiry, the authors applied a structure independent pigment index (SIPI) which incorporates NIR reflectance at 800nm to compensate for the influence of internal scattering by the leaf structure. The inclusion of both power and exponential factors was tested as the spectral response of the carotenoid-chlorophyll ratio was non-linear. The optimum results from this work demonstrated a correlation (R^2= 0.987) using an exponential SIPI and wavebands 445nm and 680nm. This

work was undertaken in a laboratory and using an integrating sphere to minimise directional reflectance factors. The use of blue wavelengths would make NDPI and SIPI difficult to use under field conditions, as noted in section. 1.3.3.

1.6.3. Turgour indices.

Some attempts have been made to detect leaf water status using the H_2O absorption band centred at 970nm. Peñuelas *et al.* (1993) found significant (R^2 =0.793, 0.893) correlation between the ratio R^{970}/R^{900} and the relative water content (RWC) in leaves from two out of three varieties of Gerbera plants (*Gerbera jameosinii*). Results from a third variety (Rozamunde) were not correlated and the authors concluded that changes in cell-wall elasticity combined with absorption by liquid water to form the reflectance change in some varieties and not others. Peñuelas *et al.* suggested that their method was best suited to canopies with complete ground cover and without significant changes in LAI. Spectral reflectance measurements were conducted under clear skies, and the method might not function effectively under conditions of cloud or high humidity. Indeed, Rollin & Milton (1998) state that any changes at these wavelengths will need to be separated from the influence of water in the atmosphere. Airborne data may prove difficult to interpret; correction for atmospheric absorption is achieved at ground level by comparing the target reflectance to that from a reference panel, both items being subject to the same irradiance (Milton, 1987; Thenkabail *et al.*, 2000). This facility is not available when collecting data with airborne or satellite instruments and may limit, or inhibit, large-scale analysis of canopy water status.

1.6.4. Hyperspectral indices.

Hyperspectral vegetation indices exploit the availability of high spectral resolution data (section 1.5) which contain more information about the target than would be available from multispectral reflectance measurements (Campbell, 1996). The large number of closely-spaced data points facilitates the deployment of derivative analysis methods.

Derivative analyses of hyperspectral data have been applied to the investigation of vegetation parameters which generate spectral features over a narrow wavelength range, with the 'red edge' (section 1.6.1) subject to particular scrutiny e.g. Boochs *et al.*, 1990; Guyot *et al.*, 1992; Lelong *et al.*, 1998. The red edge feature is usually described by the position of the inflection point of the first derivative at *c.* 730nm, although Guyot *et al.* (1992) used the wavelength at which reflectance is equal to the mean of the 670nm and 760nm values. The red edge of canopy reflectance was considered to be a poor indicator of canopy chlorophyll levels by Demetriades-Shah *et al.* (1990) who suggested using the 2nd derivative of reflectance at 636nm to measure canopy chlorosis.

1.7. Spectral data processing.

1.7.1. Continuum removal.

Continuum removal is the process of removing from the spectrum, variation which is unrelated to the spectral features to be analysed. Spectral features in the continuum-removed spectra are displayed as a deviation from the continuum, enabling a more detailed comparison between pixels or images by minimising absorption features not related to the spectral feature of interest.

A continuum is usually a convex hull, fitted over the spectrum by some mathematical equation. The continuum can be removed by subtraction or division, although Clark & Roush (1984) showed that removal by subtraction will move the inflection point and distribution of the spectral feature when the continuum has a gradient. Continuum removal by division does not alter the position of the absorption feature and can be extended to normalise band-depth. The continuum-corrected value is (Bc-Br)/Bc where Bc is the continuum band value and Br is the recorded band value. This ratio would appear to remove or greatly reduce the impact of variation in incident light. Kokaly & Clark (1999)

describe an alternative method of band depth normalisation; dividing the depth of each continuum-removed waveband by the depth at the feature minimum. This results in the minimum being equal to one at all times and will mask any correlation with a causative factor in the vicinity of the feature minimum. This method does, however, preserve the shape of the feature and may be of use for analysing overlapping features or changes at the shoulders of absorption bands.

1.7.2. Ratio analyses.

Chappelle *et al.* (1992) used the 'ratio analysis of reflectance spectra' (RARS) to analyse the reflectance spectra from the detached leaves of soybean (*Glycine max*) plants grown at three levels of nitrogen nutrition. The mean of twenty spectra from high nitrogen leaves was divided by the mean spectrum from the same number of medium-nitrogen leaves. The ratio analysis amplified the differences in reflectance due to nitrogen-induced pigment concentrations and was designed to identify the absorption peaks of the various pigments. Their ratio was multiplied by one hundred, presumably because the authors felt that percentage results were more intuitive than fractional values. Pre-multiplication of the numerator would achieve the same outcome and reduce the possibility of rounding errors where spectra converge. The ratio analysis method would be applicable to other (e.g. stress-induced) spectral response features, although plotting multiple comparisons on a single chart would lack clarity. Continuum removal and ratio analyses are perhaps best suited to the analysis of a small number of groups or treatment levels.

Carter (1993) subtracted the reflectance spectra from leaves of unstressed control plants from spectra of leaves from plants subjected to stress factors. The reference spectrum is, in effect, a continuum and subtracting this from the target spectrum may cause a displacement of absorption features as noted by Clark & Roush (1984). The difference between control and treatment spectra would be sensitive to changing illumination levels and Carter

conducted his experiments in the laboratory under controlled conditions. Carter (1994) extended the method by dividing the difference between spectra by the mean at each waveband to determine the sensitivity of the spectral response to stress factors.

1.7.3. Correllograms.

The correllogram is a plot of correlation (r , the Pearson moment) or the coefficient of correlation (R^2), of a factor against individual elements, in this case nematode infection against reflectance at each waveband. Examples of correllogram application to remote sensing can be found in the papers of Blackburn (1998), Datt (1998) and Thenkabail *et al.* (2000).

The correllogram would appear to be an ideal method of selecting candidate wavebands for a PCN-specific detection algorithm. Some caution is required, however, as correlation is not proof of cause and effect. Blackburn (1998) found a strong correlation between caretenoid concentration and red reflectance, even though caretenoids do not absorb red light (Lichtenhaler, 1987). Blackburn attributes this spurious result to a similar distribution of carotenes and chlorophyll, which does absorb red light. Many factors influence the amount and distribution of light reflected from a plant canopy (Gates, 1965; Knibling, 1970) and similar pseudo-results cannot be excluded. Indeed, Datt (1998) used the correlation between biomass and NIR reflectance to correct one such effect, to decouple leaf area from chlorophyll absorption to determine chlorophyll concentration.

1.7.4. Principal Components Analysis.

Essentially a classification/visualisation method, principal components analysis (PCA) uses a covariance or correlation matrix to determine the direction (eigenvector) of the greatest variability (eigenvalue) within the data set. Principal components are calculated in decreasing order of variance and plotted as orthogonal to each other. The first principal plane will plot PC1 along the X-axis and PC2 on the Y-axis when displayed in cartesian

form. In this arrangement, PC1 represents a linear regression line through the data and PC2 contains the scatter around that line (Mather, 1999).

Although PCA can enhance and separate elements of the data, it is clearly driven by the range and distribution of values in the current data set. It is therefore questionable whether PCA can be employed as a predictive method where random objects might be present in the image (e.g. buildings, roadways or water) and might influence the transformation parameters applied to the vegetation reflectance.

1.7.5. Empirical data transforms.

The tasselled cap transformation of Kauth & Thomas (1977) is a re-orientation of the first principal plane describing a pixel in n-space. Although the transform is similar in operation to the output stages of a principal components transform, the matrix parameters are pre-determined and specific to the waveband configuration of the instrument used (Mather, 1999). A pixel measuring reflectance from a vegetated target will migrate from a position at the lower left of the plane (wet, bare soil pre-planting) to a peak near the upper left (maximum biomass) before declining to the lower-right of the plane (dry soil, post harvest). The path described by a pixel throughout the vegetative cycle resembles the 'tasselled cap' after which this transform is named. Although the tasselled cap transform is 'universal', interpretation should take local atmospheric and soil conditions into account and Mather (1999) suggests that coefficients for a tasselled cap transformation should ideally be calculated with data from the area of study. Jackson (1983) concluded that the vegetation (greenness) parameter of the tasselled cap transform was sensitive to soil background effects.

1.7.6. Derivative analyses.

Derivative analysis measures the rate of change across the range of recorded wavebands and this is a particularly sensitive way of comparing the margins, or 'shoulders' of an

absorption feature. A change in these dimensions can be used to record minor variations in spectral reflectance or segregate overlapping spectral absorption from multiple sources (Dixit & Ram, 1985). Derivative spectra are commonly used to suppress background signals (Rollin & Milton, 1998) and, as demonstrated by Demetriades-Shah *et al.* (1990), near-linear background effects (e.g. soil) are reduced to a constant by first-order differentiation and largely eliminated from the second derivative. Hyperspectral spectra are recorded as a series of discrete signal values attributed to the nominal waveband centres of the recording instrument. The first derivative is therefore calculated as the change in signal strength between adjacent wavebands divided by the waveband interval (Mather, 1999). The second derivative measures the change in the preceding derivative across the waveband intervals and describes the 'change in the rate of change'.

Noise in spectral data is defined as sensor response not related to the target radiance (Campbell, 1996), and derivative methods become increasingly sensitive to noise at higher derivative order (Dixit & Ram, 1985). Care must be taken to determine a suitable filter algorithm as the method and degree of smoothing can modify both the position and magnitude of peak correlation (Rollin & Milton, 1998). Demetriades-Shah *et al.* (1990) found polynomial smoothing over a 24nm bandwidth to result in the highest mean signal-to-noise ratio for vegetation. This may, however, have been specific to their experiment as the optimum differentiating interval was said to have been dependent upon the amount of noise and the spectral resolution of the data.

1.8. Related studies.

1.8.1. General plant stress papers.

A large number of experiments have been conducted to measure changes in reflectance due to plant stress factors, although many studies reported on pathogens that exert a direct influence on leaf colour and reflectance e.g. blight (*Phytophthora infestans*) while others

measured crop biophysical parameters (e.g. leaf area) common to many growth-limiting factors.

Peterson & MacDonald (1996) investigated the spectral response of potato cv. Russet Burbank to limited availability of the macronutrients nitrogen (N), potassium (K) and phosphorus (P), by measuring the reduction of near-infrared and short-wave infrared reflectance plus the first derivative position at the red edge. Some variation in the reflectance ratio of the green, red and NIR bands was noted, although not confirmed as significant, and the authors were unable to distinguish between the spectral response due to deficiencies in N, P or K.

1.8.2. Root pathogen studies.

Damage caused by pathogens which have an indirect, or systemic, influence on the above-ground plant components can be identified only by the symptoms that they induce in the haulm. Take-all (*Ophiobolus graminis*), a root-rot disease of wheat, was discernible from aerial photographs and this was linked to soil conditions by Brenchley (1968). Blakeman (1990) also reported that take-all (now known as *Gaeumannomyces graminis*) could be identified from aerial photographs, although the link between pathogen and photograph was not discussed.

Johnson *et al.* (1996) observed reduced canopy development and lower chlorophyll concentrations in grape vines infested with the root-louse phylloxera (*Daktulosphaira vitifoliae*). Aerial images from a CASI spectrometer (ITRES Research, Calgary, Canada) and aerial infrared photography were found to be valuable for the management of phylloxera infestation, although their NDVI results appear to be closely related to canopy development in the widely-spaced crop. Johnson (1999) discussed laboratory reflectance measurements from the same experimental crop and found higher reflectance at 550nm,

plus a *c.* 3nm reduction in the red edge inflection point at the higher infestation level when compared to the leaves of lightly infested plants. Spectral reflectance measurements were not, however, judged to be suitable for the detection of 'pre-visual' phylloxera infestation.

1.8.3. Nematode reflectance studies.

Brenchley (1968) related nematode (*Trichodorus* spp. or *Longidorus* spp.) damage in sugar beet (*Beta vulgaris*) to light tones on panchromatic photographs. Infestation was, however, associated with soil type and conditions and may not have been the primary cause of the tonal changes. Lighter tones indicate increased reflectance from the infested crop. The spectral sensitivity of the film was not stated and the wavelengths at which reflectance was measured could not be ascertained from their paper.

Heald *et al.* (1972) observed that growth difference in mature cotton (*Gossypium hirsutum*) infested by the nematode *Rotylenchulus reniformis* was clearly visible on infrared photographs (Kodak Ektachrome 8443 film) at 61 days after planting (DAP) and, while not apparent from a visual inspection of the crop, nematode damage was detectable from infrared photography at 111 DAP. Areas of reduced crop growth appeared as lighter tones (indicating higher reflectance) in their images. By contrast, however, Gausman *et al.* (1975) measured the reflectance of detached leaves and whole canopies of cotton plants infested with *R. reniformis* and found that reflectance was reduced by infestation across the entire 500-2500nm spectral range.

Bouman *et al.* (1992) recorded the green (548 or 550nm) and near-infrared (823 or 850nm) reflectance from the crop canopies of potato cv. Bintje (uninfested) and cv Darwinia (infested with an unspecified 'severe' density of *Globodera pallida*). The authors did not set out to compare infested and uninfested canopies, and accurate comparison would have been confounded by their experimental methods. Reflectance measurements were

collected from different cultivars in different years, using different instruments and from two separate sites. Soil reflectance from the Darwinia experiment was higher than from the Bintje location, although both soils were reported as 'sandy humus'.

Green reflectance from both experiments was largely invariant throughout canopy development and senescence and the authors attribute this to the similar reflectance levels of soil and canopy in the green waveband. Near-infrared reflectance closely tracked the rise and decline of the canopy ground cover, although infested plants reflected less (*c.* 50% against *c.* 70%) near-infrared radiation. The authors conclude that the weighted difference vegetation index (WDVI) (Clevers, 1989) was an accurate method of assessing percentage ground cover of the crop. Green (near-invariant) reflectance was substituted for red in their WDVI calculations and it is apparent from the figures provided that near-infrared reflectance was primarily responsible for the success of this index in tracking canopy extent.

Haverkort & Schapendonk (1994) observed that infection by potato cyst nematodes reduced canopy development and infra-red reflectance to a greater degree than drought. No details of cultivar, species or infestation levels were presented. Haverkort & Trudgill (1995) refer to the Haverkort & Schapendonk experiment and state that leaf area and reflectance were halved by PCN infestation in both irrigated and non-irrigated plants.

Spectral reflectance of potato crops infested with PCN was investigated in a preliminary experiment by Heath *et al.* (1999) and by Stephens *et al.* (2000). Both studies reported the relationship between NDVI and nematode numbers present in the soil. Heath *et al.* used an ASD Fieldspec FR spectrometer and reported an R^2 of 0.825 between NDVI and eggs g^{-1} soil of PCN from a field experiment and R^2 of 0.866 from a concurrent pot experiment.

Stephens *et al.* (2000) mounted two digital cameras in a light aircraft which recorded radiance from the crop canopy at 640nm and 840nm. The ratio index NDVI was correlated (R^2= 0.88) with nematode density, although this was measured as cysts per 100g of soil. The authors state that cyst contents are highly variable (200-600 eggs/cyst) and counting cysts (rather than eggs) would introduce a further element of uncertainty to the PCN assay.

Nutter *et al.* (2002) measured reflectance from soybean (*Glycine max*) crop canopies infested with the nematode *Heterodera glycines* at pre-planting (Pi) levels ranging from zero to more than 10,000 eggs 100cm $^{-3}$ soil (approximately 77 eggs g^{-1} soil at an assumed soil density of 1.3). Reflectance measurements were collected from the ground using a field radiometer (Cropscan Inc, Rochester, MN), from the air (visible and near-infrared film) and from space (Landsat 7). The authors report their results solely from the 810nm (near-infrared) waveband and do not mention their measurements at other wavebands. Reflectance measurements were correlated (ground R^2= 0.48, airborne camera R^2= 0.33) with nematode density from 995 2x3 meter crop quadrats. Landsat 7 satellite images (band 4, 750-900nm) were better correlated (R^2= 0.58) with nematode density, although sample areas were aggregated (N=16) due to the larger (30m) pixel dimensions of the Landsat image. Aggregating sample areas by infestation categories might have improved their correlation from field and airborne reflectance data by reducing the influence of general crop heterogeneity. A chart plotting the difference in reflectance from zero and high infestation sample areas with time indicates that the maximum discrimination occurred at *c.* 80 days after planting and, while canopy development is not mentioned, this may have been coincident with near-complete canopy cover as the plotted difference curve appears similar to that from a crop growth cycle.

Lawrence *et al.* (2002) state that the normalised difference vegetation index (NDVI) was under evaluation for the detection of the reniform (*Rotylenchulus reniformis*) nematode in

fields of cotton (*Gossypium hirsutum*). The authors suggested that hyperspectral remote sensing data may prove valuable for future developments in variable-rate nematicide application.

Wheeler & Kaufman (2003) investigated the spectral reflectance of cotton infested with *Meloidogyne incognita* using a single airborne 35mm camera. The film used was Kodak Ektachrome Infrared EIR and a Tiffen 62M filter was fitted to exclude blue wavelengths. This configuration recorded radiance from green to near-infrared wavelengths. Photographic images were scanned into digital format and the red, green and blue pixel values recorded as the digital numbers (DN, 0-255) for near-infrared, red and green reflectance. Waveband centres, bandwidth and waveband-overlap were not reported. The authors investigated individual wavebands, simple waveband ratios and NDVI, but found a poor and inconsistent relationship with nematode burden (eggs and juveniles per $500cm^{-3}$ soil).

Wheeler & Kaufman, however, compared reflectance with the final nematode population (Pf). Multiplication of PCN is strongly dependent on the initial population level (Haydock & Evans, 1998b) and equivalent Pf levels may have derived from widely differing multiplication rates in the host crop should *M. incognita* exhibit similar density-dependent population dynamics to PCN. The level of detail given was insufficient to determine whether the spectral resolution of their method extended into other, possibly contrasting, waveband regions masking or confounding the spectral responses they sought to identify.

The nematode reflectance studies listed above used near-infrared wavebands, or ratios and indices (NDVI) which are sensitive to near-infrared reflectance. Such analysis methods are sensitive to crop cover and biomass (Baret & Guyot, 1991; Haverkort *et al.*, 1991) and therefore, to any stress factor which reduces plant growth. It appears unlikely, therefore,

that a causative factor can be identified from reflectance methods which are sensitive to a wide variety of plant stress factors.

1.9. Conclusions.

Potato cyst nematodes are a yield-limiting and economically-damaging problem for commercial potato growers. Effective management strategies are essential to maintain yield, limit the further dissemination of PCN and to ensure the future viability of infested land. An improvement in current sampling methods is required to expedite the extension of precision farming methods to PCN management and to enable growers to restrict, or reduce, PCN populations while meeting the demands of major retailers.

The patch or modulated application of granular nematostats is not recommended (Parker, 1998) as low initial populations can, if untreated, result in very high multiplication on non-resistant cultivars (Evans & Stone, 1977; Phillips & Trudgill, 1998). Supplementary control measures however, (e.g. fumigant biocides, trap cropping or biological control) appear to be more amenable to localised application, but only where the within-field distribution of PCN has been determined to a sufficiently detailed level.

The collection and processing of bulk soil samples does not give an indication of the distribution of PCN within the sample area (Evans *et al.*, 2000). A large number of individual samples must be collected and processed separately in the laboratory in order to gain detailed knowledge of a population distribution (Riding & Parker, 2000). The application of spectral analysis to the mapping of PCN infestation would allow growers to target post-harvest fumigant nematicide application, or to trap-crop discrete areas for the removal of developing foci.

Damage to infested crops, thought to have been caused by nematodes, has been detected from ground and airborne reflectance measurements. Reports in the literature reviewed were, however, unable to discriminate between nematodes and other crop-stress factors and are best suited to the direction of conventional soil sampling methods. A nematode-specific remote sensing method might reveal the heterogeneity of infestation within fields and enable agronomists to track population movement across subsequent rotations.

Of the PCN-induced effects on the potato canopy from the literature reviewed, water has (leaving aside obvious wilting symptoms) the potential to affect turgour and near-infrared reflectance. Reduced water uptake appears to be offset by a reduction in transpiration and reports of leaf water content were mixed in the papers reviewed. Nitrogen (N) has a considerable effect on leaf colour (Steven, 1985; Buschmann & Nagel, 1993), however no consistent effect of PCN on haulm nitrogen concentration is apparent from the literature. Reported nitrogen levels did not fall below the recommended leaf concentration levels (3%) of Ulrich (1993).

Potassium (K) was the element most frequently described as reduced by infestation, and the symptoms of K deficiency appear to be restricted to reduced transpiration. Some interactions between N and K were noted (Trudgill, 1980; Grove *et al.*, 1999), and it would seem that sufficient K is required for the uptake of N. Some effect on leaf colour may therefore be indirectly linked to the amount of potassium available to the plant. Phosphorus deficiency was reported as having very similar foliar symptoms to PCN-infestation and leaves are stunted and darker green (Ulrich, 1993). Several papers (e.g. Trudgill *et al.*, 1975a; Trudgill, 1980; De Ruijter & Haverkort, 1999; Grove *et al.*, 1999) report the potato haulm concentration of phosphorus to have been reduced by PCN infestation, and that this was possibly limiting to plant development.

Conventional vegetation indices, measuring the ratio between reflectance at red and near-infrared wavebands, appear to be poorly suited to the discrimination of PCN-induced stress from other pathogens present in the field. The availability of hyperspectral reflectance data will offer the opportunity to compare minor spectral response features which would not be readily apparent from the broad-band reflectance data.

Pattern analysis, hinted at by Brenchley (1968) and comparison of multi-temporal images may help to discriminate between stress factors if a) the background variability is sufficiently low to determine the pattern accurately b) the infestation is sufficiently localised and c) multi-temporal images can be obtained reliably and under suitable weather conditions. Nutter *et al.* (2002) note that temporal patterns may be distinct indicators of nematode infestation while Been & Schomaker (1996) found developing foci of PCN to have a characteristic elliptical shape, elongated in the direction of cultivation. The collection of multi-temporal images may be hindered by a maritime climate and pattern recognition will require both a clear spectral distinction between infested and other crop areas and a localised infestation.

Brown (1969) found substantial yield losses due to nematode infestation at levels which were insufficient to produce obvious symptoms in the haulm. Post-cropping (Pf) populations can reach 50 eggs g^{-1} soil where PCN had been undetectable before planting (Evans *et al.* 1998). This multiplication will have occurred within the roots of the current crop suggesting that, while low levels of PCN infestation are unlikely to be detectable by remote sensing, previously undetectable foci might induce sufficient stress in the plant to make spectral analysis a suitable method for the early location of new and developing infestations. It may then be possible to eradicate or substantially reduce these new foci and thereby limit the spread of infection to other areas of the farm or field.

1.10. Aims and objectives.

The aim of this study was to develop a spectral assay for the detection of PCN infestation using remote sensing of light reflected from the canopy of commercial potato crops. A combination of field and glasshouse experiments were designed to address the following objectives:

- To undertake a preliminary analysis of the wavelengths, ratios and derivatives most likely to describe PCN infestation;
- disprove the null hypothesis that "potato cyst nematode infestation does not produce a measurable change in reflectance from the canopy of infested plants;"
- characterise and describe the relationship between PCN infestation and canopy reflectance;
- relate the symptoms of PCN damage to aerial or satellite images for wide area survey;
- produce recommendations for the design and configuration of a device for the practical application of spectral measurement to the assay of PCN infestation.

Initial experiments focussed on establishing a relationship between reflectance at individual wavebands and nematode burden. Reflectance measurements were collected from the canopy of lightly and heavily infested plants of a field and a glasshouse experiment using a field spectrometer. The correlation between root invasion and spectral reflectance was plotted for each waveband in order to identify candidate wavebands for further analysis.

The method was subsequently extended to airborne remote sensing. Ratios between suitable wavebands were calculated and these were applied to airborne spectral images collected from the canopy of commercial field crops. Further field experiments investigated the potential use of satellite remote sensing for the detection of PCN infestation.

A glasshouse experiment was designed to differentiate between the spectral response of potato plants infected with the fungal pathogen *R. solani* with reflectance from plants infested by PCN. Recommendations for the design and configuration of a device for the practical application of spectral measurement to the assay of PCN infestation are reported in chapter seven.

2. 2000 Field Experiment.

2.1. Introduction.

An extensive field experiment was conducted in this, the first year of the investigation, to determine suitable waveband regions for use in subsequent airborne and satellite assessments. High resolution spectral reflectance measurements were collected from individual plants using a field-portable spectrometer and compared with nematode population density in the plant root system (section 1.1.8.4.2). The correlation between spectral reflectance and nematode burden was plotted for each waveband (Blackburn,1998; Datt, 1998) and wavebands selected for their potential to determine infestation of the potato crop by PCN.

Additional measurements were collected using a hand-held chlorophyll meter (Hydro-Agri, Immingham, UK).

2.2. Objectives.

1) To provide a detailed comparison of the amount and composition of light reflected from heavily and lightly PCN-infested potato plants;
2) identify specific wavebands, waveband ratios and spectral regions for the development of further experimental methods;
3) assess the potential of a spectral assay for the identification of potato cyst nematode infestation.

2.3. Materials and methods.

2.3.1. Experiment and preparation.

2.3.1.1. Experimental site.

The experiment was located in Fourgates field, Edgmond, Shropshire (Ordnance Survey grid reference SJ707195). The field is of well drained, sandy loam with a slight (2-3°) slope to the west. No trees or field margins were within 50m of the experimental area. A wide range of PCN population density was considerd to be an important factor for determining the spectral response of potato plants to PCN infestation. The experiment location had been used for PCN trials in the two years prior to this experiment and PCN population density ranged from 3 - 450 eggs g^{-1} soil (final population (Pf) from a co-located 1999 experiment).

2.3.1.2. Design and layout of the Four Gates field experiment.

A single rectangular block was allocated for this experiment, measuring 36m east-west and 12.8m north-south (10 beds). The block was divided by a lateral track, 6m wide, and by a set of tramlines at the third-bed from the northern margin. The experimental area was bounded to the north by a track, separated by one guard-bed of potatoes, and to the south by a second set of tramlines. Eastern and western boundaries were formed by a 1m discard area to adjacent potato beds.

The experimental area was divided into twenty-four, 5m x 2 bed plots, twelve to the east of the lateral track, and twelve to the west (Fig. 2.1.). This gave sixteen, 15m beds containing thirty-two 15m rows (excluding tramlines). Slight differences in spacing led to the discarding of plants adjacent to internal plot boundaries. Discard rows resulted in an uneven number of active rows per plot, eighteen plots having three active rows and the six remaining plots with four rows (Fig 2.1.).

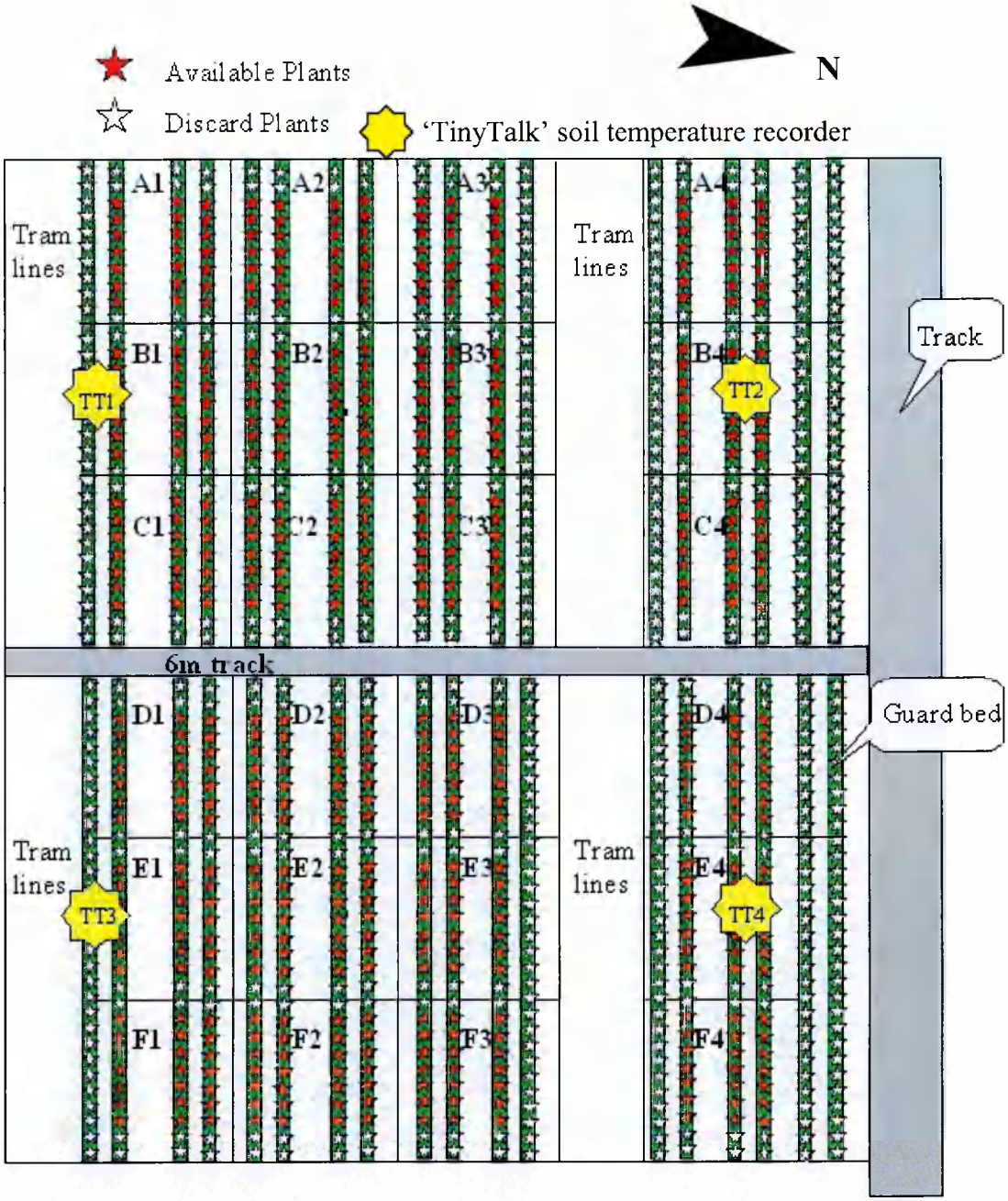

Figure 2.1. Layout of the Four Gates field experiment. Not drawn to scale. Plots are 5m in length (E-W) and 3.66m (two rows) wide.

2.3.1.3. Potato seed tubers.

Seed tubers (Desirée VTSC1 35-45 cm) were chitted in trays under 24 hour artificial light from April 13th, 2000. A heater was set to prevent the ambient temperature falling below 10°C. The chitted seed tubers were hand planted on May 11th, 2000 using a template to ensure accurate spacing of 30cm centres, selected to facilitate root separation when lifting to test for nematode root invasion. A hand planting device was used to ensure an even planting depth of 15cm (Plate 2.1.).

2.3.1.4. Monitoring and agronomic inputs.

2.3.1.4.1. Determination of existing soil nutrient status.

Soil samples were collected for NPK determination on April 20th, 2000. Four samples were taken from each bed at 1m spacing using a 1" (25.4mm) corer to 30cm depth. Two-thirds of the sample volume was frozen for N analysis and the remaining third air-dried for P and K analyses. The experimental area was accidentally treated with nitrogen on May 15th, 2000 and fresh soil samples were collected on May 19th. Four samples were taken from each plot to a depth of 30cm, one metre diagonally inward of the plot vertices.

2.3.1.4.2. Laboratory analysis of soil nutrient content.

Laboratory analyses of soil nutrient status were conducted according to standard methods (MAFF, 1986). Available nitrogen content was determined by Kjeltec steam distillation on May 22nd, 2000 (method 53). Nitrogen (N) ranged from 100 Kg/ha to 223.6 Kg/ha. Potassium (K) was measured by atomic absorption spectrophotometry (AAS) (Thermo Jarrell Ash Smith-Heiftje 1000 Atomic Absorption Spectrophotometer) at 404.4nm (method 63) and found to range from 405 to 533 ppm. Magnesium (Mg) was also measured by AAS, but at a wavelength of 202.5nm (method 40) and found to vary between 61 and 161.45 ppm. Soil pH was broadly neutral, ranging from 6.2 to 6.55 as measured from individual plots using a Russell RL 150 pH Meter (method 32). Laboratory analysis of the field plot samples for P content was carried out using a Beckman DU-600 UV/VIS flame spectrometer at 880.0nm on August 8th, 2000. Phosphorus ranged from 177.2 to 261.6 mg/l with an average of 207.86.

2.3.1.4.3. Agronomic inputs.

Agronomic inputs were applied to standard commercial practice (MAFF, 2000) and no nematicides were used. Nitrogen, as ammonium nitrate (NH_4NO_3), was hand-applied to individual plots on May 25th, 2000, to normalise to a target rate of 200 Kg/ha. Plot C1 was already at 209.3 Kg/ha and plot F2 at 223.6 Kg/ha due to the accidental application of nitrogen on the experimental area by Harper Adams Farm workers on May 15th, 2000. Supplementary potassium was also added to individual plots by hand spreading on May 25th, 2000. The target rate being 160 Kg/ha of K_2O. No correction for phosphorus (P) was applied, as the fertiliser would not have become available to the plants during the experiment duration (P. Beckwith, personal communication). Existing phosphorus was at a high level (index 7-8) and not limiting . Existing Mg ranged from 60.99 to 161.45, with an average of 125.06 (index 1-2) and no additional Mg was applied.

2.3.1.4.4. Soil temperature and soil moisture deficit (SMD).

Four 'Tinytalk' temperature dataloggers (Gemini Data Loggers UK Ltd, Chichester, West Sussex) were located in the centre of the outside beds (Fig 2.1.) and buried at a depth of 15cm. Soil temperatures rose to 18-20°C during early May, then fell back to 12-14°C in the third and fourth week of May, remaining low (14-16°C) until the middle of June. Peak soil temperature rose to 23-24°C during the third week of June before falling back to 14-18°C from the 22nd of June to the end of the experiment.

Soil moisture deficit (SMD) was assessed by weight. Soil samples were collected at 5pm on June 19th 2000, taking four cores from each plot, using a 1" (25.4mm) auger to a depth of 30cm. Soil samples were transported in polyethylene bags, weighed within one hour of sampling then transferred to metal drying containers. The samples were placed in a drying oven at 105°C for 24 hours, then re-weighed to establish soil moisture content. The dried

soil was passed through a 4mm sieve and stone weight subtracted from the sample weights to prevent variable stone content affecting the moisture calculations.

2.3.1.4.5. Plant canopy assessment.

Plant canopy development was assessed on June 21st, 2000 (41 DAP), by taking the mean of two horizontal measurements at right-angles across the plant canopy with a tape measure.

2.3.2. Selection of plants for spectral and nematode analysis.

A subset of plants for analysis ('tag plants') was chosen by stratified random selection of plants within rows, and grouped by plot boundaries. Rows contained twelve available plants in each of the end plots, and thirteen in the mid-plots. A Genstat pseudo-random number algorithm (checked for normal distribution and rounded down to integer values in Excel) was used to select four plants from each row of every plot, starting at plot 'A1'. Plants were selected by row number using the next number from the sequence that did not duplicate an existing plant. Plots and rows were processed in alphabetical and numerical order:

This procedure resulted in the selection of 312 plants from the 962 available, distributed evenly across the experimental area, although the selection was random within the plot rows (Fig. 2.2.). Each plant was marked with a plastic tag bearing the plot number, row number (Counting from the left from the centre track) and plant number (counting away from the centre track). Identification tags were located in the soil, away from the spectrometer's field of view.

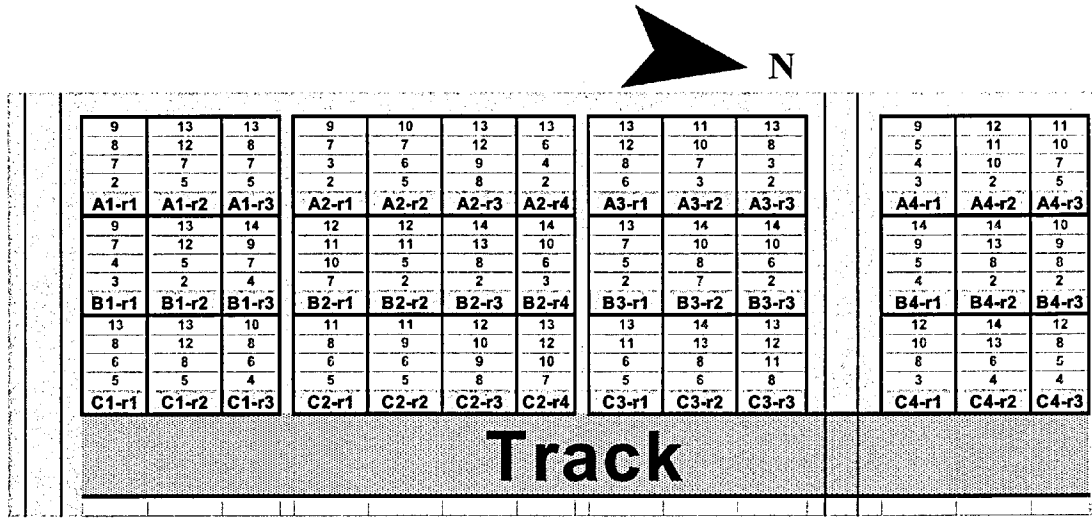

Figure 2.2. Schematic diagram listing selected 'tag plants' from the western section of the Four Gates field experiment.

2.3.3. Spectral readings.

Spectral readings were collected using a GER 1500 spectrometer, Serial No. 2039B (Geophysical and Environmental Research Corporation, Millbrook, NY) and each reading was immediately followed by a reference scan of the Spectralon (Labsphere, North Sutton NH) reference panel (Serial No. srt1011). The spectrometer head was mounted on a photographic tripod, and a 'bullseye' spirit level was placed on the spectrometer to verify that it remained vertical for each reading (Plate 2.2.). The operator stood opposite the solar azimuth, wearing dark clothing and operated the spectrometer via a laptop computer.

A random number sequence was created in Genstat and rounded down to integer values in Excel. Groups of three plots (a logical sampling path) were selected from a numeric value assigned to the entry plot. The order of each sampling session was determined by following the sequence of random numbers, ignoring within-session duplicate values (i.e. not the same plot twice in one session). This selection process was repeated to produce further random sequences for subsequent recording sessions.

Spectral reflectance readings were collected between 10:00 and 15:00 UTC on June 24th and June 25th, 2000 – 44 and 45 days after planting (DAP). Sky conditions remained

overcast throughout. The first random sampling sequence was used on July 24th, and the second on July 25th. Plots D3, E3, F3 and D4, E4, F4 were imaged on both days and the mean of both readings was applied to all subsequent analyses of these plots.

Plate 2.1. Hand planting the Four Gates field experiment.

Plate 2.2. GER1500 spectrometer positioned over a target plant of the 2000 field experiment.

2.3.4. N-Meter readings.

A Hydro N-Meter (Hydro-Agri (UK) Ltd, Immingham, Lincs) was used to record reflectance values from the field trial tag plants on June 14th and 15th, 2000 (34 and 35 DAP). This device is designed to measure chlorophyll content of the leaves and predict nitrogen requirements of cereal crops. Analysis is of spectral absorption or transmittance from a small area of leaf enclosed between two detector lenses, although the exact method and wavebands remain confidential.

The mean of thirty readings was recorded from each tag plant, selecting leaves fourth from the top of the canopy and taking readings from several areas of each leaf.

2.3.5. Harvest and processing for nematode analysis.

Three hundred and twelve 'tag' plants were harvested on June 26th, 2000 at 46 DAP. The soil ridge between plants was separated with a spade and the plants were carefully lifted and placed in plastic bags, together with the relevant plastic marker tag and *c.* 50ml of water. Plants were then placed in a cold store at 4°C prior to preparation for nematode root invasion estimation.

Plants were removed from the cold store in batches of ten and processed for root invasion analysis. Heavily infested plants were processed first to preserve cysts which were visible on the exterior of the roots and which might be lost from the samples. One sample from each plant was analysed for invasion of juveniles to the roots according to Hooper (1986). Three counts were made from the first 146 samples to reduce the error associated with sub-sampling. Analysis of these counts indicated that this approach was not productive and that the results were highly correlated (R^2=0.9 between any two counts). A single count was made from the remaining samples.

2.3.6. Harvest for yield assessment.

Four plants, closest to the centre of each plot, were harvested for yield measurement, on September 12th, 2000 at 124 DAP, avoiding plants where the next plant had been harvested before. The tubers were washed and allowed to air-dry prior to weighing.

2.4. Results.

2.4.1. Experiment preparation and monitoring.

2.4.1.1. Emergence.

All plants emerged by June 13th, 2000 (34DAP). Some plants from heavily infested plots E2 and A3 were just visible, while canopies of less infested plots had closed in the rows six days earlier (Plate 2.3.).

2.4.1.2. Soil moisture.

Soil moisture at the end of four hot, dry days (June 19th) ranged from 10.85% to 15.85% by weight. (field capacity = 22.7 %, I. Grove personal communication) There was a slight (R^2=0.25) positive correlation with root invasion – heavily infested plots had greater soil moisture, possibly due to reduced transpiration from the smaller canopy of infected plants (Plate 2.3; Plate 2.4.).

2.4.1.3. Assessment of nematode burden.

The concentration of nematodes found to have invaded the roots of experimental plants was between zero and 6,350 juveniles g^{-1} root (mean 1737). Cyst nematodes have a limited motile range and are essentially static in the soil unless moved by external forces (Been & Schomaker, 1995), and root invasion of individual plants varied considerably within the experimental plots. Standard errors of mean root invasion per experimental plot ranged from 59.47 to 473.27, with an average of 211.43.

Plate 2.3. Heavily infested plants of plot E1 at 28DAP. The canopy from plants of less infested plots was closing within the rows at this time.

Plate 2.4. Elevated view of the 2000 experimental area at the conclusion of the experiment.

2.4.1.4. Canopy development.

A strong (F= 242.93, p <0.001, $R^2_{(4)}$=0.98) correlation was found between the recorded root invasion (grouped by 1,000's) and plant canopy diameter, indicating that the selected measure of nematode-induced plant stress is closely reflected in actual plant performance (Fig. 2.3.).

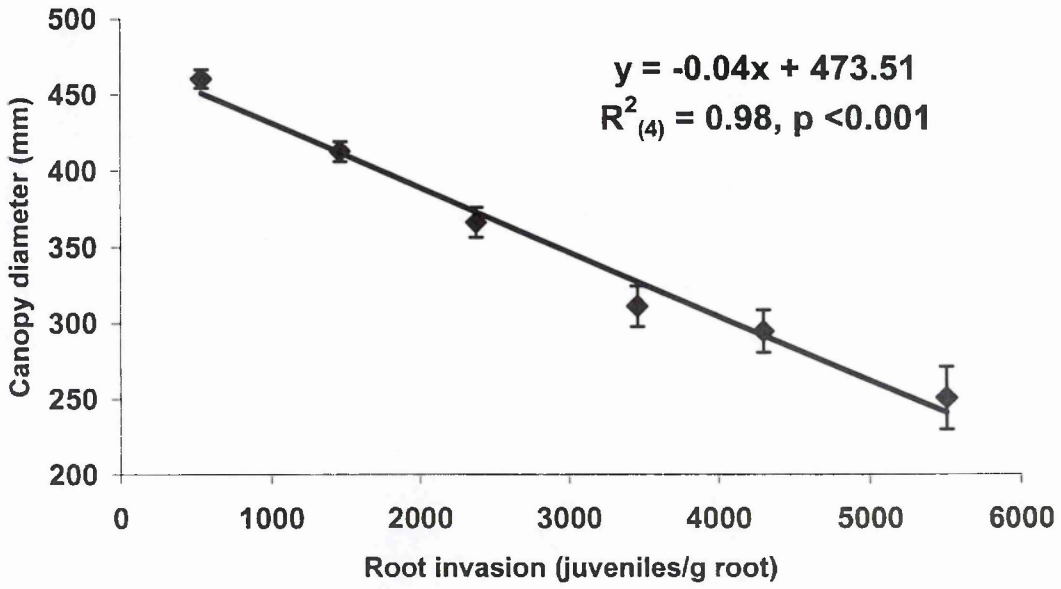

Figure 2.3. Plant canopy diameter, as influenced by nematode burden ± SEM.

2.4.2. Yield.

Yield (measured from 4 plants per plot) ranged from 8.17 to 83.9 tonnes/ha. The mean root invasion from individual plots was correlated ($F_{(1, 22)}$= 70.52, p < 0.001, $R^2_{(22)}$ =0.76) with final yield (Fig. 2.4.).

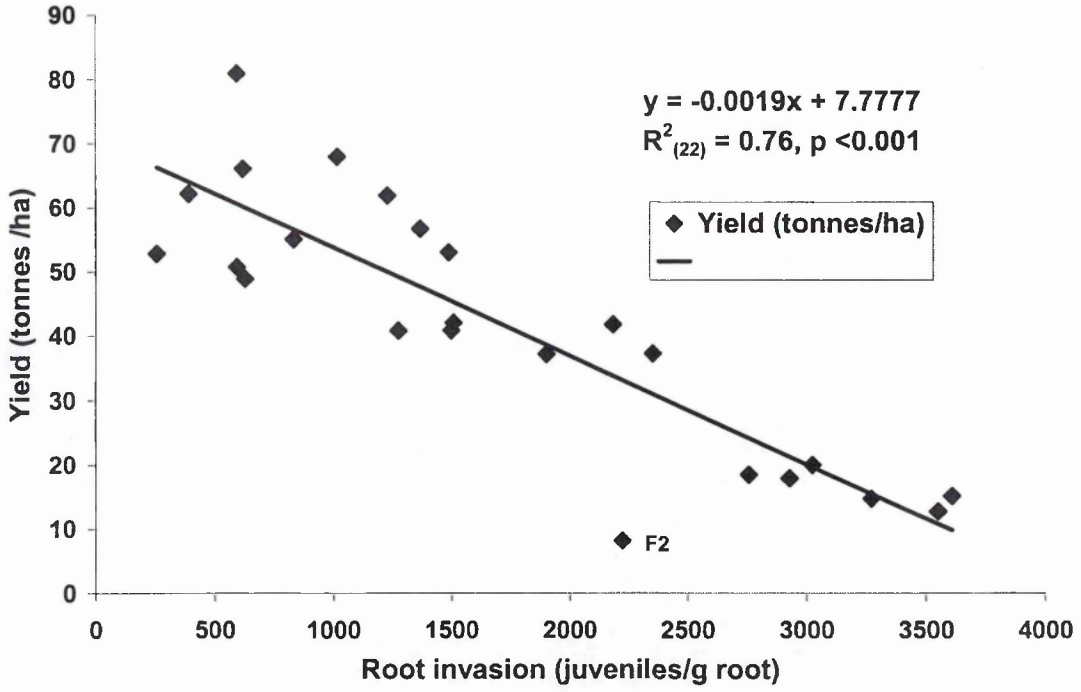

Figure 2.4. Correlation of root invasion with final yield per plot. The low outlier, Plot F2 (not excluded), was an area of two halves and yield plants, closest to the centre of the plot, may not be representative of the tag plants from all plot rows.

2.4.3. Spectral measurements.

Plants were sorted into ascending order of root invasion (juveniles g^{-1} root) and aggregated into six groups, each group having an invasion count range of 1000, e.g. 0-999, 1,000-1,999. This grouping process was designed to reduce the variability of spectral reflectance from individual plants. The correlation (r) between root invasion and spectral reflectance was then plotted for each waveband (Fig. 2.5.).

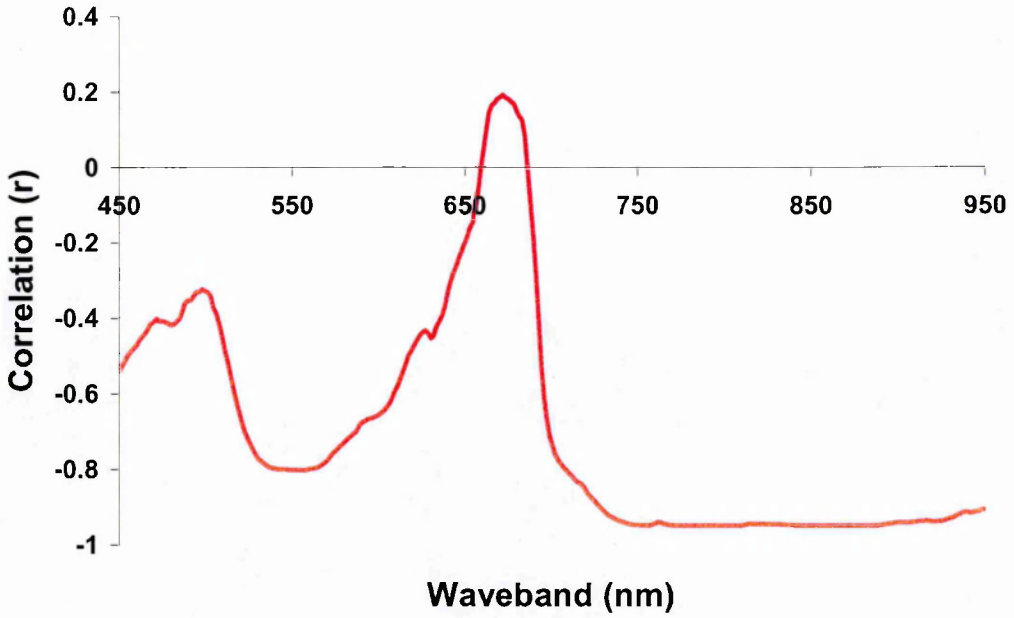

Figure 2.5. Correlation (r) of reflectance with root invasion (1000's) from the GER spectrometer data.

This method of depiction, referred to as a 'correlogram' (Blackburn,1998; Datt, 1998) was used to identify wavebands best suited to further analysis. The pattern of correlation between root invasion means (grouped by 1,000's, N=6) and reflectance was similar when comparing mean values for each plot (N=24) (Fig. 2.6.).

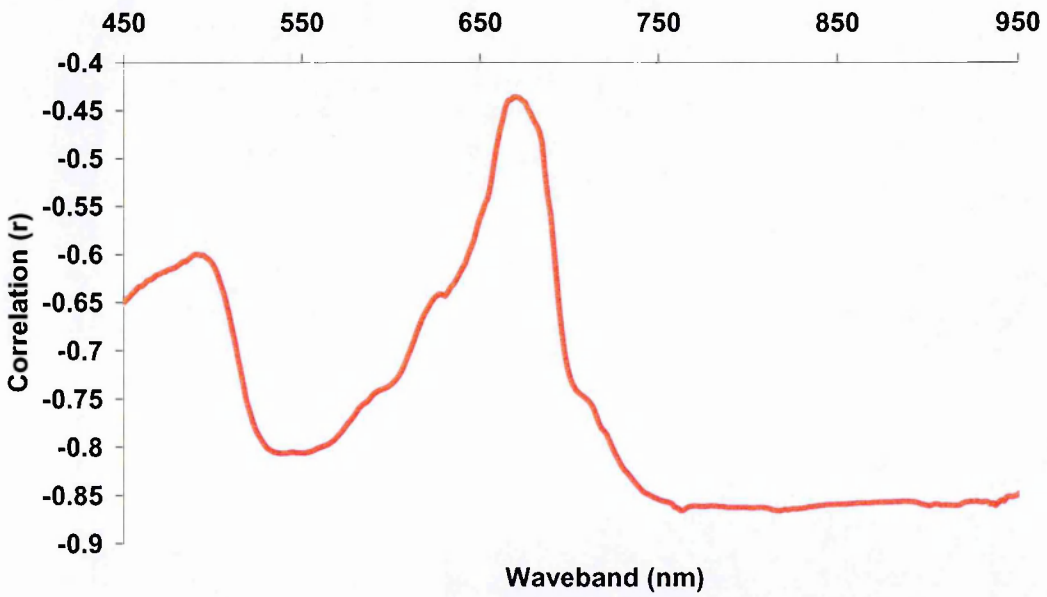

Figure 2.6. Correlation of spectral reflectance with root Invasion (juveniles g^{-1} root). Means of experimental plots (N= 24)

The ~675nm region was least correlated with nematode infection, while regions ~550nm and ~760-900nm were negatively correlated. The wavebands 551.5nm, 681.5nm and 780nm were selected for further analysis and ratios of these were compared with the nematode burden of plants grouped by experimental plot. The comparison was repeated, grouping plants into 1,000's of root invasion (Table 2.1.).

Ratio calculations similar to normalised difference indices "(band *a*-band *b*) / (band *a*+band *b*)" (Mather, 1999) were used here as these help to compensate for changes in incident light and other extraneous factors (Lillesand & Kiefer, 1993), and are not affected by absolute pixel values in their constituent wavebands (Mather, 1999). The normalised difference between green (551nm) and red (681nm) reflectance was found to be correlated ($F_{(1,4)}$= 70.84, p <0.001, $R^2_{(4)}$= 0.993) with nematode burden as determined by the number of juveniles present in the roots of the plants (Table 2.1; Fig. 2.7.). Means of this analysis, are shown grouped by experimental plot in Figure 2.8.

Table 2.1. Correlation of the red-green reflectance ratio with nematode root invasion. (Juveniles g^{-1} root).

Grouping	Red-Green	Red-NIR	Green-NIR	N
Plot	-0.823	-0.721	-0.251	24
1,000's of juveniles	-0.996	-0.978	-0.850	6

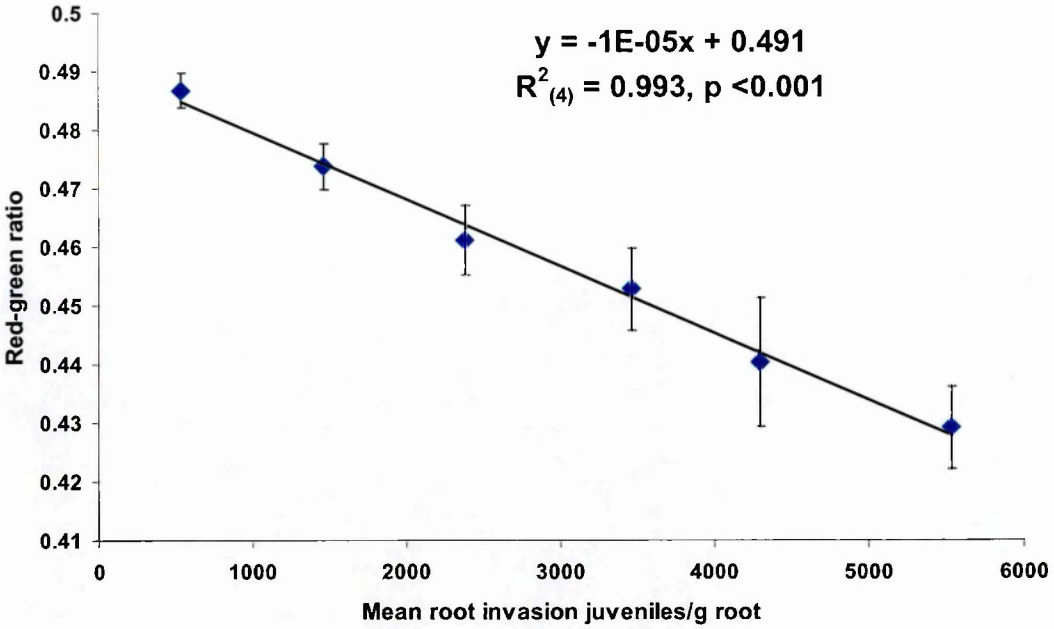

Figure 2.7. Plot of red-green reflectance ratio vs. nematode burden. Means of 1000's juveniles g^{-1} root ± SEM.

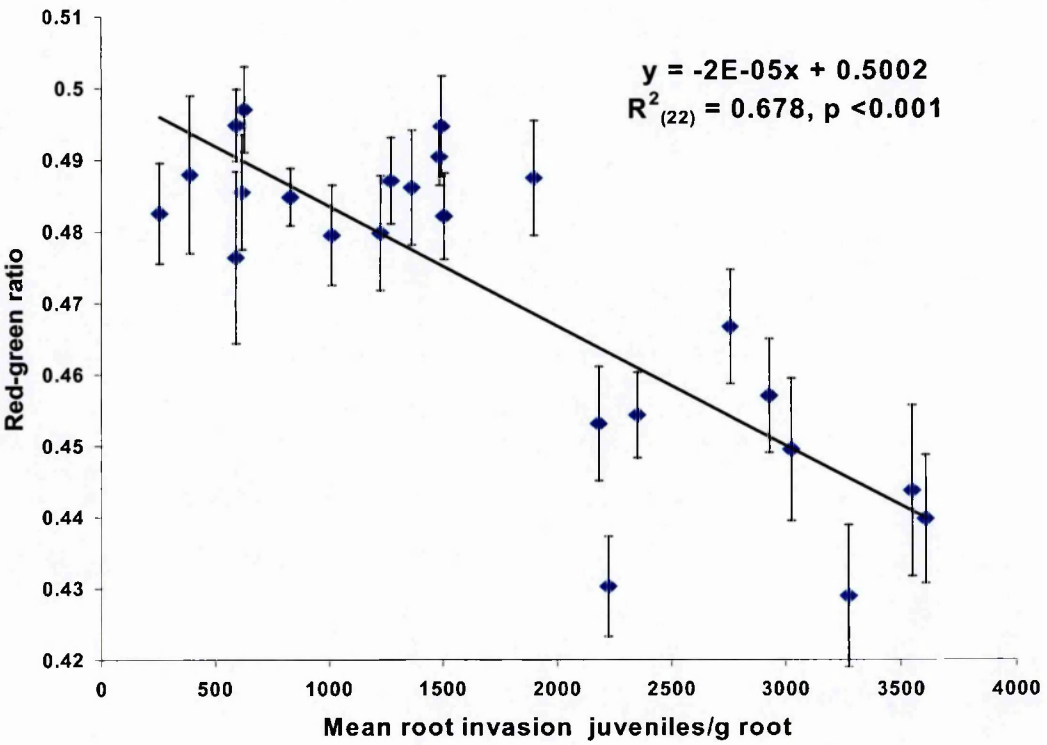

Figure 2.8. Plot of red-green reflectance ratio ± SEM vs. nematode burden (juveniles g^{-1} root). Means of experimental plots.

2.4.4. Supplementary measurements using a Hydro N-meter.

N-meter readings taken from all tag plants on June 14th and 15th, 2000 (34-35 DAP), were strongly ($F_{(1,4)}$= 99.25, p <0.001, $R^2_{(4)}$=0.96) correlated with root invasion (Fig. 2.9.).

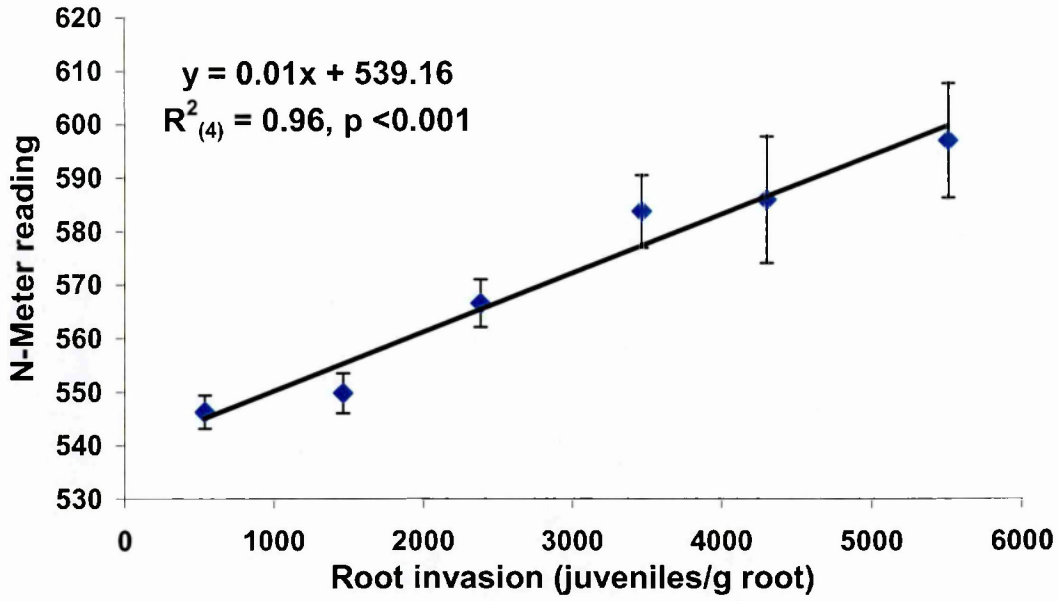

Figure 2.9. Correlation of mean root invasion with N-Meter readings ± SEM. June 14-15, 2000.

2.5. Discussion.

Knibling (1970) noted that visible reflectance changes are as responsive to plant stress as the near-infrared region. This can be due to a reduced concentration of pigments (Al-Abbas *et al.*, 1974), or sensitivity of the photosynthesising process to metabolic disturbances (Knibling, 1970; Sellars, 1987). Plant stress, whether caused by pathogens, environmental factors or nutrient deficiency reduces the absorption of incident light by photosynthesising pigments in the chloroplasts (Blazquez & Edwards, 1986; Sanwald, 1981).

Previous studies have shown reflectance from stressed plants to increase across the visible spectrum. Al-Abbas *et al.* (1974) report that deficiencies in N, P, K, Mg, S or Ca increased reflectance across the visible region when compared with the leaves of non-deficient maize (*Zea mays*) plants. Blazquez & Edwards (1986) found reflectance at visible wavebands from potato leaves to be increased by infection with *Phytophthora infestans* or *Alternaria solani*. The authors also investigated aerial colour-infrared photography in the same study and were able to detect these pathogens in the field. Carter (1993) examined the spectral

response to stress of, among others, loblolly pine (*Pineas taeda* L) (competition), golden euonymus (*Euonymus japonica*) (powdery mildew), slash pine (*Pinus elliottii Engelm*) (lack of ectomycorrizal fungi), persimmon (*Diospyros virginiana*) (herbicide DCMU) and live oak (*Quercus virginiana* Mill.) (senescence) He found reflectance to increase regardless of stress agent, particularly at 550nm and 710nm, and noted that this was a consistent response to plant stress.

The pattern of correlation between reflectance and nematode burden found in this experiment (Figures 2.5, 2.6.) differs from the expected plant stress response. An increased red (681nm) and reduced near-infrared (780nm) reflectance would accord with normal spectral response to plant stress (Wiegand *et al.*, 1991) and the ratio between these waveband regions forms the basis of most remote sensing vegetation indices (Perry & Lautenschlager, 1984; Steven *et al.*, 1990; Elvidge & Chen, 1995). Reflectance at red wavebands reaches a (minimum) asymptote at canopy densities substantially lower (*c.* LAI = 3; Guyot, 1990) than that of a mature potato crop and was not correlated with nematode burden in this experiment. A reduction in near-infrared (780nm) reflectance is linked with reduced leaf area (Knibling, 1969; Sinclair *et al.*, 1973) and is thus likely to be common to any pathogen which reduces biomass.

An apparent decrease in green (551nm) reflectance with increasing nematode burden in this experiment (Figures 2.5, 2.6.) is in contrast to the findings of other studies on plant spectral response to pathogen-induced stress. A ratio between red and green wavebands was found to have a higher correlation with nematode infection ($R^2_{(4)}$= 0.99) than the ratio between red and near-infrared ($R^2_{(4)}$=0.95). Several wavebands close to the red and green centres were tested and peak (negative) correlation was noted from the ratio between 551nm and 681nm.

The square of the correlation coefficient (R^2) was used by Blackburn (1998) to relate wavebands to chlorophyll concentrations in bracken (*Pteridium aquilinum*). This analysis method, although identifying candidate wavebands, does not indicate whether they are positively or negatively correlated with the assumed causative factor. Green reflectance trends from this experiment would have been reported as a positive R^2 value had the square of the correlation coefficient been used to describe these results. Ratio indices developed from wavebands selected for correlation could have been formed only between wavebands having greater or lesser R^2 values and the opportunity to compare negative with positive correlation would have been lost.

A potential intrusion of soil surface reflectance on the plant spectral measurements was considered as soil has a markedly different spectral signature to photosythetically-active vegetation (Huete, 1988; Guyot, 1990). Reflectance was recorded from bare soil in the experimental area and compared with a typical potato-plant spectrum. Soil reflectance was seen to be lower at 551nm, higher at 681nm and lower again at 780nm. An element of soil in the spectrometer field-of-view would, therefore, result in lower green, higher red and lower near-infrared reflectance, and produce a similar change in the red-green and red-NIR ratios as that observed from nematode infection.

However, only plants having the highest nematode density in their roots (> 5000 juveniles g^{-1} root) may have lacked sufficient leaf area to ensure that soil background was completely excluded from the reflectance measurements. A combination of dense plant canopy, restricted spectrometer field-of-view and laser-target alignment will have avoided the inclusion of soil reflectance in the spectra of plants from lower infestation levels. The ratio of red to green reflectance follows a consistent trend for all infestation levels (Figures 2.7, 2.8.). All groups, including those having a dense and extensive canopy development,

are well aligned with the regression line, indicating that this feature is independent of soil background reflectance.

A characteristic sharp rise in reflectance from green vegetation between 680nm and 760nm is referred to as the "red edge" (Boochs *et al.*, 1990). The position of the red edge was calculated as the inflection point (the waveband where the first derivative of the spectrum changes from a positive to a negative value) by Buschmann & Nagel (1993) and Blackburn (1998). Both authors noted that the red edge inflection point moved to shorter wavelengths as chlorophyll content reduced.

No correlation was found between red edge wavelength and PCN infestation during this experiment. The studies of Demetriades-Shah & Steven (1988) and Blackburn (1998, 1999) indicate that this effect is insensitive at higher chlorophyll concentrations per unit area as would be the case when measuring a dense canopy such as a mature potato crop. Demetriades-Shah & Steven were unable to reproduce the red edge shift detected from individual leaves when measuring the reflectance of a sugar beet canopy from an elevation of *c.* two metres.

The reduction in green reflectance of nematode-infested plants raises the question of why this spectral response is so markedly different when other studies have demonstrated the opposite effect? There is some indication from the literature that nematodes increase the amount of photosynthetic pigments in leaves of infested plants, leading to a reduction in reflectance at visible wavelengths. Phosphorus deficiency and an excess of sodium have been linked to nematode infestation (Trudgill *et al.*, 1975a) and both are reported as causing darker foliage in affected plants.

Gausman *et al.* (1975) found cotton plants (*Gossypium hirsutum*) infested with the nematode *Rotylenenchulus reniformis* to have fewer, smaller and darker leaves. Infected plants exhibited significantly lower ($p= 0.01$) reflectance at 550nm and 650nm from single leaves in the laboratory and from canopy reflectance in the field. Infested plants were found to have a greater concentration of chlorophyll (4.3 mg/g vs. 4.1 mg/g) per unit area of leaf. Grove *et al.* (1999) noted that leaves were darker from infested plants and stated that these can contain increased chlorophyll content per unit area.

Buschmann & Nagel (1993) report a consistent reduction in reflectance from 500nm to 700nm with increasing chlorophyll concentration of bean leaves (*Phaseolus vulgaris*) in the laboratory. Their results show the 550nm waveband to have a strong correlation with chlorophyll concentration ($R^2=0.756$). Datt (1998) also found reflectance at 550nm to be correlated with pigment content when measuring eucalyptus leaves in the laboratory. Photosynthetic pigments absorb at both blue and red wavelengths (chlorophyll *a* and *b*), or blue only (carotenoids and xanthophyll). These pigments absorb very little at green wavebands (Lichtenhaler, 1987) although Gates *et al.* (1965) found that, as chlorophyll concentration increases, red and blue chlorophyll absorption extends further into both flanks of the green peak and the leaf appears darker.

The darker colour of leaves from infected plants reported by Gausman *et al.* (1978) and Grove *et al.* (1999) might therefore be due to a higher chlorophyll concentration per unit area of leaf. This would increase chlorophyll-derived absorption as measured at leaf level, e.g. by hand-held field spectrometers and the Hydro N-meter. This effect may, however be offset by the reduction in both leaf number and leaf size (Gausman *et al.*, 1978; Haverkort & Trudgill, 1995) when measuring the reflectance from whole canopies i.e. airborne spectral imaging.

An alternative mechanism for nematode-induced darkening of leaves might be found in the disturbed cation-ion balance of infected potato plants. Trudgill *et al.* (1975b) found the sodium (Na) content of potato haulm dry matter to more than double (from 0.12% to 0.25%) in response to PCN infection, and postulated that extra Ca and Na were taken up as an ionic balance for reduced potassium (K). The leaves of cotton plants stressed by soil salinity were found to have more chlorophyll, were stunted and had a more compact cell arrangement than unstressed leaves (Gausman *et al.*, 1984) although this may have been partly caused by a delayed maturity of the stressed plants. Terry & Ulrich (1972) found the Na content in leaves of sugar beet (*Beta vulgaris*) to increase by 500% when potassium was withdrawn, although this effect was transient and Na concentration reduced to the initial level within 20 days. According to Ulrich (1993), the potato is a sodium excluder and increased sodium uptake may form a potential link between nematode infection, reduced growth, and the darkening of leaves.

The correlation between N-meter score and nematode infection ($F_{(1,4)}= 99.25$, $p < 0.001$, $R^2_{(4)}= 0.96$) suggests that some form of light-excluding spectral analysis device might produce accurate results under sub-optimal weather conditions. Measurements from the Hydro Agri N-meter are collected in a closed system, with the instrument fully enclosing the leaf-section, and are therefore scarcely affected by level or quality of ambient light. Tested leaves, however, were shaded from direct sunlight to avoid any potential for false readings due to a strong internal scattering of infrared light by the leaf (Knibling, 1970).

The workings of this instrument are not in the public domain and the results obtained cannot be attributed to the leaf colour effects noted above. It is clear, however, that the Hydro N-meter must measure the reflectance or transmittance of a leaf section clamped between the sensor lenses. Designed to predict nitrogen deficiency, it is highly probable that this device would ratio one waveband at peak chlorophyll absorption (~670nm) with a

waveband that is less affected by chlorophyll (e.g. 550nm or beyond 700nm). Whilst operational details of the Hydro N-meter are not available, the User Manual of the SPAD-502 chlorophyll meter (Minolta Camera Co., Japan) describes that near-identical instrument as using the relative transmittance (through the leaf) from two sequential light-emitting diodes (LEDs). The SPAD-502 LEDs operate with peak emission at *c.* 650nm and *c.* 940nm (orange-red and near-infrared wavebands) according to the user manual.

Limited availability of the spectrometer combined with poor weather reduced the quantity and quality of the spectral data available for analysis. The GER instrument was available for ten days, sufficient for one reading from all 312 field trial plants and second measurements from 72 plants. Poor weather and curtailment of the experiment duration due to the appearance of cysts of PCN on the exterior of the roots prevented the acquisition of more data. Spectral measurements were collected over two days, June 24th and 25th, 2000. The weather on both days was cloudy and did not improve during the period of spectrometer availability. The June 24/25th readings are the only spectral data available for this experiment.

Field spectroscopy measurement of plant canopy reflectance is, without access to elevated platforms, subject to considerable variability. The field-of-view of the GER 1500 in the this experiment (*c.* 0.8m above the canopy crown) was *c.* 4cm and heterogeneity of the canopy reflectance due to, e.g. leaf angle and shadow contribution, necessitates the collection of a large number of replicates before meaningful comparisons can be drawn between treatments.

A mobile gantry had been intended to lift the spectrometer 4m above the crop canopy (Plate 2.5.). This device had been constructed before the spectrometer equipment became available and was designed to utilise a low-cost Kodak barium-sulphate reference card. It

was subsequently deemed unwise to mount the very expensive (*c.* £1,000) and easily-damaged Spectralon™ reference panel on a lifting arm which had limited fastening capabilities. Time taken in moving the gantry between targets would have slowed the recording process and the option of more, albeit variable, spectra was considered to be of equal value to this investigation. Comparisons between groups of plants ordered by infestation level (1,000's, juveniles g^{-1} root) reduced the inherent variability of these spectral measurements and aided the identification of a correlation between wavebands and pathogen.

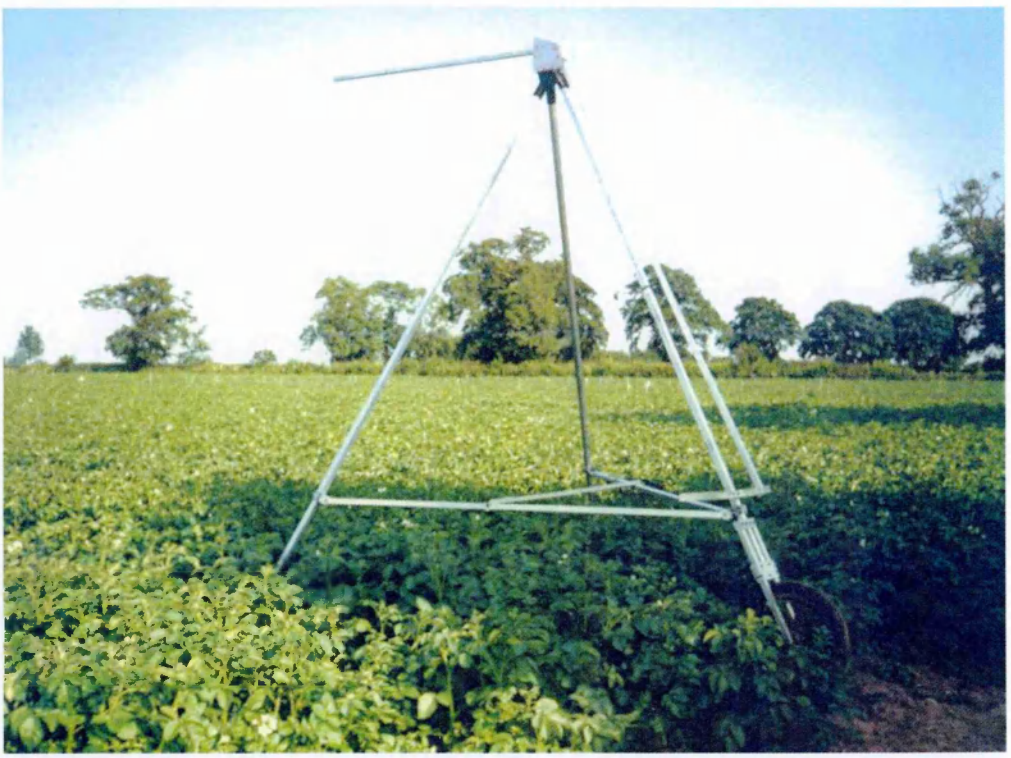

Plate 2.5. Mobile gantry designed to collect field spectra from an elevation of 4m.

2.5.1. General conclusions.

This experiment has identified a ratio between red and green reflectance as worthy of further investigation. No narrow-band spectral features were found however, and these may have been obscured by variability due to adverse weather conditions. In progressing to airborne spectral measurements, particular attention will be given to the red-green ratio, and the spectral region between 600nm and 700nm. This is intended to identify any

broadening of the red chlorophyll absorption band around 675nm. Near-simultaneous reflectance measurements and (hopefully) better weather might then reveal a level of detail that is missing from the spectra in the 2000 field experiment.

The N-meter recording process might obviate the need for laboratory analysis of soil or root samples. However, data collection remains time-consuming and this approach would appear to be less suited to the intensive survey of large areas than airborne or satellite survey.

3. 2000 Poly-tunnel pot experiment

3.1. Introduction.

Considerable effort was directed towards equalising or recording abiotic factors identified from the 2000 field experiment which might potentially confound the spectral analyses. The field experiment layout was, however, dictated by existing population levels and it must be appreciated that it may not always be possible to completely exclude localised variability in field experiments (Trudgill, 1992). A concurrent poly-tunnel experiment was therefore conducted in order to confirm the findings of the field experiment in a controlled environment, although Trudgill (1992) concluded that pot experiments were less realistic than field experiments due to many factors, including a potential limitation on root and haulm development, and suggested that results should be treated with caution. The use of a pot experiment was considered beneficial when used to support the field experiment rather than as the primary source of experimental data.

3.2. Objective.

The 2000 poly-tunnel experiment was designed to provide additional data to support the results of the 2000 field experiment conducted under more controlled agronomic conditions. This experiment was, therefore, located in an open-ended poly-tunnel rather than in a glasshouse, using carefully-mixed soil and rotating the plants to ensure equality of light and competition.

3.3. Materials and methods.

3.3.1. Experiment preparation and monitoring.

3.3.1.1. Potato cyst nematode inoculum.

Soil from a heavily-infested area of Four Gates Field, Edgmond (OS Grid ref. 3707E, 3195N) was collected on April 20th, 2000 and placed in a drying cabinet for ten days at a temperature of 24°C. Cysts of *Globodera rostochiensis* were recovered by flotation (Hooper, 1986) on May 5th, 2000 and the extracted material dried at 24°C in a fine nylon mesh wrap. The proportion of non-cyst material was reduced by repeated rolling the extract across a sheet of white paper as the spherical cysts roll more readily than other, non-target, material. The cysts were then collected in a receptacle with some residual detritus.

The extracted and refined material weighed 1.83g and this was analysed for cyst content by weighing. The material was thoroughly mixed by shaking for sixty seconds in a sample jar. Three samples were removed from the centre of the jar using a spatula and placed on the balance tray of a CAHN C-3 Microbalance (Cahn Instruments Inc. Cerritos, California, USA). The balance was allowed to stabilise for two minutes and the weight of each sample was recorded. The cysts from each sample were then extracted and weighed. The weight of cysts expressed as a percentage of the whole sample weight ranged from 41.0% to 52.3% with a mean of 46.16%.

The inoculum requirement for this experiment was calculated by using the relationship between cyst weight and the number of eggs contained in the cysts as reported by Arntzen *et al.* (1994), who counted 8.1 eggs of *Globodera pallida* and *G. rostochiensis* per µg of dry, clean cyst weight. A random number sequence was generated in Genstat (Appendix C.) and used to select a dose value for each of thirty pots. The quantity of raw inoculum

was calculated as 1,800,000μg (0.03g held in reserve) divided by the sum of all pot dose values (1229), resulting in a unit innoculum of 1464.6μg. This figure was then multiplied by each pot dose value to calculate the weight of innoculum for that pot. The initial population (Pi) for each pot was then calculated as innoculum (μg) * 0.46 (cyst content by weight) * 8.1. These figures were divided by 6000g of pot soil to give initial population values ranging between five and 100 eggs g^{-1} soil. Thirty measures were weighed out on the CAHN C-3 Microbalance on June 8th, 2000 and placed in marked sample jars prior to inoculation of the pot soil.

3.3.1.2. Seed-tubers and planting material.

Seed-tubers cv. Pentland Dell were selected for even size within the specified 35-45mm range and chitted at not less than 10°C under constant light until root primordia were visible on the shoots. The experiment was planted on June 13th, 2000. Thirty-six 10" (25cm) plant pots were filled with John Innes No. 2 (sterilised peat/loam) and numbered. Six pots were planted without inoculum. Soil from the remaining thirty pots was mixed with the innoculum for each pot by emptying into a plastic sack then shaking and inverting the sack for sixty seconds. Half of the mixed soil was then returned to the pot, a seed tuber added and the remaining soil used to fill the pot. The pots were placed in an open poly-tunnel and watered. Pot positions were rotated weekly to compensate for differences in illumination and competition from adjacent plants. A measurement of plant height, a count of the main stem number and a subjective visual assessment of leaf angle were undertaken on July 5th, 2000 (22 DAP).

3.3.2. Spectral measurements.

Plants were moved to an area of grassland away from trees and buildings on July 7th, 2000 (24 DAP). A series of 147 spectral measurements were then recorded with a GER 1500 spectrometer (Appendix D.) within two hours of solar noon. Each measurement was followed by a recording of the Spectralon™ reference panel, (serial No. st1011). The

weather was bright, cloudy and windy. Cumulus cloud frequently obscured the solar disk and work was suspended during periods of cloud transition. The potato plant stems were found to be etiolated and weak and this may have been due to their growing in a location sheltered from wind. Some stems needed support (twining with other stems) and the plant canopies were not in a natural configuration.

Plants were then transported in an enclosed vehicle to the NERC Equipment Pool for Field Spectroscopy (EPFS) facility at the University of Southampton on July 10th, 2000 (27 DAP). One hundred and sixty spectral measurements were recorded from 23 plants in a darkened laboratory using an ASD Fieldspec FR spectroradiometer, serial No. 6032/1 (Analytical Spectral Devices Inc. Boulder, Colorado, USA). A 1000w halogen lamp provided the illumination and the 8° spectrometer optic was mounted on a photographic tripod *c.* 40cm above the canopy crown, giving a *c.* 5.6cm diameter field-of-view.

Supplementary measurements using a Hydro N-meter (described in chapter two) were collected on July 5th, 2000 (22 DAP). Measurements were taken from around the plant canopy by selecting the terminal or penultimate leaflet from each fully-expanded leaf. The mean of 30 measurements was recorded as the N-meter value for each plant.

All plants were harvested on July 12th, 2000 (29 DAP) and root samples (2g) were preserved in formal acetic acid (FAA; Southey, 1970) prior to estimation of the number of nematodes in the roots.

3.3.3. PCN sampling.

Nematode burden was assessed by quantifying the number of juveniles within a sample of the plant root (Hooper, 1986) and the mean of three counts was recorded as the invasion burden for the plant.

3.3.4. Data analyses.

Attempts to group the experimental plants by invasion counts (e.g. 1,000's juveniles g^{-1} root) resulted in a very uneven number of plants in the groups. Plants were therefore sorted into ascending order of invasion and ordered into six groups of six plants. A mean invasion count and mean spectral measurement were then calculated for each group. The relationship between mean invasion and mean N-meter score was determined using linear regression in Genstat version 5.4 (Lawes Agricultural Trust, Rothamsted, UK).

3.4. Results.

The susceptible (Evans *et al.*, 1977) and relatively intolerant Pentland Dell potato plants (Evans & Haydock, 1990) displayed no apparent signs of stress when scored by eye, despite having been infested with up to 100 eggs g^{-1} soil initial nematode population density (Pi) and invaded by up to 2,283 juveniles g^{-1} root. Stem numbers, plant height and (a highly subjective) leaf-angle assessment were not correlated with nematode burden.

Root invasion counts ranged from 33 to 2,283 juveniles g^{-1} root and were correlated with the calculated initial populations ($F_{(1,34)}= 340.54$, $p < 0.001$, $R^2_{(34)}= 0.91$). Soil had been splashed between pots as they were watered by a relief horticultural worker and five of the six un-inoculated pots were found to contain juveniles of PCN in their roots.

Spectral reflectance collected using the GER 1500 instrument was not significantly correlated with root invasion (juveniles g^{-1} root), even when arranged into six groups of six plants. Spectral measurements collected with the ASD Fieldspec FR at Southampton were also not significantly correlated with nematode burden.

A comparison between the N-meter score recorded on July 5th, 2000 and nematode burden showed a significant linear relationship ($F_{(1,34)}= 7.92$, $p= 0.008$, $R^2_{(34)}= 0.19$). This

improved considerably ($F_{(1,4)}$= 60.19, p= 0.001, $R^2_{(4)}$= 0.938) when the comparison was applied to groups of six plants (Fig. 3.1.).

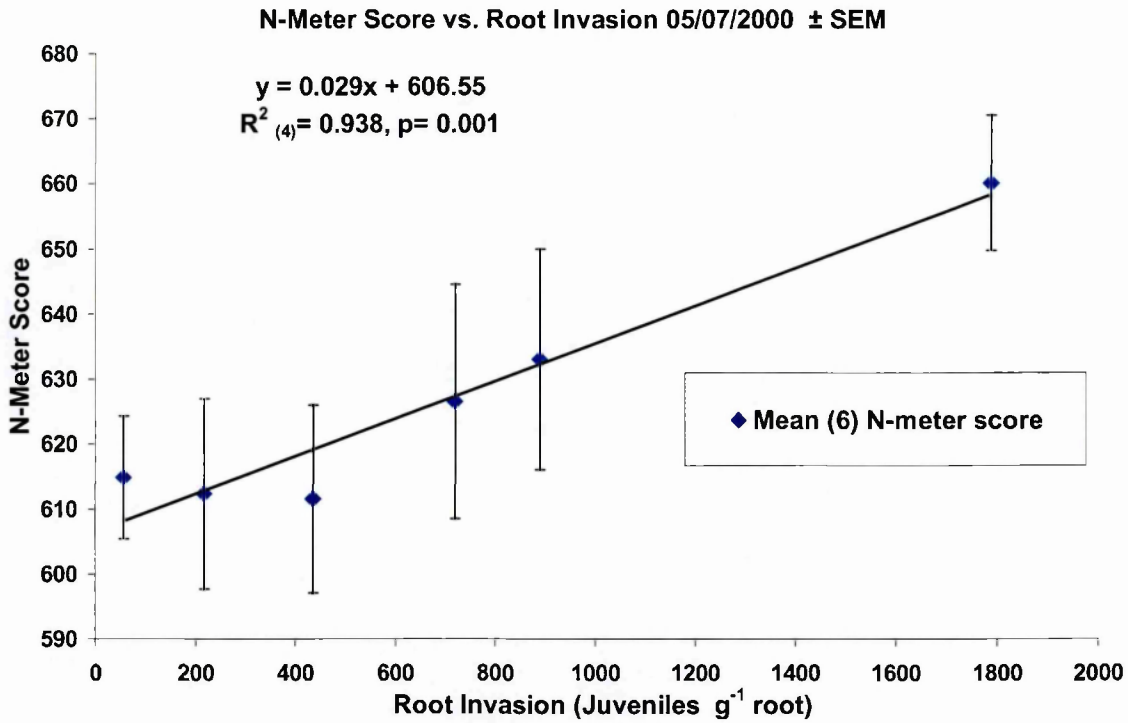

Figure 3.1. N-meter score and standard error for groups of six plants.

3.5. Discussion.

The experimental plants did not exhibit noticeable symptoms of nematode-induced stress and most physical and spectral measurements were poorly correlated with nematode burden. Trudgill (1992) noted that plants of a pot experiment may develop at a faster rate than field crops as a result of higher soil temperatures. The seed tubers had also been chitted (aged) before planting and many (14) plants had already emerged at eight days after planting (8 DAP). It is possible that the plants were able to develop an extensive root system before the full effect of nematode invasion could inhibit plant growth, thus reducing the actual stress burden on the plants. Constant watering and the organic nature of the John Innes No.2 planting medium may have also ameliorated the effects of the nematode burden.

Whilst spectral measurements collected under natural light and in the laboratory were not significant, the measurements collected using the Hydro-Agri N-meter were strongly correlated ($F_{(1,4)}$= 60.63, p= 0.001, $R^2_{(4)}$= 0.938) with nematode burden and are consistent with N-meter results recorded from the 2000 field experiment.

4. 2001 Field experiments

4.1. Introduction.

Field spectroscopy was found to be a useful tool for the investigation of the spectral response of potato plants to PCN infestation in the 2000 experiments. There were some limitations to the method, particularly in that field spectra had been collected from limited areas of the crop, over an extended period and under changeable weather conditions. Airborne spectral data collection can, by contrast, image entire fields in seconds and cloud shadow, present only as a reduced signal in field spectrometer readings, is clearly visible in airborne images. The ability to recognise cloud shadow and exclude affected areas will minimise errors caused by changes in solar irradiance between spectra from individual crop regions.

4.2. Objectives.

To evaluate the potential of airborne remote sensing for the detection of PCN infestation and to extend the spectral assay of PCN infestation to whole-field airborne imagery.

4.3. Materials and methods.

4.3.1. Experimental sites.

Two fields of commercial potato crops, New Piece field, Tibberton, Shropshire and Near Moor field, Edgmond, Shropshire, were selected for the 2001 airborne remote sensing experiments. The suitability of these sites was based on the results of an initial soil survey conducted in March 2001.

Planting of the northern half of the second experimental site at Near Moor field (Ordnance Survey grid reference SJ 705197) was delayed until May 9th, 2001 and vegetation cover consisted largely of weeds at the time of the ARSF flights. The remainder of the sampled

experimental area was planted on May 24th, 2001 and was largely devoid of vegetation. Only limited analysis was conducted on data collected from Near Moor field and details of this experiment are listed in Appendix E.

The experiment described in this chapter was located in New Piece field (Ordnance Survey grid reference SJ 687188). The soil was sandy loam and the southern half of this *c.* 10.5 ha field slopes to the south-west (*c.* 3m). New Piece field was planted with potato cv. Charlotte on March 8th, 2000, although wet weather delayed planting of the southern field area. However, all of the experimental locations were located within the area planted on March 8th.

Field boundaries, tracks, trees and other static features were recorded using a Sokkia Hawkeye Differential Global Positioning System (DGPS) and Midas software (Sokkia Ltd, Crewe, Cheshire, UK). These data were imported into Arcview 8.1 GIS software (Environmental Systems Research Inc. Redlands, Ca. USA.) and used to register the airborne images to ground features (Fig. 4.1.).

4.3.2. Sampling for PCN populations.

Exploratory soil samples were collected during March 2001 to determine the distribution of PCN within the fields. Intensive soil sampling and flightlines were then arranged to cover field areas having the largest variation in PCN population densities.

A series of 32 experimental plot areas were measured from New Piece field using the DGPS receiver and soil samples collected from 36 cores of a regular grid pattern within each plot on March 30th, 2001. The core samples were bulked (*c.* 1.5Kg) and analysed to determine the mean nematode population density of the area (Fig. 4.2.). Three hundred

point samples were collected at *c.* 5m spacing on March 29th, 2001 and their locations recorded using the DGPS receiver (Fig. 4.1.).

Soil samples were dried at 25°C for five days and sieved (4mm) to remove stones. A 200g sub-sample was taken from each sample after thorough mixing. Cyst extraction and egg counts were made according to the procedures described by Shepherd (1986). All area samples and 140 point samples were processed for PCN population density, selecting every fifth point sample where infestation was low.

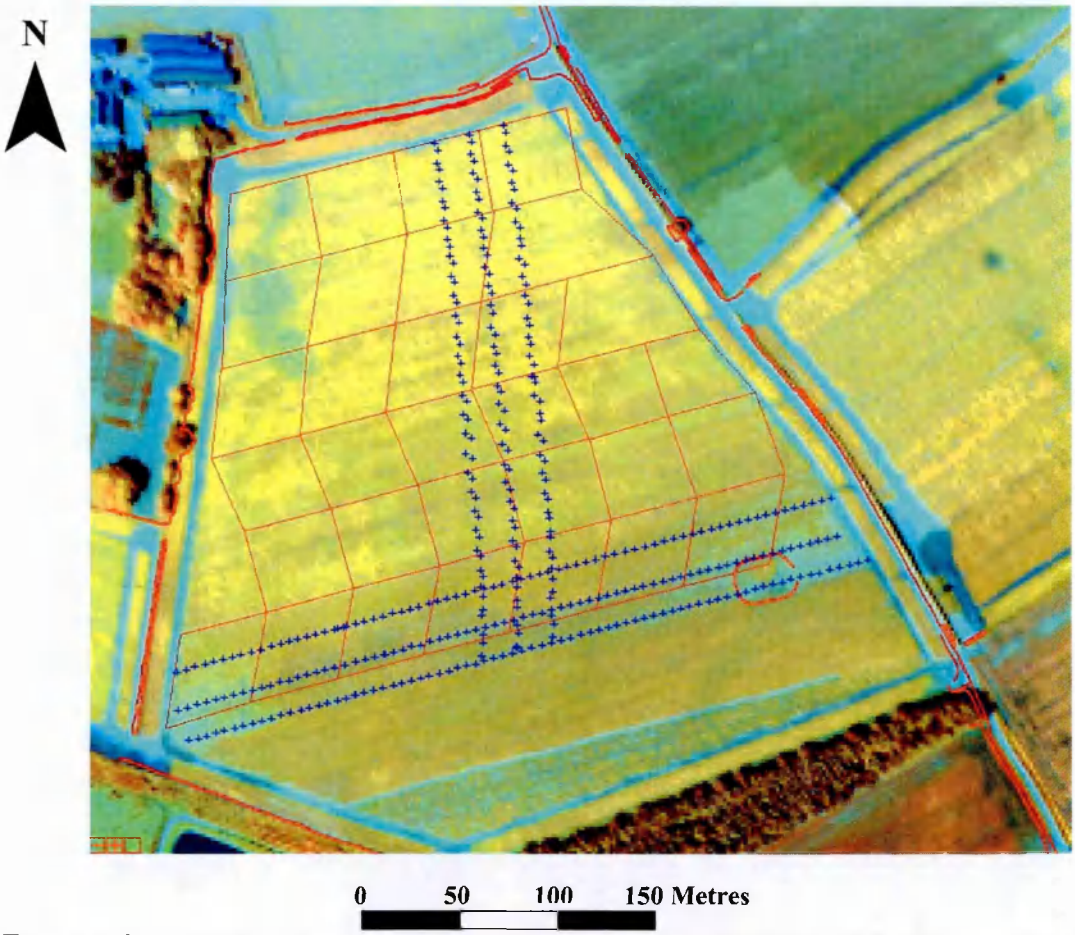

Figure 4.1. DGPS vector overlay of New Piece Field boundaries and sample locations on flight image 17202 (bands 10,6,1). Five-metre point sample locations are denoted by + symbols. An oval red line marks the extent of a shallow depression in the field.

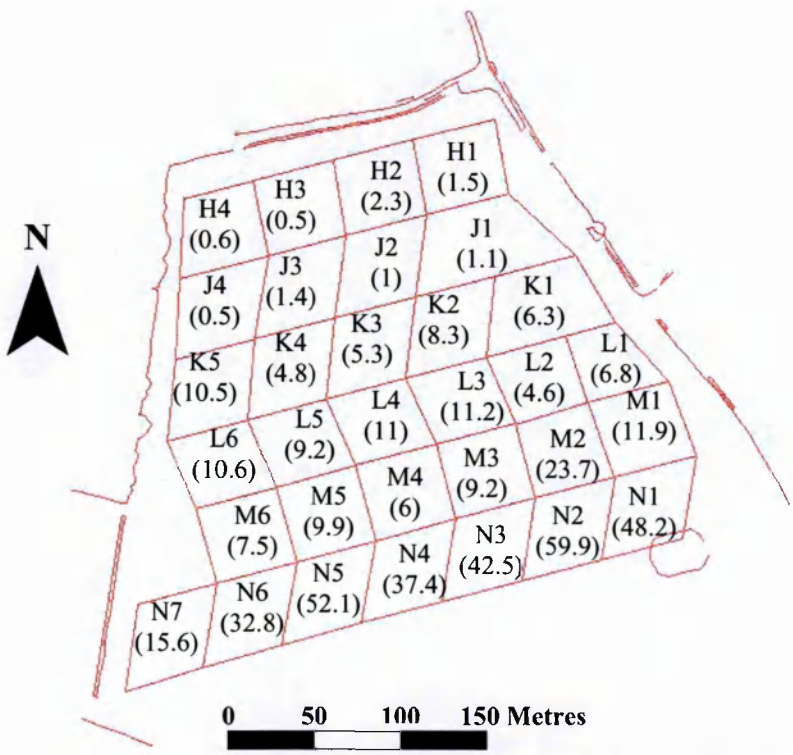

Figure 4.2. Experimental plot areas and initial PCN population density (Pi) estimation (eggs g^{-1} soil) of New Piece Field.

4.3.3. Airborne remote sensing data collection.

The NERC ARSF aircraft, a Dornier 228, flew six flight lines on June 21st, 2001 from 14:03 to14:36 GMT, imaging both experimental sites and the ground calibration areas.

Instruments carried were the CASI-2 (Itres Research, Calgary, Canada) and the Daedalus AZ-16 Airborne Thematic Mapper (ATM) (SenSyTech (formerly Daedalus Enterprises, Inc.), Newington, VA). A Wilde RC10 survey camera collected a photographic record of the target areas and this was used to identify ground features appearing in the radiometric data. Flight parameters are listed in Appendix F. and the CASI-2 instrument specifications in Appendix G.

Ground-truth reference spectra were collected from bare soil, dry grass, a sports field, the potato canopy and a small lake. Reference spectra were collected using a GER1500 spectrometer in dual-beam mode between 14:20 and 17:13 UTC on the day of the flights.

4.3.4. Spectral data processing.

4.3.4.1. Daedalus Airborne Thematic Mapper (ATM).

ATM image data from early (MultiSpec) processing showed minimal (< 0.1) correlation in the far-infrared (2244nm waveband centre) and thermal infrared (9950nm waveband centre) bands. Further processing of the ATM images was suspended due to concerns over possible directional effects from the 90° sensor view angle and the wide (24nm-185nm) wavebands. Higher spectral resolution images were available for all experimental areas from images collected with the CASI-2 instrument and the ATM data were not expected to enhance the available information.

4.3.4.2. ITRES Research CASI-2.

Scattering from the edge of clouds can alter the distribution of solar radiation (Dr E. Milton, personal communication) and images were inspected to ensure than no cloud shadow was within *c.* one kilometre of the experimental areas. Images from flights 17203 and 17204 were discarded due to cloud shadow over the targets. Images analysed for the 2001 field experiment were the vegetation bandset image from flight17202, the heath bandset image from flight 17205, and two enhanced-spectral mode images from flights 17206 and 17207. Waveband centres and approximate bandwidths for each image type are listed in Appendix G.

Image files supplied by NERC ARSF had been processed to hierarchical data format (HDF) level 1b, This level of processing comprises the radiometric correction for sensor attributes and aircraft navigation, pitch, roll and yaw information appended. Level 1b files retain the geometric distortions caused by aircraft movement due to turbulence and linear features appear as undulating lines on the image.

The level 1b HDF files were processed to level 3a using the ARSF-supplied computer program 'azgcorr' on a Sun Sparc 20 workstation. This process uses the appended navigation and displacement information to place each sensor measurement in the correct location relative to a map co-ordinate system. The output pixel size was set to 2m x 2m and the default azgcorr method of bicubic interpolation (spline value 1.0) was used to calculate the output pixel values.

Correction for pixel size and location will depend to some extent on an accurate determination of the aircraft (sensor) height above the target, with pixels at the edge of the image affected to a greater extent than at nadir (due to the angle of view). No digital elevation model (DEM) was available for the experimental sites at the time of image

processing and an attempt was made to interpolate a 50m grid from the elevation data of the DGPS points recorded for the sample locations. The interpolated DEM distorted the image and was therefore discarded. Images from the 17202 and 17205 flights were subsequently re-processed in azgcorr using a 25m DEM obtained in January 2003 from the Midas Landmap service (www.landmap.ac.uk). These spatial mode images were re-processed because a linear 'stretch' correction might over-compensate at the centre pixels of their 54° swath. Less distortion was expected from the enhanced spectral mode images 17206 and 17207 due to the limited swath (22.13°) and no geoid-spheroid separation factor was applied to these images.

Level 3a HDF images were converted to band-sequential (BSQ) or geotiff format using the NERC ARSF supplied computer program 'azexhdf' on a Sun Sparcserver 5 computer. The ENVI function 'cross-track correction' was investigated for the correction of possible limb-brightening (cosine) or off-azimuth reflectance factors. This process was subsequently discarded as the correction factors were calculated from the entire image, including many non-target features e.g. roads and cloud shadow, and the correction was considered unreliable for images covering a heterogeneous area.

Empirical line calibration factors were calculated for five target areas of the 17202 flight image as the ground truth areas were not covered by a single enhanced spectral flight image. This calibration was conducted for future reference to quantify the atmospheric attenuation at the time of data collection and was not used in the current within-field analyses.

4.3.4.3. Image location and rectification.

Early attempts at rectification using Arcview 8.1 (Environmental Systems Research Inc. Redlands, Ca. USA.) and MultiSpec 2.5 (http://dynamo.ecn.purdue.edu/ ~biehl/MultiSpec)

were superseded and discarded when the ENVI software program, version 3.5 (Research Systems Inc. Boulder, Colorado) was purchased in July 2002. Reported results are derived from images rectified using the ENVI first-order rotation, scaling, and translation (RST) registration method and nearest-neighbour resampling.

Band-sequential images and DGPS vector data were projected into Ordnance Survey Grid Reference co-ordinates, although the DGPS data had been collected using the OSGB36 datum whilst the airborne data used the WGS84 datum. Image files and DGPS vector files were retained in their original datum projection throughout the rectification process, placing each image in the approximately correct location relative to the DGPS map overlay. Geotiff files (produced from azgcorr version 4.3.3) were projected as transverse mercator on the OSGB 1936 datum by default and were within 6m of their correct registration to the DGPS vector overlay. This residual disparity was removed by editing the image map co-ordinate information contained in the ENVI header file.

4.3.4.4. Comparison of enhanced spectral mode images.

The Northern enhanced spectral mode image (17207) was noticeably darker than the Southern image (17206) (Fig. 4.3.), and this was attributed to the slightly positive pitch of the aircraft sensor viewing additional shadow when flying towards the solar position. A narrow area of the target was captured in both enhanced spectral mode images. This overlap region was used to calculate a 'difference spectrum' between the images by using the ENVI 'layer-stacking' function to amalgamate both images, then creating a polygon 'Region of Interest' (ROI) from the overlap area (Fig. 4.4.). A margin of two pixels width was retained from the image boundaries to avoid possible edge effects from the azgcorr interpolation process. The mean spectra from all pixels of the overlap ROI contained 288 channels, 144 from each image (Fig. 4.5.). These data were imported into Excel and the difference at each waveband calculated to generate a correction factor. The factor was

then applied (added) to waveband radiance values (in a spreadsheet) for each plot of the 17207 image to compensate for the difference between the images. Radiance values at all wavebands were then equal for the common overlap region of the 17206 and 17207 flight images. Corrected spectral values from the experimental plot areas covered by the 17207 flight image were therefore considered to be directly comparable with spectra from the 17206 flight image.

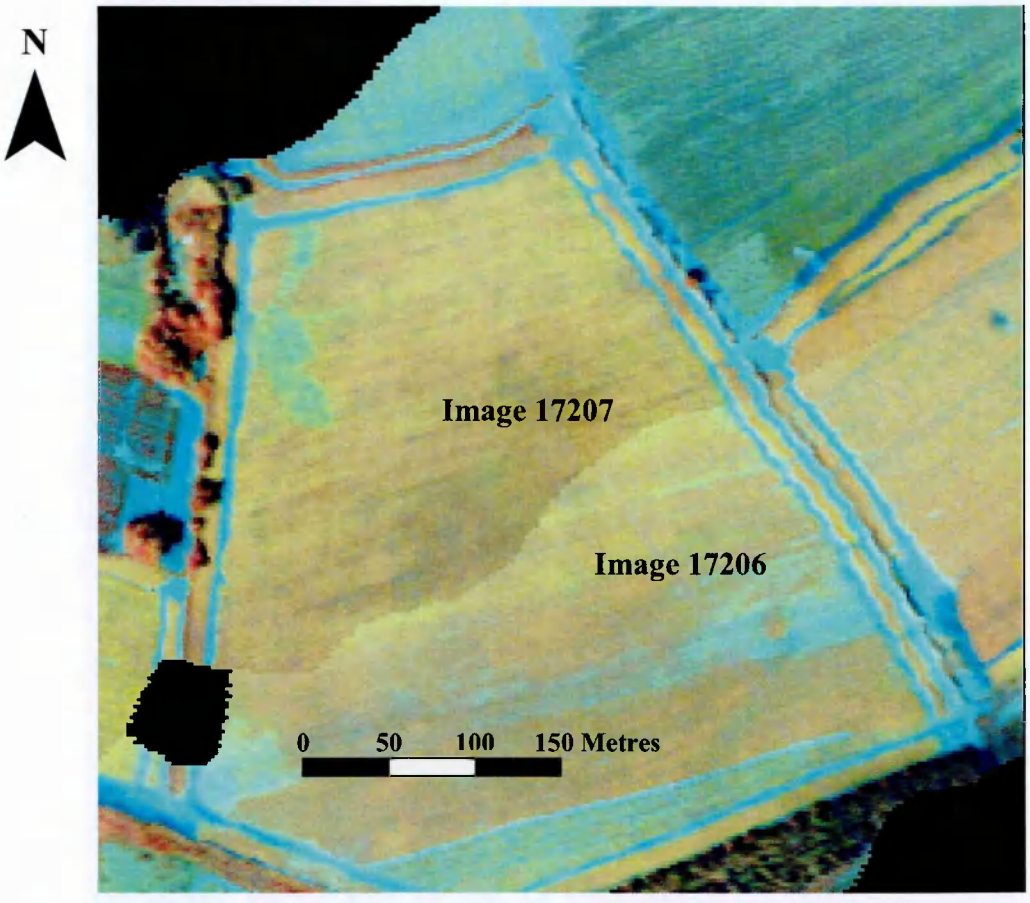

Figure 4.3. Comparison of enhanced-spectral mode flight images 17206 and 17207 of New Piece Field.

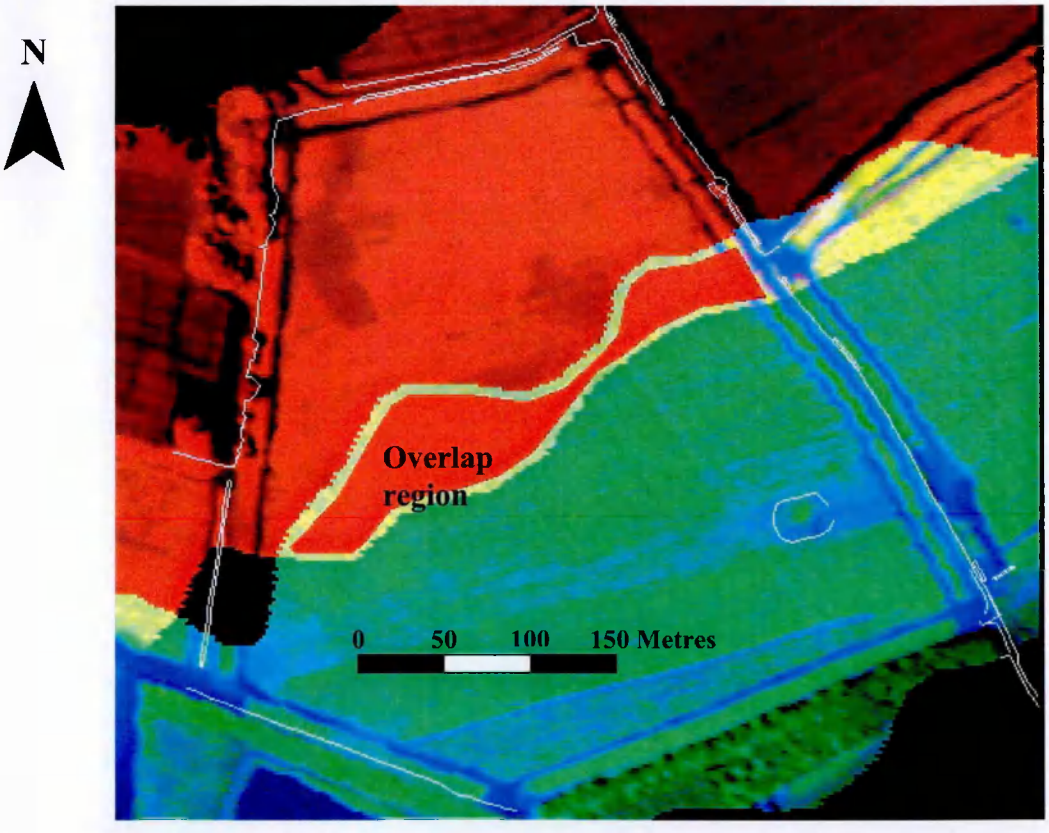

Figure 4.4. Overlap region, common to both flight images, used to calculate a correction factor between enhanced-spectral mode images 17206 and 17207.

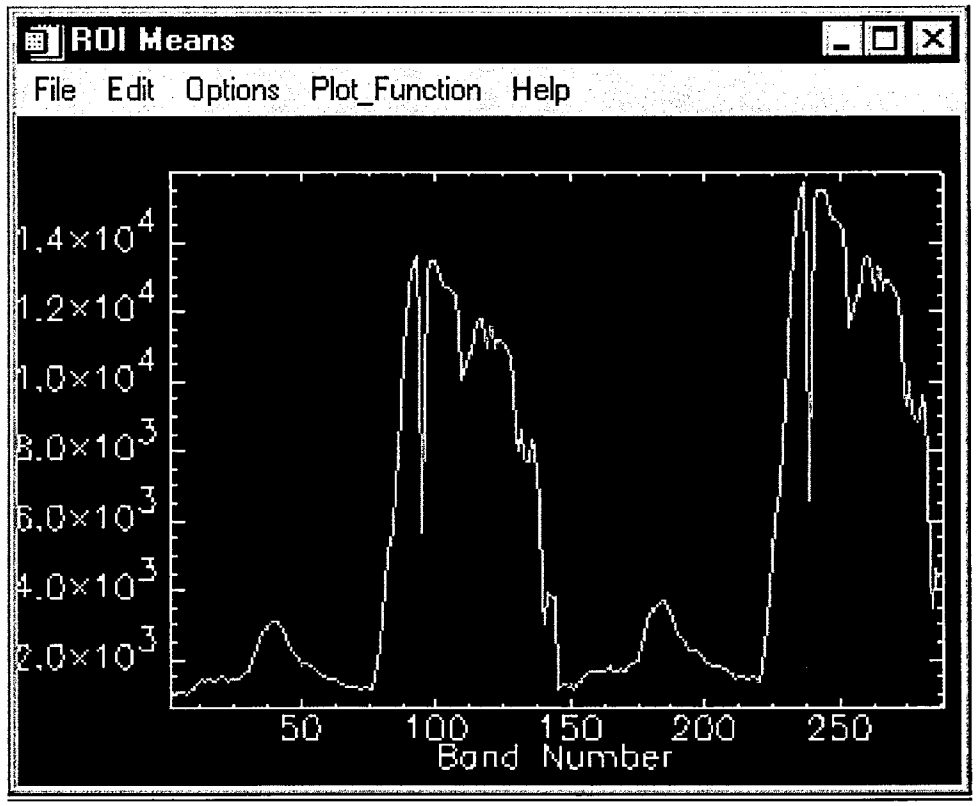

Figure 4.5. Spectra of the overlap region between two enhanced-spectral mode images. Wavebands 1-144 (X axis) show the spectrum derived from flight image 17207. The spectrum of flight image 17206 is shown by wavebands 145-288.

4.3.4.5. Vector overlay of sample areas.

Pixels corresponding to the experimental plot areas were selected using the ENVI ROI function (Fig. 4.6.) and the mean for each ROI recorded as a single spectrum. An area of the north-western corner of New Piece field is visibly distinct from the surrounding field in each image. This is an area of low PCN infestation and ROI borders were arranged to avoid the visible feature.

Spectra from the point samples were calculated from the mean of four pixels surrounding the sample location. Unsupervised classification, using a single iteration of both the isodata and K-means algorithms, was conducted on the experimental plot areas using ENVI. The isodata method was investigated for all wavebands (13), bands 3 & 4 (green & red) and band 3 singly.

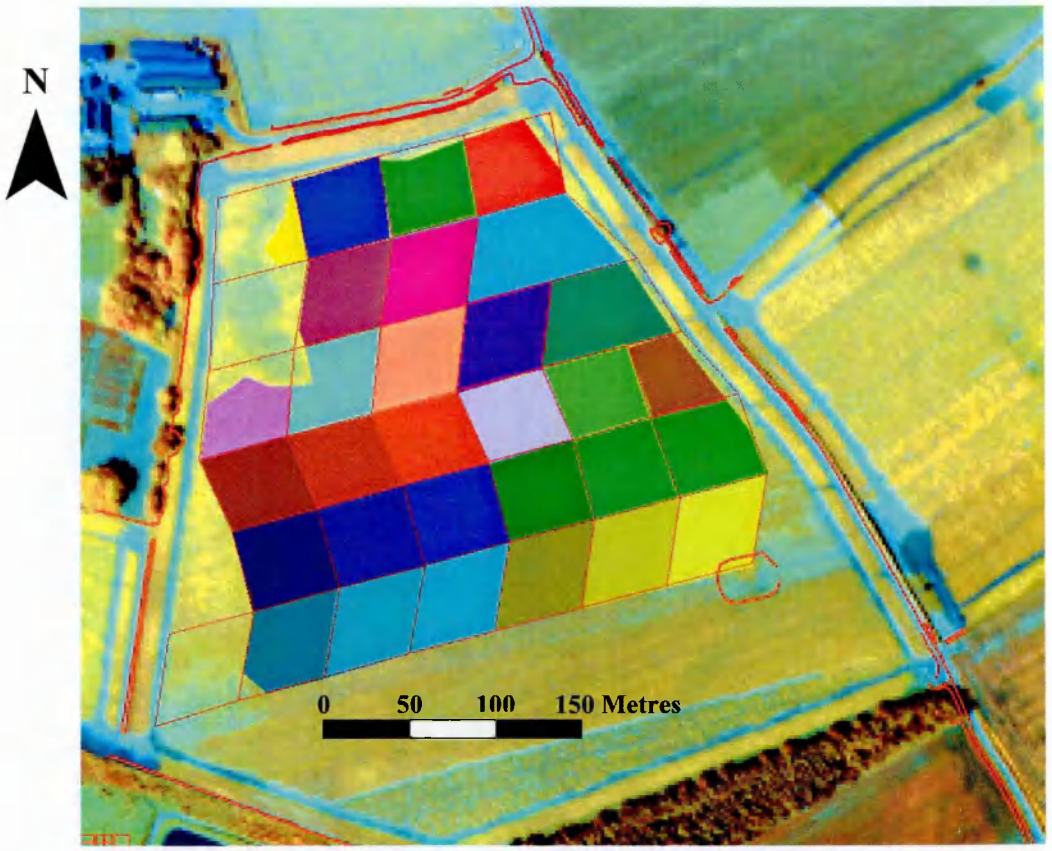

Figure 4.6. Region of interest (ROI) polygons used to calculate mean spectra from experimental plot areas of New Piece field.

4.3.5. Statistical analyses.

Counts of initial nematode populations (Pi) were skewed towards lower values. A natural logarithm (Log_n) transformation was therefore applied to the block sample data while a square root transformation was found to be superior for the point sample counts.

Correlation with Log_n Pi was plotted against waveband for the mean spectra of experimental plot areas from the c17202 image (vegetation bandset), the c17205 image (heath bandset, and the combined images c17206 and c17207 (enhanced-spectral mode) (Fig. 4.7.). The linear correlation of the green (*c.* 552nm) waveband and green-red ratio with the transformed Pi counts was calculated in Genstat version 4.2.

4.4. Results.

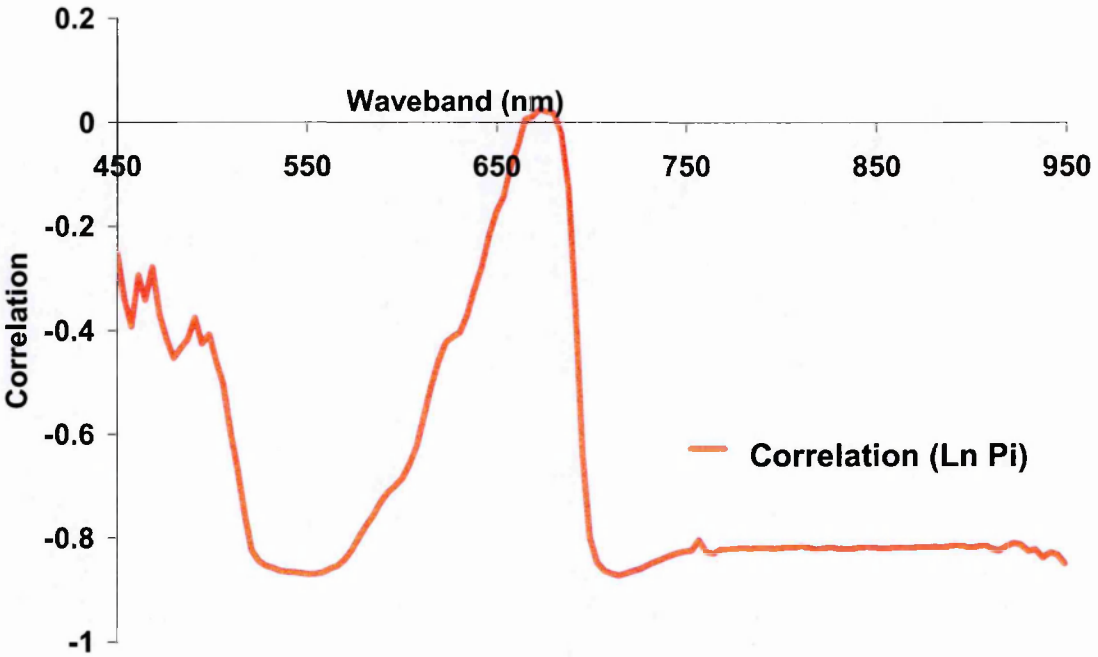

Figure 4.7. Correllogram of the combined enhanced-spectral mode images with $\log_n$ Pi (eggs g^{-1} soil) of the experimental plot areas of New Piece field.

Significant linear relationships were found between the green (551.12nm) waveband from the combined enhanced-spectral (17206 and 17207) images with $\log_n$ Pi of the experimental plot area mean data ($F_{(1,28)}$=86.34, $p < 0.001$, $R^2_{(28)}$= 0.755) and the square root of Pi for the point samples ($F_{(1,121)}$=121.36, $p < 0.001$, $R^2_{(121)}$= 0.501).

Results from the combined enhanced-spectral mode images were supported by analysis of the vegetation band image c17202, which covered the entire field in one pass. Radiance in the green waveband (552.06nm) was negatively correlated with Log_n Pi of the experimental plot area means ($F_{(1,28)}$= 111.69, $p < 0.001$, $R^2_{(28)}$ = 0.8). Spectral mode images cover a wider swath (54°) than the enhanced-spectral mode images (22.13°) and therefore might include directional reflectance effects as noted by Barnsley & Morris (1990). Their investigation of airborne images (72° swath, 36° from the principal solar plane) demonstrated a similar directional effect for green (ATM Band 3, 520nm-600nm)

and red (ATM Band 5, 630nm-690nm), suggesting that possible sensor view-angle effects would be largely cancelled out by ratioing the red and green wavebands. The ratio $\frac{\text{Green - Red}}{\text{Green + Red}}$ was therefore investigated and this revealed a significant linear relationship with Log_n Pi of the experimental plot area means ($F_{(1,28)}= 30.97$, $p < 0.001$, $R^2_{(28)}= 0.526$). Increased red reflectance from bare soil of heavily-infested plots may be generating some additional scatter in this ratio.

A slight shoulder at 630nm is visible in the correllogram derived from the combined enhanced-spectral images (Fig. 4.7.), and this is confirmed by the correllogram of data from the 17205 image, which covered the entire field in ten wavebands from 605.97nm to 696.4nm. This bandset was chosen to investigate possible effects of PCN on the overlapping absorption regions of chlorophyll *a* and chlorophyll *b*. The 630nm response is also present in the 2000 field experiment correlation, although it is absent from the 2000 pot experiment. The ratio 630nm/638nm was significantly related ($F_{(1,28)}= 27.18$, $p < 0.001$, $R^2_{(28)}= 0.493$) to $\log_n$ Pi of the experimental plot area mean data of the New Piece field experiment and would appear to have some potential for distinguishing PCN infestation from other stress factors.

A histogram equalisation stretch was applied both green and red (bands 3 & 4) of the 17202 vegetation bandset image to look for patterns which would indicate localised infestation with PCN. The green band equalisation stretch indicated a general darkening towards the south of the field where infestation was higher, but no clear patterns could be visually identified. Unsupervised classification was carried out in ENVI, using the isodata classification algorithm. A significant linear relationship was identified between the classification (mean of all pixel classes in the ROI) from the all-bands isodata classification and the natural logarithm of Pi ($F_{(1,28)}= 23.95$, $p < 0.001$, $R^2_{(28)}= 0.461$). This

relationship improved substantially when the classification was restricted to the red and green bands ($F_{(1,28)}$= 108.6, p <0.001, $R^2_{(28)}$= 0.796). A near-identical result was obtained from the green (552.06nm) band alone ($F_{(1,28)}$= 102.9, p <0.001, $R^2_{(28)}$= 0.787) (Fig. 4.8.), indicating that the red (668.68nm) band was adding little to the analysis. A single iteration of the isodata algorithm applied to the green band failed to discriminate between bare soil (having *c.* 50% higher reflectance) and the crop canopy from areas of low infestation. Five iterations of the isodata classification did discriminate between soil and crop from the green waveband and the results of this analysis are presented in figure 4.8.

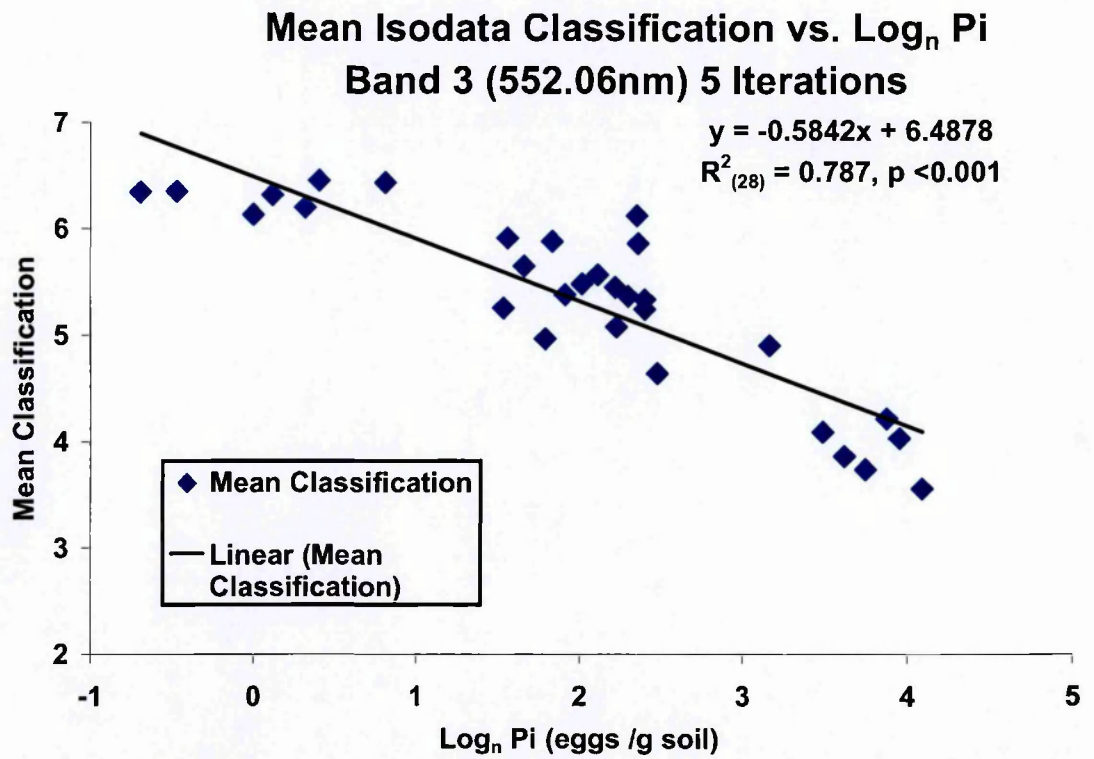

Figure 4.8. Unsupervised classification of the New Piece field experimental plot areas from the 17202 flight image vs. $\log_n$ Pi (eggs g^{-1} soil).

4.5. Discussion.

An unusual spectral region is visible in the north-west corner of New Piece field. This area was excluded by visual inspection of the images when creating the sample area ROIs. (Fig. 4.6.). However, the nearby sample areas H3 and part of H4 (Fig. 4.4.) have slightly higher red reflectance than surrounding areas, suggesting that elevated red reflectance may be present at pre-visual levels. A post-cropping field inspection revealed a slight dip in the

field with no obvious change in soil type or other factor. This region is clearly visible in all thirteen wavebands of the 17202 image, being brighter than the surrounding crop at visible wavebands and darker in infra-red wavebands (beyond *c.* 740nm).

4.5.1. Image location and rectification.

The co-location and alignment of the enhanced-spectral mode images was hampered by a lack of distinct ground features in the overlap area. Rectification and initial positioning was made with reference to the recorded boundary features (hedges and tracks) and refined by reference to minor features e.g. trees and track-intersections. Some residual error is inevitable in the vertical alignment of the two images, although this is not thought to exceed four metres (one pixel-width from each image).

Comparison of image location grid references with the DGPS point sample overlay data confirmed that a range of overlay points across the enhanced-spectral mode images were within one (2m) pixel of the recorded DGPS location, indicating that the image registration process of the enhanced-spectral mode images had not been degraded by the lack of DEM elevation correction. Along-track pixel dimensions are affected to an identical degree by altitude (excluding minor topographical variation) and a linear stretch (or, in this case, squash) will not distort the image. The across-track correction is more complex due to the range of sensor view-angles (port: -10.8264 star: 11.3035, sensor swath: 22.13°), which mix a variable cosine enlargement of pixel width with the constant tangent of each sensor field-of view (FOV). The following calculations were performed to quantify possible location errors due to the linear registration method adopted.

The geoid-spheroid correction for New Piece field was estimated at 80m (from OS map contour lines) and exaggeration of the swath width equals 32.53m (tan 22.13°

* 80). Dividing 32.53m by 203 pixels equates to 0.1603m per pixel. This is the amount by which each pixel would be adjusted by a linear correction.

The upper and lower pixels of the image are located by the registration process and (with registration applied equally to upper and lower pixels) the nadir pixel is static. The cosine effect is therefore divided by the nadir pixel and a maximum discrepancy is to be expected mid-way (25% and 75% of image height) between the nadir pixel and the upper and lower pixels (which are theoretically in their correct locations).

The mid-distance pixels are separated by 50 pixels from the nadir location (203 /4 – 1) and subtracting 0.1603m from these 50 pixels will move the mid-point pixel 8.015m towards the nadir position. The tangent of 5.5° (approximate sensor angle of the mid-point pixels) * 80m = 7.703m. Therefore the linear scaling transformation is moving the mid-point pixels 31.2cm (8.015m – 7.703m) too far towards the nadir position.

This is a rule-of thumb calculation as the maximum discrepancy is probably just outside of the mid-point pixel (due to the non-linear nature of the cosine displacement). However, the DGPS points are claimed accurate to one metre (RMS) and image registration is measured to the nearest 2m pixel: a theoretical error of 31cm is meaningless in this context. Geoid-spheroid correction was, however, used for subsequent image registration.

4.5.2. Collation of two enhanced-spectral mode images.

The NERC ARSF operator had been requested to obtain images at the highest possible spatial resolution. As a consequence of this request, the swath width of the 203 pixels-wide enhanced-spectral mode images was not sufficient to cover the experimental area in

one pass, and enhanced-spectral mode images were collected from two reciprocal flights. The two enhanced-spectral mode images were not directly comparable (Fig. 4.3.) and it is unfortunate that one image (17206) covered areas of high PCN infestation whilst the other image (17207) recorded a section of the experimental area where infestation was generally low.

The process of calculating the difference between each image from the overlap area and applying this as a factor to the whole of one image (17207) created additional work and introduced another layer of uncertainty to the image analysis process. The success of the image-correction process was confirmed by a very similar correlation from experimental plot areas of the single image (17202) data ($F_{(1,28)}$= 111.69, $p < 0.001$, $R^2_{(28)} = 0.8$) and the combined (and corrected) enhanced-spectral mode images ($F_{(1,28)}$=86.34, $p < 0.001$, $R^2_{(28)}$= 0.755) at green (~550nm) wavebands.

4.5.3. Rationale for ratio calculations.

The use of a ratio between wavebands is important in field spectroscopy, where irradiance can change substantially between target and reference-panel readings. This variability is reduced, but not excluded when using a dual-beam spectrometer, due to the different integration times of the target and reference instruments. The near-instantaneous data collection and an ability to identify cloud shadow would appear to remove the need to ratio wavebands when analysing airborne images. Slight changes in solar irradiance and bi-directional reflectance factors (BRDF), however, have the potential to introduce variability which cannot be corrected by comparison with reflectance from a reference panel.

Airborne images of New Piece field were acquired at 59m sec^{-1} (115kt airspeed), taking *c.* seven seconds to traverse the experimental area. The airborne instrument records only total energy received by the sensor (radiance) rather than a percentage of solar irradiance

(reflectance) without adjustment for changes in solar irradiance. The CASI-2 instrument is fitted with an incident light sensor (ILS) although this is not currently used for irradiance correction (Milton *et al.*, 2000). Investigations are in progress (Choi *et al.*, 2002) which aim to account for the effects of aircraft attitude and thus enable the ILS to be used as a reference measure of solar irradiance in the future. Milton & Goetz (1997) describe how invisible patches of water vapour can cause short-term variation in the magnitude and distribution of solar irradiance, despite apparently cloud-free conditions. Their investigation focussed on the spectral region 700nm-1000nm and did not include the visible wavebands used in this experiment. However, their spectra differed by up to four percent at 700nm (the upper limit of the visible spectral region) over a period of nine minutes. Solar irradiance across the visible region may fluctuate in a similar manner and cannot be assumed to be constant. Energy reflected or re-radiated from the target and measured by the sensor will fluctuate according to irradiance and Milton & Goetz (1997) used reflectance from a white reference panel as a proxy to determine solar irradiance. A ratio between two wavebands is considered to be less sensitive to fluctuating irradiance as both numerator and denominator wavebands will be affected in a similar (if not identical) manner.

The direction in which the aircraft (and hence the instruments) are pointing (heading), rather than the ground track, determines how an airborne sensor is aligned with the principal solar plane. The headings for reciprocal flights of June 21st, 2001 differ by 192°-195°, indicating a wind-drift correction of 6°-7.5° from the planned track. An investigation of sensor view-angle effect on airborne image data by Barnsley & Morris (1990) indicated that BRDF was similar for both red and green wavebands (section 4.4.).

The 17202 vegetation bandset image used in this experiment was acquired at an aircraft heading generally aligned with the principal solar plane (*c.* 12.4° difference, details in

Appendix F.), thereby minimising BRDF reflectance factors from the wide (54°) sensor view-angle of the NERC ARSF CASI-2 instrument. Some residual BRDF effect cannot, however, be discounted and calculating the ratio of two visible-region wavebands is expected to substantially reduce this unwanted variability.

In contrast to soil reflectance from the 2000 field experiment, radiance from soil areas in the airborne images was higher than the crop canopy across the visible spectrum. Canopy closure was not complete in some heavily infested areas of the experimental field, allowing radiance from soil to contribute to the overall sensor response. Radiance from bare soil adjacent to the experimental area (beyond the eastern hedge margin of New Piece field) was recorded as *c.* 50% higher than canopy radiance at 550nm. The effect of (dry) soil in the sensor field-of-view would therefore increase radiance in the green waveband and reduce the negative correlation with PCN infestation. Correlation with infestation reported from this experiment was achieved despite the contribution from soil in heavily infested plots.

Radiance from vegetated areas is very low (*c.* 5-10%) at red wavelengths and radiance from soil was some three-and-a-half times greater at 680nm. This overwhelming influence on red radiance is thought to be responsible for the lower correlation ($F_{(1,28)}= 30.97$, $p < 0.001$, $R^2_{(28)}= 0.526$) of the red-green ratio when compared with the correlation of the green waveband ($F_{(1,28)}= 111.69$, $p < 0.001$, $R^2_{(28)} = 0.8$). Experimental plots where soil was visible in the images had a lower red-green ratio, introducing some scatter to the ratio chart (not shown). Some bare soil of the target area will have been due to reduced growth caused by PCN infestation, although soil and weather conditions at planting may have exerted an unknown influence on the canopy development and, although co-located, increased soil reflectance should not be interpreted as a clear symptom of infestation in this experiment.

4.5.4. Within-field heterogeneity.

The reduction in correlation ($F_{(1,121)}$=121.36, p <0.001, $R^2_{(121)}$= 0.501) of the green (551.12nm) waveband, derived from the means of four pixels surrounding point samples when compared with the means of 450-600 pixels from the experimental plot area samples ($F_{(1,28)}$=86.34, p <0.001, $R^2_{(28)}$= 0.755) of the combined enhanced-spectral mode images is seen as an indication that background heterogeneity of crop radiance is not fully accounted for by the 4m-by-4m point sample spectra. Mean values from larger areas of the crop canopy should therefore be considered for the detection of PCN infestation, unless the infestation foci are known to be strongly aggregated and pathogenesis is severe.

4.5.5. Classification.

An unsupervised classification method (as opposed to supervised where 'typical' areas are submitted as training examples) was used as this has the potential to reduce manual input in the detection process and to enable classification of areas where *a. priori* knowledge of PCN population density and distribution is not available.

The success of unsupervised classification in identifying infested crop areas may offer potential to automate the assay of PCN from airborne imagery. Grouping into classes will depend on the range of pixel values in the image and may be specific to image and location. The classification from this experiment, however, was conducted on an image that contained many non-target features, e.g. a small lake, a wooded area, bare soil and neighbouring fields, suggesting that the classification process can be robust.

4.5.6. General conclusions.

Green wavebands (~550nm) have been used in this experiment. The negative correlation of near infrared wavebands (> 700nm) with PCN infestation would deliver similar results to that of the green waveband. However, reduced near-infrared reflectance (or radiance) is

not unique to PCN infestation whereas the majority of stress factors result in increased reflectance at 550nm (Wiegand *et al.*, 1991).

The relationship between PCN infestation and green reflectance reported in section 2.2.3. is confirmed by results from the 2001 airborne data. The red-green ratio is also supported, despite some scatter in red radiance of highly-infested plots. This experiment has, despite some minor setbacks, succeeded in extending the application of spectral reflectance/radiance from localised field measurement to the wide-area airborne identification of PCN infestation. The consistency of results from the 2000 and 2001 field experiments, measured from ground and airborne imaging methods and using different cultivars, would suggest that these are genuine spectral responses to infestation and not artefacts. The possibility that results from the 2000 field experiment were influenced by changeable weather conditions or diurnal factors is largely discounted by results from near-instant spectra collected under cloud-free conditions in 2001. The 2000 field spectra support the 2001 airborne measurements and reduce the likelihood of these being due to spatial factors in the experimental area. Subsequent experiments were designed to confirm the results of this experiment and to investigate the potential of satellite imagery for the detection of PCN populations.

5. 2001 Outside pot experiment

5.1. Introduction.

Many factors impact upon the vitality of field crops, e.g. drought (Epstein & Grant, 1973), nutrient deficiencies (Ulrich, 1993) and viral or fungal pathogens (Hansen, 1991; Evans & Haydock, 1993; Back *et al.*, 2000). Several studies have indicated that plant spectral responses are similar across a wide range of stress-inducing factors e.g. Carter (1993) and Peterson & MacDonald (1996). The identification of measurable change unique to nematode infection is therefore an ambitious endeavour.

Commercial potato crops are susceptible to many viral and fungal organisms e.g. potato leaf-roll virus (PLRV) or stem canker (*Rhizoctonia solani*). Such pathogens affect plant health and vitality and potentially generate confounding spectral response features in crop canopies imaged for PCN detection. Nematode infection has been linked with increased plant susceptibility to fungal pathogens (Evans & Haydock, 1993) including *R. solani* on potato (Grainger & Clark, 1963; Back *et al.*, 2000). The spectral response of a potato crop's canopy to *R. solani* infection will be liable to detract from the spectral assay of PCN. The ability to segregate the spectral response patterns of PCN-infested crops from that caused by other plant pathogens can be expected to substantially enhance the accuracy and benefit of remote sensing for PCN detection.

Canopy reflectance is subject to many variables not present when working with single leaves. These variables include leaf angle, leaf area and background material (Bacci *et al.*, 1991; Hatfield & Pinter, 1993; Blackburn, 1998). Whilst this complicates the extrapolation of single-leaf data to canopy reflectance, the imaging of single leaves might

expose subtle differences in the spectral response to individual pathogens that would otherwise be masked by the greater complexity of canopy spectral reflectance.

A preliminary study was conducted on June 25th, 2000, on a field experiment in Four Gates Field, Edgmond Shropshire (OS Grid ref. 3707E, 3195N) which was established by the Ph.D student Matthew Back to investigate the interaction between PCN and *R. solani*. (Back *et al.*, 2000). Spectral measurements were collected by the methods described in section 2.2.1.1. Forty spectra were collected from four plants in each of ten experimental plots subjected to a range of PCN populations. Six of the ten plots had been inoculated with spores of *R. solani* at planting. Plotting NDVI values against root invasion data showed a correlation ($F_{(1,8)}$= 7.14, p= 0.028, $R^2_{(8)}$= 0.472) for the means of four plants per experimental plot. Visual examination of the data points revealed that plants inoculated with *R. solani* exhibited a consistently lower NDVI value than plants having a similar nematode burden (Fig. 5.1.).

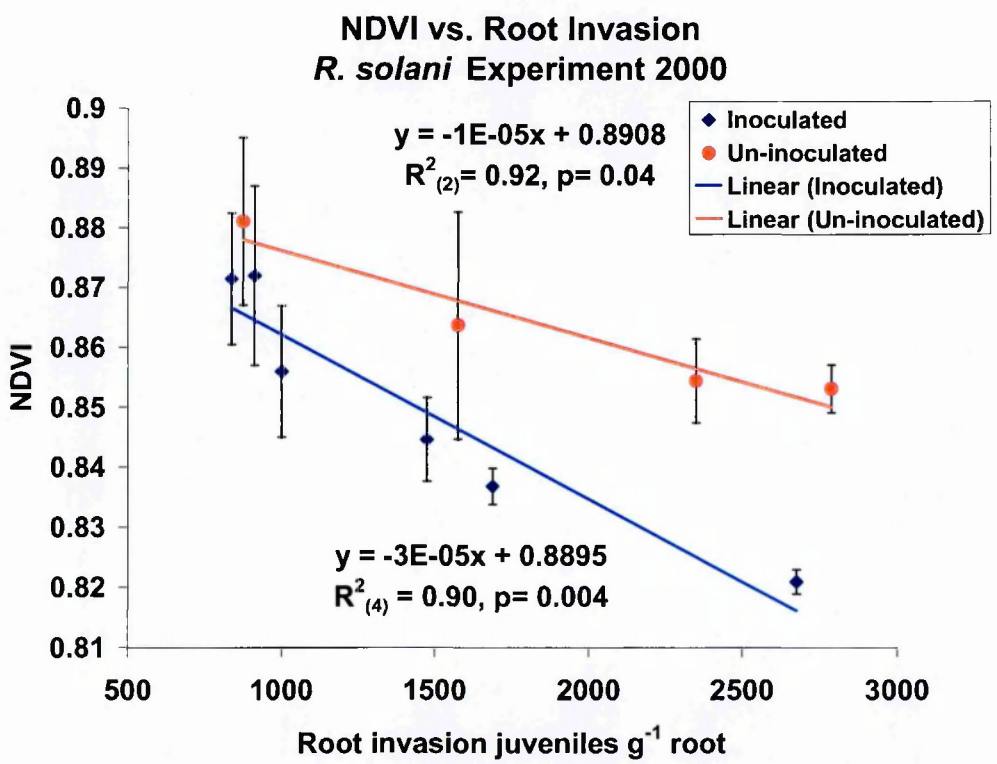

Figure 5.1. Plants inoculated with *R. solani* form a second, lower curve. NDVI ±SEM of four plants.

This observation suggested that the spectral response of *R. solani* could be interpreted as PCN infection, or distort a quantitative measure of PCN density obtained from spectral reflectance. The limited number of spectra and diurnal illumination factors rendered these data unsuitable for a more detailed analysis of spectral response to the two pathogens and a replicated pot experiment was therefore conducted in 2001.

1) To identify spectral response patterns caused by PCN infection in a controlled environment;
2) identify spectral response patterns caused by infection with *R. solani*;
3) examine differences in the spectral response patterns from each pathogen for a potential method of discriminating between them;
4) compare the spectral response pattern of plants infected with either or both pathogens to that from healthy (no-pathogen) plants.

5.2. Materials and methods.

Starting from a null hypothesis that there exists no difference in the spectral response of potato plant leaves when infected with *R. solani* or PCN, this experiment was designed to compare spectra between groups of plants infected with either pathogen. A further comparison, closer to field conditions where *R. solani* might not be excluded, comparing the spectra from plants infected with both pathogens to uninfected plants was conducted to look for spectral response to a possible interaction between PCN and *R. solani*.

5.2.1. Experiment design and preparation.

A pot experiment with fifteen replicates of four treatments was designed. The treatments were:

1) PCN	Soil inoculated with cysts of *G. rostochiensis*;
2) *R. solani*	Soil inoculated with *R. solani* (AG3);
3) PCN and *R. solani*	Soil inoculated with PCN and *R. solani*
4) No pathogens	Control plants, no inoculum used.

Plastic plant pots of 23cm diameter, 20cm depth were used to avoid constriction of the root mass prior to image collection, as such restriction may preferentially affect the healthier pathogen-free plants. Each pot had six drainage holes of 20mm diameter in the base, and pots were situated on gravel to facilitate the egress of surplus moisture. An unshaded outdoor location was selected and pots were arranged in four rows of fifteen, with treatments randomly distributed across the rows (four treatments per block, fifteen-fold replication). This arrangement was changed weekly to compensate for possible unequal illumination from adjacent plants and lack of competition for plants on the edge of the blocks. Blocks were redistributed within the rows and the inner and outer plants from each block exchanged position.

5.2.1.1. Potato seed tubers.

Sixty seed tubers, cv. Desireé, grade VTSC2 (Certified Scottish seed supplied by Scott & Newman, Shrewsbury.) were planted at 10cm depth in 23cm diameter pots (20cm depth) on May 5th, 2001. Seed tubers were selected for similar size within the 35-45mm supply specification and used in sequential order from the storage tray to avoid inadvertent bias between treatments.

5.2.1.2. *Rhizoctonia solani* inoculum.

A mixture of 20g maize, 980g silver sand and 250ml water was autoclaved at 120°C for 50 minutes on April 6th, 2001 and allowed to cool. This mixture was then inoculated with six mycelial plugs taken from the growth margin of a seven-day old culture of *R. solani*, anastomosis group 3 (AG3) supplied by M. Back, and placed in conical flasks, sealed with aluminium foil and cultured at 20C for 5 weeks. A similar sand/maize mixture was prepared for the uninoculated pots, although this was not autoclaved.

5.2.1.3. Potato cyst nematode inoculum.

Soil from Four Gates Field, Edgmond (OS Grid ref. 3707E, 3195N) was collected on March 13th, 2001 and placed in a drying cabinet prior to the extraction of PCN cysts by flotation. The source location had been under continuous potato cultivation for the previous three years, leading to the expectation of a high number of viable cysts. Cysts of *Globodera rostochiensis* (S. Minnis, personal communication) were washed from 9kg of dried soil on April 30th and May 1st, 2001, and were separated from other organic matter by repeatedly rolling across a sheet of white paper on May 2nd and 3rd, 2001. This process was repeated until only cysts were visible to the naked eye.

5.2.1.4. Preparation of the planting medium and agronomic inputs.

A mixture of 80% sterilised loam and 20% sand (William Sinclair Horticulture Ltd, Lincoln, UK) was prepared on May 4th, 2001. The soil purchase requirement for sixty pots was calculated as 426Kg of loam and 115Kg of horticultural sand. The supplier confirmed that the N, P and K content of this soil was low, and this would have been further reduced by the addition of horticultural sand. Nutrient input was as per MAFF Fertiliser recommendations RB 209 (MAFF, 2000), assuming index two. The appropriate amounts were calculated by dividing the surface area of sixty pots into one hectare, then multiplying the hectare nutrient rate by the resulting fraction. Nitrogen input was limited to half of the

total requirement to allow for replenishment of an expected higher rate of leaching at a later date.

The quantity of N, P and K added to the total soil mixture was as follows:

N: 82.6 g of 34.5% ammonium nitrate (NH_4NO_3) (34.5%N)
= 50% of calculated requirement.

P: 132.3g of 47% calcium phosphate ($Ca(H_2PO_4)_2.H_2O$ (47% P_2O_5)

K: 124.3 g of 60% potassium chloride (KCl) (60% K_20)

Loam and sand were measured out in pots of 23cm diameter, 20cm depth on May 5th, 2001. Forty-eight pots were filled level to the rim with sterilised loam and twelve pots with horticultural sand. The pots were emptied onto a swept concrete surface and N, P and K inputs added in granular form. The soil, sand and nutrient mix was then passed through a cement mixer three times, mixing by hand to amalgamate the mixer loads before each five minute mixer session. Thirty pots were then filled with soil before cysts of PCN were sprinkled over the remaining soil mix. This infested soil was then passed through the cement mixer a further four times and hand-mixed before each mixer load. The remaining thirty pots were then filled with the PCN-infested soil mixture.

The contents of each pot were emptied into a plastic sack and a 30ml scoop of the appropriate silver sand/maize mix added. The sack was then shaken for one minute to distribute the sand/maize throughout the soil. The pot was then half-filled from the bag, the seed tuber added and covered with the remaining soil. Separate sacks were used for each treatment to avoid cross-contamination. The no-pathogen plants were planted first, followed by the PCN-only pots. The workbench was then carefully swept before the *R.*

solani-only pots were planted, followed by the PCN+*R. solani* pots. Plants were placed outside immediately on planting (Plate 5.1.). Emergence was recorded on eight separate dates, at 17, 20, 23, 26, 27, 29, 30 and 31 days after planting (DAP).

Only 50% of the calculated nitrogen requirement had been incorporated during the planting process. A further 40% was applied on June 13th, 2001, by dissolving 70g of Nitram (34.5%) in 7000ml of water and pouring 100ml onto the soil of each pot. This process was repeated on July 13th, 2001, bringing the nitrogen input to 130% of calculated requirement in response to suspected leaching by heavy rain and constant watering.

5.2.1.5. Assessment of *R. solani* infection.

Assessment of *R. solani* severity followed a scoring protocol devised by Back *et al.* (2000) in which a numerical score is applied to each stem. The sum of these scores is divided by the number of main stems, with secondary stems counted as half of a main stem. Damaged stolons, tuber-bearing underground stems, are also included in the overall assessment and scores range from 0 (no disease) to 9 (plant dead). Although scores can be derived in a number of permutations, plants with a score equal to the mean for the current experiment (4.74) will have suffered substantial damage e.g. pruning of a main stem or complete girdling by necrotic lesions.

5.2.1.6. Sampling for PCN population density estimation.

A 200g soil sample was taken from the pots during the planting proceedure. Cyst extraction and egg counts were made according to the procedures described by Shepherd (1986) and initial nematode population density estimation (Pi) for each pot recorded as eggs g^{-1} soil.

5.2.1.6.1. Harvest for plant residue measurement.

Plants were harvested on 07/08/2001 at 93 DAP and the effects of treatment on plant growth parameters recorded. Tubers were seperated from the plant, weighed and counted. Total plant weight (without tubers) was then recorded. The haulm was separated from the remaining plant material, weighed immediately and oven dried for 48 hours at a temperature of 95° C. Dried haulm material was weighed within 30 minutes of removal from the drying oven and the residual weight recorded as percentage of fresh weight to determine haulm dry matter.

5.2.2. Spectral reflectance measurements.

Two spectral assays were performed on the experimental plants. Whole plants were measured under natural (solar) illumination, and excised single leaves were recorded in a laboratory.

5.2.2.1. Spectral measurements under natural (solar) illumination.

A series of spectral reflectance measurements were taken from plants of the pot experiment on July 4th, 2001, using a GER 1500 dual-beam spectrometer (Plate 5.2.) in an open space, free from shadow and remote from trees and shrubbery which might scatter light into the experimental area. Plants were placed under the target sensor and the GER laser guide used to ensure that the plant was central beneath the instrument. Five spectra were recorded from each sample in quick succession and plants were rotated *c.* 60 degrees between each recording. The reference sensor remained static over the calibration panel at all times. Two hundred and eighty spectra were recorded from fifty-six plants. The means of five spectra per plant were carried forward to the subsequent spectral analyses.

Plate 5.1. Plants of the 2001 pot experiment.

Plate 5.2. GER 1500 dual-beam spectrometer.

5.2.2.2. Spectral imaging of leaves under controlled laboratory conditions.

The experimental plants were transported to the Institute of Grassland Research, Aberystwyth (IGER) on July 25th, 2001, packed securely in an enclosed vehicle and placed in a sheltered outdoor location on arrival. Twenty-eight plants were measured during this visit, eight replicates of no pathogen, PCN and *R. solani*, plus four replicates of PCN+*R. solani*.

Groups of four plants, one from each treatment, were taken into the IGER building and placed under a window. Three leaves were measured from each plant, with individual leaves being detached from the plant immediately before measurement . The order in which plants from the treatments were processed rotated with every group to compensate for possible desiccation or reduced photosynthetic activity whilst inside the building. Imaging continued on July 26th, 2001, although PCN+*R. solani* plants were omitted to enable the imaging of more replicates from the other treatments as imaging was taking longer than anticipated. Plants were imaged in groups of three on this occasion.

The room used for imaging was a normal office, fitted with light-excluding curtains, but with light-coloured walls. Internal blackout measures were makeshift with sheets of black card arranged around the computer monitors to shield the camera from direct illumination. All operator movement and computer-activity was suspended during the imaging process.

Imaging equipment, consisting of a digital camera (Photometrics Sensys 1401E digital camera with a Kodak KAF 1401E Grade 1 CCD chip (1317 x 1035 pixels) fitted with a tuneable filter (VariSpec VIS2 tuneable Lyot-type birefringent filter, Cambridge Research and Imaging Inc.), both controlled by dedicated software (MetaMorph, Universal Imaging Corporation) on a desktop computer (plate 5.3.). The camera collected a series of images as the filter switched between wavebands (Plate 5.6.). The output for each leaf was a

series 46 TIF format picture files (Plate 5.6.) ranging from 520nm to 700nm, the upper limit of the filter, at intervals of four nanometres (nm). The filter bandwidth – full width, half maximum (FWHM) of the transmission curve - varied with wavelength, from *c.* 9.2nm at 520nm to *c.* 18nm at 700nm, and there was some overlap between images separated by a nominal 4nm. Image files were saved on to sixty compact disks.

Two fibre-optic 'cold-light' laboratory lamps were arranged on either side of the camera. Each lamp had two lenses, and the four beams of light were arranged radially around the leaf and as close as possible to the camera lens, so as to reduce shadowing.

The terminal leaflet from each stem was selected, unless small (< 2cm wide) or damaged. Lower leaves were used when a plant had less than 3 stems. Leaves did not fill the camera field-of view and a background area of black cardboard is visible in the images. The white adhesive fixing material is also visible in images taken early on the first day. Glare from this substance was seen to be affecting images of the surrounding leaf area, and a black card overlay with an aperture cut to show most of the leaf was substituted at midday (Plate 5.3.). The aperture card remained in use for all plants imaged during this visit

5.2.2.2.1. Calibration measurements.

Calibration measurements were recorded immediately following each group of four plants by imaging a block of Spectralon (Labsphere, Inc. North Sutton, NH, USA.) material having near-100% reflectance (Plate 5.4.).

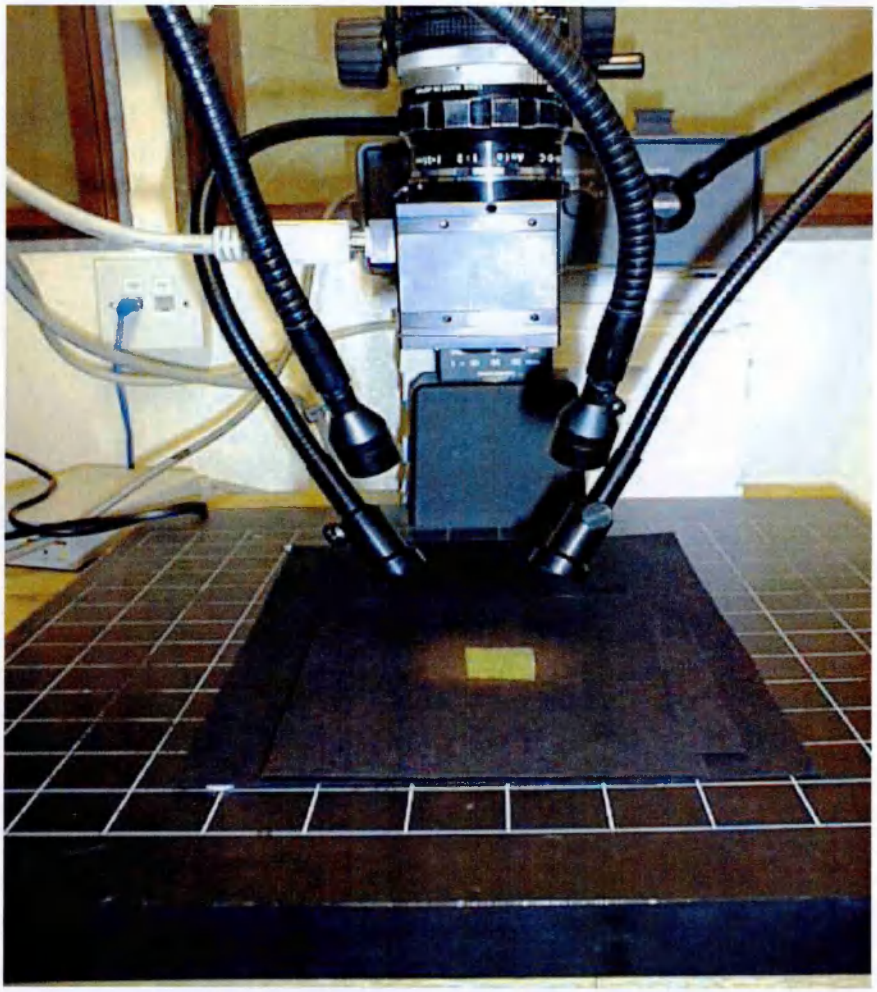

Plate 5.3. IGER camera and card aperture.

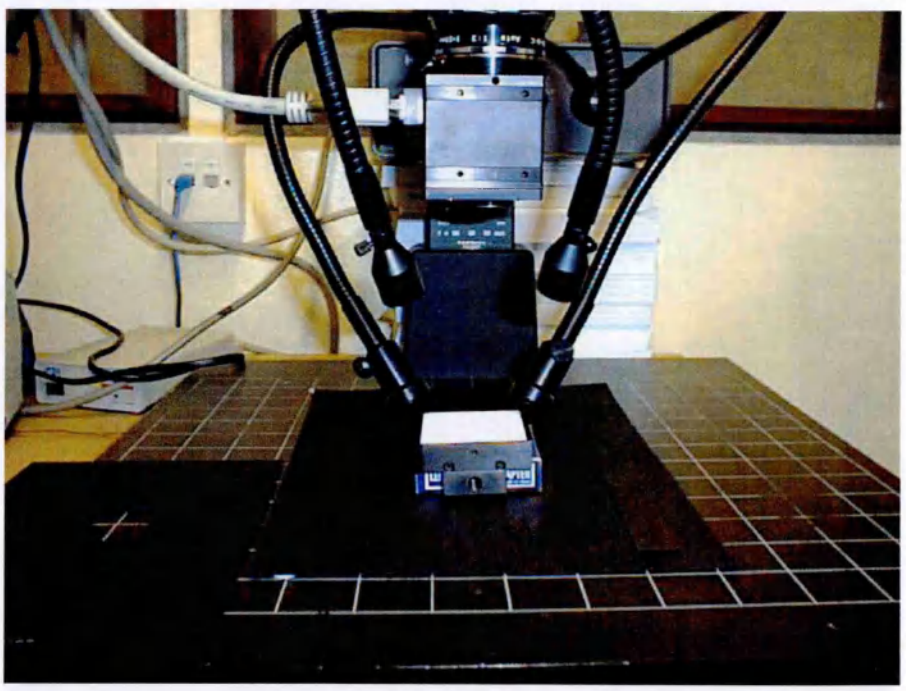

Plate 5.4. Spectralon calibration panel.

A second visit was made to IGER on August 1st and 2nd, 2001 with the 28 remaining plants: seven no-pathogens, seven PCN, four *R. solani*, and ten PCN+*R. solani*. A rectangle of wood, covered with black card had been fabricated to secure the leaves. Four narrow fingers of black plastic, cut from the casing of a computer disk, held the leaf in place (Plate 5.5.) and this device was used to hold all leaves measured during the second visit. Calibration spectra were again recorded after every group of four plants

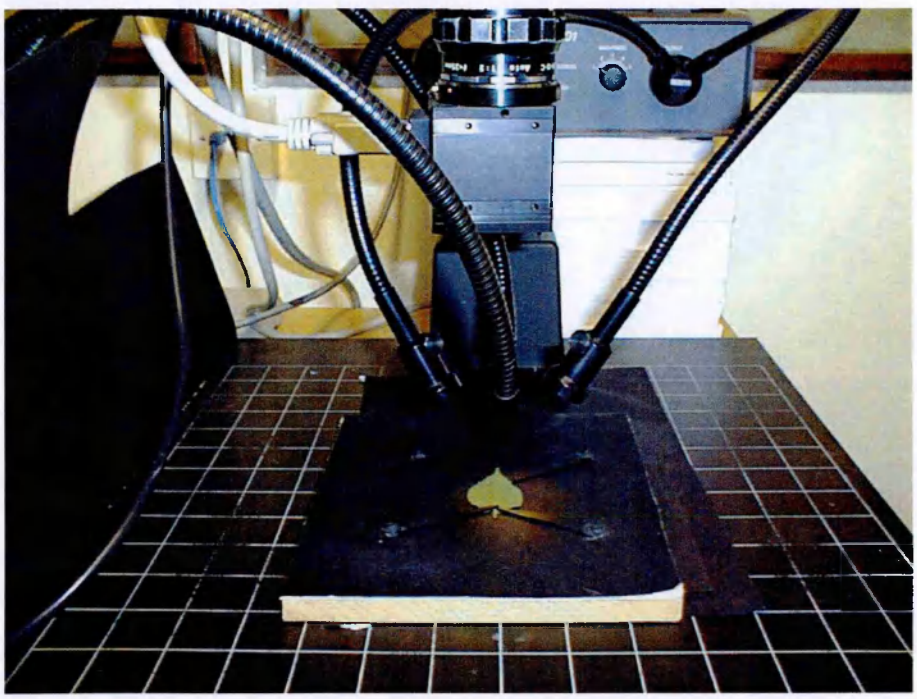

Plate 5.5. Finger card used in the 01/08 and 02/08/2001 imaging sessions.

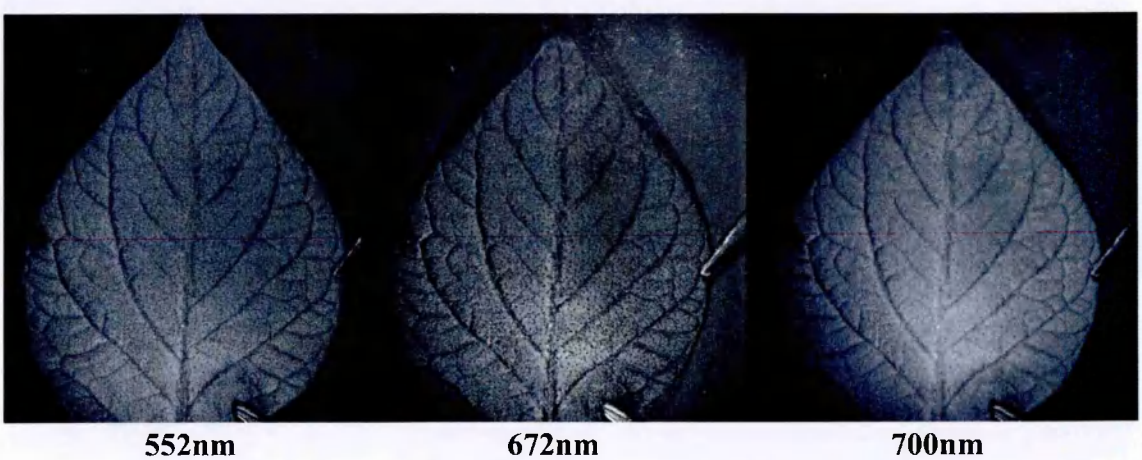

Plate 5.6. Typical leaf shown at three wavelengths, 552nm (green), 672nm (red) and 700nm (far-red). IGER digital camera and variable filter.

One fibre-optic laboratory lamp developed an electrical fault on the morning of August 1st. Subsequent examination of the images indicated that this lamp had been fluctuating imperceptibly during the entire session. Two plants, one from treatment PCN and one PCN+*R. solani*, were measured under the faulty lamp and have been excluded from the IGER data set.

5.2.3. Processing of the IGER spectral reflectance measurements.

Spectral data collected at IGER were examined with the aid of the ImageTool software program and scripting language. Imagetool software was developed for the analysis of medical imagery by the University of Texas Health Science Centre, San Antonio, Texas (UTHSCSA) (ftp://maxrad6.uthscsa.edu).

The camera records the intensity of light reaching each of its sensor elements as a digital number (DN). ImageTool is able to read the DN value from individual pixels of a tagged image format (TIF) picture file. This software was used to select suitable pixels, calculate their mean at each wavelength and write the results to a spreadsheet-compatible results file. A comprehensive scripting program, supplied with the ImageTool software, facilitates the automation of a complex sequence of actions. ImageTool script programs were written to select a series of plants and process the image files from the three leaves of each plant. A typical script would process eight plants – 24 leaves, 1,104 images and 2,880Mb of data. Scripts were left to run overnight, taking up to 12 hours to complete. Several problems were encountered when lack of computer memory caused the script to terminate, and the process was often repeated with four plants only. A sample ImageTool script is listed in Appendix H.

When energy reaching a sensor exceeds the upper limit of the sensor's dynamic range, that sensor is saturated -it is unable to measure a further increase in energy (light). Changes in

sensor response and illumination strength were to have been corrected by ratioing the plant spectra with calibration measurements collected after each session. In practice, reflectance from the Spectralon panel often exceeded the sensor capacity and large areas of the image became saturated. The exceptional reflectance during calibration also diffused a large amount of light into the room where it might be reflected back to the camera lens. Calibration of the leaf images gave variable results and analysis was undertaken on raw reflectance only. Every change of settings or equipment therefore marked the beginning of a new session, and each session has been treated as a separate experiment.

Some specular reflectance from leaf veins was visible at 616nm. This, and non-contributory reflectance from the dark background material was reduced by setting minimum (MIN) and maximum (MAX) pixel selection criteria in the image processing scripts. These upper and lower limits were set to correspond with the illumination level of the current data set and were session-specific. Changing the limits altered the spectral response curve and all plants within a data set were processed using the same parameters.

Although the dynamic range of the camera extended to DN 4096 (= 2^{12}), examination of the output spectra indicated that sensor response was reduced as pixel values neared this limit. Scripts recorded the number of pixels, if any, which reached a DN value of 3850, and wrote this information to the results file.

5.2.3.1. Processing sequence.

1) Select the first plant;
2) select the first leaf;
3) open the reference file (600nm);
4) select all pixels having a DN value between MIN and MAX;
5) create a .CSV output file;

6) open each image (waveband) file in turn;

7) record the DN values for all pixel locations selected in step 4;

8) record the number of saturated pixels (if any);

9) calculate the mean DN for all selected pixels;

10) write the mean, and saturated pixel count to the output file;

11) repeat for each leaf;

12) repeat for each plant.

This process was dependent on a specific pixel location recording the same leaf area across all 46 images. Leaves were firmly mounted throughout each imaging sequence and only diffraction by the filter could alter the pixel location. Inspection of a prominent visual feature from a sample leaf indicated that no movement had taken place. The images were rectangular and the leaves were not: images contained either some background material or a sub-set of the leaf. Selecting a sub-set would have been a manual process and a potential source of bias. The decision was taken make the images larger than the leaves and to process a rectangle that just covered the leaf, while minimising the inclusion of background material. Leaves imaged using white adhesive on the morning of 25/07 were, however, processed using the largest possible within-leaf rectangle while avoiding proximity to the white adhesive, as this was the only way of preventing glare from the adhesive affecting leaf reflectance.

There was some overlap between spectral reflectance curves from the leaves and the backing card. This made comparison between data sets unreliable as the spectral values were a composite of all pixels selected from the reference file, and the spectral curve of black card was markedly different to that of the target material. The variable ratio of leaf to background also introduced a potential confounding factor between plants from the

same session, although careful selection of the MIN parameter and image area eliminated this factor where possible.

A second analysis was performed using tighter minimum and maximum pixel values, selected from the 25th file (616nm, peak reflectance). The selection of 616nm as the reference wavelength was seen to be successful in excluding saturated pixels at all wavelengths. Background reflectance was excluded from this data set by selecting the largest possible rectangle that could be located entirely within the leaf. A small element of subjectivity remained, however, as several rectangles (tall, thin or short, wide) could be fitted within a single leaf. Comparison of the first and second image analysis revealed that the spectral curve from each differed, primarily in *c.* 5% lower red reflectance, increasing towards infrared (+15% at 700nm).

Plants imaged on July 26th, 2001 (session three) were re-analysed using file 46 (700nm) as the reference. Some 'saturated' pixels were noted and four leaves from two *R. solani* plants were identified as having 0.1% pixels exceeding the 3850 saturation limit. As this is DN 246 below the sensor limit, and does not represent a sudden change in sensor response, the contribution of one pixel per thousand exceeding this value was expected to be insignificant. Indices of the ratio between two wavebands, e.g. NDVI = (NIR-Red)/(NIR+Red) should have been independent of signal strength, but remained sensitive to variable spectral response curves from different sessions. In addition to differences in illumination levels, individual sessions produced different spectral curves and this was reflected in the variance of ratio indices.

5.2.4. Statistical analysis of the IGER image data.

Analysis was conducted on spectra collected from four treatments over five sessions. The treatment PCN+*R. solani* was omitted from session three (26/07/2001) and no plants from treatment *R. solani* remained for analysis by session five (02/08/2001).

Plant N= 42 No-pathogen= 11, PCN= 12, *R. solani*= 7, PCN+*R. solani*= 12

Session N= 20 (5 sessions per treatment)

Preliminary examination of the data was carried out in the Microsoft Excel 97 spreadsheet program (Microsoft Corp, Seattle, Washington, USA) as this enabled rapid visualisation of the spectral relationships. Line plots charting the correlation between spectral response and treatment were plotted in the Excel charting feature and five candidate wavebands were selected from these charts where the means of treatment spectra diverged.

Four waveband combinations were examined:

1)	IGER-NDVI	calculated as	(700nm-672nm)/(700nm+672nm)
2)	GREEN-RED+1		1+((552nm-672nm)/(552nm+672nm))
3)	GREEN-ORANGE		(552nm-608nm)/(552nm+608nm)
4)	RED-ORANGE		(672nm-608nm)/(672nm+608nm)

The constant (1) was added to the GREEN-RED ratio index to avoid the introduction of negative values to the statistical analyses. The ratio between these wavebands was reversed from that of previous (solar illumination) spectral measurements due to a red-bias in the laboratory light source.

Five candidate wavebands were also examined:

1) 552nm (green)
2) 608nm (orange)
3) 624nm (orange)
4) 672nm (red)
5) 700nm (near infra-red)

A conventional analysis of variance (ANOVA) could not be used as the data structure was unbalanced. Consequently, a Generalised Linear Model (GLM) approach using normal errors was adopted using Genstat (Lawes Agricultural Trust, Rothamsted) allowing the effects of session, treatment and the interaction between session and treatment to be determined.

In the analysis, a single pooled reflectance value for each of the four candidate waveband combinations and five individual wavebands for each plant were calculated as the mean reflectance of sub samples of three leaves. In this way, individual plants formed the replicates and potential issues of pseudoreplication were avoided.

5.2.5. Statistical analysis of the GER dual-beam spectrometer data.

Ratio indices, similar to those used to analyse the IGER spectra, were calculated from the mean spectra of forty five plants imaged with the GER dual-beam spectrometer on July 4th, 2001.

1) NDVI: (780nm-675nm)/(780nm+675nm)
2) IGER-NDVI: (700nm-675nm)/(700nm+675nm)
3) GREEN-NDVI: (780nm-552nm)/(780nm+552nm)
4) ORANGE-RED: (608nm-675nm)/(608nm+675nm)
5) ORANGE-GREEN: (552nm-608nm)/(552nm+608nm)
6) GREEN-RED: (552nm-675nm)/(552nm+675nm)

The NDVI ratio constructed from the GER data used 780nm as the NIR waveband as the upper limit of the IGER filter (700nm) is closer to visible red than true NIR The ratio 'IGER-NDVI' was included in the GER spectral data when the IGER results indicated that this ratio might be significant, and in order to compare the GER spectra directly with the IGER results.

All GER spectra were collected in a single session and under identical conditions. The range of emergence dates (17 to 31 DAP) of these plants was considered to be a possible confounding factor. Imaging took place at 60 DAP, 43 days after the first plant emerged, but only 29 days from the last emergence. Mean emergence per treatment differed by almost two days (Table 5.1) and, as this difference might be a symptom of the infection, DAP was included in the analysis in order to investigate a possible effect on spectral reflectance.

5.3. Results.

5.3.1. Results from the experimental preparation.

Plants emerged from seventeen to thirty-one days after planting (DAP) (Table 5.1.).

Table 5.1. Mean emergence and standard error of means, days after planting (DAP).

Treatment	All plants	Plants used
No pathogens	22.60 ±0.40	22.18 ±0.42
PCN	22.60 ±0.65	23.00 ±0.74
R. solani	23.75 ±0.87	23.71 ±1.29
PCN+*R. solani*	24.07 ±0.79	24.15 ±0.85

Four plants failed to emerge, three from treatment *R. solani* and one from treatment PCN+*R. solani*. Two no-pathogen plants, three from treatment PCN and four from

treatment *R. solani* were excluded from the analysis due to infection with a pathogen from one of the other treatments. No-pathogen plants 10a and 12a were mono-stem and very light in colour, visibly different from the other plants, and also excluded. Forty-five plants remained available for analysis:

No pathogen	11 plants
PCN	12 plants
R. solani	8 plants
PCN+*R. solani*	14 plants

The recorded average Pi of 94.5 eggs g^{-1} of dry soil was close to the target value of 100 eggs g^{-1} soil (Table 5.2.), although the range, from 36 to 187 eggs g^{-1} soil of the thirty pots is surprising in view of the extensive mixing performed as part of the planting procedure. Cyst counts are less variable (107 – 156 cysts per 200g sample) and Pi variability is largely due to a wide range of eggs per cyst (60-240).

Table 5.2. Mean nematode infestation (eggs g^{-1} soil) and standard error of means.

	Mean Pi (PCN)			
Treatment	All plants		Plants used	
PCN	95.66	±6.95	96.07	±8.70
PCN+*R. solani*	93.87	±9.49	92.79	±10.18

Every surviving plant inoculated with *R. solani* became infected to a significant degree (Table 5.3.). Although *R. solani* scores can be derived in a number of permutations using the method of Back *et al.* (2000), plants with a score equal to the mean for the current experiment (4.74) will have suffered substantial damage e.g. pruning of a main stem or complete girdling by necrotic lesions.

Table 5.3. Mean *R. solani* score and standard error of means.

	Mean *R. solani* score			
Treatment	All plants		Plants used	
R. solani	5.08	±0.32	5.09	±0.40
PCN+*R. solani*	4.46	±0.31	4.39	±0.32

5.3.2. Results of the spectral analyses.

5.3.2.1. IGER digital camera data.

Session was a significant factor for all candidate wavebands and waveband ratios from the IGER digital camera spectral data (Table 5.4.). The effect of treatment was significant for the ratio indices IGER-NDVI (p=0.01) and Orange-Red (p=0.05), which were able to discriminate between treatments no-pathogen and PCN+*R. solani* (Figures 5.2. and 5.3.). The ratio Orange-Red was also able to discriminate between PCN and *R. solani* (Figure 5.3.).

Table 5.4. Analysis of session, treatment and session-treatment interaction effects of the IGER digital camera measurements..

	IGER Data		
Waveband/Ratio	Session	Treatment	Session x Treatment
IGER-NDVI	$F_{(4,25)}$=35.09, p<0.001	$F_{(3,25)}$=4.63, p=0.01	$F_{(10,25)}$=1.15, NS
ORANGE-RED	$F_{(4,25)}$=35.05, p<0.001	$F_{(3,25)}$=2.94, p=0.05	$F_{(10,25)}$=0.43, NS
ORANGE-GREEN	$F_{(4,25)}$=32.62, p<0.001	$F_{(3,25)}$=0.86, NS	$F_{(10,25)}$=0.65, NS
GREEN-RED+1	$F_{(4,25)}$=38.97, p<0.001	$F_{(3,25)}$=2.59, NS	$F_{(10,25)}$=0.62, NS
NM552	$F_{(4,25)}$=100.39, p<0.001	$F_{(3,25)}$=1.41, NS	$F_{(10,25)}$=0.21, NS
NM608	$F_{(4,25)}$=155.88, p<0.001	$F_{(3,25)}$=2.46, NS	$F_{(10,25)}$=0.4, NS
NM624	$F_{(4,25)}$=184.34, p<0.001	$F_{(3,25)}$=2.19, NS	$F_{(10,25)}$=0.62, NS
NM672	$F_{(4,25)}$=67.34, p<0.001	$F_{(3,25)}$=0.59, NS	$F_{(10,25)}$=0.55, NS
NM700	$F_{(4,25)}$=21.76, p<0.001	$F_{(3,25)}$=0.81, NS	$F_{(10,25)}$=0.11, NS

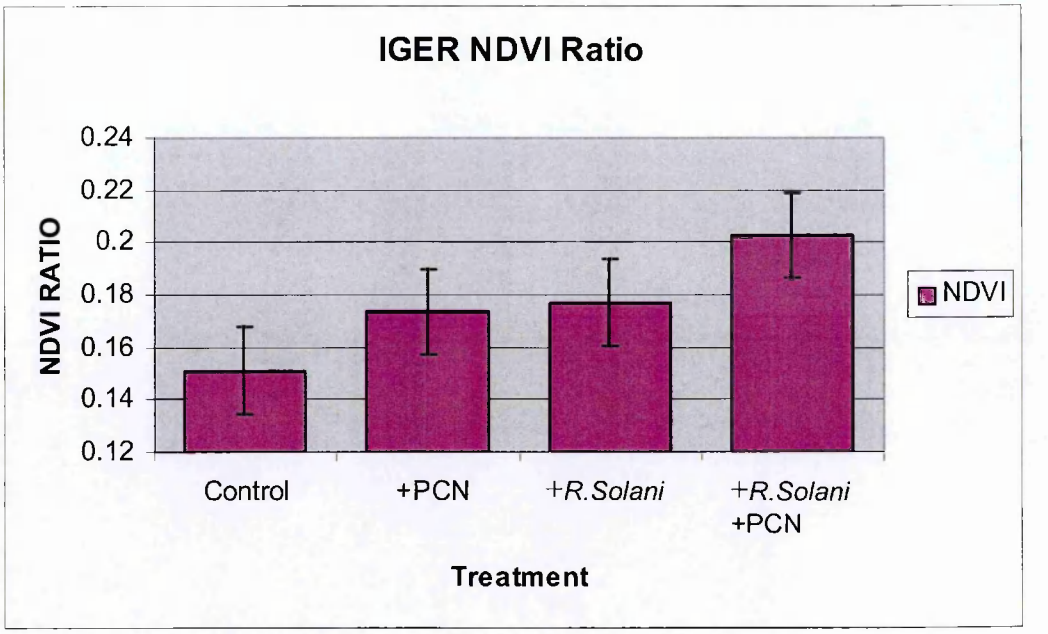

Figure 5.2. NDVI treatment means from the IGER camera reflectance spectra and least significant differences (min replicates) from potato plants of the 2001 outside pot experiment.

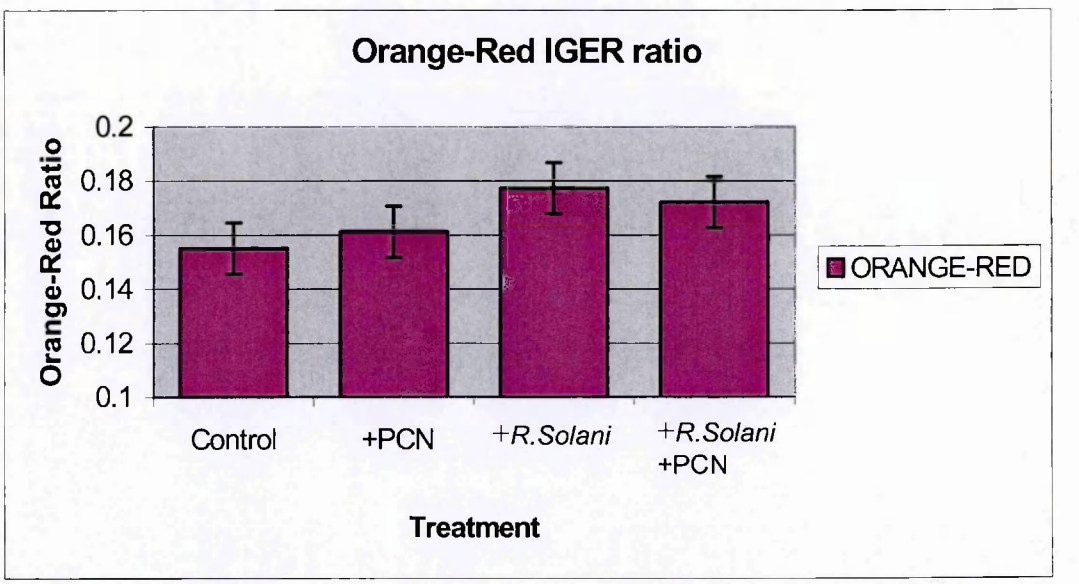

Figure 5.3. Orange-Red treatment means from the IGER camera reflectance spectra and least significant differences (max-min replicates) from potato plants of the 2001 outside pot experiment.

5.3.2.2. GER dual-beam spectra.

Plant N= 45 No-pathogen= 11, PCN= 12, *R. solani*= 8, PCN+*R. solani*= 14

DAP N= 8 Emergence recorded on eight occasions.

The GER instrument collects spectra in 512 individual wavebands, each of a nominal 1.5nm bandwidth. This fine division of the limited incoming energy reduces the signal-to-

noise ratio (SNR) and narrow wavebands offer no advantage to this ratio analysis. Wavebands were therefore calculated as the mean of five waveband values, centred around the nominal wavelength, to reduce the effects of SNR on the very subtle differences in treatment means.

The ratio indices Green-Red and Orange-Green showed significant ($p<0.05$) effects of treatment and both were able to discriminate between treatments PCN and *R. solani* (Figures 5.4. and 5.5.). Neither ratio was able to produce a significant difference between the means of treatments no-pathogen and PCN+*R. solani* and the two pathogens may be moving the ratio in opposite directions (Figures 5.4. and 5.5.). Days after planting (DAP) was not significant for any of the ratios or wavebands investigated (Table 5.5.).

Table 5.5. Summary for the effects of DAP, treatment and DAP-treatment interaction on reflectance at target ratios and wavebands of GER dual-beam spectra from potato plants of the 2001 outside pot experiment..

GER dual-beam spectrometer data.

Waveband/Ratio	DAP	Treatment	DAP x Treatment
NDVI	$F_{(7,42)}$=1.81, NS	$F_{(3,42)}$=0.42, NS	$F_{(5,42)}$=0.18, NS
GREEN-NDVI	$F_{(7,42)}$=1.65, NS	$F_{(3,42)}$=1.32, NS	$F_{(5,42)}$=0.12, NS
IGER-NDVI	$F_{(7,42)}$=0.51, NS	$F_{(3,42)}$=2.53, NS	$F_{(5,42)}$=0.40, NS
GREEN-RED	$F_{(7,42)}$=0.40, NS	$F_{(3,42)}$=3.13, p=0.04	$F_{(5,42)}$= 0.29, NS
ORANGE-GREEN	$F_{(7,42)}$=0.69, NS	$F_{(3,42)}$=3.34, p=0.03	$F_{(5,42)}$=0.49, NS
ORANGE-RED	$F_{(7,42)}$=0.31, NS	$F_{(3,42)}$=2.16, NS	$F_{(5,42)}$=0.22, NS
NM552	$F_{(7,42)}$=1.11, NS	$F_{(3,42)}$=0.50, NS	$F_{(5,42)}$=2.79 p=0.04
NM608	$F_{(7,42)}$=1.07, NS	$F_{(3,42)}$=0.43, NS	$F_{(5,42)}$=2.92 p=0.03
NM624	$F_{(7,42)}$=1.06, NS	$F_{(3,42)}$=0.42, NS	$F_{(5,42)}$=2.86 p=0.03
NM675	$F_{(7,42)}$=1.10, NS	$F_{(3,42)}$=0.56, NS	$F_{(5,42)}$=2.71 p=0.04
NM700	$F_{(7,42)}$=1.10, NS	$F_{(3,42)}$=0.32, NS	$F_{(5,42)}$=3.01 p=0.03
NM780	$F_{(7,42)}$=1.22, NS	$F_{(3,42)}$=0.39, NS	$F_{(5,42)}$=2.38, NS

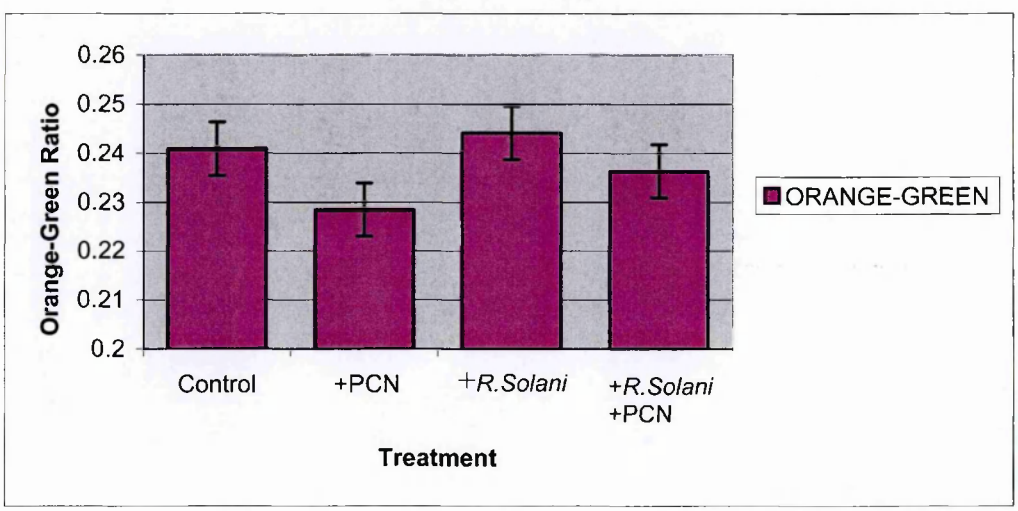

Figure 5.4. Orange-Green treatment means from the GER reflectance spectra and least significant differences (min replicates) from potato plants of the 2001 outside pot experiment.

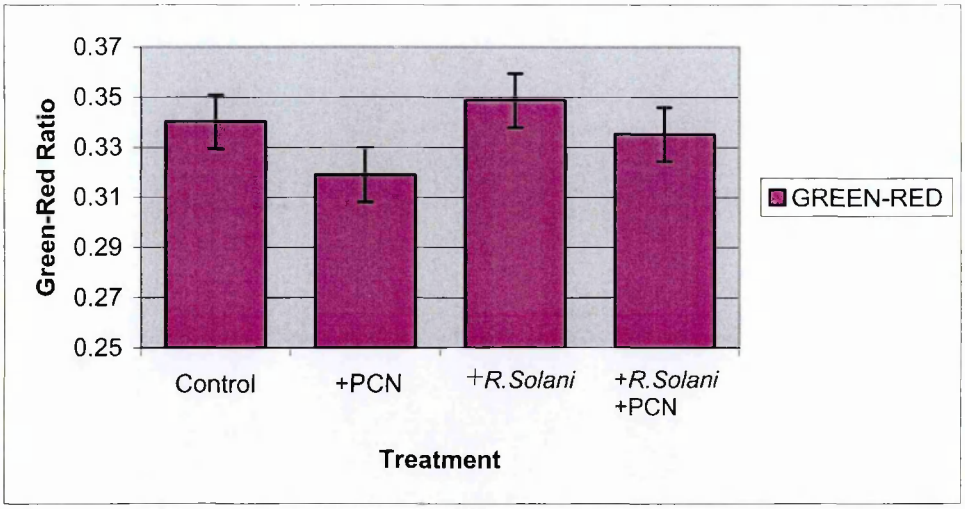

Figure 5.5. Green-Red treatment means from the GER reflectance spectra and least significant differences (min replicates) from potato plants of the 2001 outside pot experiment.

5.3.2.3. Analysis of plant residue.

N= 56 No-pathogen= 15, PCN= 15, *R. solani*= 12, PCN+*R. solani*= 14

Plants were harvested on 07/08/2001 and the relationship between treatment and plant growth parameters recorded (Table 5.6; 5.7.).

Table 5.6. Analysis of plant residue measurements from potato plants of the 2001 outside pot experiment..

Plant parameter	
No. Primary Stems	$F_{(3,43)}$=9.32, p<0.01
No. Secondary Stems	$F_{(3,43)}$=3.85, p=0.02
Whole Plant Weight (excluding tubers)	$F_{(3,43)}$=7.97, p<0.01
Haulm Weight	$F_{(3,43)}$=8.31, p<0.01
No. of Tubers	$F_{(3,43)}$=6.05, p=0.02
Total Tuber Weight	$F_{(3,43)}$=10.45, p<0.01
Mean Weight per Tuber	$F_{(3,43)}$=4.37, NS
Percent Dry Matter	$F_{(3,43)}$=1.26, NS

Table 5.7. Means and standard errors of plant residue measurements. Mean weight per tuber is reported as treatment means for the derived mean weight per tuber parameter of individual plants.

Mean Plant parameter	No-pathogen	PCN	*R. solani*	PCN+*R. solani*
No. Primary Stems	5.22 ±0.28	4.33 ±0.45	3.11 ±0.42	2.86 ±0.23
No. Secondary Stems	0.00	0.25 ±0.18	2.22 ±0.95	1.36 ±0.45
Whole Plant Weight (g) (excluding tubers)	203.84 ±7.72	189.31 ±8.87	167.36 ±9.56	153.38 ±6.23
Haulm Weight (g)	147.93 ±6.48	126.22 ±6.13	124.60 ±7.63	105.07 ±4.82
No. of Tubers	16.22 ±1.01	18.42 ±1.70	13.67 ±0.80	11.79 ±1.02
Total Tuber Weight (g)	298.88 ±9.05	257.67 ±6.43	300.84 ±8.99	255.13 ±6.90
Mean Weight per Tuber (g)	18.91 ±1.15	15.59 ±1.74	22.80 ±1.72	24.17 ±2.30
Percent Dry Matter	8.18 ±0.16	8.26 ±0.11	8.05 ±0.15	8.37 ±0.07

5.4. Discussion.

5.4.1. Leaf spectroscopy under laboratory conditions.

Johnson (1999) examined the spectral reflectance of vine leaves infested with the grape root louse phylloxera (*Daktulosphaira vitifoliae* Fitch) under laboratory conditions and with limited success, being able to distinguish between leaves from infected and uninfected plants, but not between leaves from lightly and heavily infected samples. Blazquez & Edwards (1983) imaged leaves from potato and tomato plants under laboratory conditions, seeking to identify suitable wavebands for aerial infrared photographic survey of crop disease. They imaged ten leaves each from potato plants with no infection, early blight (*Alternia solani*) and late blight (*Phytophthora infestans*). These pathogens produce necrotic lesions that directly affect the surface colour and structure of the leaf while PCN and *R. solani* do not act directly on the leaf. The discrimination of spectral response to pathogens in the root and stems is likely to be harder to define. Laboratory reflectance measurements from detached leaves are frequently obtained using an integrating sphere connected to a spectrometer (e.g. Gates *et al.*, 1965; Fourty *et al.*, 1995; Peñuelas *et al.*, 1995), thereby minimising directional effects of illumination and reflectance. An

integrating sphere was not available to the 2001 experiment, which was planned at short notice in response to availability of the IGER digital camera equipment.

5.4.2. Individual leaf measurements with a digital camera.

The interpretation of spectra collected with the IGER digital camera equipment is complicated by unequal conditions between different sessions and a lack of suitable calibration spectra to correct for those differences. Variability in overall session levels, seen in the sharp rise of session significance for individual wavebands (Table 5.4.), are matched to a reduction in treatment significance. Ratio indices are less susceptible to session differences as both sides of the equation are similarly affected. Session remains the most significant factor however, as differences in the shape of spectral response curves, due to changed lighting conditions or varying background reflectance interact with the contrasting waveband reflectance of the ratio indices. The ratio index 'IGER-NDVI' was able to distinguish between healthy and stressed plants when both pathogens were present, while the ratio Orange-Red was able to discriminate between spectra from the two pathogens, ($p=0.05$) in the IGER spectral measurements. The ratio indices Green-Red+1 ($p=0.075$) and the waveband 608nm ($p=0.86$), each selected as a potential predictor of PCN - *R. solani* difference, were approaching significance and further development of the method might bring these measures into renewed consideration.

5.4.3. Imaging of whole plants under conditions of natural illumination.

The GER 1500 dual–beam spectrometer enables the rapid collection of a large number of spectra in quick succession. File sizes are small, typically one-hundredth of the data volume from the IGER camera, and post-processing takes minutes rather than hours.

Ratio indices between green and red, or green/orange wavebands were able to discriminate between PCN and *R. solani* while only NDVI discriminated between healthy plants and those infected with both pathogens. Carter (1993) suggested the wavelength regions 535-

640nm and 685-700nm as potential indicators of plant stress and all significant ratios from the present study use wavebands within, or close to these regions.

Field spectrometer measurements are extremely sensitive to changes in ambient light, despite a near-simultaneous calibration measurement in dual-beam mode. The spectrometer field-of view is also very small, typically 2-3 cm diameter, and leaf angle or shadowing can have a disproportionate influence on the magnitude of individual spectra. A large number of replicates are therefore required before conclusions may be drawn from the mean reflectance values recorded in this manner, as seen in the lack of significance attributable to individual wavebands (Table 5.5.).

The ratio index 'IGER-NDVI', significant in the IGER data set, was not significant when measured with the GER dual-beam spectrometer. No single waveband was significant, possibly as a result of the substantial fluctuation in solar illumination, and therefore signal strength, during the GER imaging session.

5.4.4. Plant residue measurements.

Grainger & Clark (1963) found no reduction in yield from either PCN or *R. solani* in isolation, although they do suggest that very high levels of PCN infection can reduce yield in the absence of *R. solani*. Their findings were based on a pot experiment (cv. Epicure) and are only partially supported by the tuber weight measurements from the current experiment, where both treatments with PCN reduced tuber yield by *c.* 14% (Table 5.7) while *R. solani* in isolation did not reduce tuber yield. *Rhizoctonia solani* infection from this experiment produced fewer and heavier tubers than the no-pathogen and PCN treatments, contradicting Grainger & Clark (1963) who reported an increased number of lighter tubers for treatments infected with either pathogen, and, (by calculations derived from the table provided) experienced a substantial decrease in mean tuber weight for

individual and combined pathogens when compared with their control plants. Comparison of their results with the present study is subject to considerable uncertainty, as the authors do not indicate the capacity of their pots or the number of replicates per treatment and report PCN infection only in terms of cysts g^{-1} soil. Cysts can contain a variable number of embryonated juveniles, depending partially upon age and condition (Brodie *et al.* 1993; Turner, 1998) and cyst numbers alone do not present a reliable indication of the actual nematode population. The volume of soil – and, ergo, the number of nematodes – available to a plant grown in a potentially limiting container cannot be determined from the information provided.

An increase in haulm dry matter with nematode density, reported by Trudgill *et al.* (1975b) was not observed, although their finding of reduced haulm weight is reproduced in this study. Seinhorst (1981) reports a strong negative correlation between dry matter content and water consumption in several species of infected plants. Irrigation may have been less limiting in this controlled pot experiment than for the field experiment of Trudgill *et al.*, possibly ameliorating the effect of nematode damage in the roots.

5.5. General conclusions.

The leaves of potato plants exhibit considerable variance of spectral reflectance, even between leaves from the same plant, and a large number of replicates is required to account for this natural variability. Image collection under conditions of natural illumination is further subject to fluctuation of incident radiation. The narrow field of view of a field spectrometer poses additional problems as there is no record of the area measured or the amount of leaf, background or shadow contributing to the single, mean reflectance value recorded at each waveband.

The imaging of individual leaves under laboratory conditions was undertaken specifically to identify differences between the spectral reflectance of healthy plants and those infected with PCN or *R. solani.* Laboratory conditions removed the variability of solar illumination and environmental conditions associated with field spectroscopy, although results were not directly comparable due to the different distribution of light from artificial and natural sources. This method does not, however, facilitate the imaging of a large number of replicates. Both image collection and subsequent analysis place heavy demands on time and resources and the volume and complexity of data produced represents a considerable disadvantage when compared with conventional spectroscopy.

Whilst a digital camera and tuneable filter cannot match the precision and convenience of a dedicated spectrometer, equipment cost are significantly lower, possibly one-tenth that of a spectrometer and integrating sphere. This method might form a second tier of spectral analysis, available to a wider group of researchers. Further development of this imaging method would require a stabilised light-source and fixed positioning of the lamps and target within a small, enclosed and non-reflective chamber. The calibration panel should be held in a fixed position relative to the camera and suitable exposure times determined to avoid saturation at all wavelengths. The variable ratio of leaf to background material remains problematic, and a different foreoptic will be required if the camera field of view is to be contained within the leaf area. A black overlay card, as used in sessions two and three, would go some way to resolving this problem if the positioning of the card and leaf can be accurately reproduced for all replicates, i.e. fixed guide stops to locate the card and leaf. The card aperture would need to be sized to cover the smallest leaf, and this will exclude sections of larger leaves. Grossman *et al.* (1994) punched a standard-sized disk from each leaf and their method could substantially reduce the image data volumes and background reflectance by selecting a sub-set from each image containing only the leaf disk. Any selection of a leaf region for sub-sampling would require the application of a

carefully-considered protocol if it is to be objective. Aggregating pixels would reduce data volumes, as will reducing the number of wavebands recorded.

This experiment has confirmed the results from a preliminary experiment conducted in 2000. The ratio IGER-NDVI reveals a similar response to each pathogen plus a cumulative effect from both pathogens (Fig. 5.2.) in laboratory measurements, supporting the conclusions drawn from the preliminary field study that plants infested with PCN exhibit a greater spectral response in the presence of *R. solani.* Notable, however, is that the IGER-NDVI ratio is derived from two wavebands within the visible spectrum (672nm and 700nm). The preliminary study used wavebands 680nm and 780nm, the latter being in located the near-infrared spectral region used in conventional vegetation indices.

From the field spectrometer measurements, the ratio Orange-Green emerged as capable of discriminating between the pathogens PCN and *R. solani*, and between PCN and no-pathogen plants (Fig. 5.4.). The ratio Green-Red follows a similar trend with higher ratio values (compared to the no-pathogen samples) for *R. solani* replicates and lower ratios for the PCN-infested plants (Fig. 5.5.). These results support the green-red findings from two field experiments and the previous pot experiment. Importantly, they also indicate that a non-PCN pathogen (*R.solani*) is moving the ratio between red and green reflectance in the opposite direction to PCN infestation, reinforcing the prospect that the green-red ratio will contribute to the discrimination between PCN infestation and other stress factors in the field.

6. Field experiments 2002

6.1. Introduction.

Two field experiments were conducted in 2002 with the objectives of reinforcing the airborne results from the 2001 experiment and to investigate the potential of satellite imagery for the detection of PCN infestation. Experimental methodology was revised in response to limitations identified from the 2001 experiments. Image registration was supported by constructing visible ground features at strategic points around the experimental areas and higher flight levels requested to avoid the need to mosaic and correct multiple images. The procurement of images from orthogonal flight directions was requested to enable the correction of directional reflectance factors where images might be acquired at an azimuth divergent to the principal solar plane.

6.2. Materials and methods.

6.2.1. Experimental sites.

Two fields of commercial potato crops were selected after consultation with the landowners, using PCN population density distribution data provided by their agronomist (Andrew Wade, Agrovista UK Ltd). These fields were then divided into quarter-hectare (50m * 50m) areas which formed the survey units for PCN population density sampling and airborne data analysis. The survey areas were arranged to include the majority of the crop whilst avoiding the anticipated headland margins.

The first experiment was located in Challinors Field, Pave Lane Farm, Newport, Shropshire (Ordnance Survey Grid Reference SJ 764 159), a 10.69 ha field of sandy-loam soil, tending to loam and sloping *c.* 26m to the east. The second experimental site was located in Big Field, Deepdale Farm, Newport, Shropshire (Ordnance Survey Grid

Reference SJ 709 234). Big field covers *c.* 12 ha and soil type ranges from loam to sandy loam, with heavier soil in the north-west corner. A southern field extension slopes to the south and there is a slight rise mid-field.

Challinors Field was planted (cv. Maris Piper) on April 1st, 2002 in wet conditions, working from the south. Planting was suspended due to adverse weather and soil conditions and the northern section and headlands were planted on April 8th, 2002. One row from the earlier planting was located four rows into the later planting area. One third of Big Field (from the west) was planted (cv. Maris Piper) on March 18th 2002, with the remainder planted on March 28th 2002.

6.2.2. DGPS mapping.

Field boundaries, tracks, trees and other static features were recorded using a Sokkia Hawkeye Differential Global Positioning System (DGPS) and Midas software (Sokkia Ltd, Crewe, Cheshire, UK) and used to register the airborne images to ground features as described in section 4.3.1. All field boundaries were recorded using the Sokkia Hawkeye DGPS receiver, including both sides of hedges where possible to improve the accuracy of image registration (Figures 6.1., 6.4.). The extents of a depression and a wet area within Big Field were also recorded with the DGPS receiver.

Thirty experimental plot areas were located in Challinor's Field and thirty-seven in Big Field. Fifty-metre grid points were pre-programmed into the DGPS Midas software for each experimental site to ensure regular and even plot layouts. The experimental plots were then set out by navigating to the programmed location and placing marker canes in the field. The boundary between the earlier and later planting in Challinors Field was recorded on April 9th, 2002 when turned soil from the previous day's planting was still

clearly visible. Further DGPS recordings were made of tram-lines and headland margins from both experimental sites once the crops had become established.

6.2.3. Soil sampling for PCN population density estimation.

Thirty soil samples were collected from the quarter-ha experimental plots in Challinors Field on February 25th & 26th, 2002 (Figures 6.1., 6.2.), and thirty-seven samples from Big Field on March 5th & 6th, 2002 (Figures 6.4., 6.5.). Thirty-six cores in a six-by-six grid were obtained from each plot area using a 25mm x 200mm auger and bulked (*c.* 1.5Kg) for determining the mean nematode population density of the area. Five quarter-ha plots of Challinors Field were sub-divided into twenty 25m x 25m sub-plots and these were selected to encompass a wide range of population levels (Figures 6.1., 6.3.). Soil samples for population density estimation were collected from the sub-plots on March 20th & 21st, 2002, also by taking 36 cores of a 6 x 6 grid. Samples were dried at 25°C for five days and sieved (4mm) to remove stones. Two hundred grams of soil was taken from each sample after thorough mixing. Cyst extraction and egg counts were then made on these subsamples according to the procedures described by Shepherd (1986). The species of PCN present was determined for both experimental sites as being *G. pallida* by the use of PCN-specific primers in a polymerase chain reaction (PCR) (Ibrahim *et al.*, 2001).

6.2.4. Location markers.

Image registration of the 2001 ARSF images had been hampered by a lack of clearly-defined ground features in some parts of the experimental area. Artificial ground features were constructed from sheets of (shiny, new) galvanised corrugated iron in order to avoid a repeat of this problem. Marker sheets were placed at locations around the experimental areas on June 24th and 25th, 2003. Each metal marker formed a 2m square with some soil covering the corners to prevent them from blowing away (Plate 6.1.).

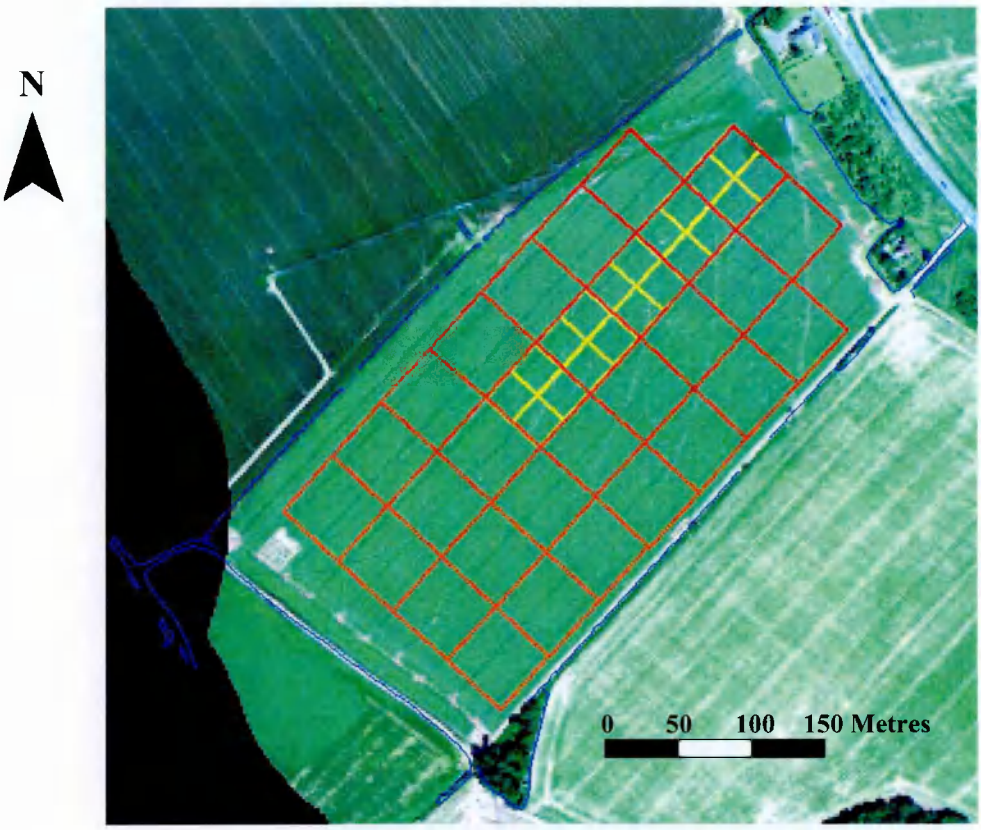

Figure 6.1. Vector overlay of quarter-hectare experimental plot areas and 25m sub-plots on flight image 17706 (bands 6,3,1) of Challinors Field, Pave Lane Farm.

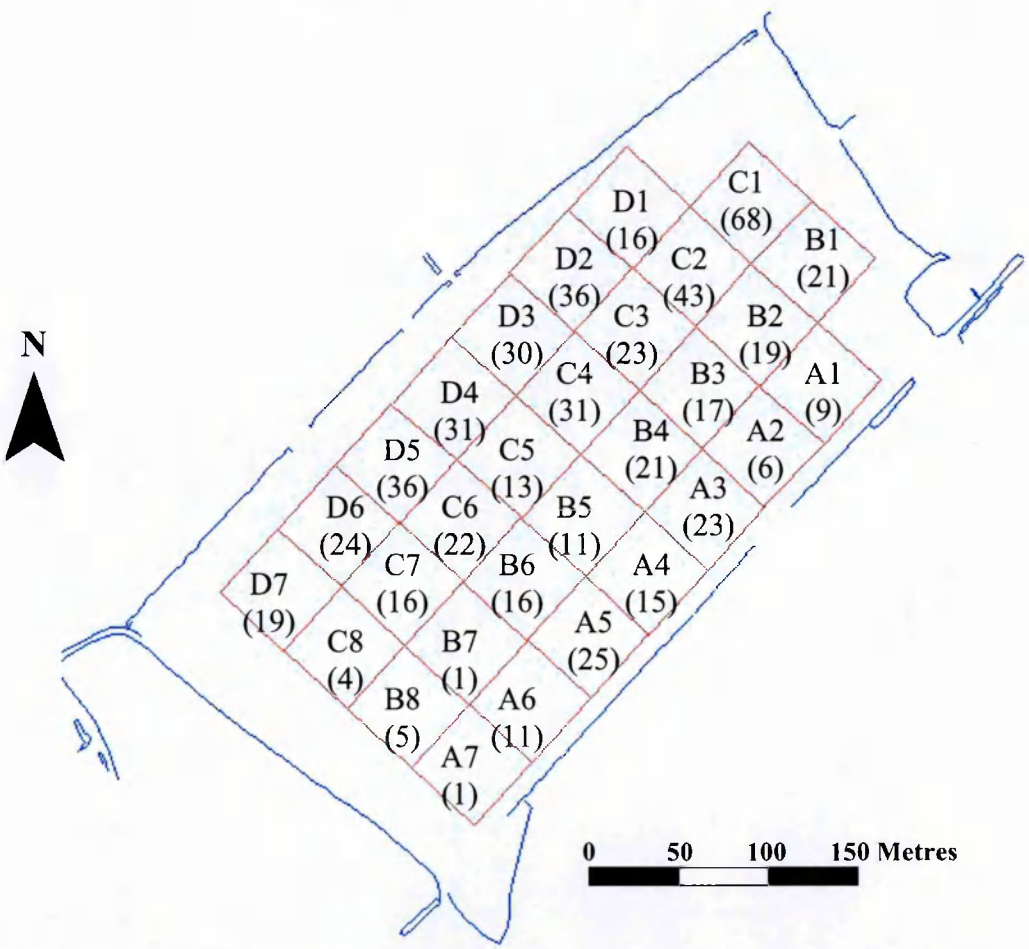

Figure 6.2. Quarter-hectare experimental plot areas and PCN initial population density estimation (eggs g^{-1} soil), Challinors Field, Pave Lane Farm.

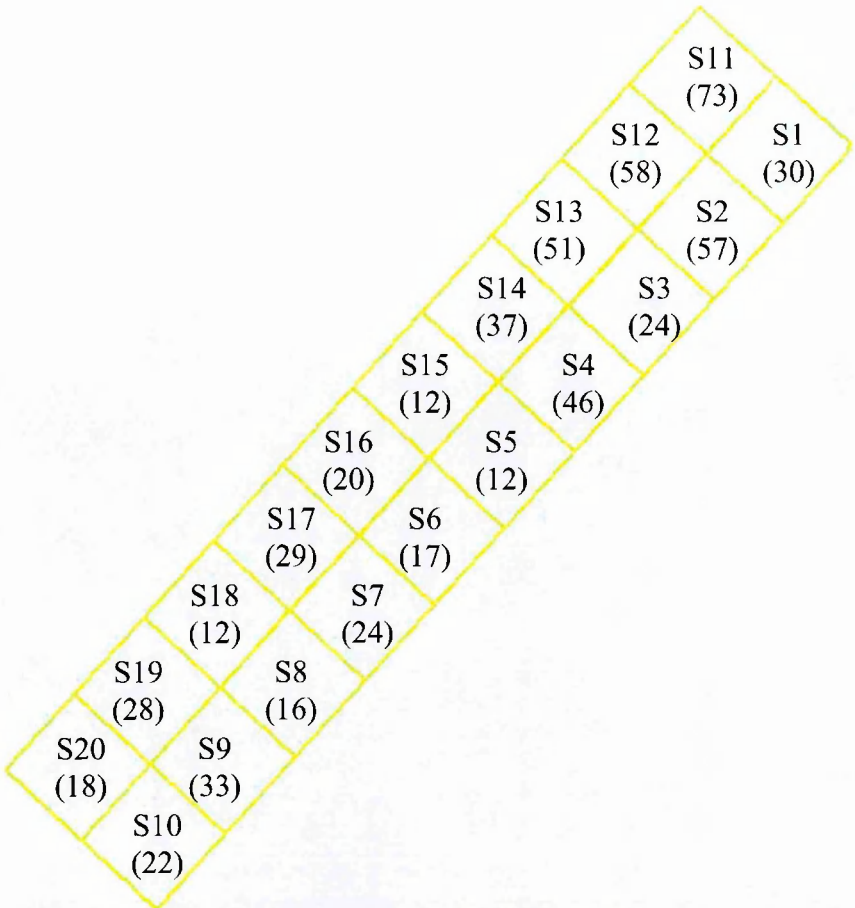

Figure 6.3. Layout and PCN initial population density estimation (eggs g^{-1} soil) of the 25m experimental sub-plot areas, Challinors Field, Pave Lane Farm. The sub-plots are divisions of experimental plot areas C1-C5.

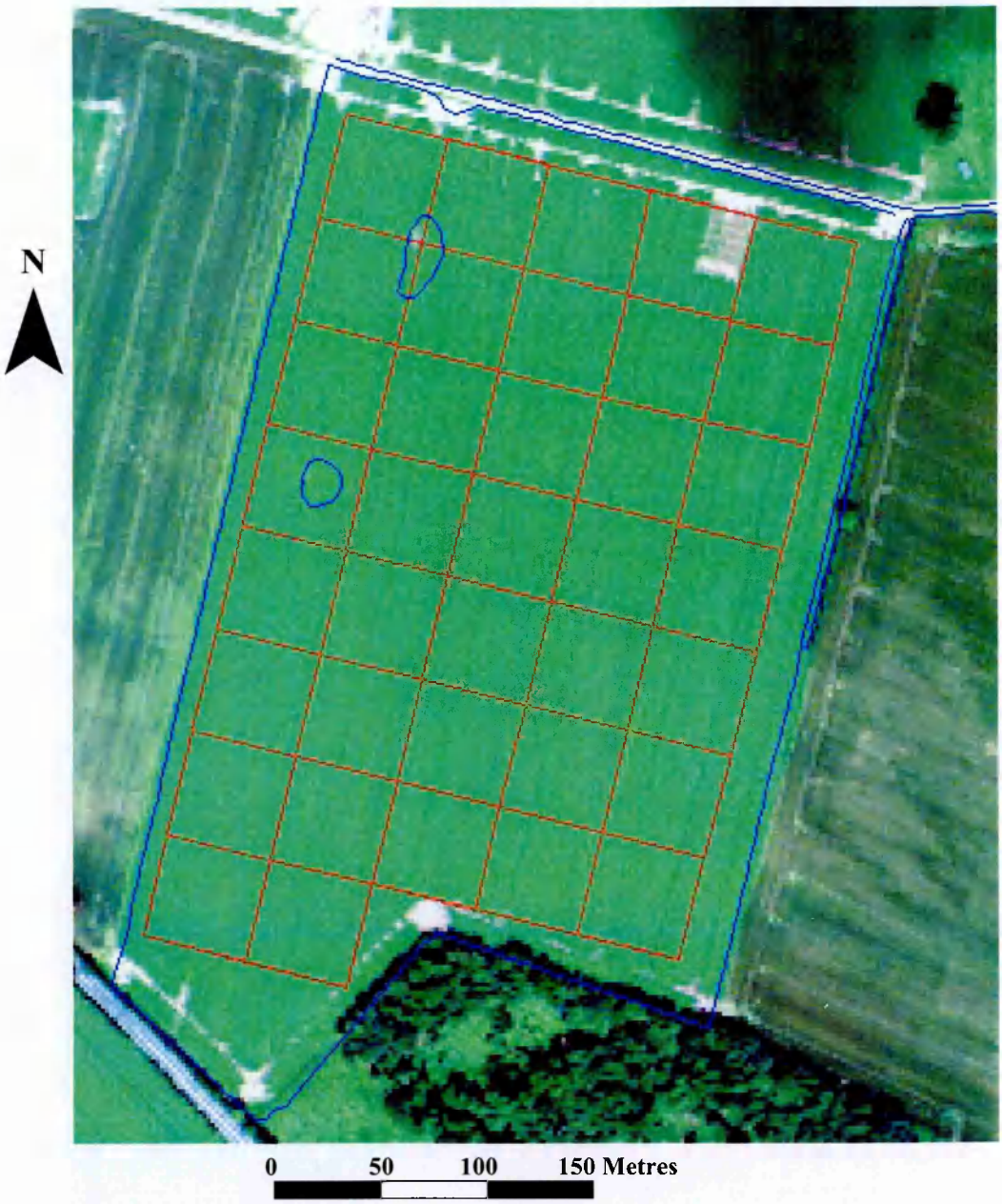

Figure 6.4. Vector overlay of quarter-hectare experimental plot areas on flight image 19615 (bands 6,3,1) of Big Field, Deepdale Farm. Two shallow field depressions are marked in blue.

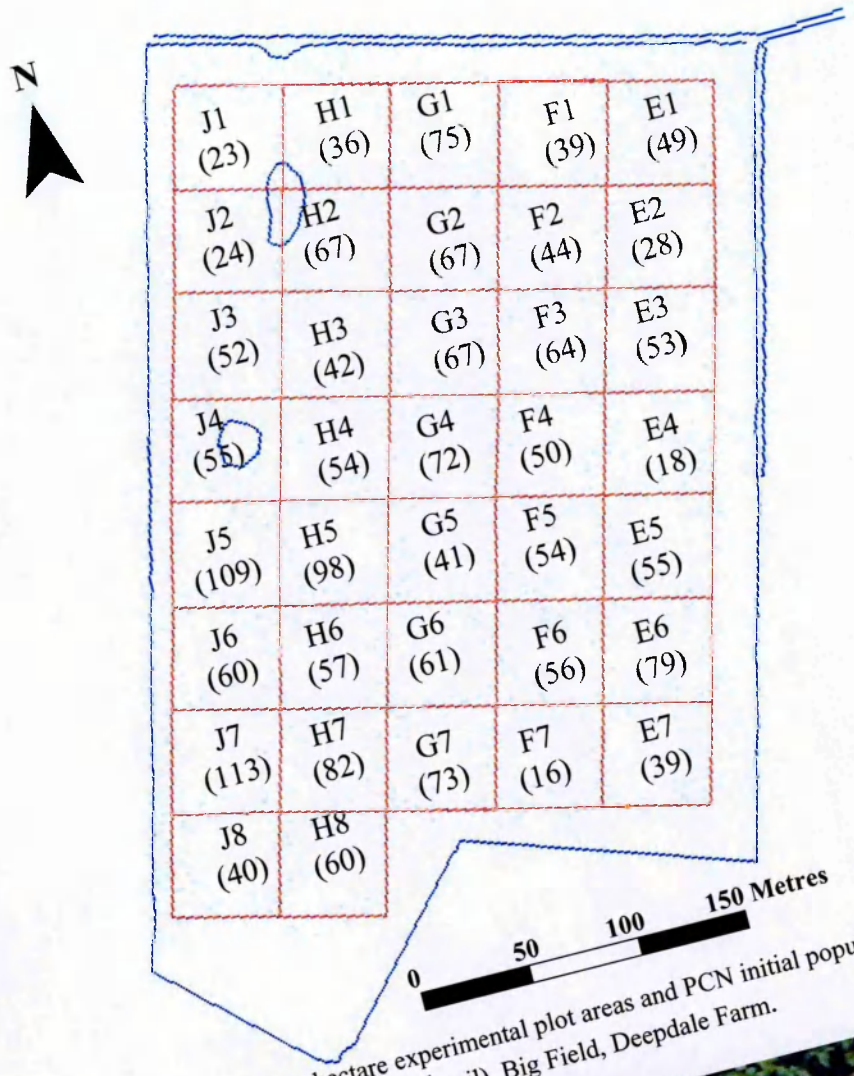

Figure 6.5. Quarter-hectare experimental plot areas and PCN initial population density estimation (eggs g^{-1} soil), Big Field, Deepdale Farm.

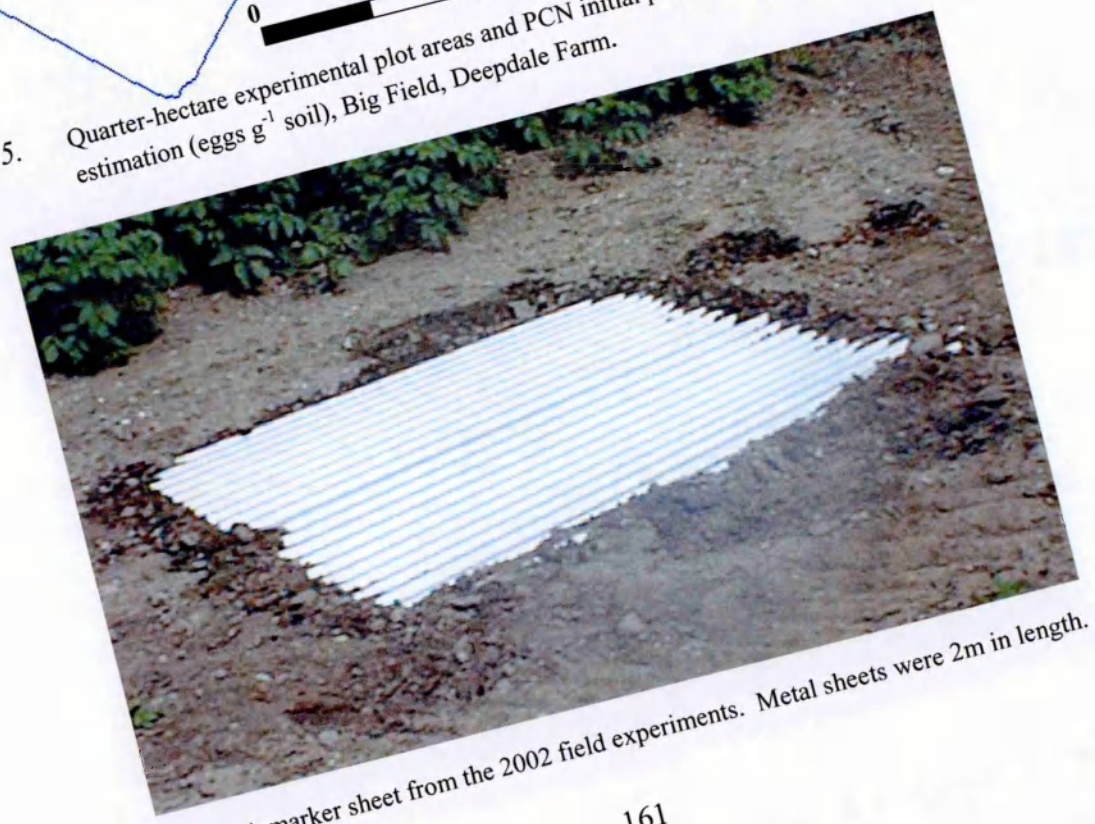

Plate 6.1. A marker sheet from the 2002 field experiments. Metal sheets were 2m in length.

Four markers were placed in Challinors field, with a fifth just over the hedge in a field to the north. Seven markers were positioned in Big Field, with two locations intended to be within the overlap area if the experimental area was to be covered by multiple images. The marker locations were recorded with the DGPS receiver and the mean of four points (the marker vertices) used to reduce positional error. A reference satellite signal could not be obtained for one marker in Challinors Field due to masking by trees from an adjacent woodland and the position was estimated by recording the position of white canes and sighting along the canes to the marker.

6.2.5. Ground-truth measurements.

Ground-truth reference spectra were collected using a GER1500 spectrometer in dual-beam mode on July 15th, 2002 between 13:01 and 13:23 UTC. Ten measurements from a Spectralon™ reference panel were collected (both spectrometers aimed at the panel) and used to generate a calibration file to compensate for differences between the two instruments. Thirty spectra were then collected from bare rolled soil from the south-western corner of Swan's Leasow field (Ordnance Survey Grid Reference SJ 715 201), followed immediately by thirty spectra from adjacent experimental grass plots. The weather was overcast throughout the reference spectra collection session.

6.2.6. GER dual-beam measurements.

Spectral reflectance measurements were recorded from the crop canopy in Challinors Field with a GER dual beam spectrometer on July 26th, 2002. Two 25m square areas were marked with canes; the south-east corner of experimental plot C8 (Pi = 3.6) and the north-east corner of plot C1 (sub-plot S1, Pi = 30.3). Forty spectra were collected from plot C8 before moving to sub-plot S1 where 72 spectra were collected. A further 47 spectra were then collected from plot C8 to compensate for possible diurnal changes during the sampling period (10:38 to 13:46 UTC). Calibration measurements (inter-calibration of the two spectrometer heads) were conducted prior to the collection of spectra from the C8

area, the S1 area and the second C8 measurements. Weather conditions were clear with only isolated cumulus clouds remote from the solar position and all spectra were recorded from the area of the April 1st planting session (116 DAP).

6.2.7. ARSF flights.

The NERC ARSF aircraft flew seven flight lines on June 26th, 2002 from 10:47 to 11: 33 UTC. A further six flight lines were flown on July 15th, 2002, imaging the two experimental sites and the ground-truth calibration area on both days. A persistent technical problem with the CASI-2 instrument prevented the acquisition of flight images in enhanced-spectral mode. All CASI images were collected in spatial mode using a vegetation bandset altered to include fifteen spectral bands (listed in Appendix G.) instead of thirteen bands from the 2001 flight data. The June 26th 2002 ARSF flight parameters are listed in Appendix I. and details of the July 15th, 2002 flights in Appendix J.

6.2.8. Satellite images.

6.2.8.1. SPOT (Satellite Pour l'Observation de la Terre).

Three SPOT images were obtained and each image was correctly located, covering both experimental locations. The first image was recorded at 11:02:36 UTC on July 14th, 2002 by the SPOT-4 satellite which carries the four-band HRVIR instrument. The second SPOT image was collected by the SPOT-2 satellite on July 26th, 2002 at 11:00:33 UTC. The SPOT-2 satellite carries the three-band HRV instrument. A third SPOT image was collected at 11:00:41 on August 21st, 2002 by the SPOT-2 satellite. SPOT instrument specifications and SPOT image details are listed in Appendix A.

6.2.8.2. Ikonos satellite image (Space Imaging Inc.).

A single 10km x 10km multispectral Ikonos image was ordered from EarthScan Network Inc. Albuquerque, NM, USA. The Ikonos satellite acquired an image on June 20th, 2002. This image was located *c.* eighteen kilometres due west of the intended location and did

not encompass either experimental location. The error had been caused by incorrect entry of the (correctly supplied) latitude and longitude coordinates, either by the resale agents or when tasking the satellite. A second Ikonos image was acquired on July 26th, 2002 at 11:41 UTC. This image was located *c.* six kilometres west of the intended location, but just including the Big Field experimental site. The image co-ordinates did not accord with the location requested and no explanation for this discrepancy was received from Earthscan Network Inc. Ikonos waveband details and the July 26th Ikonos image parameters are listed in Appendix B.

The order window had been quoted as sixty days from mid-June (i.e. to mid August). A third Ikonos image was collected on October 24th, 2002, despite this limitation. The third image was correctly positioned although the potato crop had already been harvested by this time. The order timing confusion appears to have been due to the satellite operators (Space Imaging Inc. Thornton, Colorado, U.S.A.) taking over the order processing from the resale agents Earthscan Network Inc.

6.2.9. Image processing.

6.2.9.1. CASI airborne images.

Four level 1b CASI HDF image files were processed to level 3a in Azgcorr version 4.3.3 (Azimuth Systems, UK) on a Sun Sparc 20 workstation as described in section 4.3.4.2 The 2002 flight images were processed with the inclusion of elevation data supplied by the Midas Landmap service (www.landmap.ac.uk). Bicubic interpolation (spline value 1.0) was selected and output pixel dimensions were set to 2m x 2m. Level 3a HDF files were exported to the geotiff image file format using the azexhdf computer program (Azimuth Systems, UK) on a Sun Sparcserver 5 computer. Flight images 17704, 17705, 17707, 17709,17710 (26/06/2002) were discarded as unsuitable due to cloud shadow over the

targets. Flight images 19610, 19611, 19612, 19614, and 19615 (15/07/2002) were also discarded due to cloud shadow.

Geotiff format image files were imported into the ENVI computer program, version 3.5 (Research Systems Inc. Boulder, Colorado). The image map co-ordinate values of the ENVI header file were edited by 3-4m so as to align each image with the DGPS vector mapping. The image from flight 19615 represented Big Field, Deepdale Farm as 4m wider (E-W) than the DGPS mapping of the field boundaries. A sub-set of this image covering the Big Field site and immediate vicinity was extracted and registered with the ENVI map-to-image registration function, using the metal markers as control points. Nearest-neighbour interpolation was used for the 1st degree polynomial registration and the RMS error (6 points) was 1.23. A further 1m easting was then subtracted from the header file co-ordinates to refine the image border alignment.

The19613 flight image was sub-sampled to cover the Swans Leasow ground-truth targets and immediate area. Four metres northing was added to the ENVI header file to align the recorded DGPS points with ground features. This was further compared with Ordnance Survey Land-Line data and the registration seen to be accurate to within *c.* 2m. Alignment is less critical here as the ground-truth targets (experimental grass plots and bare, rolled soil) are clearly defined on the image.

6.2.9.2. SPOT satellite images.

Some difficulty was encountered when locating the SPOT satellite images due to the 20m pixel size. Linear features are not distinct and some estimation was required to align the image with the DGPS map lines. The SPOT images were supplied processed to level 1b which comprises radiometric processing (detector normalisation) and geometric correction for distortion due to the earth's rotation and off-nadir view angles (using bi-cubic

interpolation). The SPOT images were orientated along the orbital path and were not registered to a map projection. (http://www.spot.com/home/support/sheet/level1b).

The first SPOT image of July 14th, 2002 was rotated by +9.9° using nearest-neighbour interpolation. A sub-set of the image was then selected to cover the vicinity of the Challinors Field experimental site using the ENVI 'Resize Data Spatial/Spectral' facility and entering line and column numbers to either side of the field. Assumed Ordnance Survey grid reference values were then entered into the ENVI header file and the image projected to 'United Kingdom National Grid' using the WGS84 datum. The image grid reference values were then repeatedly edited until the image was aligned with the DGPS mapping of the field boundaries.

The second and third SPOT images were rotated by 9.7° and registered to the mapping data in the identical manner to the first image. The rotation of these images was required to align the images to true north by correcting for the offset orbital track of the SPOT-2 and SPOT-4 satellites.

6.2.9.3. Ikonos satellite image.

The Ikonos image of July 26th, 2002 was supplied as four geotiff image files (blue, green, red and near infrared bands). These images had been geometrically corrected by the supplier using the cubic convolution interpolation method and projected to the Universal Transverse Mercator (UTM) projection zone 30 north, using the WGS84 datum. The four images were collated by using the ENVI 'layer-stack' function and a sub-set of the resulting four-band image selected to cover the Big Field experimental site. Ten metres was then subtracted from the ENVI header easting co-ordinate to align the image with the DGPS mapping of the field boundaries and the metal marker sheets.

6.2.10. Statistical analyses.

6.2.10.1. GER dual-beam measurements from Challinors Field.

Spectra collected from the sub-plot S1 of Chalinors Field experimental site were compared with the aggregated spectra recorded from plot C8. The C8 spectra had been collected before and after the S1 measurements and were combined to compensate for diurnal factors which might influence reflectance from the crop canopy. The ratio between mean S1 spectra and the combined C8 mean spectra was plotted at each waveband in the manner described as the ratio analysis of reflectance spectra (RARS) by Chappelle *et al.* (1992).

6.2.10.2. CASI and satellite images.

Pixels from CASI and satellite images corresponding to the quarter-hectare experimental areas were selected using the ENVI ROI function and the mean for each ROI recorded as a single spectrum. The correlation between the estimated PCN population density (Pi) and ROI mean pixel values from individual images was plotted at each waveband. The quarter-ha sample counts from Challinors field were transformed to square root values in Genstat version 5.1 (Lawes Agricultural Trust, Rothamsted, UK) as the untransformed data did not approximate a normal distribution. A larger pixel size (20m) and uncertain registration accuracy may have allowed radiance from boundary features to contribute to the mean pixel values of the outer plot areas from the SPOT satellite images. Analysis from the 20m satellite images was therefore restricted to the inner experimental plot rows.

6.2.10.3. Ground truth measurements.

An empirical line calibration of the 19613 flight image was conducted using ground-truth spectra collected from bare, rolled soil and grass using a GER dual-beam field spectrometer on July 15th 2002, 2.5 hours after the flight. This calibration was undertaken to enable comparison with future investigations and has not been applied to the within-field comparisons of the 2002 experiments.

6.3. Results.

6.3.1. Metal marker sheets.

The bright metal marker sheets were intended to contrast with bare soil around the field perimeter. The spread of white daisies (*Bellis perennis*) across the surrounding soil may have reduced the desired contrast. Scattering of NIR from the crop canopy also reduced contrast when markers were placed close to the crop, although the spectral signature of the markers could be amplified by calculating the ratio of a visible and a near-infrared waveband for pixels in the marker vicinity. The marker position was then determined by examining the ratio values of a line of pixels from each axis. Marker sheets provided a valuable check on image registration, being better defined than hedgerows, although they were not strictly necessary as the availability of a DEM improved and simplified the registration process and sufficient DGPS features were available in 2002.

6.3.2. GER dual-beam measurements.

The ratio between mean spectra from the sub-plot S1 (Pi = 30 eggs g^{-1} soil) and those collected from a 25m square within plot C8 (Pi = 3.6 eggs g^{-1} soil) in Challinors Field indicated that reflectance is reduced (to 89.86%) by infestation at 552nm and increased at 680nm (Fig. 6.6.). A slight change in correlation at 630nm, recorded from the 2000 and 2001 field experiments, was also present in the ratio between the S1 and C8 spectral means.

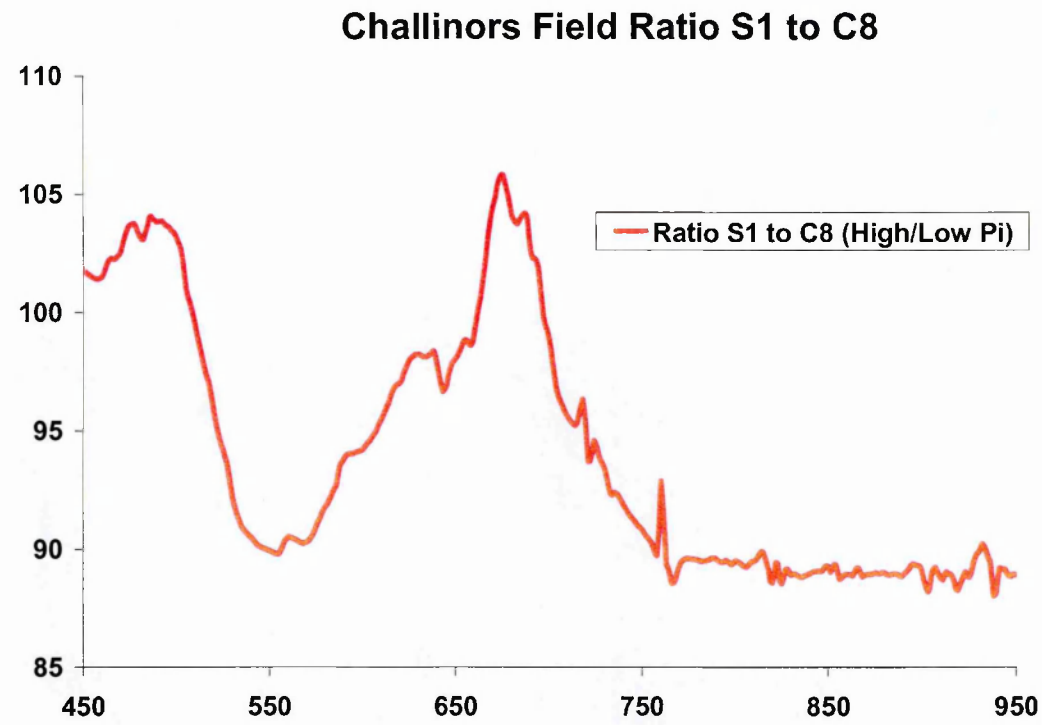

Figure 6.6. Ratio analysis of reflectance spectra means from two experimental areas of Challinors Field.

6.3.3. CASI airborne images.

Images from flights 17706 and 17708 on June 26th, 2002 each covered the entire experimental area from Challinors Field at approximately orthogonal flight directions (headings 326° - 232° = 94°) with no cloud shadow visible within one kilometre of the experimental area. All flight images of Big Field, Deepdale Farm were obscured by cloud on this day.

Flight image 17706 was almost (to 6.1°) aligned with the principal solar plane, thereby minimising bidirectional reflectance factors (BRDF). Flight image 17708 was collected along the axis of PCN variability, but at 75.7° to the principal solar plane. Spectra from this image were affected by BRDF, resulting in elevated radiance from the northern crop areas. The ratio between image spectra increases by *c.* 13% from south to north (A plots to D plots) at 552nm and 670nm, and is *c.* 6% higher at 780nm when comparing the 17708 flight data (means of plot-row spectra) with the 17706 flight image.

The correllogram curve derived from flight image 17706 of the Challinors Field experimental site is of the same general distribution as those from earlier experiments (Fig. 6.7.). However, the entire curve is aligned further towards a positive relationship than has been recorded from earlier experiments.

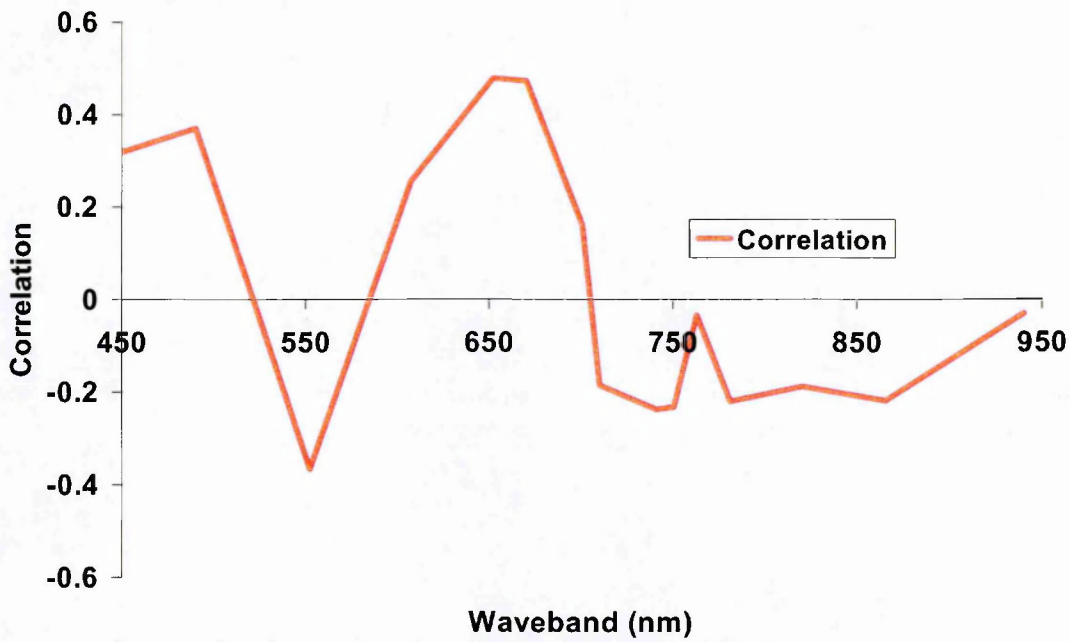

Figure 6.7. Correlation of spectra from flight image 17706 with square root transformed PCN initial population density estimation (eggs g^{-1} soil) from the quarter-ha experimental areas of Challinors Field (all plots).

An unsupervised classification (isodata algorithm, 5 iterations, 1% class separation) was conducted on band 3 (552.36nm) of the quarter-ha plot areas in the ENVI computer program. Isodata class values were calculated as the mean class value of all (*c.* 600) pixels for the plot (Table 6.1.).

Table 6.1. Wavebands and ratio indices from flight image 17706 regressed against square-root transformed initial nematode population density estimation (eggs g^{-1} soil) for the quarter-ha plot areas of Challinors Field.

Parameter	Flight Image 17706, Challinors Field All Plots		
NM552_36	$F_{(1,28)}= 4.35$,	p= 0.046	$R^2_{(21)}= 0.135$
NM670	$F_{(1,28)}= 8.06$,	p= 0.008	$R^2_{(21)}= 0.224$
NM780_96	$F_{(1,28)}= 1.43$,	N/S	$R^2_{(21)}= 0.048$
Red_Green	$F_{(1,28)}= 7.63$,	p= 0.01	$R^2_{(21)}= 0.214$
NDVI	$F_{(1,28)}= 4.78$	p= 0.037	$R^2_{(21)}= 0.146$
Isodata Class	$F_{(1,28)}= 4.66$	p= 0.04	$R^2_{(21)}= 0.143$

The relationship of spectral means with (the square root of) nematode population density followed the expected pattern when analysing crop rows A, B and C (Fig. 6.2.), listed from the south). Results from the northern row of experimental plots (D1-D7) were markedly different to all other plot areas and the analysis was repeated without the northern D plots, which had been planted at a later date (Table 6.2.).

Table 6.2. Wavebands and ratio indices from flight image 17706 regressed against square-root transformed initial nematode population density estimation (eggs g^{-1} soil) for the A-C quarter-ha plot areas of Challinors Field.

Parameter	Flight Image 17706, Chalinors Field Plots A-C		
NM552_36	$F_{(1,14)}= 14.88$	p< 0.001	$R^2_{(14)}= 0.415$
NM670	$F_{(1,14)}= 18.88$	p< 0.001	$R^2_{(14)}= 0.473$
NM780_96	$F_{(1,14)}= 21.04$	p< 0.001	$R^2_{(14)}= 0.5$
Red_Green	$F_{(1,14)}= 21.14$	p< 0.001	$R^2_{(14)}= 0.501$
NDVI	$F_{(1,14)}= 23.27$	p< 0.001	$R^2_{(14)}= 0.526$
Isodata Class	$F_{(1,14)}= 15.88$	p< 0.001	$R^2_{(14)}= 0.430$

Mean spectra from flight image 17706 were extracted and compared with PCN population density estimates of the 25m sub-plots in Challinors Field (Table 6.3.).

Table 6.3. Wavebands and ratio indices from flight image 17706 regressed against initial nematode population density estimation (eggs g^{-1} soil) for the 25m sub-sample areas of Challinors Field.

Parameter	Challinors Field 25m Sub-samples		
NM552.36	$F_{(1,18)}= 15.06$,	p= 0.001	$R^2_{(18)}= 0.456$
NM670	$F_{(1,18)}= 3.12$,	N/S	$R^2_{(18)}= 0.147$
NM780.96	$F_{(1,18)}= 7.38$,	p= 0.014	$R^2_{(18)}= 0.291$
Red-Green	$F_{(1,18)}= 8.75$,	p= 0.008	$R^2_{(18)}= 0.327$
NDVI	$F_{(1,18)}= 5.75$,	p= 0.028	$R^2_{(18)}= 0.242$

Flight image 19615 covered Big Field, Deepdale Farm on July 15th, 2002, flying towards the sun (7.4° to the principal solar plane). Big Field was only just clear of cloud shadow and some scattering effect from the cloud leading-edge is possible (E. Milton, personal communication). This was, however, the only clear airborne image from the Big Field experimental site.

A curve plotting the linear relationship between spectral reflectance in fifteen wavebands and PCN population density estimation for the Big Field experimental site followed a similar pattern to results obtained from earlier experiments, and to results obtained from the Challinors Field experimental site in the current experiments (Fig. 6.8.). The relationship was orientated further to positive values than expected, resulting in significance transferring from green (552nm) to red (670nm) wavelengths (Table 6.4.).

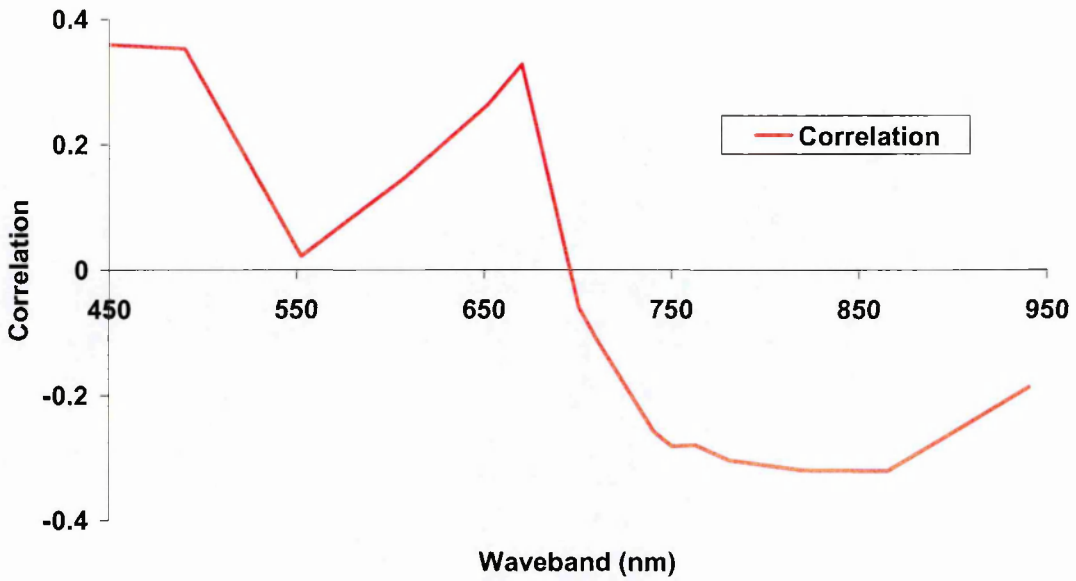

Figure 6.8. Correlation of waveband data from flight image 19615 regressed against initial nematode population density estimation (eggs g^{-1} soil) of the Big Field experimental plots.

Table 6.4. Wavebands and ratio indices from flight image 19615 regressed against initial nematode population density estimation (eggs g^{-1} soil)of the Big Field experimental plots.

Parameter	Image 19615, Big Field Quarter-ha Plots		
NM552_36	$F_{(1,35)}$= 4.21,	N/S	$R^2_{(35)}$= 0.001
NM670	$F_{(1,35)}$= 4.21,	p= 0.048	$R^2_{(35)}$= 0.108
NM780_96	$F_{(1,35)}$= 3.56,	N/S	$R^2_{(35)}$= 0.092
Red_Green	$F_{(1,35)}$= 4.23,	p= 0.047	$R^2_{(35)}$= 0.108
NDVI	$F_{(1,35)}$= 6.79,	p= 0.013	$R^2_{(35)}$= 0.162

6.3.4. SPOT satellite images.

SPOT data were calculated from plot rows B and C of Challinors Field only as pixel size and potential registration errors may affect the pixel values from the outer experimental plots. Few pixels were located entirely within the outer experimental plot areas and contrasting radiance from widely different surfaces (e.g. tracks and hedges) would have a

disproportionate influence on the mean recorded for the crop. The issue of large pixels is discussed further in section 6.4.

A cloud was covering the Big Field experimental site in the first SPOT image (July 14th, 2002). Challinors Field was free of cloud although cloud shadow was present at 200m to the south and east of the experimental area. The linear relationship between PCN initial population density estimation and radiance recorded in band one of the first SPOT image ($F_{(1,14)}$=24.05, p <0.001, $R^2_{(14)}$= 0.632) was stronger than from other wavebands and ratios tested (Table 6.5.). Isodata classification of these data failed, however, to discriminate between areas within the crop at up to 10 iterations of band 1 .

Table 6.5. Correlation from the first SPOT image (14/07/2002) with initial nematode population density estimation (eggs g^{-1} soil) of the B+C plots of Challinors Field.

Parameter	First SPOT Image, Challinors Field		
Band_1	$F_{(1,14)}$= 24.05,	p< 0.001	$R^2_{(14)}$= 0.632
Band_2	$F_{(1,14)}$= 0.04,	N/S	$R^2_{(14)}$= 0.003
Band_3	$F_{(1,14)}$= 9.06,	N/S	$R^2_{(14)}$= 0.393
Band_4	$F_{(1,14)}$= 24.05,	N/S	$R^2_{(14)}$= 0.189
Red_Green	$F_{(1,14)}$= 3.26,	p= 0.042	$R^2_{(14)}$= 0.263
NDVI	$F_{(1,14)}$= 6.45,	p= 0.024	$R^2_{(14)}$= 0.316

The second SPOT image (July 26th, 2002) showed cloud shadow *c.* 400m to the east and west of the Challinors Field experimental area. The mean pixel values of band one (green) and the red-green ratio were significantly correlated (p <0.001) with nematode population density of the sixteen B and C plots from Challinors Field (Table 6.6.). An isodata classification (5 iterations) of band 1 was not significant (p=0.073)

Table 6.6. Correlation from the second SPOT image (26/07/2002) with initial nematode population density estimation (eggs g^{-1} soil) from the B+C plots of Challinors Field.

Parameter	Second SPOT Image, Challinors Field		
Band_1	$F_{(1,14)}= 19.13$,	$p < 0.001$	$R^2_{(14)}= 0.578$
Band_2	$F_{(1,14)}= 3.9$,	N/S	$R^2_{(14)}= 0.218$
Band_3	$F_{(1,14)}= 0.76$,	N/S	$R^2_{(14)}= 0.052$
Red_Green	$F_{(1,14)}= 11.26$,	$p= 0.005$	$R^2_{(14)}= 0.446$
NDVI	$F_{(1,14)}= 2.13$,	N/S	$R^2_{(14)}= 0.132$
Band 1 Isodata (5)	$F_{(1,14)}= 3.76$,	N/S	$R^2_{(14)}= 0.212$

A large cloud shadow was visible at *c.* 350m south-west of Challinors Field in the third SPOT image of August 21st, 2002. Band 1 (green) was no longer significant ($p= 0.06$) and band 2 (red) attained significance ($p = 0.017$) in this image from a visibly senescent crop. The red-green ratio remained significant ($p= 0.014$, Table 6.7.). Big Field had been harvested before this image was acquired by the satellite.

Table 6.7. Correlation from the third SPOT image (21/08/2002) with initial nematode population density estimation (eggs g^{-1} soil) from the B+C plots of Challinors Field.

Parameter	Third SPOT Image, Challinors Field		
Band_1	$F_{(1,14)}= 4.17$	N/S	$R^2_{(14)}= 0.229$
Band_2	$F_{(1,14)}= 7.39$	$p= 0.017$	$R^2_{(14)}= 0.346$
Band_3	$F_{(1,14)}= 1.21$	N/S	$R^2_{(14)}= 0.080$
Red_Green	$F_{(1,14)}= 7.89$	$p= 0.014$	$R^2_{(14)}= 0.360$
NDVI	$F_{(1,14)}= 2.62$	N/S	$R^2_{(14)}= 0.158$

6.3.5. Ikonos satellite image.

The Ikonos satellite image appeared to be completely cloud-free in the vicinity of the Big Field experimental site. It did not, however, provide a significant result from the bands and ratios tested.

6.4. Discussion.

6.4.1. GER dual-beam spectrometer measurements.

The ratio analysis of mean spectra from two crop areas with different nematode population densities has reinforced results from earlier experiments and confirmed that canopy reflectance at green wavebands is reduced by infestation with PCN. A slight reversal of the ratio of reflectance is visible at 639nm – 644nm, a slightly longer wavelength than had been observed in earlier experiments. This spectral shift may have been due to cultivar or phenological factors and would complicate the application of this spectral feature to the assay of PCN infestation. It was not possible to analyse this feature from two infestation levels and the 2002 airborne images were not of sufficient spectral resolution to identify this narrow spectral response due to technical problems with the CASI-2 sensor.

The dual-beam field spectrometer equipment was difficult to transport through the crop and movement through the field was causing damage to the haulm at a time when further airborne and satellite images were anticipated. Great care was required to avoid straining the many cable connections between the spectrometer heads, laptop computer and the auxiliary power packs. Field spectroscopy of such dense vegetation would benefit greatly from a radio link between the target spectrometer and a base station attached to the (static) reference instrument.

6.4.2. CASI airborne images.

Consistent poor weather and problems of aircraft serviceability were limiting to the collection of airborne remote sensing data from the 2002 experiments. The NERC ARSF CASI-2 instrument developed a technical fault which prevented the acquisition of hyperspectral (144 waveband) images and restricted airborne spectral data to fifteen wavebands.

The availability of a digital elevation model (DEM) improved and simplified the image geocorrection process, largely eliminating the rotation, stretching and translation (RST) required when registering airborne images from the 2001 experiments.

The relationship between spectral data from flight image 17706 and PCN population density estimation of the Challinors Field experimental plots was investigated in greater detail. Three of the four plot-rows (23 plots) exhibited reduced green (552nm) and higher red (672nm) radiance with increasing PCN infestation levels and this was consistent with results from earlier experiments (Fig. 6.9.).

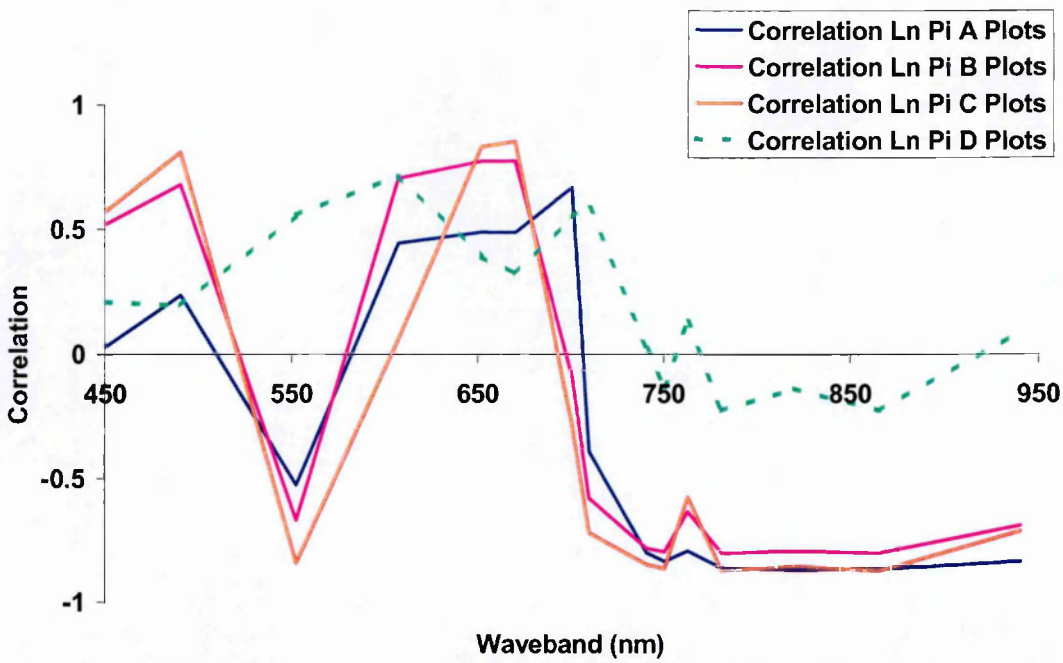

Figure 6.9. Relationship between airborne spectral data and the natural logarithm (Log_n) of PCN population density estimation (eggs g^{-1} soil) from the quarter-ha experimental plot rows of Challinors Field. Flight image 17706.

The relationship between spectra from Plots D1-D7 and initial PCN population density estimates did not accord with results from earlier experiments or from the majority of the experimental site. The crop in plots D1-D7 had been planted one week later than the other plots (excepting a narrow strip in C1-C8) and this may have had some bearing, although a logical explanation for this divergent result could not be determined.

A linear spectral feature was present in the eastern row of experimental plots in band 6 (red) of the 19615 flight image from the Big Field experimental site, although not apparent in the composite image (Fig. 6.4.). This may have been caused by reduced application of nitrogen to the crop. Some areas of light green crop colour (a symptom of reduced nitrogen application) were noted during inspection of the crop. The landowner does not recall varying the agronomic inputs to this field. He did, however, experience some difficulty in obtaining an even nitrogen application rate from his spreading equipment and may have inadvertently changed settings mid-field when attempting to improve the spread pattern.

Quarter-hectare plot areas from the Big Field experimental site were examined with reference to the row (e.g. E1-E7, F1-F7) to investigate whether one or more rows had been affected by agronomic factors. Plot rows were orientated in an approximately north-south direction (Fig. 6.5.). Western plot rows (H-J) displayed a positive relationship with Pi at visible wavelengths and a negative relationship in the NIR region (Fig. 6.10.). The eastern plot rows (E-F) exhibited a consistently negative relationship to Pi, except at 670nm. No conclusions could be drawn from analysis of the individual row spectra, except that the east and west of the field had markedly different radiance curves which could not be resolved to the area of possibly reduced nitrogen application.

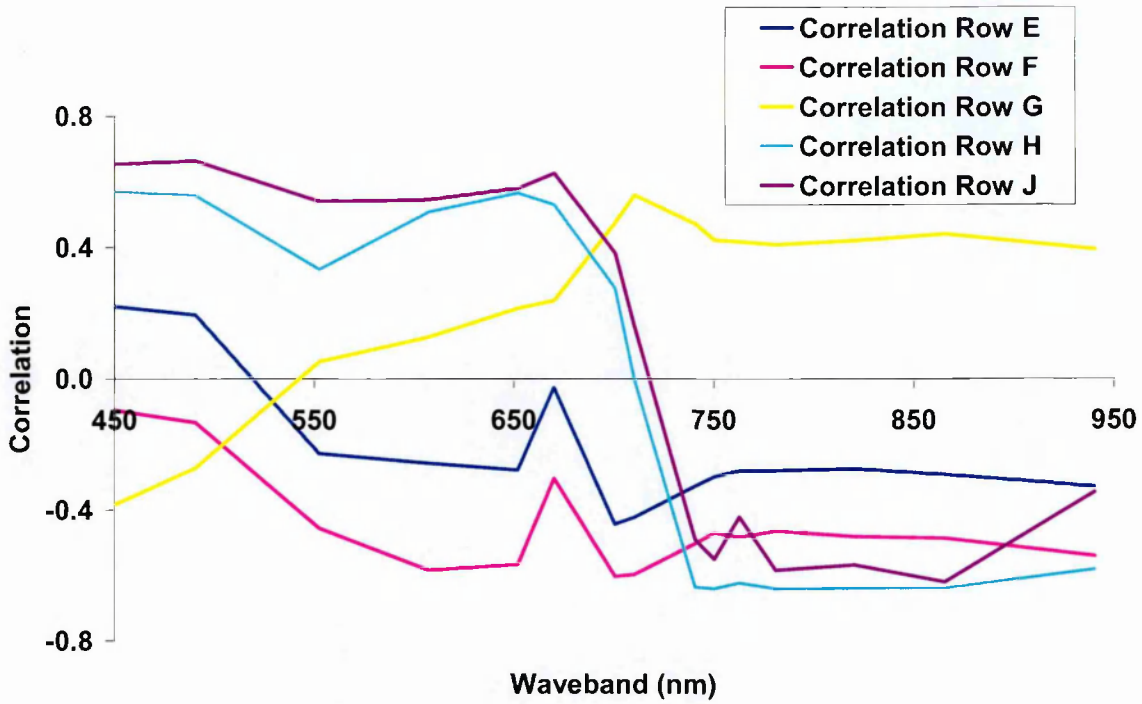

Figure 6.10. Relationship between airborne spectral data and initial PCN population density estimation (eggs g-1 soil) from the quarter-ha experimental plot rows of Big Field. Flight image 19615.

6.4.3. General conclusions.

The linear relationships identified between initial PCN population density estimation and green wavebands, or red-green ratio calculations of the 2002 experiments are less conclusive than those recorded in earlier experiments. The application of the normalised difference vegetation index (NDVI, calculated as $\frac{780\text{nm}-670\text{nm}}{780\text{nm}+670\text{nm}}$, a conventional measure of crop stress) to the aircraft and satellite image data would appear to indicate that these crops have been subjected to levels of stress lower than would be commensurate with estimated PCN population density levels. The NDVI ratio remained above a value of 0.89 in airborne images of Big Field, and was no lower than 0.83 in Challinors Field. Normalised difference ratio values of these magnitudes are indicative of a healthy crop: the NDVI ratio values from the New Piece field airborne image (17202) in 2001 ranged from 0.72 to 0.85 by comparison.

The potato crop canopy of the Big Field experimental site was observed to be dense and of healthy appearance, with no signs of stress visible during field inspections. The crop in Challinors Field also appeared healthy and canopy closure was complete in all experimental areas, although canopy height was estimated to be reduced by *c.* 100-150mm in the vicinity of high PCN infestation levels.

The potato cultivar Maris Piper was grown at both experimental sites and is susceptible to the *G. pallida* PCN species detected in these fields. Evans *et al.* (1977) noted that Maris Piper plants infested with 168 eggs g^{-1} soil of *G. pallida* developed an extensive root system with longer, thinner roots and were able to exploit a greater volume of soil when compared with Pentland Dell plants heavily infested with *G. rostochiensis*. Maris Piper plants grew larger and senesced later: the haulm fresh weight of Maris Piper replicates was reported as being *c.* 50% greater than Pentland Dell plants at all but one infestation level (10 eggs g^{-1} soil). The findings of Evans *et al.* (1977) suggest that Maris Piper plants are able to develop an extensive canopy and root system when heavily infested with PCN. A resilient grown performance of cv. Maris Piper under exposure to PCN infestation may have contributed to the reduced stress symptoms noted from these experiments.

A correllogram curve derived from spectral data of flight image 17706 from the Challinors Field experimental site (Fig. 6.7.) (79-86 DAP) is aligned further towards a positive relationship than had been recorded from earlier experiments. Similar analysis of spectra from flight image 19615, the sole airborne image of Big Field (109-119 DAP), revealed an entirely positive relationship between radiance and PCN population density estimation (Fig. 6.8.) in the visible spectral region. The negative relationship between green radiance and PCN population density estimation of the Challinors Field experimental site would appear to be stronger from the earlier SPOT image (97-104 DAP) (Tables 6.5, 6.6., 6.7.). Images of Big Field may have been collected beyond the optimum time for the detection of

PCN-induced crop stress. The Ikonos satellite image of Big Field experimental site was acquired at 120-130 DAP.

SPOT image data were applied to the inner experimental plot areas only due to the size of SPOT pixels (20m) and possible interaction between radiance from adjacent non-crop areas (due to scattering by atmospheric particles) and the crop boundary region. The image pixels are not divisible and a region derived from 20m SPOT pixels will include reflectance from all pixels in the region, including those that are partly outside of the experiment plot area. The spectral means reported by the ENVI software program were tested on SPOT image data by comparing the mean values of two regions. One polygon was drawn between pixel vertices and covered half of the outer pixels, the second polygon covered the whole of the same pixel range. Mean band values were identical in both cases. Figure 6.11. illustrates the problem of selecting valid pixels from limited areas of the field.

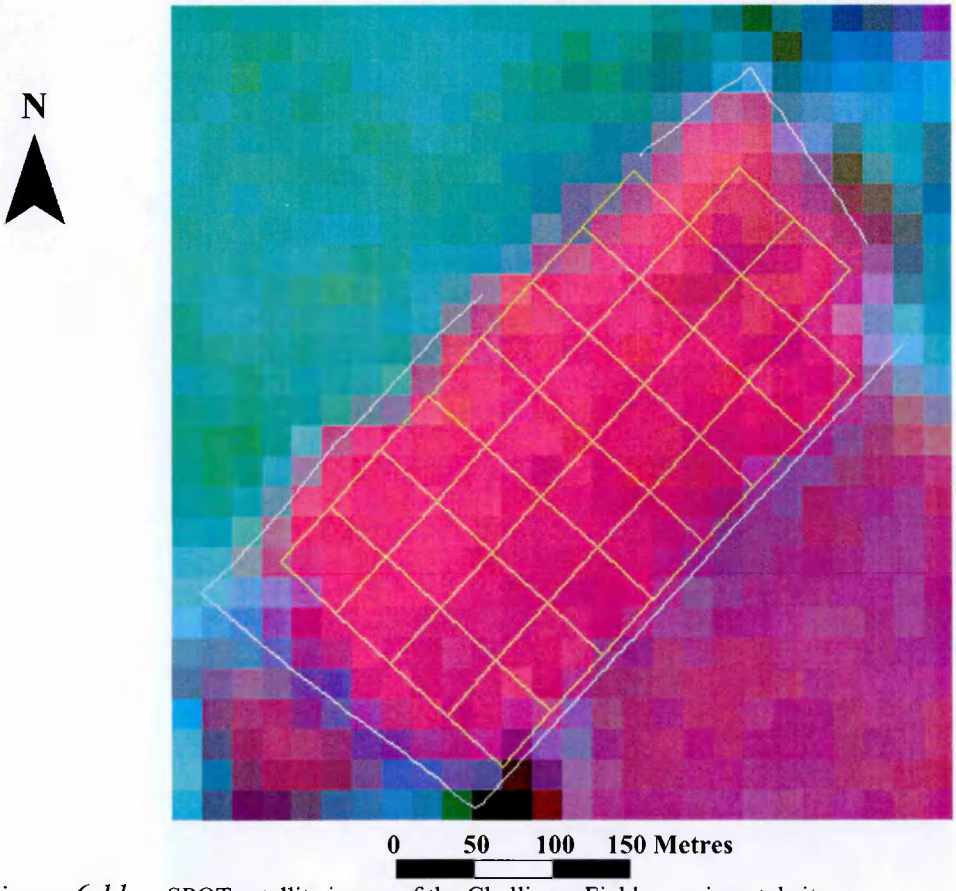

Figure 6.11. SPOT satellite image of the Challinors Field experimental site.

An image of the Challinors Field experimental site from the Ikonos satellite should have provided a useful comparison with the SPOT data. This opportunity was missed because of errors in tasking the satellite.

The broad green and red wavebands (SPOT 90nm and 70nm, Ikonos 80nm and 60nm) of current satellite instrumentation had been expected to mask some of the green-red spectral response by incorporating wavelengths where the correlation with PCN infestation density is reduced or opposed to that from the wavelength of interest. However, band one (500nm-590nm) from the first and second SPOT images has been successful in describing PCN infestation from the inner sixteen experimental plot areas of Challinors Field ($R^2_{(14)}$= 0.632 and 0.578 respectively).

The relationship between PCN infestation and spectral reflectance/radiance in these experiments was tempered by inconstancies within the experimental areas which may have been due to tolerance of the cultivar, delayed image collection or by non-PCN stress factors in the field. The 2002 field experiments have, however, confirmed the results of the 2000 and 2001 field experiments, using both airborne and satellite images. Green wavebands are seen once again to be an important parameter for the spectral assay of PCN infestation and satellite imagery has been demonstrated as capable of detecting spectral changes consistent with infestation by PCN.

7. Discussion

A consistent linear relationship between reflectance in the region of 550nm (green) with PCN population density estimates was observed in three seasons of field experiments, using field spectrometers, airborne multispectral and hyperspectral sensors and from satellite images. This spectral response was sufficiently broad to be measurable by the SPOT HRV instrument band one (500nm-590nm). The broad spectral response indicates a potential for detecting PCN-induced reduction of green radiance using a simple, low-cost and robust detector system.

Image acquisition in this investigation was partially dependent on aircraft and instrument availability, although weather conditions were the major factor in determining the time at which spectra and images could be recorded from the growing crop. Field spectrometer measurements from the 2000 Four Gates Field experimental area were obtained at 44-45 days after planting (DAP), albeit from plants that were early to mature due to extensive chitting of the seed tubers and the late planting date (May 11th). Green reflectance alone could not be associated with PCN population density estimation due to the very substantial differences in solar irradiance between the collection of target and reference spectra under overcast conditions. The ratio $\frac{681nm - 551nm}{681nm + 551nm}$ was related to root invasion counts (1000's juveniles g^{-1} root) ($F_{(1,4)}$= 70.84, $p < 0.001$, $R^2_{(4)}$= 0.993) early in the crop cycle and the Hydro N-Meter measurements produced a strong linear relationship ($F_{(1,4)}$= 99.25, $p < 0.001$, $R^2_{(4)}$=0.96) at just 34-35 DAP. Airborne images of the 2001 New Piece experimental site were obtained at 105 DAP. Green radiance (CASI-2 551.12nm waveband) was linearly related ($F_{(1,28)}$=86.34, $p < 0.001$, $R^2_{(28)}$= 0.755) with PCN population density estimation of the experimental plot areas.

Three SPOT satellite images from central plots of the 2002 Challinors Field experimental site represent the only temporal data series obtained during this investigation. The strongest linear relationship between reduced green radiance and PCN population density estimation was seen in the first SPOT satellite image ($F_{(1,14)}$= 24.05, p <0.001, $R^2_{(14)}$= 0.632) at 104 DAP and this reduced to ($F_{(1,14)}$= 19.13, p <0.01, $R^2_{(14)}$= 0.578) in the second SPOT image twelve days later (116 DAP). The potato canopy in Challinors Field was senescing visibly at the time of the third SPOT image (142 DAP) and the relationship between radiance in SPOT band one (500nm-590nm) with PCN population density estimation was no longer significant ($F_{(1,14)}$= 4.17, p <0.06, $R^2_{(14)}$= 0.229). The relationship between reduced radiance at green wavelengths and PCN-induced plant stress spans a wide range of crop maturity (5-16 weeks) and, although experiments from each year are not directly comparable, would appear to be stronger when measured from younger plants.

Whilst field spectrometer measurements may be obtained (with care) before canopy closure is complete, soil background reflectance is liable to detract from the information conveyed by aircraft and satellite images of fractional vegetation cover. Soil reflectance can be higher or lower than canopy reflectance at green wavelengths, according to e.g. soil type and moisture. The signal of interest is contained in the vegetation reflectance fraction and reflectance from soil or other background matter will reduce the potential to discriminate between levels of green reflectance from the canopy (section 1.6.1.2.). Aircraft and satellite images were therefore requested at a time when the target canopy was expected to have achieved closure across the crop rows.

A ratio between two (or more) wavebands is required where fluctuating irradiance or variable sensor view-angles might distort the absolute radiance levels measured from survey areas under comparison. The use of red wavebands (670-680nm, depending on

instrument) in a ratio with a green waveband resulted in the strongest relationship with PCN population density estimation, although this was weaker than the response of the green waveband alone. Radiance from dry soil (recorded from a field adjacent to the 2001 New Piece experimental area) was over three times greater than from the crop canopy at 670nm, inflating the sensitivity of a red-green ratio to the presence of soil in the sensor field-of-view.

Reduced green radiance and near-invariant radiance at red wavebands (except in senescent crops) would suggest that infestation by PCN raises the concentration of chlorophyll in the leaves of potato plants. Leaf reflectance at 550nm was described as increasing in a near-exponential manner with reducing chlorophyll content by Hodáňová (1985). The sensitivity of spectral reflectance to changes in photosynthetic pigments of eucalyptus leaves was reported as at a maximum at 550nm and 709nm wavelengths by Datt (1998) although red wavelengths (660nm-690nm) were insensitive to changes in pigment content. Darker green leaves of plants infested by nematodes have been reported by Gausman *et al.* (1978) and Grove *et al.* (1999). Gausman *et al.* measured increased chlorophyll content (4.3mg g^{-1} vs. 4.1mg g^{-1}) in leaves of cotton plants (*Gossypium hirsutum*) stressed by infestation with the nematode *R. reniformis.* Photosynthetic pigments accumulate as the leaf matures and reflectance at visible wavelengths is reduced (Walter-Shea & Norman, 1991). Leaf growth in potato ceases at tuber initiation (Nelson & Hwang, 1975) and change in reflectance due to leaf maturity is unlikely to account for the reduction in green reflectance measured from plants at up to sixteen weeks in this investigation.

Early reports of lighter tones (indicating higher reflectance) from infested crops on panchromatic (Brenchley, 1968) and infrared (Heald *et al.*, 1972) photographic film were not supported by the results in this project. More recently, Stephens *et al.* (2000) reported a strong curvilinear relationship between NDVI measurements obtained from paired digital

cameras mounted on a light aircraft with counts of PCN cysts collected from soil samples of a known infestation. Their camera equipment was fitted with filters which restricted sensitivity to 640nm and 840nm (at 11nm FWHM bandwidth) and was not configured to record the reduced green radiance reported in this project. Green radiance has been shown in this investigation to contain the greatest amount of information on PCN-induced plant stress and this was consistent across seasons, cultivars and imaging methods, although significance was seen to transfer to the red spectral region as the crop matured. Nutter *et al.* (2002) examined the spectral response of soybeans (*Glycine max*) to infestation by the cyst nematode *Heterodera glycines*. The authors reported results at 810nm (near-infrared) and did not discuss the relationship between nematode population density and reflectance at visible wavebands. Wheeler & Kaufman (2003) found little correlation between the spectral reflectance of cotton (*Gossypium hirsutum*) and post-harvest population densities (Pf) of the nematode *M. incognita.* Post-harvest nematode population densities are considered to be an unreliable indicator of pre-planting distribution. Multiplication rates in the current crop are strongly dependent on initial population levels (Haydock & Evans, 1998b). A wide variation in invasion and multiplication may therefore result in similar post-harvest population densities, confounding an attempted analysis of plant stress due to nematode pathogenicity.

The reduction in green reflectance from plants infested with PCN is contrary to an expected increase in visible reflectance due to a reduced chlorophyll content of stressed vegetation (Wiegand *et al.*, 1991). Carter (1993) reported increased reflectance at 550nm in response to a range of stress factors and concluded that this was a consisted response to plant stress. Reports of reduced green reflectance found in the literature were limited to deficiency in phosphorus (Ulrich, 1993), infestation by the nematode *Rotylenchulus reniformis* on leaves of cotton plants) (Gausman *et al.*, 1975; Gausman *et al.,* 1978) and soil salinity (Gausman *et al.*, 1984).

A comparison with spectra from plants stressed by other pathogens was not obtained under field conditions. Cyst nematodes are essentially static and their occurrence can be determined in advance of a planned spectral survey. Other pathogens, e.g. aphids, fungal or viral diseases, are less predictable and a spectral assay of these pathogens would require much shorter lead-in times than are currently available for spectrometer hire or aircraft and satellite image collection. Spectral measurements were therefore collected from potato plants infected with the fungal pathogen *Rhizoctonia solani* in a concurrent field experiment (conducted by the Ph.D. student Matthew Back), and from plants grown in pots for the explicit purpose of differentiating between the spectral responses to PCN and *R. solani*.

The comparison of spectra from plants infested with PCN and those infected with *R. solani* has indicated that the orange spectral region (*c.* 625nm) can be used to distinguish between these two pathogens. Spectral measurements to discriminate between PCN and *R. solani* were, however, collected under unfavourable weather conditions. Spectra recorded using a GER 1500 Dual-Beam spectrometer were of highly variable signal levels, notwithstanding the near-concurrent target and reference measurements. Data acquired from the digital camera equipment at the Institute of Grassland Research, Aberystwyth (IGER) were subject to changes in lighting, leaf mounting methods and exposure settings between imaging sessions.

These highly-variable spectra were used to produce ratio indices between two wavebands, each of which were expected to have been influenced to a similar degree by variability in irradiance or camera settings. These data were re-evaluated at the conclusion of this project by converting mean spectral curves (per treatment) into dimensionless distribution curves. The conversion was achieved by converting the signal at each waveband to a

percentage of the spectrum mean from 450nm-700nm for GER 1500 spectra and 520nm-700nm for the IGER camera as $\frac{(\text{Waveband} * 100)}{\text{Mean spectrum } (450\text{nm} : 700\text{nm})}$. The linear relationship between these distribution curves and root invasion by PCN and *R. solani* disease scores is shown in Fig. K.1. in Appendix K. The simple ratio between distribution curves for PCN and *R. solani* with no-pathogen replicates is shown for the 2001 GER Dual-Beam spectrometer data (Fig. K.2.) and the IGER Digital Camera measurements (Fig. K.3.). Field spectrometer data from the experiment of M. Back in 2000 and the 2001 pot experiment indicated that infestation by PCN reduced green reflectance whilst the *R. solani* pathogen did not.

7.1. Limitations.

Specific narrow-band spectral features could not be related to PCN population density estimates from the spectra obtained in the course of this investigation. The single candidate feature, a slight reversal in the curve produced by plotting the ratio of infested to uninfested plant spectra against waveband was located at different wavelengths in each of the three experiments where it was observed. Some promising results were obtained, although a suitable algorithm in one year performed poorly in subsequent experiments. An anticipated relationship between pathogen burden and radiance close to the 970nm water absorption band was not found. The CASI-2 instrument spectral range extends to 947nm, on the fringe of this absorption band, and the GER 1500 spectrometer covered the entire feature (to 1095nm) while the negative relationship with PCN remained essentially constant from *c.* 750nm to the upper limit of the instrument spectral range.

Substantial heterogeneity was found in reflectance from the canopy of the potato crop and the aggregation of a large number of spectra (or image pixels) was required to identify areas of PCN infestation. Values recorded with a hand-held chlorophyll meter were initially discarded as not indicative of PCN pathogenicity. Aggregating these

measurements into infestation groups (1000's juveniles g^{-1} soil), however, revealed a strong linear relationship with nematode burden ($F_{(1,4)}$= 99.25, p <0.001, $R^2_{(4)}$=0.96) and similar trends were noted when aggregating field spectrometer readings. The relationships between green radiance (551nm) calculated from four 2m pixels of the 17206/17207 flight images and PCN population density of the 2001 field experiment were lower ($F_{(1,121)}$=121.36, p <0.001, $R^2_{(121)}$= 0.501) than for the *c.* 2500m^2 area samples ($F_{(1,28)}$=86.34, p <0.001, $R^2_{(28)}$= 0.755), indicating that a 4m rectangle was not sufficient to fully determine PCN infestation levels.

7.2. Future work.

The origins of a minor spectral feature noted at 630nm are worthy of further investigation. This feature is located at the approximate overlap of the longer-waveband absorption features of chlorophylls *a* and *b* (Lichtenhaler, 1987) and may indicate that the ratio between these pigments is influenced by nematode pathogenesis.

The influence of cultivar, growth stage and environment on the absolute values of green reflectance or red-green reflectance ratio might be determined by examination of spectra from crops grown across multiple seasons, in various soil types, and a wide range of cultivars. Experience gained from the operation of a within-field assay would then be applied to the development of site, soil, temporal and cultivar-specific input parameters for reflectance-based PCN detection.

7.3. Practical application.

Unfavourable weather conditions have hampered or delayed this investigation in each of its three years duration. Some independence of climatic conditions will be required if a spectral assay method is to be reliably useable in a maritime climate. Aircraft and satellite imaging methods are at the mercy of clouds, wind and rain, as are reflectance measurements collected with a field spectrometer. Only the closed-system of the Hydro N-

meter was able to collect spectra under the majority of prevailing weather conditions. This points to a closed, or near-closed instrumentation system as being most likely to deliver a commercially-viable spectral assay method for the detection of PCN infestation.

A closed imaging system, completely enclosing a leaf or plant, would not be conducive to the rapid and economical survey of large crop areas. A semi-open system, whereby the sensor and target are shielded from fluctuating solar irradiance and high wind, but which allows rapid movement across the field is suggested. A tractor-mounted (or trailed) imaging system would offer several advantages over airborne and satellite remote sensing. The sensor and illumination source can be located in a fixed geometry to each other and might be arranged at an angle to the canopy with a fixed background located behind the target. Vehicle, and therefore sensor movement over uneven ground would affect view-angle and may lead to erroneous measurement. Sensor movement can be minimised by use of a gyro-stabilised mounting within the vehicle, although this will add complexity and expense to a system which is required to be both robust and cost-effective. A wider, longer trailed vehicle, spanning several crop-rows and with multiple sprung wheels along each side would be less prone to roll and pitch movement than a sensor mounted directly on the tractor. A large, light-excluding canopy would substantially reduce variability due to incident irradiation and the tractor generator can be used to power a focussed and stabilised light source across the target towards the fixed background plate. Differential Global Positioning System (DGPS) receivers are already in use to map the position of e.g. grain harvesters in the field. The incorporation of a DGPS receiver into the data recording equipment of a dedicated PCN-sensor vehicle would enable measured reflectance values to be mapped to actual field locations

The many wavebands of a conventional radiometer add expense and complexity. A single sensor, sensitive to radiance at 550nm is proposed, based on controlled illumination and

the provision of a constant background surface with similar reflectance characteristics to the target. The sensor can be designed to cover a broad waveband (~60nm appears suitable from the results of this investigation) and would be less expensive and more robust than a spectrometer having high spectral resolution. The addition of red and NIR channels might extend the application of this sensor to other crop-monitoring functions, e.g. nitrogen requirement, the design function of the Hydro N-Meter.

A covered PCN-sensor vehicle would be less subject to changes in solar irradiance and might be useable in the dark. Leaves of the dicotyledon potato plant are differentiated with additional chloroplasts located below the upper (adaxial) surface where reflectance is lower than from the abaxial side (Guyot *et al*, 1992). A partial sheltering of the target canopy by a covered sensor vehicle would reduce the likelihood of wind inverting canopy elements and thus enable the system to be used under a wider range of weather conditions.

Whilst a sensor vehicle can be designed to protect the instruments from rain, the presence of raindrops or dew on leaves of the target canopy might affect the spectral values recorded and spectral assay of PCN infestation should be limited to occasions where the crop canopy is dry.

7.4. Conclusions.

Southey (1974) noted that foliar symptoms of PCN infestation were influenced by soil type and environmental factors. The spectral assay of infestation by PCN is proposed as a within-field comparison as cultivar, maturity stage and growing conditions may influence leaf colour. However, the unsupervised classification of a 2001 CASI-2 flight image was conducted over an area which extended beyond the experimental area and included reflectance from many non-target surfaces. Results from this classification would appear

to indicate a reduced sensitivity to absolute reflectance values. Unsupervised classification might facilitate the automation of PCN assay from airborne imagery.

A swift and accurate measure of populations under a growing crop would open up many otherwise prohibitive options to the grower:

1. Trap cropping, particularly for organic growers, could become viable if foci can be identified and removed before the infestation is spread by subsequent tillage;

2. targeted application of nematicides can control populations while, at the same time, responding to the demands for reduced chemical application from supermarket buyers;

3. short rotation becomes possible if developing foci are removed before they have time to multiply;

4. localised information can be used to prevent the spread of infestation by changing tillage direction and reviewing the direction of vehicle movement between infested and uninfested fields.

Appendix A. Spot satellite image parameters.

SPOT (Satellite Pour l'Observation de la Terre)

Spot Image

5, rue des Satellites

BP 4359

F 31030 Toulouse cedex 4

France

Details from Mather (1999), Jensen (2000) and

http://www.spot.com/home/proser/Level12A%20tech%20Aug2002.pdf

SPOT 2:

Instrument HRV (High Resolution Visible) (3 bands)

Orbit: sun synchronous at 822km. Inclination 98.2°

Spatial resolution at nadir: Multispectral 20m Panchromatic (510nm-730nm) 10m

Sensor: linear array

Data:	11 bit (2048 levels)
Band 1:	500nm-590nm
Band 2:	610nm-680nm
Band 3:	790nm-890nm

SPOT 4:

Instrument HRVIR (4 bands)

Orbit: sun synchronous at 822km. Inclination 98.2°

Spatial resolution at nadir: Multispectral 20m Panchromatic (510nm-730nm) 10m

Sensor: linear array

Data:	11 bit (2048 levels)
Band 1:	500nm-590nm
Band 2:	610nm-680nm
Band 3:	790nm-890nm
Band 4:	1580nm-1750nm

Ist SPOT image

Scene ID	4 026-242 02-07-14 11:02:32 1 I
K-J identification	026-242
Date 2002-07-	14 11:02:36
Instrument	HRVIR 1
Shift Along	Track 4 1200
Preprocessing	level 1B
Spectral mode	XI
Number of spectral bands	4
Spectral band indicator	XS1 XS2 XS3 XS4
Gain number	5, 5, 3, 4
Absolute calibration gains (W/m2/sr/μm)	2.16226, 2.73051, 1.24567, 13.48687
Orientation angle	9.9 degree
Incidence angle	R27.6 degree
Sun angles	Azimuth: 148.7, Elevation: 56.0
Number of lines	2986
Number of pixels per line	3889
Scene Centre Location	Latitude N052° 58' 43" Longitude W002° 33' 09"
Pixel number	1983
Line number	1493

2nd SPOT image

Scene ID	2 026-242 02-07-26 11:00:27 1 X
K-J identification	026-242
Date	2002-07-26 11:00:33
Instrument	HRV 1
Shift Along Track	7 2100
Preprocessing level	1B
Spectral mode	XS
Number of spectral bands	3
Spectral band indicator	XS1 XS2 XS3
Gain number	8, 8, 6
Absolute calibration gains (W/m2/sr/μm)	1.30509, 1.27265 1,.53995
Orientation angle	9.7 degree

Incidence angle	R30.4 degree
Sun angles	Azimuth: 149.1, Elevation: 53.9
Number of lines	2984
Number of pixels per line	4062
Scene Centre Location	Latitude N052° 49' 15" Longitude W002° 19' 52"
Pixel number	2076
Line number 1	492
Corners Location	

3rd SPOT image

Scene	ID 2 026-242 02-08-21 11:00:35 1 X
K-J identification	026-242
Date	2002-08-21 11:00:41
Instrument	HRV 1
Shift Along Track	6 1800
Preprocessing level	1B
Spectral mode	XS
Number of spectral bands	3
Spectral band indicator	XS1 XS2 XS3
Gain number	8, 8, 6
Absolute calibration gains (W/m2/sr/μm)	1.30509, 1.27265, 1.53995
Orientation angle	9.7 degree
Incidence angle	R30.4 degree
Sun angles	Azimuth: 153.6, Elevation: 47.2
Number of lines	2983
Number of pixels per line	4063
Scene Centre Location	Latitude N052° 52' 24" Longitude W002° 20' 53"
Pixel number	2077
Line number	1492

Appendix B. Ikonos satellite sensor and image details.

Ikonos-2 satellite: Space Imaging Inc. Thornton, Colorado, U.S.A

Details from Jensen (2000) and http://www.infoterra-global.com/ikonos.htm

Orbit:	Sun synchronous at 681km.
Spatial resolution at nadir:	Multispectral 4m, Panchromatic(450nm-900nm) 1m
Sensor:	Linear array
Data:	11 bit (2048 levels)
Band 1:	450nm-520nm
Band 2:	520nm-600nm
Band 3:	630nm-690nm
Band 4:	760nm-900nm

Ikonos Image July 26th, 2002:

Processing Level:	Standard geometrically corrected image
Type:	MSI
Interpolation Method:	Cubic convolution
Map Projection:	Universal Transverse Mercator, zone 30 north.
Datum:	WGS84
Nominal Collection Azimuth:	257.2505 degrees
Nominal Collection Elevation:	70.65574 degrees
Sun Angle Azimuth:	164.8927 degrees
Sun Angle Elevation:	56.10309 degrees
Acquisition Date/Time:	2002-07-26 11:41 GMT

Coordinate1:		Coordinate 2:	
Latitude:	52.73410994 degrees	Latitude:	52.82403204 degrees
Longitude:	-2.57042970 degrees	Longitude:	-2.56954342 degrees

Coordinate 3:		Coordinate 4:	
Latitude:	52.82340094 degrees	Latitude:	52.73348088 degrees
Longitude:	-2.42110013 degrees	Longitude:	-2.42229200 degrees

Appendix C. Pseudo-random number generation.

Pseudo-random number generation in Genstat, version 5, release 4.21. (Lawes Agricultural Trust, Rothamsted, UK). 2000 field and pot experiments.

Plant selection. 2000 field experiment

GRANDOM [DISTRIBUTION=uniform; NVALUES=2000; SEED=0; LOWER=1; UPPER=15] pselect

* MESSAGE: Default seed for random number generator used with value 374004

(*Message retained so reader can create an identical 'random' sequence*)

Read-sequence order. 2000 field experiment

GRANDOM [DISTRIBUTION=uniform; NVALUES=500; SEED=0; LOWER=1; UPPER=9] order

*MESSAGE: Default seed for random number generator used with value 519178

Pot dose. 2000 pot experiment

GRANDOM [DISTRIBUTION=uniform; NVALUES=30; SEED=0; LOWER=5; UPPER=100] dose2

* MESSAGE: Default seed for random number generator used with value 581550

Appendix D. GER 1500 instrument details.

Source: http://www.ger.com/1500print.html. Accessed on 02/04/2003.

GER (Geophysical and Environmental Research) Corporation
16 Bennett Common Millbrook New York 12545 USA

Instrument:	GER 1500	
Spectral range:	350nm-1050nm	
Channels:	512	
Nominal bandwidth:	1.5nm	
Wavelength repeatability:	+0.1nm	
Radiometric calibration:	400nm:	±5%
(Traceable to NIST)	700nm:	±4%
	1000nm:	±5%
Digitisation:		16 bit (65536 discrete levels)

Note: the NERC EPFS instruments used in this investigation record in the range 300nm-1100nm.

Dual-beam mode is considered to be unreliable beyond *c.* 1050nm (E.M. Rollin, personal communication)

2000 field and pot experiments.

Instrument:	GER 1500
Serial No:	2039
Mode:	Single-beam
Reference panel:	Spectralon^{tm} srt1011
Field of view (foreoptic):	3°

2001 field and pot experiments plus ground-truth spectra.

Instrument:	GER 1500
Serial No:	2038 (Target) 2039 (Reference)
Mode:	Dual-beam
Reference panel:	Spectralon^{tm} srt3446
Field of view (foreoptic):	3° (Unity function set in software)

2002 field experiment and ground-truth spectra.

Instrument:	GER 1500
Serial No:	2038 (Target) 2039 (Reference)
Mode:	Dual-beam
Reference panel:	Spectralon^{tm} srt4240b
Field of view (foreoptic):	3° (Unity function set in software)

Appendix E. Near Moor Field experimental site 2001.

Late planting and poor weather delayed the canopy development of the potato crop (cv. Yukon Gold) in the Near Moor experimental area, illustrated in Figure E.1. Analysis of data from this experiment was not progressed beyond initial image registration. Initial PCN population density estimation(Pi, eggs g^{-1} soil) is shown in Table E.1.

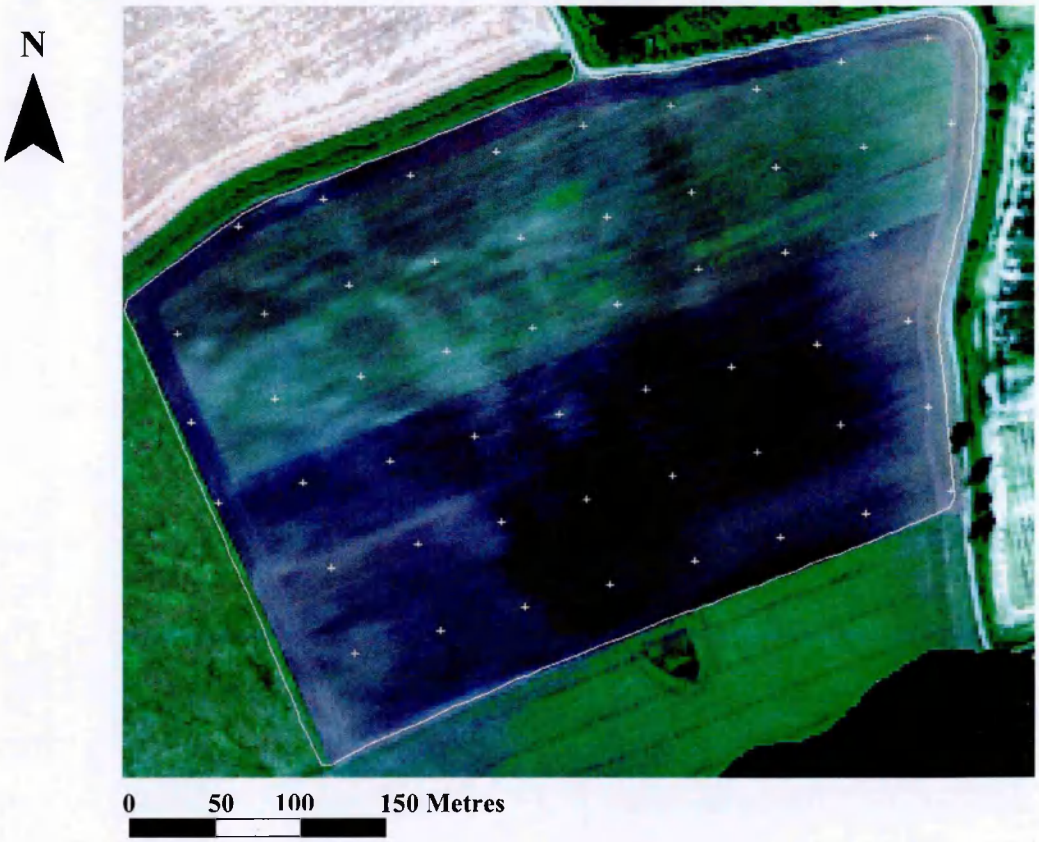

Figure E.1. False-colour (bands 6,3,1) image showing limited vegetation cover and experimental area vertices. CASI-2 flight image 17202, June 21st, 2001.

Table E.1. Initial PCN population density (Pi, eggs g^{-1} soil) estimation from quarter-ha experimental areas of Near Moor Field experimental site. Listed from the north-east. (Plot AA1).

Sample	Eggs g^{-1}	Sample	Eggs g^{-1}	Sample	Eggs g^{-1}
AA1	57	AB6	44	AD3	16
AA2	53	AB7	45	AD4	21
AA3	24	AB8	45	AD5	113
AA4	53	AC1	205	AD6	36
AA5	71	AC2	48	AD7	17
AA6	80	AC3	47	AE1	62
AA7	78	AC4	37	AE2	139
AA8	54	AC5	49	AE3	145
AB1	232	AC6	89	AE4	90
AB2	194	AC7	26	AE5	62
AB3	152	AC8	46	AE6	12
AB4	150	AD1	155	AE7	9
AB5	97	AD2	97		

Appendix F. ARSF flight details June 21st, 2001.

CASI-2 instrument, Serial Number 2007. Aircraft: D-CALM.

Flight image c172021b.hdf: 2001 vegetation bandset

c. 860m spheroid height (geoid-spheroid correction in post-processing).

Time	13:55 to 13:58 UTC
Aircraft heading:	NE *c.* 58° true
CASI-2 FOV: (Email from A.K. Wilson)	54.4° (Custom lens)
(Azexhdf listing of image file c172021b.hdf:	FOV= 53.20 (-26.824° to 26.286°).
Solar azimuth at 14:00:	225.6°
Solar elevation at 14:00:	54.2°
Divergence from principal solar plane:	12.4°

Flight image c172061b.hdf: Enhanced Spectral Mode - southern section of New Piece Field.

No cloud shadow visible within *c.* 1km of the New Piece Field experimental area.

c. 830m spheroid height (no geoid-spheroid correction).

Time:	14:26 to 14:29 UTC
Aircraft heading:	NE *c.* 58° true
CASI-2 FOV: (Email from A.K. Wilson).	*c.* 22°
Solar azimuth at 14:30:	235.4°
Solar elevation at 14:30:	50.7°
Divergence from principal solar plane:	2.6°

Flight image c172071b.hdf: Enhanced Spectral Mode - northern section of New Piece Field. No cloud shadow visible within *c.* 1km of the New Piece Field experimental area.

c. 814m spheroid height (no geoid-spheroid correction).

Time:	14:33 to 14:36 UTC
Aircraft heading:	WSW *c.* 250° true
CASI-2 FOV: (Email from A.K. Wilson).	*c.* 22°
Solar azimuth at 14:30:	235.4°
Solar elevation at 14:30:	50.7°
Divergence from principal solar plane:	14.6°

Astronomical Applications Dept. U.S. Naval Observatory

(web address http://aa.usno.navy.mil/data/docs/AltAz_noJS.html). Accessed 07/08/2003.

Altitude and Azimuth of the Sun. June 21st, 2001 Universal Time 2 25, N52 45.

13:50	55.2	222.1
14:00	54.2	225.6
14:10	53.1	229.0
14:20	51.9	232.3
14:30	50.7	235.4
14:40	49.4	238.3

Appendix G. CASI-2 instrument details.

Itres Research, Calgary, Alberta, Canada.

Source: NERC ARSF user documentation.

Compact Airborne Spectrographic Imager (CASI).

The CASI-2 sensor utilises a two-dimensional CCD detector array with 512 pixel elements across-track and 288 channel elements along-track. The imaging method is 'Push-broom'; all elements of the across-track swath are imaged simultaneously.

Spectral range:	405nm-950nm
Channels:	288 (aggregated according to imaging mode and user requirements)
Digitisation:	12 bit (4096 discrete levels)
Operating Modes:	
Spatial:	512 across-track elements. Maximum of 18 selectable wavebands.
Spectral:	Maximum of 39 across-track elements at 288 wavebands. Other permutations programmable.
Enhanced-Spectral:	Maximum of 101 across-track elements at 288 adjacent wavebands. Other permutations programmable.

Table G.1. Waveband settings: Spatial Mode images in 2001 and 2002.

Vegetation bandset 2001 CASI-2 flights 17202 and 17203.

Band	NM	FWHM
1	449.93	18.9514
2	490.06	20.91688
3	552.06	9.74382
4	669.68	9.82774
5	700.22	9.8446
6	709.78	9.84942
7	740.41	9.86358
8	749.99	6.0338
9	762.46	4.11816
10	780.69	9.87914
11	820.07	7.96818
12	865.29	9.9005
13	940.41	9.90678

Heath bandset 2001. CASI-2 flights 17204 and 17205.

Band	NM	FWHM
1	605.97	11.6826
2	616.4	9.79356
3	625.9	9.80016
4	635.4	9.8065
5	645.87	11.71654
6	656.34	9.81976
7	665.87	9.82554
8	675.4	9.8311
9	685.9	11.74614
10	696.4	9.84258

Vegetation bandset 2002. CASI-2 (all 2002 flights).

Band	NM	FWHM
1	450.18	18.959
2	490.33	20.92556
3	552.36	9.74664
4	607.23	9.78844
5	651.89	11.7213
6	670	9.82726
7	700.54	9.8427
8	710.09	9.84704
9	740.71	9.8596
10	750.28	6.03154
11	762.74	4.1168
12	780.96	9.87272
13	820.3	7.96142
14	865.45	9.88792
15	940.42	9.88744

Table G.2. Waveband settings: Enhanced-Spectral Mode images 17206 and 17207 in 2001.

Band	NM	FWHM	Band	NM	FWHM	Band	NM	FWHM
1	405.4	4.04858	49	585.12	4.09264	97	768.21	4.11864
2	409.1	4.04968	50	588.91	4.09338	98	772.05	4.11906
3	412.8	4.05074	51	592.7	4.09404	99	775.89	4.11932
4	416.5	4.05184	52	596.49	4.09478	100	779.73	4.11968
5	420.21	4.05294	53	600.28	4.0955	101	783.57	4.12004
6	423.92	4.054	54	604.07	4.09618	102	787.41	4.12034
7	427.62	4.05504	55	607.86	4.09686	103	791.25	4.12066
8	431.34	4.0561	56	611.66	4.09758	104	795.09	4.12096
9	435.05	4.05714	57	615.45	4.0982	105	798.93	4.12126
10	438.76	4.05818	58	619.25	4.09892	106	802.77	4.12156
11	442.48	4.05926	59	623.05	4.0996	107	806.62	4.12182
12	446.2	4.06026	60	626.85	4.1002	108	810.46	4.12212
13	449.92	4.06126	61	630.65	4.10082	109	814.31	4.12236
14	453.65	4.06228	62	634.45	4.10148	110	818.15	4.1226
15	457.37	4.06328	63	638.25	4.1021	111	822	4.12286
16	461.1	4.06428	64	642.06	4.10264	112	825.84	4.1231
17	464.83	4.06526	65	645.86	4.10332	113	829.69	4.12328
18	468.56	4.06622	66	649.67	4.10394	114	833.54	4.12358
19	472.29	4.06722	67	653.48	4.10448	115	837.38	4.12382
20	476.03	4.06816	68	657.29	4.1051	116	841.23	4.12396
21	479.77	4.0691	69	661.1	4.1057	117	845.08	4.1242
22	483.51	4.07006	70	664.91	4.10624	118	848.93	4.12438
23	487.25	4.071	71	668.73	4.10686	119	852.78	4.12456
24	490.99	4.07192	72	672.54	4.10734	120	856.63	4.12474
25	494.73	4.07284	73	676.35	4.1079	121	860.47	4.12492
26	498.48	4.07374	74	680.17	4.10844	122	864.32	4.12504
27	502.23	4.07466	75	683.99	4.10894	123	868.18	4.12524
28	505.98	4.07558	76	687.81	4.10954	124	872.03	4.12536
29	509.73	4.07646	77	691.63	4.11004	125	875.88	4.12554
30	513.49	4.07732	78	695.45	4.11052	126	879.73	4.12566
31	517.24	4.07824	79	699.27	4.11108	127	883.58	4.12578
32	521	4.07902	80	703.09	4.1115	128	887.43	4.1259
33	524.76	4.07994	81	706.91	4.11198	129	891.28	4.12602
34	528.52	4.0808	82	710.74	4.11248	130	895.14	4.12608
35	532.28	4.0816	83	714.56	4.1129	131	898.99	4.1262
36	536.04	4.0825	84	718.39	4.1134	132	902.84	4.12626
37	539.81	4.0833	85	722.22	4.11382	133	906.69	4.12634
38	543.58	4.0841	86	726.05	4.1143	134	910.55	4.12646
39	547.35	4.08488	87	729.88	4.11474	135	914.4	4.12646
40	551.12	4.08574	88	733.71	4.11516	136	918.25	4.12658
41	554.89	4.0866	89	737.54	4.11558	137	922.1	4.12658
42	558.66	4.08732	90	741.37	4.11596	138	925.96	4.12664
43	562.44	4.08806	91	745.2	4.11644	139	929.81	4.1267
44	566.22	4.08886	92	749.03	4.1168	140	933.66	4.1267
45	569.99	4.08964	93	752.87	4.11718	141	937.52	4.1267
46	573.77	4.09038	94	756.7	4.1176	142	941.37	4.1267
47	577.56	4.09118	95	760.54	4.11796	143	945.22	4.1267
48	581.34	4.09184	96	764.37	4.11828	144	949.08	4.1267

Source: azexhdf listing of level 1b HDF image files.

Appendix H. Sample ImageTool script

{Opens a series of files, selects pixels within upper and lower bound and calculates the mean of all selected pixels to a text window. Modified to use a variable rectangle}

```
var
  path,firstfilename,filename, textfile,p9:string;
pot1,pot2,pot3,pot4,pot5,pot6,pot7,pot8,pot9,pot10,pot11,pot12,leaf1,leaf2,leaf3,selectfile,
selectleaf:string;
  n,n2,n3,max,min,x,y,z,nano,sum,file,leafnum,posit,satpix,x1,x2,y1,y2:integer;
  mean:real;
  accept:boolean;
  xval,yval,zval,orgX,orgY,topleft,lowright:array;

begin

min := 800;                                   {Variable according to session}
max := 2300;
path := 'd:\\images\\pot';
{path := 'j:\\iger\\pot';}

{********************** Edit these for current pots ************************}
pot1 := '3a';
pot2 := '18b';
pot3 := '32c';
pot4 := '49d';
pot5 := '20b';
pot6 := '34c';
pot7 := '8a';
pot8 := '53d';

{****************** Rectangle positions for each PLANT **********************}
orgX[1]:= 600;              {pot 1} {top left and lower right coordinates}
orgX[2]:= 600;
orgY[1]:= 620;
orgY[2]:= 620;

orgX[3]:= 200;              {pot 2}
orgX[4]:= 650;
orgY[3]:= 160;
orgY[4]:= 650;

orgX[5]:= 150;              {pot 3}
orgX[6]:= 650;
orgY[5]:= 170;
orgY[6]:= 580;

orgX[7]:= 170;              {pot 4}
orgX[8]:= 700;
orgY[7]:= 160;
orgY[8]:= 630;
```

```
orgX[9]:= 110;                {pot 5}
orgX[10]:= 600;
orgY[9]:= 290;
orgY[10]:= 850;

orgX[11]:= 210;               {pot 6}
orgX[12]:= 530;
orgY[11]:= 190;
orgY[12]:= 870;

orgX[13]:= 175;               {pot 7}
orgX[14]:= 680;
orgY[13]:= 300;
orgY[14]:= 850;

orgX[15]:= 210;               {pot 8}
orgX[16]:= 550;
orgY[15]:= 220;
orgY[16]:= 870;

{********************  Start of program  ******************************}
leaf1 := '1';
leaf2 := '2';
leaf3 := '3';

{********************* Start of Plant loop ******************************}
for file := 1 to 8 do begin                                  {for each pot}
leafnum :=1;                                                 {reset leaf for each pot}

{****************** Loop for each leaf from current plant (3) ***************}
satpix := 0;
topleft[1] := orgX[((file*2)-1)];          {set sample rectangle for each plant}
topleft[2] := orgX[(file*2)];
lowright[1] := orgY[((file*2)-1)];
lowright[2] := orgY[((file*2)-1)];

topleft[3] := orgX[(file*2)];              {for annotation rectangle }
topleft[4] := orgX[((file*2)-1)];
lowright[3] := orgY[(file*2)];
lowright[4] := orgY[(file*2)];

x1 := topleft[1];
x2 := topleft[2];
y1 := lowright[1];
y2 := lowright[3];

 for leafnum := 1 to 3 do begin                              {leaf loop within pot }

if (file = 1) then begin
                filename := pot1;                            {pot directory}
  end;
  if (file = 2) then begin
                filename := pot2;
```

```
  end;

  if (file = 3) then begin
                filename := pot3;
  end;

  if (file = 4) then begin
                filename := pot4;
  end;

  if (file = 5) then begin
                filename := pot5;
  end;

  if (file = 6) then begin
                filename := pot6;
  end;

  if (file = 7) then begin
                filename := pot7;
  end;

  if (file = 8) then begin
                filename := pot8;
  end;

end;

p9 := concat(filename,'-');
filename := concat(path,filename);

if (leafnum = 1) then begin
                filename := concat(filename,'\\',p9:1,leaf1,'\\',p9:1,leaf1);
end;

if (leafnum = 2) then begin
                filename := concat(filename,'\\',p9:1,leaf2,'\\',p9:1,leaf2);

end;

if (leafnum = 3) then begin
                filename := concat(filename,'\\',p9:1,leaf3,'\\',p9:1,leaf3);
end;

  firstfilename := filename;
  textfile := concat(filename,'b.csv');          {must reset at end of leaf loop!}
  MakeNewTextWindow(textfile);
  movewindow(600,300);                           {position text window on screen}
  SelectWindow(textfile);                                  {make output file active}
  writeln('NM,',P9,leafnum:1,',File,SatPix');  {write header information}

{***************** Open file *25 to select pixels to use*********************}
filename := concat(filename,'25.tif');          {25 is 616 nmn = peak reflectance}
```

```
Open(filename);
SelectWindow(filename);
accept := true;
movewindow(10,60);                          {position image on screen}

{******************** DEBUG ONLY ************************************}
                {accept :=ShowmessageCancel('filename - Continue ? ');
                if (accept=true) then begin
                                exit;
                end;}

{************* Select pixels within upper and lower bounds ******************}
x:=0;
y:=0;
z:=0;
posit:=1;

SetForegroundColor(255,0,0);                {draw rectangle for visual reference}
Makepolygonroi(topleft,lowright,4);
MakeAnnotation;
killroi;

{****************** Row and Column loops ******************************}
for y := y1 to y2 do begin                                  {each row}
 for x := x1 to x2 do begin   }                             {pixels in row}
                z := Getpixel((x+1),(y+1));
                if (z > min) and (z < max)  then begin
                                xval[posit] := (x);
                {populate arrays}
                                yval[posit] := (y);
                                zval[posit] := z;
                                posit := posit+1;
                {move to next array position}
                end;
 end;                           {end of row}
 wait(0.0025);                  {let other programms run!}
end;                            {end of test file loop}

selectwindow(textfile);
writeln('source value , ',x,',',y,',',z);
selectwindow(filename);

Dispose;                                                    {close pixel select file}
filename := firstfilename;

{****************** Loop for each wavelength file ************************}
for n := 1 to 46 do begin                                   {loop for each file}
                satpix := 0;
                if (n < 10) then begin
                                filename := concat(filename,'0');  {add leading zero}
                end;
                filename := concat(filename,n:1);
                filename := concat(filename,'.tif');
```

```
            Open(filename);
            SelectWindow(filename);
            movewindow(10,60);                    {position image on screen}
            nano := (n*4)+516;                    {wavelength of current file}

{***************** Get selected pixels from wavelength file ******************}
            {for n2 := 1 to (posit-1) do begin
                        x:= xval[n2];
                        y:= yval[n2];}
                        z:= GetPixel((x+1),(y+1));
        if (z > 3850) then begin
          satpix := satpix+1;              {check for saturated pixels}
        end;
                        sum:= sum+z;
            {end;}

            mean := z;                    {calculate mean of all selected pixels}

            SelectWindow(textfile);       {make output file active}

            writeln(nano,',',mean,',',n,',',satpix); {write nm, comma and mean to file}
            SelectWindow(filename);               {select image window to close}
            Dispose;
            filename := firstfilename;            {revert to initial name}
            mean := 0;                            {reset mean}
            sum := 0;                             {reset sum}
            z := 0;
            {reset z}
end;
{************** End wavelength file process loop - write results *****************}
writeln(posit,' Pixels used\n', min,' Minimum\n',max, ' Maximum\n');
writeln(satpix,' Saturated pixels');
writeln('Rectangle from ',x1,':',y1:1,' to ',x2,':',y2:1);
SelectWindow(textfile);
Save;
Dispose;
Beep;
leafnum := leafnum+1;
end;
{************************ End of leaf loop ******************************}
file := file+1;
end;
{************************ End of file loop ******************************}
end;
{************************** end of Program ******************************}
```

Appendix I. ARSF flight details June 26th 2002

CASI-2 instrument, Serial Number 2007. Aircraft: D-CALM.

Flight image c177041b.hdf: 2002 vegetation bandset.
Ground-truth only

c. 783m spheroid height (geoid-spheroid correction in post-processing).

Time	10:47 to 10:49 UTC
Aircraft heading:	NW *c.* 310° true
CASI-2 FOV: (Email from A.K. Wilson)	53.2° (-26.824° to 26.286°)

Solar azimuth at 10:50:	144.1°
Solar elevation at 10:50:	56.7°
Divergence from principal solar plane:	13.9°

Flight image c177061b.hdf: 2002 vegetation bandset.
Challinors Field experimental area.

c. 810m spheroid height (geoid-spheroid correction in post-processing).

Time	11:07 to 11:09 UTC
Aircraft heading:	NNW *c.* 326° true
CASI-2 FOV:	53.2° (-26.824° to 26.286°)

Source: azexhdf listing of image file c177061b.hdf.

Solar azimuth at 11:10:	152.1°
Solar elevation at 11:10:	58.3°
Divergence from principal solar plane:	6.1°

Flight image c 177081b.hdf: 2002 vegetation bandset.
Challinors Field experimental area.

c. 770m spheroid height (geoid-spheroid correction in post-processing).

Time	11:19 to 11:21 UTC

Aircraft heading:	WSW *c.* 232° true
CASI-2 FOV:	53.2° (-26.824° to 26.286°)

Source: azexhdf listing of image file c177081b.hdf.

Solar azimuth at 11:20:	156.3°
Solar elevation at 11:20:	59.0°
Divergence from principal solar plane:	75.7°

Relative headings of flights 17706 and 17708:

Track differences:	337° - 228° = 109°
Heading differences:	326° - 232° = 94°

Astronomical Applications Dept. U.S. Naval Observatory

(web address http://aa.usno.navy.mil/data/docs/AltAz_noJS.html) Accessed 07/08/2003.

Altitude and Azimuth of the Sun. June 26th, 2002. W 2 20, N52 45.

10:50:	56.7°	144.1°
11:10:	58.3°	152.1°
11:20:	59.0°	156.3°

Appendix J. ARSF flight details July 15th 2002

CASI-2 instrument, Serial Number 2007. Aircraft: G-CALM.

Flight 19613: 2002 vegetation bandset.
(Ground-truth only)

c. 758m spheroid height (geoid-spheroid correction in post-processing).

Time	11:48 to 11:50 UTC
Aircraft heading:	South *c.* 172.4° true
CASI-2 FOV:	53.20° (-26.824° to 26.286°

(Source: azexhdf listing of image file c196131b.hdf)

Solar azimuth at 11:50 UTC:	168.6°
Solar elevation at 11:50 UTC:	58.31°
Divergence from principal solar plane:	3.8°

Flight 19615: 2002 vegetation bandset.
Big Field Experimental area Cloud to north and south of the target within *c.* 60m.

c. 750m spheroid height (geoid-spheroid correction in post-processing).

Time	11:58 to 12:00 UTC
Aircraft heading:	South *c.* 180.4° true
CASI-2 FOV:	53.20° (-26.824° to 26.286°

(Source: azexhdf listing of image file c196151b.hdf)

Solar azimuth at 12:00 UTC:	173.0°
Solar elevation at 12:00 UTC:	58.6°
Divergence from principal solar plane:	7.4°

Astronomical Applications Dept. U.S. Naval Observatory
(web address http://aa.usno.navy.mil/data/docs/AltAz_noJS.html) Accessed on 07/08/2003.
Altitude and Azimuth of the Sun. July 15th, 2002 Universal Time. W 2 20, N52 45.

11:50	58.31°	168.6°
12:00	58.6°	173.0°

Appendix K. Review of PCN vs. *R. solani* spectral data

Spectra collected from a 2000 field experiment of the Ph.D. student Matthew Back and leaves and plants of the 2001 pot experiment had been collected under conditions of variable illumination. Analysis of these data was limited to the investigation of ratios calculated between pairs of wavebands subject to identical irradiance, and did not facilitate the generation of ratio or correlation curves. The data were re-evaluated at a late stage in this investigation by converting the spectra into dimensionless distribution curves. All spectra (treatment means) were converted to a percentage of the reflectance across the spectral range as $\frac{(\text{Waveband} * 100)}{\text{Mean spectrum } (450\text{nm} : 700\text{nm})}$ It should be noted that a change in reflectance in one part of the spectral range will exert an inverse effect on the remaining curve. This method should be interpreted as an exposition of the distribution of reflectance from each treatment. The data are dimensionless and the relative magnitude of the curves does not convey any information.

Figure K.1. illustrates the correlation (r) between distribution curves and pathogen burden from the 2000 field experiment of M. Back. Some interaction between spectral responses to PCN and *R. solani* is inherent in these data as many plant samples were subject to both pathogens.

Distribution curves derived from spectra collected from whole plants of the 2001 pot experiment are shown in figure K.2. The curve for each pathogen is shown relative to the control (no pathogen) samples as a ratio analysis. The treatments are discrete; there was no overlap between pathogens in any replicate used in this analysis.

Figure K.3. displays the distribution curves derived from spectra recorded from excised leaves of the 2001 pot experiment plants. The spectra were collected under artificial

illumination (two cold-light laboratory lamps) using a digital camera and tuneable filter (section 5.2.2.2.) at the Institute of Grassland Research, Aberystwyth (IGER). Radiance Spectra recorded at IGER were of measurements of radiance as reference spectra collected from a Spectralon™ panel were found to have exceeded the dynamic range of the camera sensors.

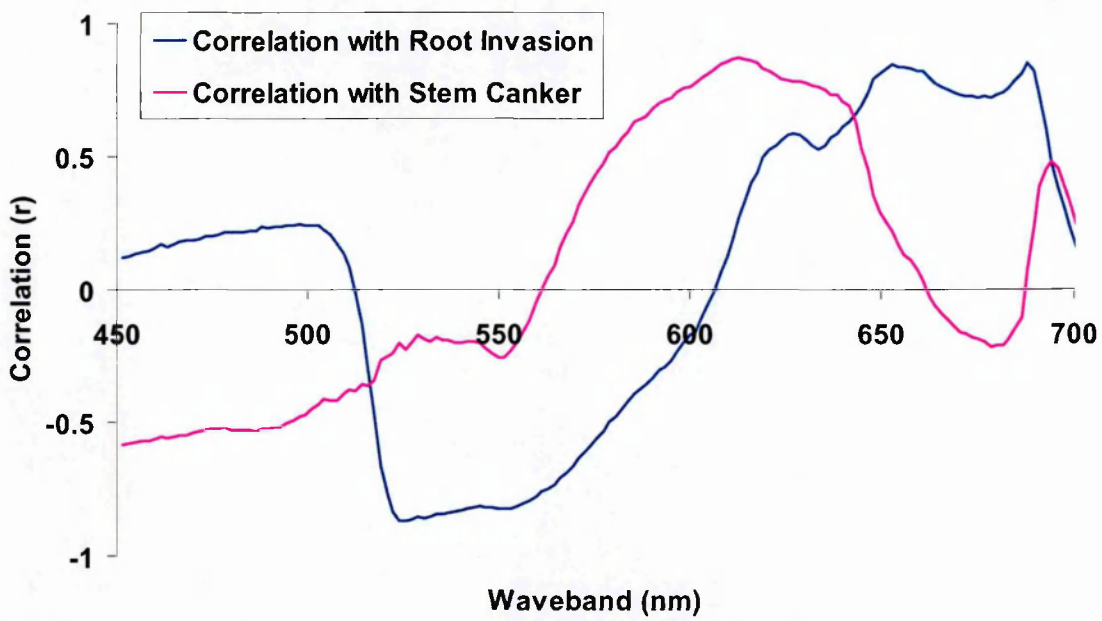

Figure K.1. Correlation between root invasion (juveniles g^{-1} root) and stem canker assessment scores (Back & Jenkinson, 2000) with spectral reflectance as a percentage of the spectral mean 450-700nm. *R. solani* experiment, Four Gates Field (M. Back), June 2000.

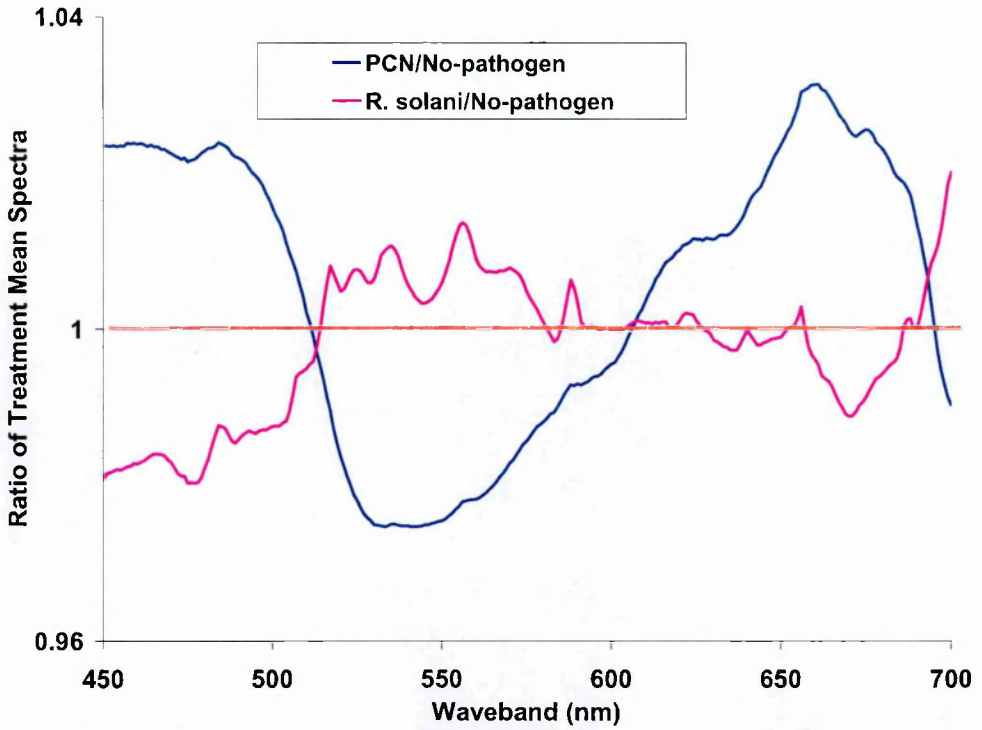

Figure K.2. Ratio of spectral reflectance between treatments and no-pathogen (control) replicates. Spectra collected under solar illumination on July 4th, 2001 using a GER 1500 Dual-Beam Field Spectrometer. Reflectance converted to a percentage of the spectral mean 450-700nm.

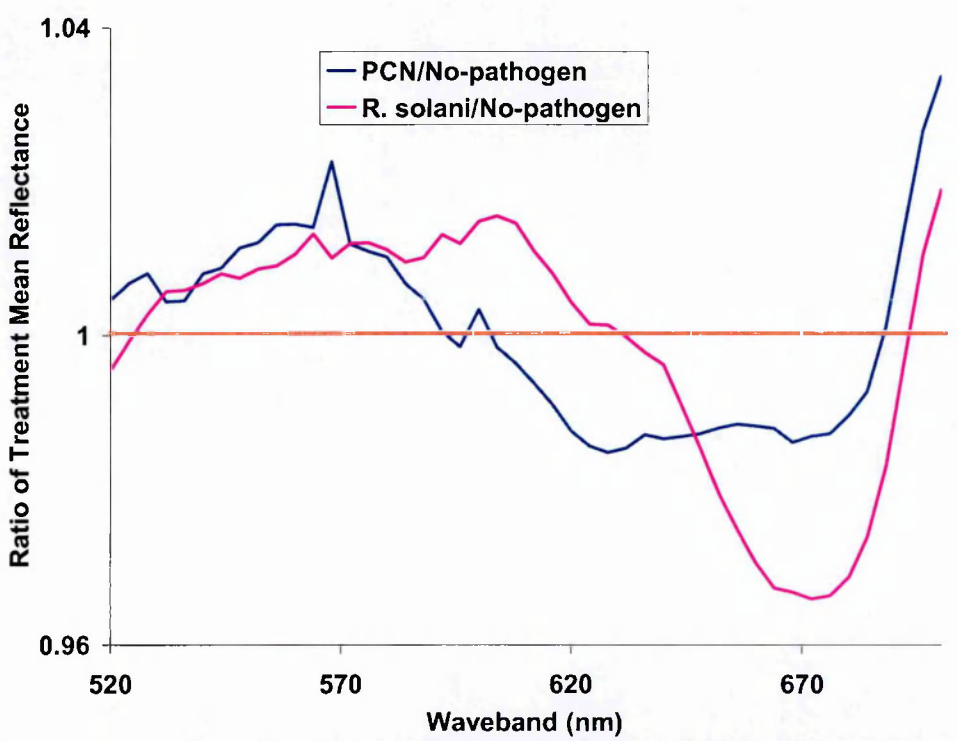

Figure K.3. Ratio of spectral reflectance between treatments and no-pathogen (control) replicates. Spectra collected using a digital camera and tuneable filter from experimental pot samples in 2001. Reflectance converted to a percentage of the spectral mean 520-700nm.

The distribution curves for each pathogen are dissimilar to those derived from field spectrometer measurements obtained under solar illumination. This may have been caused by a lower-intensity artificial light source failing to activate sufficient chloroplasts in the leaf, although this has not been confirmed. A disparity between the treatments is visible in the orange (*c.* 620nm) spectral region.

References

Al-Abbas, A.H., Barr, R., Hall, J.D., Crane, F.L. and Baumgardener, M.F. 1974. Spectra of normal and nutrient-deficient maize leaves. *Agronomy Journal* **66:** 16-20.

Anon. 1972. Vacuuming the golden nematode, *Agricultural Research*, Washington. **21:3** 10.

Ambrose, E., Haydock, P.P.J. and Wilcox, A. 2000. Degradation of the nematicide Oxamyl in field conditions. *Aspects of Applied Biology* **59:** 41-51.

Arntzen, F.K., Mulder, J.G. and Visser, J.H.M. 1994. Rapid and non-destructive assessment of the number of eggs in cysts of potato cyst nematodes by weighing. *Fundamentals of Applied Nematology* **17(4):** 299-302.

Asner, G.P. 1998. Biophysical and biochemical sources of variability in canopy reflectance. *Remote Sensing of Environment* **64:** 234-253.

Bacci, L. Benincasa, F., Maracchi, G. and Zipoli, G. 1991. Ground based remote sensing measurements for the early detection of plant stresses. *EPPO Bulletin* **21:** 673-681.

Back, M.A., Haydock, P.P.J. and Jenkinson, P. 2002. Disease complexes involving plant parasitic nematodes and soilborne pathogens. *Plant Pathology* **51:** 683-697.

Back, M.A., Jenkinson, P. and Haydock, P.P.J. 2000. The interaction between potato cyst nematodes and *Rhizoctonia solani* diseases in potatoes. *Proceedings of the Brighton Crop Protection Conference, Pests and Diseases.* Farnham, UK: British Crop Protection Council. 503-506.

Baret, F. 1995. Use of spectral reflectance to retrieve canopy biophysical characteristics. **In:** Eds Danson, F.M. and Plummer, S.E. *Advances in Environmental Remote Sensing.* John Wiley & Sons, New York 33-51.

Baret, F. and Guyot, G. 1991. Potentials and limits of vegetation indices for LAI and APAR assessment. *Remote Sensing of Environment* **35:** 161-173.

Baret, F., Guyot, G., and Major, D. 1989. TSAVI: a vegetation index which minimizes soil brightness effects on LAI or APAR estimation. *12th Canadian Symposium on Remote Sensing and IGARSS* 1990, Vancouver, Canada, July 10-14.

Barnsley, M. and Morris, K. 1990. Correction of sensor view angle effect in multispectral imagery. **In:** Eds. Steven, M.D., Clark, J.A. *Applications of Remote Sensing in Agriculture.* Butterworths, London. 186-197.

Bauer, M.E. 1986. Field spectroscopy of agricultural crops. *IEEE Trans. Geo-science. Remote Sensing* GE-24: 65-75.

Been, T.H. and Schomaker, C.H. 1986. Quantitative-analysis of growth, mineral-composition and ion balance of the potato cultivar Irene infested with *Globodera-pallida* (Stone). *Nematologica* **32:3** 339-355.

Been, T.H. and Schomaker, C.H. 1995. Sampling. *Nematologica* **41:3** 358-360.

Been, T.H. and Schomaker, C.H. 1996. A new sampling method for the detection of low population densities of potato cyst nematodes (*Globodera pallida and G. rostochiensis*). *Crop Protection* **15:** 375-382.

Blackburn, G.A. 1998. Quantifying chlorophylls and caroteniods at leaf and canopy scales: an evaluation of some hyperspectral approaches. *Remote Sensing Of Environment* **66:3** 273-285.

Blakeman, R.H. 1990. The identification of crop disease and stress by aerial photography. **In:** Eds. Steven, M.D., Clark, J.A. *Applications of Remote Sensing in Agriculture.* Butterworths, London. 229-254.

Blankenship, R.E. 2002. *Molecular mechanisms of photosynthesis.* Blackwell Science, Malden, MA. 321 pp.

Blazquez, C.H. and Edwards, G.J. 1983. Infra-red color photography and spectral reflectance measurements of tomato and potato diseases. *Journal of Applied Photographic Engineering* **9:** 33-37.

Blazquez, C.H. and Edwards, G.J. 1986. Spectral reflectance of healthy and diseased watermelon leaves. *Annals of Applied Biology* **108:2** 243-249.

Boag, B. 1985. The localised spread of virus-vector nematodes adhering to farm machinery. *Nematologica* **31:** 234-235.

Boag, B., Filipe, J. and Niesten, D. 2000. Spatial distribution of *Globodera rostochiensis* foci in a potato field in Scotland. *Aspects of Applied Biology* **59:** 99-102.

Boag, B. and Neilson, R. 1994. Nematode aggregation and its effect on sampling strategies. *Aspects of Applied Biology* **37:** 103-111.

Boag, B. and Topham, P.B. 1984. Aggregation of plant parasitic nematodes and Taylor's Power Law. *Nematologica* **30:3** 348-357.

Boochs, F., Kupfer, G., Dockter, K. and Kühbauch, W. 1990. Shape of the red edge as vitality indicator for plants. *International Journal of Remote Sensing* **11:10** 1741-1753.

Brenchley, G.H. 1968. Aerial photography for the study of plant diseases. *Annual Review of Phytopathology* **6:** 1-22.

Brodie, B.B. 1998. Potato cyst nematodes (*Globodera* species) in Central and North America. **In:** Eds Marks, R.J. and Brodie, B.B. *Potato Cyst Nematodes, Biology, Distribution and Control,* Oxon. CAB International. 317-331.

Brodie, B.B., Evans, K. and Franco, J. 1993. Nematode parasites of potatoes. **In:** Eds Evans, K., Trudgill, D.L. and Webster, J.M. *Plant parasitic nematodes in temperate agriculture.* Oxon: CAB International. 87-132.

Brodie, B.B. and Mai, W.F. 1989. Control of the golden nematode in the United States. *Annual Review of Phytopathology* **27:** 443-461.

Bouman, B.A.M., Uenk, D. and Haverkort, A.J. 1992. The estimation of ground cover of potato by reflectance measurements. *Potato Research* **35:** 111-125.

Brown, E.B. 1969. Assessment of the damage caused to potatoes by potato cyst eelworm, *Heterodera rostochiensis* Woll. *Annals of Applied Biology* **63:** 493-502.

Buschmann, C. and Nagel, E. 1993. *In vivo* spectroscopy and internal optics of leaves as basis for remote sensing of vegetation. *International Journal of Remote Sensing* **14:4** 711-722.

Campbell, J.B. 1996. *Introduction to Remote Sensing.* Taylor & Francis, London, UK. 622 pp.

Carter, G.A. 1993. Responses of leaf spectral reflectance to plant stress. *American Journal of Botany* **80:3** 239-243.

Carter, G.A. 1994. Ratios of leaf reflectances in narrow wavebands as indicators of plant stress. *International Journal of Remote Sensing* **15:** 697-703.

Chappelle, E.W., Kim, W.S. and McMurtrey, J.E. III. 1992. Ratio analysis of reflectance spectra (RARS): an algorithm for the remote estimation of the concentrations of chlorophyll *a*, chlorophyll *b*, and carotenoids on soybean leaves. *Remote Sensing of Environment* **39:** 239-247.

Choi, K-Y., Milton, E. and Brown, K. 2002. Image normalisation using data from the CASI Incident Light Sensor (ILS): a model-based approach designed for operational applications. *Proceedings. NERC ARSF Workshop, Rutherford Appleton Laboratory, Didcot, UK.* 16/17 December, 2002.

Church, B.M., Gough, H.C. and Southey, J.F. 1959. Soil sampling procedures for potato root eelworm cysts. *Plant Pathology* **8:** 146-151.

Clark, R.N. and Roush, T.L. 1984. Reflectance spectroscopy: quantitative analysis techniques for remote sensing applications. *Journal of Geophysical Research* **89:** 6329-6340.

Clevers, J.G.P.W. 1989. The application of a weighted infrared-red vegetation index for estimating leaf-area index by correcting for soil-moisture. *Remote Sensing Of Environment* **29 :1** 25-37.

Cooke, D.A., McKinney, H.E. and Thomason, I.J. 1979. A rapid method for sampling surface soil. *Journal of Nematology* **11:2** 202-204.

Cotten, J. 1991. Quarantine Procedure No. 30. *EPPO Bulletin* **21**: 233-240.

Crump, D.H. 1998. Biological control of potato and beet cyst nematodes. *Aspects of Applied Biology. Protection and Production of Sugar Beet and Potatoes* **52:** 383-386.

Curran, P.J. 1985. *Principles of Remote Sensing.* Longman Scientific & Technical, Harlow, UK. 282 pp.

Dale, M.F.B. and Brown, J. 1989. The use of foliage assessment to improve the identification of tolerance to damage by nematodes (*Globodera pallida*) in potatoes. *Annals of Applied Biology* **115:** 313-319.

Danson, F.M., Plummer, S.E. and Briggs, S.A. 1995. Remote sensing and the information extraction problem. **In:** Eds Danson, F.M. and Plummer, S.E. *Advances in Environmental Remote Sensing.* John Wiley & Sons, New York 171-177.

Datt, B. 1998. Remote sensing of chlorophyll a, chlorophyll b, chlorophyll a+b, and total carotenoid content in eucalyptus leaves. *Remote Sensing Of Environment* **66: 2** 111-121.

Daughtry, C.S.T., Vanderbilt, V.C. and Pollara, V.J. 1982. Variability of reflectance measurements with sensor altitude and canopy type. *Agronomy Journal* **74:** 744-751

Davies, K.G. 1998. Natural parasites and biological control. **In:** Ed. Sharma, S.B. *The Cyst Nematodes.* Kluwer, Dordrecht. 369-387.

De Koeijer, K.J., Steven, M.D. and Colls, J.J. 2000. Integration of earth observation data with a crop model for yield forecasting. *Aspects of Applied Biology* **60:** 91-98.

Demetriades-Shah, T.H. and Steven, M.D. 1988. High spectral resolution indices for monitoring crop growth and chlorosis. *Proceedings of the 4th International Colloquium of Spectral Signatures of Objects in Remote Sensing,* Aussois, France, 18-22 January 1988. ESA SP-287, European Space Agency, Paris 299-302.

Demetriades-Shah, T.H., Steven, M.D., and Clark, J.A. 1990. High resolution derivative spectra in remote sensing. *Remote Sensing of Environment* **33:** 55-64.

De Ruijter, F.J. and Haverkort, A.J. 1999. Effects of potato-cyst nematodes (*Globodera pallida*) and soil pH on root growth, nutrient uptake and crop growth of potato. *European Journal of Plant Pathology* **105:** 61-76.

Dixit, L. and Ram, S. 1985. Quantitative analysis by derivative electronic spectroscopy. *Applied Spectroscopy Reviews* **21:** 311-418.

Elvidge, C.D. and Chen, Z. 1995. Comparison of broad-band and narrow-band red and near-infrared vegetation indices. *Remote Sensing of Environment* **54:1** 38-48.

Endo, B.Y. 1975. Pathogenesis of nematode-infected plants. *Annual Review of Phytopathology* **13:** 213-238.

Endo, B.Y. 1987. Histopathology and ultrastructure of crops invaded by certain sedentary endoparasitic nematodes. **In:** Eds Veech, J.A. & Dickson, D.W. *Vistas on Nematology.* Society of Nematologists, Hyattsville, Maryland. 196-210.

Epstein, E. and Grant, W.J. 1973. Water stress relations of the potato plant under field conditions. *Agronomy Journal* **65:** 400-404.

Evans, K. 1982. Water use, calcium uptake and tolerance of cyst-nematode attack in potatoes. *Potato Research* **25:** 71-88.

Evans, K. 1987. The interactions of potato cyst nematodes and *Verticillium dahliae* on early and maincrop potato cultivars. *Annals of Applied Biology* **110:** 329-339.

Evans, K. 1993. New approaches to potato cyst nematode management. *Nematropica* **23:** 221-231.

Evans, K., Franco, J. And De Scurrah, M.M. 1975a. Distribution of species of potato cyst-nematodes in South America. *Nematologica* **21:3** 365-369.

Evans, K. and Haydock, P.P.J. 1990. A review of tolerance by potato plants of cyst nematode attack, with consideration of what factors may confer tolerance and methods of assaying and improving it in crops. *Annals of Applied Biology* **117**: 703-740.

Evans, K. and Haydock, P.P.J. 1993. Interactions of nematodes with root-rot fungi. **In:** Ed. Wajid Khan, M. *Nematode Interactions*. Chapman & Hall, London, UK. 104-133.

Evans, K. and Haydock, P.P.J. 2000. Potato cyst nematode management – present and future. *Aspects of Applied Biology. Potato Cyst Nematode Management* **59:** 91-97.

Evans, K., Niesten, D. and Haydock, P.P.J. 2000. Sampling patterns and estimation of potato cyst nematode densities. *Aspects of Applied Biology. Potato Cyst Nematode Management* **59:** 141-147.

Evans, K., Parkinson, K.J. and Trudgill, D.L. 1975b. Effects of potato-cyst nematodes on potato plants. 3 Effects on the water relations and growth of a resistant and a susceptible variety. *Nematologica* **21:** 273-280.

Evans, K., Stafford, J., Webster, R., Halford, P., Russell, M., Barker, A. and Griffen, S. 1998. Mapping potato cyst nematode populations for modulated applications of nematicide. *Aspects of Applied Biology. Protection and Production of Sugar Beet and Potatoes* **52:**101-108.

Evans, K. and Stone, A.R. 1977. A review of the distribution and biology of the potato cyst-nematodes *Globodera rostochiensis and G. pallida. PANS* **23:** 178-189.

Evans, K. and Trudgill, D.L. 1992. Pest aspects of potato production part 1. The nematode pests of potatoes. **In:** Ed. Harris, P. *The Potato Crop*, Chapman Hall, London. 438-475.

Evans, K., Trudgill, D.L. and Brown, N. J. 1977. Effects of potato cyst nematodes on potato plants V. Root system development in lightly- and heavily-infested susceptible and resistant varieties, and its importance in nutrient and water uptake. *Nematologica* **23:** 153-164.

Evans, K., Niesten, D. and Haydock, P.P.J. 2000. Sampling patterns and estimation of potato cyst nematode densities. *Aspects of Applied Biology. Potato Cyst Nematode Management* **59:** 141-147.

Fatemy, F. and Evans, K. 1986. Growth, water uptake and calcium content of potato cultivars in relation to tolerance of cyst nematodes. *Revue de Nématologie* **9:2** 171-179.

Fatemy, F., Trinder, K.E., Wingfield, J.N. and Evans, K. 1985. Effects of *Globodera rostochiensis* and exogenous abscisic acid on stomatal function and water use of Cara and Pentland Dell potato plants. *Revue de Nématologie* **8:3** 249-255.

Fisher, R.A. 1968. Stomatal opening : role of potassium uptake by guard cells. *Science* **160:** 784-785.

Fleming, C.C., Turner, S.J., Powers, T.O. and Szalansky, A.L. 1998. Diagnostics of cyst nematodes: use of polymerase chain reaction to determine species and estimate population levels. *Aspects of Applied Biology. Protection and Production of Sugar Beet and Potatoes* **52:** 375-382.

Fourty, T.H., Baret, F., Jacquemoud, S., Schmuck, G. and Verdebout, J. 1996. Leaf optical properties with explicit description of its biochemical composition: direct and inverse problems. *Remote Sensing of Environment* **56:** 104-117.

Franco, J. 1980. Effect of potato cyst-nematode *Globodera rostochiensis* on photosynthesis of potato plants. *Fitopatologica* **15:** 1-6.

Franco, J., Oros, R., Main, G. and Ortuno, N. 1998. Potato cyst nematodes (*Globodera* species) in South America. **In:** Eds Marks, R.J. and Brodie, B.B. *Potato Cyst Nematodes, Biology, Distribution and Control,* Oxon. CAB International. 239-269.

Gates, D.M., Keegan, H.J., Schleter, J.C. and Weidner, V.R. 1965. Spectral qualities of plants. *Applied Optics* **4:** 11-20.

Gausman, H.W. 1974. Leaf reflectance of near-infrared. *Photogrammetric Engineering* **40:** 183-192.

Gausmann, H.W., Allen, W.A. and Escobar, D.E. 1974. Refractive index of plant cell walls. *Applied Optics* **13:** 109-111.

Gausman, H.W., Burke, J.J. and Quisenberry, J.E. 1984. Use of leaf optical-properties in plant stress research. *Acs Symposium Series* **257:** 215-233.

Gausman, H.W., Escobar, D.E. and Rodriguez, R.R. 1978. Effect of stress and pubescence on plant leaf and canopy reflectance. **In.** *Proceedings, International Symposium on Remote Sensing for Observation and Inventory of Earth Resources and the Endangered Environment.* Friburg, F.R.G. July, 1978. *International Archives of Photogrammetry* **23:** 719-749.

Gausman, H.W., Heald, C.M. Jr, and Escobar, D.E. 1975. Effect of *Rotylenchulus reniformis* on reflectance of cotton plant leaves. *Journal of Nematology* **7:** 368-374.

Goetz, A.F.H. 1992. Imaging spectroscopy for earth remote sensing. **In:** Eds Toselli, F. & Bodechtel, J. *Imaging Spectroscopy: Fundamentals and Prospective Applications.* Kluwer Academic Publishers, Dordrecht. 1-19.

Grainger, J. and Clark, M.R.M. 1963. Interactions of *Rhizoctonia* and potato root eelworm. *European Potato Journal* **6:2** 131-132.

Grossman, Y.L., Sanderson, E.W. and Ustin, S.L. 1994. Relationships between leaf chemistry and reflectance for plant species from Jasper Ridge Biological Preserve,

California. **In:** IGARSS 94: *Proceedings of the International Geosciences and Remote Sensing Symposium,* Pasadena, CA, August 8-12, 1994, **4:** 2357-2359.

Grove, I.G., Haydock, P.P.J., Evans, K. and Lewis, D.J. 1999. Supplementary foliar N, P and K, applied individually or in combinations, and the tolerance of potatoes to infection by the potato cyst nematodes *Globodera rostochiensis* and *G. pallida*. *Annals of Applied Biology* **134**: 193-204.

Guyot, G. 1990. Optical properties of vegetation canopies. **In:** Eds Steven, M.D. and Clark, J.A. *Applications of Remote Sensing in Agriculture.* Butterworths, London. 19-43.

Guyot, G., Baret, F. and Jacquemoud, S. 1992. Imaging spectroscopy for vegetation studies. **In:** Eds Toselli, F. & Bodechtel, J. *Imaging Spectroscopy: Fundamentals and Prospective Applications*. Kluwer Academic Publishers, Dordrecht. 145-165.

Hammond, H.K., Warren, L.H. and Kuder, M.L. 1960. Ratio recording spectroradiometer. *Journal of Research of the National Bureau of Standards, C.* **64:** 151-157.

Hansen, J.G. 1991. Use of multispectral radiometry in wheat yellow rust experiments. *EPPO Bulletin* **21:** 651-658.

Hatfield, J.L. and Pinter, P.J. Jr 1993. Remote sensing for crop protection. *Crop Protection* **12:6** 403-413.

Haverkort, A.J. and Schapendonk, A.H.C.M. 1994. Crop reactions to environmental stress factors. **In:** Eds. Struik, P.C., Vredenberg, W.J., Renkema, J.A. and Parlevliet, J.E. *Plant Production on the Threshold of a New Century.* Kluwer Academic Publishers, Dordrecht, NL. 339-347.

Haverkort, A.J. and Trudgill, D.L. 1995. Crop physiological responses to infection by potato cyst nematode (*Globodera* spp.). **In**: Eds Haverkort, A.J. and MacKerron, D.K.L. *Potato Ecology and Modelling of Crops under Conditions Limiting Growth.* Kluwer, Dodrecht. 167-184.

Haverkort, A.J., Uenk, D. Veroude, H. and Van de Waart, M. 1991. Relationships between ground cover, intercepted solar radiation, leaf area index and infrared reflectance of potato crops. *Potato Research* **34:** 113-121.

Haydock, P.P.J. and Evans, K. 1998a. Integrated crop management (ICM) protocols and the management of potato cyst nematodes. *Aspects of Applied Biology. Protection and Production of Sugar Beet and Potatoes* **52:** 361-366

Haydock, P.P.J. and Evans, K. 1998b. Management of potato cyst nematodes in the UK: an integrated approach? *Outlook on Agriculture* **27:4** 253-260.

Haydock, P.P.J. and Perry, J.N. 1998. Sampling practice and principles. **In:** Eds R J Marks and B B Brodie. *Potato Cyst Nematodes, Biology, Distribution and Control,* CAB International, Oxon. 61-74.

Heald, C.M., Thames, W.H. and Wiegand, C.L. 1972. Detection of *Rotylenchulus reniformis* infestations by aerial infrared photography. *Journal of Nematology* **4:4** 298-300.

Heath, W.L., Haydock, P.P.J., Wilcox, A. and Evans, K. 1999. Could the analyses of light reflected from the potato crop be used as a diagnostic assay for infection by potato cyst nematodes? *Offered Papers in Nematology.* Association of Applied Biologists, Linnean Society, London, 14 December 1999.

Huete, A.R. 1988. A soil-adjusted vegetation index (SAVI). *Remote Sensing of Environment.* **25:** 295-309.

Hodáňová, D. 1985. Leaf optical properties. **In:** Ed. Šesták, Z. *Photosynthesis during leaf development.* Dr W. Junk Publishers, Dordrecht, NL. 106-127.

Hoffer, R.M. and Johannsen, C.J. 1969. Ecological potentials in spectral signature analysis. **In:** Ed. Johnson, P.L. *Remote Sensing in Ecology.* University of Georgia Press, Athens, Georgia. 1-16.

Hominick, W.M. 1982. Selection of a rapidly maturing population of *Globodera rostochiensis* by continuous cultivation of early potatoes in Ayrshire, Scotland. *Annals of Applied Biology* **100:** 345-351.

Hooper, D.J. 1986. Extraction of nematodes from plant material. **In:** Ed. J F Southey. *Laboratory Methods for Work with Plant and Soil Nematodes.* HMSO, London. 51-58.

Hunter, A.H. 1958. Nutrient absorption and translocation of phosphorus as influenced by root-knot nematodes. *Soil Science* **86:** 245-250.

Hunter, R.S. 1942. Photoelectric tristimulus colorimetry with three filters. *Journal of the Optical Society of America* **32:** 509-538.

Ibrahim, S.K., Minnis, S.T., Barker, A.D.P., Russell, M.D., Haydock, P.P.J., Evans, K., Grove, I.G., Woods, S.R. and Wilcox, A. 2001. Evaluation of PCR, IEF and ELISA techniques for the detection and identification of potato cyst nematodes from field soil samples in England and Wales. *Pest Management Science* **57:11** 1068-1074.

Ives, H.E. 1915. A precision artificial eye. *Physics Review* **6:** 334-344.

Jackson, R.D. 1983. Spectral indices in N-space. *Remote Sensing of Environment* **13:** 409-421.

Jackson, R.D. 1986. Remote sensing of biotic and abiotic plant stress. *Annual Review of Phytopathology* **24:** 265-287.

Jenkins, W.R. and Malek, R.B. 1966. Influence of nematodes on absorption and accumulation of nutrients in vetch. *Soil Science* **101:** 46-49.

Jensen, J.R. 2000. *Remote Sensing of the Environment.* Prentice Hall, New Jersey. 544 pp.

Johnson, L.F. 1999. Response of grape leaf spectra to Phylloxera infestation. NASA Report #CR-208765, NASA Center for AeroSpace Information, Hanover, MD.

Johnson, L.F., Lobitz, B., Armstrong, R., Baldy, R., Weber, E., De Benidictis, J. and Bosch, D. 1996. Airborne imaging aids vineyard canopy evaluation. *California Agriculture* **50:4** 14-18.

Jones, F.G.W. 1970. The control of the potato cyst-nematode. *Journal of the Royal Society of Arts* **118**: 179-199.

Jordan, C.F. 1969. Derivation of leaf area index from quality of light on the forest floor. *Ecology,* **50:** 663-666.

Kauth, R.J. and Thomas, G. 1976. The tasselled cap – a graphic description of the spectral-temporal development of agricultural crops as seen by Landsat. *Proceedings of the Symposium on Machine Processing of Remotely-Sensed Data. Purdue University, West Lafayette, Indiana. Vol. 4B,* 41-51.

Knibling, E.D. 1969. Leaf reflectance and image formation on color infrared film. **In:** Ed. Johnson, P.L. *Remote Sensing in Ecology.* University of Georgia Press, Athens, Georgia. 17-29.

Kokaly, R.F. and Clark, R.N. 1999. Spectroscopic determination of leaf biochemistry using band-depth analysis of absorption features and stepwise linear regression. *Remote Sensing of Environment* **67:** 267-287.

Kollenkark, J.C., Vanderbilt, V.C., Daughtry, C.S.T. and Bauer, M.E. 1982. Influence of solar illumination angle on soybean canopy reflectance. *Applied Optics* **21:7** 1179-1184.

Lauer, M.J., Pallardy, S.G., Blevins, D.G. and Randall, D.D. 1989. Whole leaf carbon exchange characteristics of phosphate deficient soybeans (*Glycine max* L.). *Plant Physiology* **91:** 848-854.

Lawrence, G.W., Kelley, A.T., King, R.L., Vickery, J., Lee, H.K. and McLean, K.S. 2002. Remote sensing and precision nematicide applications for reniform nematode management in Mississippi cotton. *Nematology* 4: 128.

Lelong, C.C.D., Pinet, P.C. and Poilvé, H. 1998. Hyperspectral imaging and stress mapping in agriculture: a case study on wheat in Beauce (France). *Remote Sensing Of Environment* **66:2** 179-191.

Lichtenthaler, H.K. 1987. Chlorophylls and caretenoids: pigments of photosynthetic biomembranes. *Methods in Enzymology* **148:** 350-383.

Lili, Z., Duchesne, J., Nicolas, H. and Rivoal, R. 1991. Détection infrarouge thermique des maladies du blé d'hiver. *OEPP Bulletin* **21:** 659-672.

Lillesand, T. M. and Kiefer, R. W. 1993. *Remote Sensing and Image Interpretation,* 3rd edition, John Wiley and Sons, New York. 750 pp.

Lo, C.P. 1986. *Applied Remote Sensing.* Longman Scientific & Technical, Harlow, Essex, UK. 393 pp.

MAFF. 1986. *The Analysis of Agricultural Materials.* 3rd ed. Ministry of Agriculture, Fisheries and Food, London.

MAFF. 2000. *Fertiliser recommendations* (RB 209) *for agricultural and horticultural crops*. 7th ed. Ministry of Agriculture, Fisheries and Food, London.

Magnusson, M.L. 1986. Development of *Globodera rostochiensis* under simulated nordic conditions. *Nematologica* **32:** 438-45.

Mather, P.M. 1999. *Computer Processing of Remotely-Sensed Images.* Wiley & Sons, Chichester, UK. 292 pp.

Milton, E.J. 1987. Principles of field spectroscopy. I*nternational Journal of Remote Sensing.* **8:12.** 1807-1827.

Milton, E.J. and Goetz, A.F.H., 1997. Atmospheric influences on field spectrometry: observed relationships between spectral irradiance and the variance in spectral reflectance. *Seventh International Symposium on Physical Measurements and Signatures in Remote Sensing (ISPRS), Courchevel, France*, 109-114.

Milton, E.J., Rollin, E.M. and Brown, K.M. 2000. Practical methodologies for the reflectance calibration of *CASI* data. **In:** Ed. Tadina, F. *Proceedings of the Annual Conference of the NERC Airborne Remote Sensing Facility. Keyworth, Nottingham*, 12-13 December 2000.

Milton, E.J., Rollin, E.M. and Emery, D.R. 1995. Advances in field spectroscopy. **In:** Eds Danson, F.M. and Plummer, S.E. *Advances in Environmental Remote Sensing.* John Wiley & Sons. Chichester, UK. 9-32.

Minnis, S.T. 2000. Distribution of potato cyst nematodes in England and Wales and the use of 1,3 dichloropropene for their control. Ph.D. Thesis, Harper Adams University College, Newport, Shropshire, England.

Minnis, S., Haydock, P.P.J., Ibrahim, S., Grove, I.G., Evans, K. and Russell, M.D. 2002. Potato cyst nematodes in England and Wales – occurrence and distribution. *Annals of Applied Biology* **140:** 187-195.

Myers, V.I. and Allen, W.A. 1968. Electrooptical remote sensing methods as nondestructive testing and measuring techniques in agriculture. *Applied Optics* **7:** 1819-1838.

Nelson, S.H. and Hwang, K.E. 1975. Water usage by potato plants at different stages of growth. *American Potato Journal* **52:** 331-339.

Nutter, F.W., Tylka, G.L., Moreira, A.J.D., Marett, C.C., Rosburg, T.R., Basart, J.P. and Chong, C.S. 2002. Use of remote sensing to detect soybean cyst nematode-induced plant stress. *Journal of Nematology* **34:3** 222-231.

O'Hare, G. and Sweeney, J. 1986. *The Atmospheric System.* Oliver & Boyd, Harlow, Essex, UK.

Ou, L-T, Chung, K-Y, Thomas, J.E., Obreza, T.A, and Dickson, D.W. 1995. Degradation of 1,3-dichloropropene (1,3-D) in soils with different histories of field applications of 1,3-D. *Journal of Nematology* **27:3** 249-257.

Peñuelas, J., Baret, F. and Filella, I. 1995. Semi-empirical indices to assess carotenoids/chlorophyll a ratio from leaf spectral reflectance. *Photosynthetica* **31:2** 221-230.

Peñuelas, J., Filella, I., Serrano, L., Biel, C. and Save, R. 1993. The reflectance at the 950-970 nm region as an indicator of plant water status. *International Journal of Remote Sensing*. 14: 1887-1905.

Peñuelas, J., Gamon, J.A., Fredeen, A.L., Merino, J. and Field, C.B. 1994. Reflectance indices associated with physiological changes in nitrogen and water-limited sunflower leaves. *Remote Sensing of Environment* **48:** 135-146.

Perry, C.R. and Lautenschlager, L.F. 1984. Functional equivalence of spectral vegetation indices. *Remote Sensing of Environment* **14:** 169-182.

Peterson, J.R. and MacDonald, M.C. 1996. TRW AG resource mapping: Agricultural remote sensing phenomenology. *Proceedings, Second International Airborne Remote Sensing Conference and Exhibition* **3:** 397, San Francisco CA, 24-27 June 1996 (pub: Environmental Research Institute of Michigan,

Phillips, M.S. and Trudgill, D.L. 1998. Population modelling and integrated control options for potato cyst nematodes. **In:** Eds Marks, R.J. and Brodie, B.B. *Potato Cyst Nematodes, Biology, Distribution and Control*, CAB International, Oxon. 153-163.

Qi, J., Chehbouni, A., Huete, A.R., Kerr, Y.H., and Sorooshian, S. 1994. A modified soil adjusted vegetation index (MSAVI). *Remote Sensing of Environment* **48:** 119-126.

Raven, P.H., Evert, R.F. and Eichhorn, S.E. 1998. *Biology of Plants* 6th ed. Freeman Worth, New York. pp. 944.

Rawsthorne, D. and Brodie, B.B. 1986. Root growth of susceptible and resistant potato cultivars and population dynamics of *Globodera rostochiensis* in the field. *Journal of Nematology* **18:4** 501-504.

Richardson, A.J. and Wiegand, C.L. 1977. Distinguishing vegetation from soil background information. *Photogrammetric Engineering and Remote Sensing* **43:** 1541-1552.

Riding, A.E., Anthony, S.G. and Parker, W.E. 1998. Topographic indices and the spatial distribution of potato cyst nematodes (PCN). *Aspects of Applied Biology* **52:** 339-344.

Riding, A.E. and Parker, W.E. 1998. The spatial distribution of potato cyst nematode populations: implications for reliable sampling strategies. *Aspects of Applied Biology* **59:** 121-126.

Robinson, M.P., Atkinson, H.J., Perry, R.N. 1987a. The influence of temperature on the hatching activity and lipid utilization of second stage juveniles of the potato cyst nematodes *Globodera rostochiensis* and *G. pallida. Revue de Nématologie* **10: 3.** 349-354.

Robinson, M.P., Atkinson, H.J., Perry, R.N. 1987b. The influence of soil moisture and storage time on the motility, infectivity and lipid utilization of second stage juveniles of the potato cyst nematodes *Globodera rostochiensis G. pallida. Revue de Nématologie* **10: 3.** 343-348.

Rollin, E.M. and Milton, E.J. 1998. Processing of high spectral resolution reflectance data for the retrieval of canopy water content information. *Remote Sensing of Environment* **65:** 86-92.

Rondeaux, G., Steven, M.D. and Baret, F. 1996. Optimisation of soil-adjusted vegetation indices. *Remote Sensing of Environment* **55:** 95-107.

Rouse, J.W., Haas, R.H., Schell, J.A., and Deering, D.W. 1973. Monitoring vegetation systems in the great plains with ERTS. *Third ERTS Symposium, NASA SP-351*, vol. 1, pp.309-317.

Sabins, F.F. 1996. *Remote Sensing: Principles and Interpretation, 3rd edition.* W.H. Freeman & Company, New York. pp. 494.

Salisbury, F.B., and Ross, C.W. 1992. *Plant Physiology.* Wadsworth. Belmont, CA. pp. 682.

Sanwald, E.F. 1981. Laboratory-determined spectral signatures of leaves of healthy and rizomania-diseased sugar beets and disease interpretability from aerial IRC photographs. **In:** *Spectral Signatures of Objects in Remote Sensing.* International Colloquium, Avignon, France. 201-208.

Schans, J. 1991. Reduction of leaf photosynthesis and transpiration rates of potato plants by second stage juveniles of *Globodera Pallida. Plant, Cell and Environment* **14:** 707-712.

Schans, J. and Arntzen, F.K. 1991. Photosynthesis, transpiration & plant growth characters of different potato cultivars at various densities of *Globodera pallida. Netherlands Journal of Plant Pathology* **97:** 297-310.

Schomaker, C.H. and Been, T.H. 1992. Sampling strategies for the detection of potato cyst nematodes; developing and evaluating a model. **In:** Eds Gommers F J, Mass P W Th. *Nematology: From Molecule to Ecosystem. Proceedings Second International Nematology Congress, 11-21 August 1990, Veldhoven, The Netherlands.* 182-194.

Seinhorst, J.W. 1981. Water consumption of plants attacked by nematodes and mechanisms of growth reduction. *Nematologica* **27:** 34-51.

Sellars, P.J. 1987. Canopy reflectance, photosynthesis and transpiration. II. The role of biophysics in the linearity of their interdependence. *Remote Sensing of Environment* **21:** 143-183.

Shepherd, A.M. 1986. Extraction and estimation of cyst nematodes. **In:** Ed. J F Southey. *Laboratory Methods for Work with Plant and Soil Nematodes.* HMSO, London. 31-49.

Sinclair, T.R., Schreiber, M.M., and Hoffer, R.M. 1973. Diffuse reflectance hypothesis for the pathway of solar radiation through leaves. *Agronomy Journal* **65:** 276-283.

Slatyer, R.O. 1967. *Plant-Water Relationships.* Academic Press, London 366 pp.

Smelt, J.H., Crum, S.J.H., Teunissen, W. and Leistra, M. 1987. Accelerated transformation of Aldicarb, Oxamyl and Ethoprophos after repeated soil treatments *Crop Protection* **6:5** 295-303.

Southey, J.F. 1970. *Laboratory Methods for Work with Plant and Soil Nematodes.* Technical Bulletin 2. Ministry of Agriculture, Fisheries and Food. London, Her Majesty's Stationery Office.

Southey, J.F. 1974. Methods for detection of potato cyst nematodes. *EPPO Bulletin* **4:** 463-473.

Stephens, M, Wood, G.A. and Taylor, J.C. 2000. Opportunities for targeted control of potato cyst nematode using remote sensing. *Aspects of Applied Biology* **60:** 213-218.

Steven, M.D. 1985. The physical and physiological interpretation of vegetation spectral signatures. **In:** *Proceedings 3rd International Colloquim on Spectral Signatures of Objects in Remote Sensing*, Les Arcs, France, 16-20 December 1985. ESA SP-247, European Space Agency, Paris.

Steven, M.D. and Jaggard, K.W. 1995. Advances in crop monitoring by remote sensing. **In:** Eds Danson, F.M. and Plummer, S.E. *Advances in Environmental Remote Sensing.* John Wiley & Sons, New York. 143-156.

Steven, M.D., Malthus, T.J., Demetriades-Shah, T.H., Danson, F.M. and Clark, J.A. 1990. High spectral resolution indices for crop stress. **In:** Eds. Steven, M.D., Clark, J.A. *Applications of Remote Sensing in Agriculture.* Butterworths, London. 209-227.

Stone, A.R. 1972. *Heterodera pallida* N. SP. (Nematoda: Heteroderidae). A second species of potato cyst nematode. *Nematologica* **18**: 591-606.

Terry, N. and Ulrich, A. 1973. Effects of potassium deficiency on the photosynthesis and respiration of leaves of sugar beet. *Plant Physiology* **51:** 783-786.

Thenkabail, P.S., Smith, R.B. and DePauw, E. 2000. Hyperspectral vegetation indices and their relationships with agricultural crop characteristics. *Remote Sensing Of Environment* **71: 2** 158-182.

Trudgill, D.L. 1980. Effects of *Globodera rostochiensis* and fertilisers on the mineral content and yield of potato plants. *Nematologica* **26:** 243-254.

Trudgill, D.L. 1992. Mechanisms of damage and tolerance in nematode infested plants. **In:** Eds Gommers, F.J. & Maas, P.W.T. *Nematology from Molecule to Ecosystem.* European Society of Nematologists, Dundee. 133-144.

Trudgill, D.L., Evans, K. and Parrott, D.M. 1975a. Effects of potato cyst nematodes on potato plants I: Effects in a trial with irrigation and fumigation on the growth and nitrogen and potassium contents of resistant and susceptible varieties. *Nematologica* **21:** 169-182.

Trudgill, D.L., Evans, K. and Parrott, D.M. 1975b. Effects of potato cyst nematodes on potato plants II: Effects on haulm size, concentration of nutrients in haulm tissue and yield of a nematode resistant and a nematode susceptible potato variety. *Nematologica* **21:** 183-191.

Trudgill, D.L., Phillips, M.S. and Alphey, T.J.W. 1987. Integrated control of potato cyst nematode. *Outlook on Agriculture* **16:4** 167-172.

Turner, S.J. 1990. The identification and fitness of virulent potato cyst nematode populations (*Globodera pallida*) selected on resistant *Solanum vernei* hybrids for up to eleven generations. *Annals of Applied Biology* **117**: 385-397.

Turner, S.J. 1993. Soil sampling to detect potato cyst-nematodes (*Globodera* spp.). *Annals of Applied Biology* **123**: 349-357.

Turner, S.J. 1996. Population decline of potato cyst nematodes (*Globodera rostochiensis, G. pallida*) in field soils of Northern Ireland. *Annals of Applied Biology* **129:** 315-322.

Turner, S.J. 1998. Sample preparation, soil extraction and laboratory facilities for the detection of potato cyst nematodes. **In:** Eds R J Marks and B B Brodie. *Potato Cyst Nematodes, Biology, Distribution and Control*, CAB International, Oxon. 75-90.

Turner, S.J. and Evans, K. 1998. Origins, distribution and biology of PCN. **In:** Eds R J Marks and B B Brodie. *Potato Cyst Nematodes, Biology, Distribution and Control*, Oxon: CAB International. 7-26.

Ulrich, A. 1993 Potato. **In:** Ed. Bennett, W.F. *Nutrient Deficiencies & Toxicities in Crop Plants*. ASP Press St. Paul, Minnesota. 149-156.

Van Staden, J. and Dimalla, G.G. 1977. A comparison of the endogenous cytokinins in the roots and xylem exudate of nematode-resistant and susceptible tomato cultivars. *Journal of Experimental Botany* **28:107** 1351-1356.

Verhoeff, W. and Bunnik, N.J.J. 1981. Influence of crop geometry on multispectral reflectance determined by the use of canopy reflectance models. **In**: *Proceedings, International Colloquium Spectral Signatures of Objects in Remote Sensing.* Avignon, France. 8-11 September 1981. *Les Colloques de l'INRA* **5:** 273-290.

Verma, S.B., Sellers, P.J., Walthall, C.L., Hall, F.G., Kim, J. and Goetz, S.J. 1993. Photosynthesis and stomatal conductance related to reflectance on the canopy scale. *Remote Sensing of Environment* **44:** 103-116.

Viglierchio, D.R. 1987. Elemental distribution in tissues of plants heavily infected with nematodes. *Nematologica* **33:** 433-450.
Vogelmann, T.C. 1989. Penetration of light into plants. *Photochemistry and Photobiology* **50:** 895-902.

Volk, T. 1998. *Gia's Body: Toward a Physiology of Earth.* Copernicus, Springer Verlag, New York.

Von Mende, N., Gravato Nobre, M.J., Perry, R.N. 1998. Host finding, invasion and feeding. **In:** Ed. Sharma, S.B. *The Cyst Nematodes.* Kluwer, Dordrecht. 217-238.

Wallace, H.R. 1987. Effects of nematode parasites on photosynthesis. **In:** Eds Veech, J.A. & Dickson, D.W. *Vistas on Nematology.* Society of Nematologists, Hyattsville, Maryland. 196-210.

Walter-Shea, E.A. and Norman, J.M. 1991. Leaf optical properties. **In:** Eds Myneni, R.B. & Ross, J. *Photon-Vegetation Interactions.* Springer Verlag, Berlin. 229-251.

Ward, M.G. and Hockland, S. 1996. Nematodes and plant health: legislation and sampling strategies in decision making for nematode management. *Pesticide Science* **47**: 77-80.

Webley, D.P. and Jones, F. G. W. 1981. Observations on *Globodera pallida and G. Rostochiensis* on early potatoes. *Plant Pathology* **30:** 217-224.

Wheeler, T.A. and Kaufman, H.W. 2003. Relationship of aerial broad band reflectance to *Meloidogyne incognita* density in cotton. *Journal of Nematology* **35:1** 48-57.

Whitehead, A.G. 1986. Chemical and integrated control of cyst nematodes. **In:** Eds Lamberti, F. and Taylor, C.E. *Cyst Nematodes*, Plenum Press, New York. 413-432.

Whitehead, A.G., Nichols, A.J.F. and Senior, J.C. 1994. The control of potato pale cyst-nematode (*Globodera pallida*) by chemical and cultural methods in different soils. *Journal of Agricultural Science, Cambridge* **123:** 207-218.

Whitehead, A.G. and Turner, S.J. 1998. Management and regulatory control strategies for potato cyst nematodes (*Globodera rostochiensis* and *Globodera pallida*). **In:** Eds Marks, R.J. and Brodie, B.B. *Potato Cyst Nematodes, Biology, Distribution and Control*, CAB International, Oxon. 135-152.

Wiegand, C.L., Richardson, A.J., Escobar, D.E. and Gerbermann, A.H. 1991. Vegetation indexes in crop assessments. *Remote Sensing Of Environment* **35:** 105-119.

Wilcox-Lee, D. and Loria, R. 1987. Effects of nematode parasitism on plant-water relations. **In:** Eds. Veech, J.A. and Dickson, D.W. *Vistas on Nematology.* Society of Nematologists, Inc. Hyattsville, Maryland, USA. 260-266.

Willmer, C.M. and Mansfield, T.A. 1969. A critical examination of the use of detached epidermis in studies of stomatal physiology. *New Phytologist* **68:** 363-375.

Wood, F.H., Foot, M.A., Dale, P.S. and Barber, C.J. 1983. Relative efficiency of plant sampling and soil sampling in detecting the presence of low potato cyst nematode infestations. *New Zealand Journal of Experimental Agriculture* **11:** 271-273.

Wooley, J.T. 1971. Reflectance and transmittance of light by leaves. *Plant Physiology* **47:** 656-662.